

Spring 2024

## Impact of Climate Change on Carbon and Nitrogen Balance in *Zostera Marina* L. (Eelgrass)

Malee Jinuntuya  
*Old Dominion University*

Follow this and additional works at: [https://digitalcommons.odu.edu/oeas\\_etds](https://digitalcommons.odu.edu/oeas_etds)



Part of the [Biogeochemistry Commons](#), [Climate Commons](#), and the [Oceanography Commons](#)

---

### Recommended Citation

Jinuntuya, Malee. "Impact of Climate Change on Carbon and Nitrogen Balance in *Zostera Marina* L. (Eelgrass)" (2024). Doctor of Philosophy (PhD), Dissertation, Ocean & Earth Sciences, Old Dominion University, DOI: 10.25777/e9hb-x931  
[https://digitalcommons.odu.edu/oeas\\_etds/394](https://digitalcommons.odu.edu/oeas_etds/394)

This Dissertation is brought to you for free and open access by the Ocean & Earth Sciences at ODU Digital Commons. It has been accepted for inclusion in OES Theses and Dissertations by an authorized administrator of ODU Digital Commons. For more information, please contact [digitalcommons@odu.edu](mailto:digitalcommons@odu.edu).

**IMPACT OF CLIMATE CHANGE ON CARBON AND NITROGEN BALANCE IN  
*ZOSTERA MARINA* L. (EELGRASS)**

by

Malee Jinuntuya  
B.S. May 2003, Michigan State University  
M.S. May 2007, Michigan State University

A Dissertation Submitted to the Faculty of  
Old Dominion University in Partial Fulfillment of the  
Requirements for the Degree of

DOCTOR OF PHILOSOPHY

OCEANOGRAPHY

OLD DOMINION UNIVERSITY  
May 2024

Approved by:

Richard C. Zimmerman (Director)

Victoria J. Hill (Member)

David J. Burdige (Member)

Gary Schafran (Member)

## ABSTRACT

### IMPACT OF CLIMATE CHANGE ON CARBON AND NITROGEN BALANCE IN *ZOSTERA MARINA* L. (EELGRASS)

Malee Jinuntuya  
Old Dominion University, 2024  
Director: Dr. Richard C. Zimmerman

Seagrasses face vulnerability to both global stressors like Ocean Acidification (OA) and climate warming compounded by local stressors such as eutrophication that reduces light availability, leading to a complex dynamic of positive and negative effect on their growth and survival. Increased dissolved aqueous CO<sub>2</sub> (CO<sub>2(aq)</sub>) benefits seagrasses by enhancing photosynthetic and growth rates, but it may increase nutrient demand, potentially depleting nutrient supply, especially in oligotrophic environments.

In this study, the long-term impact of CO<sub>2</sub> on *Zostera marina* L. (eelgrass) were investigated across a gradient of CO<sub>2(aq)</sub> concentrations (55 – 2200 μM CO<sub>2(aq)</sub>) and leaf area indices (LAI). The focus was on quantify changes in carbon (C) and nitrogen (N) content, composition, and metabolism in response to CO<sub>2</sub>-stimulated photosynthesis and growth. Absolute growth rates, shoot sizes, leaf density, sucrose concentrations, and carbon and nitrogen growth demands increased with increasing CO<sub>2(aq)</sub> availability. However, there was no notable decline in biomass-specific N content of leaf at higher CO<sub>2(aq)</sub> concentrations primarily due to dilution effects caused by carbon accumulation in thicker leaves, rather than N-limitation. Rather than increasing plant survival in the context of CO<sub>2(aq)</sub> enrichment, this study found that nutrient enrichment of the sediment reduced plant survival as a result of NH<sub>4</sub><sup>+</sup> toxicity. In contrast, the high H<sub>2</sub>S concentrations reaching millimolar levels in sediment, which was stimulated by organic carbon addition, was not particularly toxic to eelgrass.

CO<sub>2</sub> effects on N uptake were complicated by changes in canopy architecture due to increasing leaf area index (LAI), affecting N uptake patterns of leaves and roots. Combining a nutrient uptake model with the radiative transfer *GrassLight* (v2.14) model, this study explored how CO<sub>2</sub>-driven photosynthesis affected N uptake patterns and requirements for growth. Model predictions across varying LAIs and CO<sub>2(aq)</sub> concentrations indicated low N demand for eelgrass under all CO<sub>2(aq)</sub> conditions, with roots playing a key role in N acquisition as CO<sub>2(aq)</sub> concentrations increased. Overall, my results highlight the importance of photosynthesis in regulating N metabolism and acquisition between the above- and belowground components, and suggest that most eelgrass meadows are unlikely to experience N limitation, even in high CO<sub>2(aq)</sub> environments.

Copyright, 2024, by Malee Jinuntuya, All Rights Reserved

*This work is dedicated to Rob and family.*

## ACKNOWLEDGEMENTS

I attribute this academic achievement to a multitude of individuals; without them this work would not have come to fruition. Foremost among them is my advisor and committee chair, Dr. Richard Zimmerman. I express deep gratitude for his intellectual wisdom, both in the realms of science and in life, and for his unwavering financial support. Dick, I am truly thankful for you taking me under your wings and welcoming me into the BORG family those pivotal years ago. Your consistent encouragement to pursue my interests, your challenges to a mindful writer and speaker, and your insistence on seeing the bigger picture have been invaluable. Thanks for pulling me out of the grass so that I could appreciate the forest. I also extend my gratitude to my dissertation committee members, Drs. Victoria Hill, David Burdige, and Gary Schafran. Their exceptional patience has allowed me to complete this work. Victoria, your boundless enthusiasm, humor, and can-do attitude kept me motivated during moments of doubt. David, I appreciate your guidance and financial support during the initial years of graduate school, allowing me to carve out my unique path at ODU.

I extend my heartfelt gratitude to the exceptional BORG crew, a group I am fortunate to call my second family. A sincere acknowledgement goes to David Ruble, for your help that transcends beyond the field and lab. I am especially grateful for all your expertise in the construction of various experimental rigs that were crucial to my research. My seagrass sisters: Billur Celebi-Ergin, Meredith McPherson and Carmen Zayas, your companionship, your support, and our endless discussions on topics spanning from science to life have enriched me. Brian Collister, you are a mechanical genius, a brilliant scientist, and an exceptional friend. Miranda and Chelsea, my two incredible and hardworking mentees, part of this work also belongs to you.

I would like to express my gratitude and acknowledge the following individuals, whose assistance and expertise were instrumental to the work presented here: Drs. Greg Cutter, Margie Mulholland, and Roger Harvey, for generously granting access to their labs and their instruments. I am immensely grateful to Laura Perry and Brittany Widner, for sharing their profound knowledge and expertise in setting up various instruments essential for running my tissues and water samples. A special thanks to Rachel McMahon for her assistance in running my amino acid samples on the LC/MS Orbitrap Mass Spectrometer, and Wes Myers for conducting grain size analysis.

I owe my sanity to both my ODU and non-ODU colleagues and friends. There are not enough blank spaces to capture all the names and the significance each one of you holds me. I am grateful that our paths crossed, guiding me through some very dark times, and your friendships help keep my spirits. Special thanks to John Knight, Drs Xiping Hu and Susan Park for your encouragements and uplifting pep talks. Additionally, I extend my appreciation to past and present departmental staff for their administrative assistance as I navigate through various forms and registrations.

If not for the love and support of my family and partner, I would not be where I am today. Thank you for all your sacrifices so that I could achieve my goal. Rob, you are my constant, my compass. Thanks for constantly guiding me in the right direction, ensuring that I never stray far from the finish line. Thanks for keeping Shoga and I fed and for giving us a loving home.

Financial support for this work was generously provided by the National Science Foundation (OCE-1061823) and Virginia Aquarium and Marine Science Center. Additional funding was provided by Dorothy Brown Smith Scholarship and Jacques S. Zaneveld Endowed Scholarship for travels and stipends.

## TABLE OF CONTENTS

|   | Page |
|---|------|
| LIST OF TABLES .....  | ix   |
| LIST OF FIGURES .....   | xi   |
| 1. INTRODUCTION .....   | 15   |
| 1.1 BACKGROUND .....  | 15   |
| 2. EFFECTS OF LONG-TERM CO <sub>2</sub> ENRICHMENT ON BIOCHEMICAL<br>COMPOSITIONS, GROWTH, AND GROWTH DEMAND OF <i>ZOSTERA MARINA</i> L.<br>(EELGRASS)..... | 20   |
| PREFACE .....   | 20   |
| 2.1 INTRODUCTION .....  | 20   |
| 2.2 MATERIALS AND METHODS.....  | 23   |
| 2.2 RESULTS .....   | 35   |
| 2.3 DISCUSSION .....  | 67   |
| 3. IMPACTS OF ELEVATED CO <sub>2</sub> AND SEDIMENT EUTROPHICATION ON<br><i>ZOSTERA MARINA</i> L.: AN ENRICHMENT STUDY .....                                | 75   |
| 3.1 INTRODUCTION .....  | 75   |
| 3.2 MATERIALS AND METHODS.....  | 78   |
| 3.3 RESULTS .....   | 84   |
| 3.4 DISCUSSION .....  | 112  |
| 4. MODELING THE EFFECTS OF CO <sub>2</sub> AND LAI ON NITROGEN UPTAKE<br>PATTERN IN <i>ZOSTERA MARINA</i> L. (EELGRASS).....                                | 120  |
| 4.1 INTRODUCTION .....  | 120  |
| 4.2 MATERIALS AND METHODS.....  | 123  |
| 4.3 RESULTS .....   | 139  |
| 4.4 DISCUSSION .....  | 161  |
| 5. CONCLUSION.....  | 169  |
| 6. REFERENCES .....   | 173  |
| 7. VITA.....  | 200  |

## LIST OF TABLES

| Table  | Page |
|--|------|
| 1. Fixed parameter values assigned to <i>GrassLight</i> runs from May 2013 to October 2014. ....   | 34   |
| 2. Summary statistics for boxplot shown in Fig. 3D.....  | 39   |
| 3. Summary ANCOVA tables for the Type III tests of fixed effects using a 1-factor (Month) Linear Mixed-Effects Model in SPSS with log CO <sub>2(aq)</sub> (pH levels = 6.1, 6.4, 6.9, 7.4, 7.7) as a covariate; DW: dry weight. ....   | 40   |
| 4. Linear regression for the effect of CO <sub>2(aq)</sub> on sucrose, FAA, total C and N contents on leaf, rhizome, and roots at the termination of the experiment (October 2014) after 18 months of CO <sub>2</sub> enrichment at treatments: 55, 107, 371, 823 and 2121 μmol CO <sub>2</sub> Kg <sup>-1</sup> SW..... | 56   |
| 5. Summary ANCOVA tables for Type III tests of fixed effects (Tissue types) using the mixed linear model routine performed in SPSS with log CO <sub>2(aq)</sub> as a covariate. ....   | 60   |
| 6. Two-way ANOVA results for the effects of log CO <sub>2(aq)</sub> (pH levels = 6.1, 6.4, 6.9, 7.4, 7.7) and treatments on pore water NH <sub>4</sub> <sup>+</sup> , NO <sub>3</sub> <sup>-</sup> , and PO <sub>4</sub> <sup>3+</sup> concentrations from May to July 2014.....   | 87   |
| 7. Two-way ANOVA results for the effects of log CO <sub>2(aq)</sub> (pH levels = 6.1, 6.4, 6.9, 7.4, 7.7) and treatments (Control, NPK, OC, and NPKOC) on porewater H <sub>2</sub> S concentrations from May to July 2014. ....  | 89   |
| 8. Two-Way ANOVA results for the effects log CO <sub>2(aq)</sub> (pH levels = 6.1, 6.4, 6.9, 7.4, 7.7) and treatments (Control, NPK, OC, and NPKOC) on log-transformed shoot numbers from May to July 2014. ....   | 92   |
| 9. Summary ANCOVA tables for Type III tests of fixed effects (Time and Treatments) using the mixed linear model routine performed in SPSS.....   | 94   |
| 10. Tukey's test results comparing the mean percent survival (I) between treatments (J). ....  | 95   |
| 11. Summary ANCOVA tables for the Type III tests of fixed effects using a 2-factor (Time and Treatment) Linear Mixed-Effects Model in SPSS with log CO <sub>2(aq)</sub> (pH levels = 6.1, 6.4, 6.9, 7.4, 7.7) as a covariate. ....   | 98   |
| 12. Summary of symbols (in alphabetical order), their definitions, and dimensions. ....  | 129  |
| 13. Fixed parameter values assigned to each <i>GrassLight</i> run.....   | 137  |
| 14. Fixed parameter values assigned to each N-growth model run. ....   | 138  |

| Table   | Page |
|---|------|
| 15. Effects of $\text{CO}_{2(\text{aq})}$ on uptake kinetics: maximum potential uptake rate, $V_{\text{pmax}}$ ( $\mu\text{mol shoot}^{-1} \text{d}^{-1}$ ), half-saturation constant, $K_{\text{S}}$ ( $\mu\text{M}$ ), and affinity coefficient $\alpha$ ( $V_{\text{pmax}}/K_{\text{S}}$ ) of ammonium and nitrate in leaves and roots. .... | 152  |

## LIST OF FIGURES

| Figure  | Page |
|---|------|
| 1. Outdoor CO <sub>2</sub> enrichment facility located at the Virginia Aquarium for Marine Science (Virginia Beach, VA) (originally published by Zimmerman et al. (2017)).  | 26   |
| 2. Environmental conditions during the experiment from May, 2013 to October, 2014 for (A) above water natural down-welling irradiance ( $E_d$ ) at 100% (full sun) and 60% (40% shading) light levels, (B) daily mean salinity (PSS), (C) daily mean water temperature (°C), and (D) daily mean aqueous CO <sub>2</sub> concentrations. | 36   |
| 3. Concentrations of macronutrients (NH <sub>4</sub> <sup>+</sup> , NO <sub>2</sub> <sup>-</sup> +NO <sub>3</sub> <sup>-</sup> , and PO <sub>4</sub> <sup>3-</sup> ) in Owls Creek surface water from 1998 to 2016 are presented in panels A, B, and C.   | 38   |
| 4. Heat maps of (A) absolute growth rates, and (B) specific growth rates of <i>Zostera marina</i> L. contoured as a function of pH or CO <sub>2(aq)</sub> treatments (vertical left axis) and months (horizontal axis) from May 2013 until October 2014.  | 42   |
| 5. Heat maps of (A) mean shoot size, and (B) leaf density contoured as a function of pH or CO <sub>2(aq)</sub> treatments (vertical left axis) and months (horizontal axis) from May 2013 to October 2014.  | 44   |
| 6. Heat maps of (A) biomass-specific sucrose concentrations, and (B) area-specific sucrose concentrations in leaf tissues contoured as a function of pH or CO <sub>2(aq)</sub> treatments (vertical left axis) and months (horizontal axis).  | 46   |
| 7. Heat maps of (A) biomass-specific free amino acids (FAA), and (B) area-specific FAA concentrations contoured as a function of pH or CO <sub>2(aq)</sub> treatments (vertical left axis) and months (horizontal axis).  | 49   |
| 8. Concentrations of specific free amino acids (FAA) concentrations in <i>Zostera marina</i> L. leaf tissues from the highest CO <sub>2(aq)</sub> (hash lines) and ambient CO <sub>2(aq)</sub> (solid color) treatments, contrasting between December 2013 (red) and July 2014 (black).   | 50   |
| 9. Heat maps of carbon (A, B), nitrogen (C, D), and sulfur (E, F) content in leaves normalized to biomass (top row) or leaf area (bottom row) contoured as a function of pH (or CO <sub>2(aq)</sub> ) treatments and months.  | 53   |
| 10. Heat maps of (A) molar C:N ratio, and (B) molar N:S ratio contoured as a function of pH or CO <sub>2(aq)</sub> treatments (vertical left axis) and months (horizontal axis).  | 54   |
| 11. Differences in eelgrass shoot sizes across pH (or CO <sub>2(aq)</sub> ) gradient at the end of the experiment in October 2014.  | 55   |

| Figure  | Page |
|---|------|
| 12. Sucrose (left) and free amino acids (FAA) (right) concentrations for leaves (top), rhizome (middle), and roots (bottom) plotted against $\text{CO}_{2(\text{aq})}$ concentrations with corresponding pH scale presented on the secondary x-axis. .... | 58   |
| 13. Leaf, rhizome, and root total C (left axis) and N (right axis) content in <i>Zostera marina</i> L., shown as a function of log $\text{CO}_{2(\text{aq})}$ concentrations and pH (secondary x-axis). ....  | 59   |
| 14. Seasonal patterns of <i>Zostera marina</i> L. C demand in response to pH (or $\text{CO}_{2(\text{aq})}$ ) treatments, depicted in scatter plot with observations spanning from May 2013 until October 2014. ....                                      | 61   |
| 15. Seasonal patterns of <i>Zostera marina</i> L. N demand in response to pH (or $\text{CO}_{2(\text{aq})}$ ) treatments, depicted in scatter plot with observations spanning from May 2013 until October 2014. ....                                      | 62   |
| 16. Predicted growth demand for carbon (A, B) and for nitrogen (C, D) in summer vs winter as a function of aqueous $\text{CO}_2$ ( $\text{CO}_{2(\text{aq})}$ ) concentrations. ....  | 63   |
| 17. Time series depiction of the effects of $\text{CO}_{2(\text{aq})}$ (or pH) on the abundance of carbon as sucrose ( $\text{C}_{\text{sucrose}}$ ) per shoot available for new growth, from June 2013 until October 2014. ....                          | 65   |
| 18. Time series depiction of the effects of $\text{CO}_{2(\text{aq})}$ (or pH) on sucrose reserves from June 2013 until October 2014. ....  | 66   |
| 19. Sediment fertilization and $\text{CO}_{2(\text{aq})}$ enrichment experimental design. ....  | 79   |
| 20. Percentage distribution of sediment grain sizes from Elizabeth River, obtained at the Sailing Center (Old Dominion University, Norfolk, Virginia). ....   | 86   |
| 21. The porewater concentrations of $\text{NH}_4^+$ (A), $\text{NO}_3^-$ (B), and $\text{PO}_4^{3-}$ (C) for each sediment treatment: Control (red), NPK (orange), OC (yellow), NPKOC (green). ....   | 88   |
| 22. Porewater $\text{H}_2\text{S}$ concentrations measured in Control, NPK, OC, and NPKOC sediment treatments from May to July 2014. ....   | 90   |
| 23. Percent survival (A) plotted as a function of time for the four sediment types: Control (red), NPK (orange), OC (yellow), and NPKOC (green) from May to July 2014. ....   | 93   |
| 24. Percent survival plotted as a function of log-nutrient concentrations and log $\text{H}_2\text{S}$ concentration for days 11 (start of porewater sampling), 32, and 68 (end of porewater sampling). ....  | 96   |
| 25. Shoot size ( $\text{cm}^2$ ) of <i>Zostera marina</i> L. plotted as a function of time (in experimental days) for (A) Control, (B) NPK, (C) OC, (D) NPKOC sediment treatments. ....   | 100  |

| Figure  | Page |
|---|------|
| 26. Absolute growth rates ( $\text{cm}^2 \text{d}^{-1}$ ) of <i>Zostera marina</i> L. in Control (A), NPK (B), OC (C), and NPKOC (D) treatments plotted against time. ....  | 101  |
| 27. Specific growth rates (SGR) ( $\% \text{d}^{-1}$ ) of <i>Zostera marina</i> L. in Control (A), NPK (B), OC (C), and NPKOC (D) treatments plotted against time. ....   | 102  |
| 28. Heat map of leaf sucrose concentrations plotted as a function of pH and corresponding $\text{CO}_{2(\text{aq})}$ concentrations (left axis) across time for all (except NPKOC) sediment treatments combined (Control, NPK, OC were not significantly different, Table 11).....  | 104  |
| 29. Heat maps of leaf FAA concentrations plotted as a function of pH with the corresponding aqueous $\text{CO}_2$ concentrations (left axis) across time for Control (A), NPK (B), OC (C), and NPKOC (D) sediment treatments. ....  | 105  |
| 30. Heat maps of total nitrogen (TN) content per unit dry weight of leaf plotted as a function of pH and corresponding $\text{CO}_{2(\text{aq})}$ concentrations (left axis) across time for Control (A), NPK (B), OC (C) and NPKOC (D) sediment treatments. ....   | 108  |
| 31. Heat map of total carbon (TC) ( $\text{mmol g}^{-1}$ DW of leaf) plotted as a function of pH and corresponding $\text{CO}_{2(\text{aq})}$ concentrations (left axis) across time for all sediment treatments combined (Control, NPK, OC and NPKOC were not significantly different, Table 11). ....                       | 109  |
| 32. Heat map of total sulfur (TS) ( $\text{mmol g}^{-1}$ DW of leaf) plotted as a function of pH and corresponding $\text{CO}_{2(\text{aq})}$ concentrations (left axis) across time for all sediment treatments combined (Control, NPK, OC and NPKOC were not significantly different, Table 11). ....                       | 110  |
| 33. Heat maps of C:N (A) and N:S (B) ratios (mole:mole) plotted as a function of pH and corresponding $\text{CO}_{2(\text{aq})}$ concentrations (left axis) across time for all sediment treatments combined (Control, NPK, OC and NPKOC were not significantly different, Table 11). ....                                    | 111  |
| 34. Conceptual diagram illustrating the interactive effects of $\text{CO}_{2(\text{aq})}$ , light, and nutrient ( $\text{NO}_3^-$ , $\text{NH}_4^+$ ) availability on nitrogen (N) uptake in <i>Zostera marina</i> L.....   | 125  |
| 35. Parameter space defining the N-growth model.....  | 128  |
| 36. A property-property plot demonstrating the linear relationship between light and $\text{CO}_2$ -saturated rate of photosynthesis ( $P_E$ ) and maximum aerobic respiratory demand of roots+rhizome ( $R_{\text{root+rhi}}^{\text{max}}$ ) determined for <i>Zostera marina</i> L.....                                     | 140  |
| 37. Each panel illustrates the diurnal pattern of (A-F) shoot specific instantaneous canopy photosynthesis ( $P_c$ , and (G-L) shoot specific instantaneous aerobic respiration for roots+rhizome ( $R_{\text{root+rhi}}$ ) predicted over 14.7 hours of daylength under different $\text{CO}_{2(\text{aq})}$ treatments..... | 141  |

| Figure   | Page |
|--|------|
| 38. Heatmap illustrating the (A) water column $\text{NO}_3^-$ concentrations, and (B) porewater $\text{NH}_4^+$ concentrations required to saturate eelgrass growth plotted as a function of $\log \text{CO}_{2(\text{aq})}$ ( $\mu\text{M}$ ) (or pH presented on the secondary x-axis) for fixed LAI values.....   | 143  |
| 39. Daily integrated rate of realized ( $V_r^{\text{LNH}_4}$ ) (black symbols) and potential ( $V_p^{\text{LNH}_4}$ ) (color hyperbolic curve) uptake rate of $\text{NH}_4^+$ by leaves at steady state plotted as a function of log-transformed $\text{CO}_{2(\text{aq})}$ concentrations (dash lines) and $\text{NH}_4^+$ concentrations. ....               | 145  |
| 40. Daily integrated rate of realized ( $V_r^{\text{LNO}_3}$ ) (black symbols) and potential ( $V_p^{\text{LNO}_3}$ ) (color hyperbolic curve) uptake rate of $\text{NO}_3^-$ by leaves at steady state plotted as a function of log-transformed $\text{CO}_{2(\text{aq})}$ concentrations (dash lines) and $\text{NO}_3^-$ concentrations. ....               | 146  |
| 41. Daily integrated rate of realized ( $V_r^{\text{RNH}_4}$ ) (black symbols) and potential ( $V_p^{\text{RNH}_4}$ ) (color hyperbolic curve) uptake rate of $\text{NH}_4^+$ by roots at steady state plotted as a function of log-transformed $\text{CO}_{2(\text{aq})}$ concentrations (dash lines) and $\text{NO}_3^-$ concentrations. ....                | 147  |
| 42. Effects of $\text{CO}_{2(\text{aq})}$ concentrations and LAI on the daily integrated maximum potential uptake rate for (A) $\text{NH}_4^+$ by leaves ( $V_{\text{pmax}}^{\text{LNH}_4}$ ), (B) $\text{NO}_3^-$ by leaves ( $V_{\text{pmax}}^{\text{LNO}_3}$ ), and (C) porewater $\text{NH}_4^+$ by roots ( $V_{\text{pmax}}^{\text{RNH}_4}$ ). ....       | 150  |
| 43. Effects of $\text{CO}_{2(\text{aq})}$ and LAI on the half-saturation constants ( $K_s$ in $\mu\text{M}$ ) of leaves for (A) $\text{NH}_4^+$ , (B) $\text{NO}_3^-$ , and of roots for (C) porewater $\text{NH}_4^+$ . The $\text{CO}_{2(\text{aq})}$ concentrations are expressed as a log scale.....   | 151  |
| 44. Percentage of total N uptake by leaves and roots under standard nutrient simulation (5 $\mu\text{M}$ water column $\text{NH}_4^+$ ; 5 $\mu\text{M}$ water column $\text{NO}_3^-$ , 100 $\mu\text{M}$ porewater $\text{NH}_4^+$ ) plotted as a function of $\log \text{CO}_{2(\text{aq})}$ concentrations for different leaf area index (LAI) (color). .... | 154  |
| 45. Percentage of total N taken as $\text{NH}_4^+$ by leaves (top), as $\text{NO}_3^-$ by leaves (middle), and as porewater $\text{NH}_4^+$ by roots, plotted as a function of water column $\text{NH}_4^+$ (0-50 $\mu\text{M}$ ) and log-transformed $\text{CO}_{2(\text{aq})}$ concentrations for fixed LAI. ....  | 155  |
| 46. Percentage of total N taken as $\text{NH}_4^+$ by leaves (top), as $\text{NO}_3^-$ by leaves (middle), and as porewater $\text{NH}_4^+$ by roots, plotted as a function of water column $\text{NO}_3^-$ (0-50 $\mu\text{M}$ ) and log-transformed $\text{CO}_{2(\text{aq})}$ concentrations for fixed LAI. ....  | 156  |
| 47. Percentage of total N taken as $\text{NH}_4^+$ by leaves (top), as $\text{NO}_3^-$ by leaves (middle), and as porewater $\text{NH}_4^+$ by roots, plotted as a function of porewater $\text{NH}_4^+$ (0-100 $\mu\text{M}$ ) and log-transformed $\text{CO}_{2(\text{aq})}$ concentrations for fixed LAI. ....  | 157  |
| 48. Isoleth of equal (50%) N uptake by leaves and roots/rhizome defined by $\text{CO}_{2(\text{aq})}$ (in log scale) and porewater $\text{NH}_4^+$ concentrations for LAI values ranging from 0.15 to 3.0.....   | 159  |
| 49. Comparison of N uptake rate (i.e. N demand) and N remineralization rate (blue solid and red dash lines; values obtained from the literature) across different LAI.....   | 160  |

## CHAPTER 1

### INTRODUCTION

#### *1.1 Background*

Seagrasses are found in shallow subtidal areas spanning across tropical and temperate latitudes, and are amongst the most prominent primary producers on our planet (Duarte and Chiscano 1999). Occupying less than 0.2% of the world's oceans (McKenzie et al. 2020), seagrass meadows are an important blue carbon ecosystem (Greiner et al. 2013). They act as a vital carbon sink by removing CO<sub>2</sub> from the atmosphere through photosynthesis and storing it in both biomass and sediments (Gacia et al. 2002; McLeod et al. 2011; Fourqurean et al. 2012). This action underscores their importance in contributing to negative climate feedback and supporting mitigation efforts (Duarte et al. 2005; Fourqurean et al. 2012; Johannessen 2022).

Shallow water marine habitats are under increasing pressure from climate change and human activities, resulting in global seagrass population declines and habitat loss. The primary contributors to the loss of these ecosystem engineers (Fonseca 1989; Hemminga and Duarte 2000; Green and Short 2003; Heck et al. 2003; Orth et al. 2006) include degraded water quality from widespread eutrophication leading to light limitation and rising temperatures resulting from unchecked emissions of greenhouse gases. Since the 1900s, an estimated 30% of the known seagrass area have been lost, at a rate of 7% per year since 1990 (Waycott et al. 2009). Therefore, conserving and restoring this blue carbon ecosystem is crucial for mitigating the rise in global atmospheric CO<sub>2</sub> ( $p\text{CO}_2$ ).

The ocean absorbs about 30% of annual  $p\text{CO}_2$  emissions (Quay et al. 1992; Orr et al. 2001). As of February 2024, atmospheric  $p\text{CO}_2$  reported by the NOAA Global Monitoring Laboratory (<https://gml.noaa.gov/ccgg/trends/>) now exceed 420 ppm, increasing oceanic  $[\text{CO}_{2(\text{aq})}]$  by 50% compared to pre-industrial level. Projections suggest  $p\text{CO}_2$  will exceed 900 ppm by 2100 (IPCC 2014; Dlugokencky et al. 2019), potentially lowering ocean pH to 7.8, and increasing oceanic  $[\text{CO}_{2(\text{aq})}]$  by 220% (IPCC 2022) (Zeebe 2012). Increasing ocean acidification (OA) will trigger non-linear ecological responses leading to winners and losers at individual, population, and ecosystem levels (Kleypas et al. 1999; Harley et al. 2006; Lee et al. 2022). Calcifying organisms are expected to suffer due to their vulnerable biominerals, which are susceptible to dissolution in undersaturated seawater with respect to calcium carbonate (Azevedo et al. 2015). Conversely, seagrasses and other photosynthetic organisms, currently  $\text{CO}_2$ -limited, should benefit from rising OA because more carbon will exist in the form of aqueous  $\text{CO}_2$  rather than  $\text{HCO}_3^-$  at lower pH (the  $\text{CO}_2:\text{HCO}_3^-$  ratio at pH 8.2 is 1:160 and at pH 6.0 is 1:1 (Beer and Koch 1996)). Numerous studies consistently reported that various seagrass species experienced increased leaf photosynthetic rates and sugar accumulation after brief  $\text{CO}_2$  exposure (hours to weeks) (Durako 1993; Zimmerman et al. 1995; Beer and Koch 1996; Zimmerman et al. 1997; Jiang et al. 2010; Ow et al. 2015). Prolonged exposure to increased  $\text{CO}_{(\text{aq})}$  availability has a quantitative impact on photosynthesis, growth and reproduction of *Zostera marina* L. (Palacios and Zimmerman 2007) that is capable of counteracting the negative effects of high temperatures on plant performance (Zimmerman et al. 2017). In addition to stimulating photosynthetic rates, long-term exposure to elevated  $\text{CO}_{(\text{aq})}$  reduces light-harvesting pigment concentrations in the leaves (Celebi-Ergin et al. 2021) mimicking the photoacclimation response to high light (Cummings and Zimmerman 2003).

Enhanced carbon metabolism under elevated CO<sub>2</sub> is anticipated to significantly impact N metabolism in seagrasses. Photosynthetic organisms feature a complex regulatory mechanism that coordinates carbon metabolism with nitrogen assimilation. The increased sucrose concentrations generated under elevated CO<sub>2</sub> not only provides more energy and carbon skeletons for plant growth, they are key regulators of N assimilation and protein synthesis (Ruan 2012). For instance, the assimilation of inorganic nitrogen such as nitrate (NO<sub>3</sub><sup>-</sup>) and ammonia (NH<sub>4</sub><sup>+</sup>) into amino acids is highly regulated by the availability of  $\alpha$ -ketoglutarate (a Krebs cycle intermediate), which serves as a precursor for the synthesis of glutamate, an important amino acid.

Currently, our understanding of the long-term effects of elevated CO<sub>2</sub> on seagrass N metabolism is rudimentary. While terrestrial plant studies are often used as reference, their results cannot be directly applied to explain seagrass response to elevated CO<sub>2</sub> due to differences in environmental conditions and ecological dynamics between marine and terrestrial ecosystems. The impact of CO<sub>2</sub> on land plants is primarily linked to improved water use efficiency (WUE, amount of carbon gained as biomass per unit of water lost) (Hatfield and Dold 2019) and changes in stomatal conductance (Ainsworth and Rogers 2007). However, water use efficiency and stomatal conductance are not an issue for fully submerged aquatic plants. Unlike terrestrial plants, seagrasses can acquire nutrients through both their leaves and roots (Thursby and Harlin 1982; Short and McRoy 1984; Pedersen and Borum 1992) in approximately equal proportions (Iizumi and Hattori 1982; Zimmerman et al. 1987), increasing the potential nutrient resources. Yet, this dissertation will show that CO<sub>2</sub> enrichment reduces the N content of seagrasses, just as it does in terrestrial plants (Ainsworth and Long 2005). Ongoing research is needed to explore whether the reduction in leaf N in seagrasses is due to changes in N uptake, N-limitation, or a dilution effect, where a proportion of nitrogen in plant tissues decreases relative to carbon.

The positive physiological responses from exposure to elevated CO<sub>2</sub> will be significant for seagrasses, particularly in eutrophic systems if the carbon and nitrogen metabolisms are integrally coupled. Seagrass habitats are frequently subjected to anthropogenic eutrophication and this enrichment has been shown to adversely affect seagrass function and physiology (Delgado et al. 1999). Excessive inorganic nitrogen concentrations (NO<sub>3</sub><sup>-</sup> and NH<sub>4</sub><sup>+</sup>) have been hypothesized to exert a direct toxic effect on seagrass, perhaps by promoting continuous nitrogen uptake and assimilation, leading to internal carbon drain and consequent die-off (Turpin et al. 1991; Burkholder et al. 1992; Touchette 2003). At 20<sup>th</sup> Century [CO<sub>2</sub>], this “runaway N metabolism” was hypothesized to force re-direction of carbohydrates from other essential metabolic pathways, therein potentially exacerbating the effects of carbon limitation on seagrass growth and survival. If carbon is indeed diverted to support nitrogen assimilation, then rising atmospheric CO<sub>2</sub> may relieve this carbon drain problem by enhancing the rates of carbon-fixation and accumulation of mobile C reserves in seagrass, increasing the likelihood of eelgrass survival in nutrient enriched environments.

Predicting seagrass health and success in the face of a changing climate requires a thorough examination of their responses over timescales that span multiple growth periods. While seagrasses should benefit from increase in CO<sub>2</sub> concentrations, understanding their future ecological success requires careful consideration of the interaction of photosynthesis with other critical factors, such as nitrogen uptake and assimilation. Despite suggestions that seagrasses may face N-limitation in high CO<sub>2</sub> environments (Alexandre et al. 2012), conclusive evidence supporting this claim is lacking and warrants further investigation. This requires determining the growth requirements for both nitrogen and carbon, a goal of this study. Moreover, with the persistence and likely intensification of anthropogenic activities leading to coastal eutrophication, intricate interactions

between eutrophication and ocean acidification will impact seagrass physiology, a topic that also remains poorly addressed. Through 18 months of long-term experimentations and modelling endeavors, this research aims to provide valuable insights that enhance our predictive understanding of how N metabolism of seagrass will respond to environmental change, particularly elevated CO<sub>2</sub> levels, spanning from physiological to whole-plant performance levels.

The research conducted here addressed several important questions regarding the response of *Z. marina* to escalating anthropogenic pressures in the context of future climate change. As a key temperate seagrass species, *Z. marina* plays a vital ecological role in supporting economically valuable fisheries and protection of shorelines, particularly in the Chesapeake Bay.

## CHAPTER 2

# EFFECTS OF LONG-TERM CO<sub>2</sub> ENRICHMENT ON BIOCHEMICAL COMPOSITIONS, GROWTH, AND GROWTH DEMAND OF *ZOSTERA MARINA* L. (EELGRASS)

### PREFACE

A part of the results presented in this chapter was published in the journal *Marine Ecology Progress Series* ([https://doi: 10.3354/meps12051](https://doi.org/10.3354/meps12051)). The right to reproduce the data in theses or dissertations is retained by the author as per the Publisher and author rights and agreements.

### 2.1 Introduction

Present day atmospheric CO<sub>2</sub> concentrations (424 ppm measured at Mauna Loa) have increased >60% since pre-industrial times (~260 ppm) (Wigley 1983). This rise in *p*CO<sub>2</sub> will directly affect the dissolved inorganic carbon (DIC) in coastal waters by altering the carbonate chemistry profile of seawater. The resulting shifts in the relative distributions of DIC towards aqueous CO<sub>2</sub> will greatly favor many photosynthetic autotrophs (Riebesell 2004; Leakey et al. 2009; Kowalczyk and Lee 2022; Velthuis et al. 2022) including seagrasses (Zimmerman et al. 1997; Apostolaki et al. 2014; Celebi 2016; Zimmerman 2021).

Predicting the responses of seagrass to future CO<sub>2</sub> levels constitutes a complex challenge due to an array of environmental drivers such as light, nutrient, and temperature, all of which collectively shape the overall performance of these plants. Responses also vary with seagrass species under examination (Invers et al. 2001) and experiment duration (Zimmerman 2021). For

instance, short-term CO<sub>2</sub> enrichment experiments conducted in laboratory settings (hours to weeks) have consistently shown positive effects on photosynthetic rates, sugar production, and leaf growth across many seagrass species ranging from temperate eelgrass, *Zostera marina* L., Mediterranean seagrass, *Posidonia oceanica* (Invers et al. 2002; Hall-Spencer et al. 2008) to tropical seagrass, *Thalassia testudinum* (Banks ex König) (Durako 1993; Beer and Koch 1996; Campbell and Fourqurean 2013), and *Thalassia hemprechii* (Jiang et al. 2010). However, it was through longer enrichment experiments (over 12-months) that key traits such as shoot density, survival, reproduction, and thermal tolerance become apparent (Palacios and Zimmerman 2007; Zimmerman et al. 2017). Furthermore, these longer-term experiments yielded mechanistic insights into the acclimatory response to CO<sub>2</sub> from metabolic to whole plant levels (Zayas-Santiago et al. 2020; Celebi-Ergin et al. 2021; Celebi-Ergin et al. 2022) that would not have otherwise been evident from short-term experiment.

Although a high CO<sub>2</sub> world is expected to enhance carbon assimilation by seagrasses, the subsequent influence on nitrogen metabolism and its distribution among leaves, rhizomes and roots has not been thoroughly investigated. Recent studies have reported lower leaf N content in *T. hemprechii* subjected to short-term (21 days) CO<sub>2</sub> enrichment (Jiang et al. 2010) and for *T. testudinum* following longer-duration (6 months) CO<sub>2</sub> exposure (Campbell and Fourqurean 2013). Conversely, no CO<sub>2</sub> effects on leaf N content were observed in a year-long CO<sub>2</sub> enrichment for *T. testudinum* (Campbell and Fourqurean 2018), suggesting that the experimental timescale may play a crucial role in determining the long-term N responses in seagrasses.

Due to the nutrient balance of seagrass (Duarte 1990), increased biomass production anticipated in high CO<sub>2</sub> environment will require a corresponding increase in N supply to meet growth demands. An imbalance between N supply and growth demands could lead to N-limitation,

thereby influencing the internal elemental stoichiometry of the plants. While N-limitation has been suggested in a number of CO<sub>2</sub>-seagrass studies (Jiang et al. 2010; Alexandre et al. 2012; Apostolaki et al. 2014), the specific N requirements for growth has rarely been provided to support N-limitation. The potential shift in stoichiometry requires us to investigate and quantify the specific N requirements of seagrass for achieving balanced growth under future CO<sub>2</sub> enriched environments. This study intends to address this knowledge gap, contributing to a comprehensive understanding of how seagrass respond to elevated CO<sub>2</sub> in terms of their N metabolism and growth requirements.

Environmental factors, such as temperature, light availability, and nutrient concentrations may interact with CO<sub>2</sub> in antagonistic ways, influencing seagrass functions. Temperature, for example, plays a crucial role in modulating physiological functions related to photosynthesis, respiration, and N assimilation, impacting the overall C and N balance, as well as seasonal growth in seagrass (Evans et al. 1986; Marsh et al. 1986; Zimmerman et al. 1989; Moore et al. 1993; Short and Neckles 1999; Touchette 2003).

This study examined how the nitrogen composition of *Z. marina* from the coastal mid-Atlantic region responds to increasing CO<sub>2</sub> concentration under controlled experimental conditions using outdoor aquaria over 18 months. By examining the impact of CO<sub>2</sub> enrichment under natural environmental conditions, the research aims to provide insights into seasonal variations in growth demands and the underlying processes controlling nitrogen balance. Additionally, the study aims to quantify differences in the biochemical composition of leaves, rhizomes, and roots, and assess the consequent impacts on C:N elemental ratios in these tissues.

## **2.2 Materials and methods**

### **2.2.1 Experimental Design**

The experiment occurred in an outdoor CO<sub>2</sub> experimental facility at the Virginia Aquarium and Marine Science Center in Virginia Beach, VA (36.8207, -75.9841). The facility consisted of 20 open top fiberglass aquaculture aquaria (each with a volume of 3 m<sup>3</sup>), supplied with seawater from Owls Creek, a nearby tidal estuary (Zimmerman et al. 2017). Seawater was pumped into a 70 m<sup>3</sup> holding tank and gravity fed into each aquarium at a flow rate of 20 L min<sup>-1</sup>, achieving 10 complete turnovers in each aquarium per day (Fig. 1). Owls Creek, located south of the Chesapeake Bay and connected to the Atlantic Ocean via the Rudee Inlet, is a polyhaline estuary and experiences semi-diurnal tide. Its salinity typically ranges between 15 and 28 Practical Salinity Scale 1978 (PSS-78) due to mixing between seawater from the Atlantic Ocean and freshwater from non-point source terrestrial runoff. The mixture of these two water sources also controls the water quality of the creek (Sisson et al. 2010). All aquaria were shaded with a neutral density mesh screen to reduce light transmission by 40%, preventing photo-damage and better replicating the light environment from which the plants were collected (see Sec 2.2.2 below).

Compressed air, delivered through a 2 m diffuser tube running along the bottom of each aquarium, kept the water column mixed and reduced the boundary layer that impedes carbon uptake (McPherson et al. 2015). Beverage grade gaseous CO<sub>2</sub> was injected into each diffuser (except ambient treatments) through solenoid valves operated pH controllers (Eutech Alpha pH 190) and glass pH electrodes. The valves were set at five distinct pH levels (with 4 aquaria per pH treatment) ranging from ambient (pH ~7.7, no CO<sub>2</sub> addition) to 6.1 (2100 μM CO<sub>2(aq)</sub>), spaced at intervals of approximately 0.5 pH units. The 1-minute averaged pH of each tank was

recorded every 10 minutes over 18 months from June 2013 to October 2014 using a National Instruments data logger controlled by custom software written in LabView. Electrodes were cleaned and calibrated weekly with a 2-point NBS buffer calibration (4 and 7 for pH treatments < 7, 7 and 10 for pH treatments > 7). Aqueous CO<sub>2</sub> (CO<sub>2(aq)</sub>) concentrations were calculated by CO2SYS version 1.1 (van Heuven et al. 2011) using the K1 and K2 dissociation constants of Mehrbach et al. (1973) refit by Dickson and Millero (1987), from simultaneously measured values of salinity (from CTD sensor in one aquarium), temperature (recorded by the thermistors in each aquarium), pH, and alkalinity. Initial total alkalinity (TA) was determined by the Gran titration method (Gieskes and Rogers 1973), and showed a robust linear relationship with salinity ( $r^2 = 0.86$ ) (Celebi-Ergin et al. 2021). Subsequent TA was estimated using the regression model: Alkalinity ( $\mu\text{mol kg SW}^{-1}$ ) =  $49.61 \times \text{Salinity} + 694.79$ ).

While a pH of 6.1 falls considerably below the ocean pH projected by IPCC (2013) for 2100, the study's broad pH (or CO<sub>2(aq)</sub>) range is useful for elucidating the functional responses (slopes and intercepts) that facilitated my ability to make predictions concerning eelgrass performance for any future climate scenario involving CO<sub>2</sub>.

The aquaria experienced natural variations in sunlight, temperature, and salinity on a daily and seasonal cycles. Downwelling irradiance in air (measured as photosynthetically active radiation (PAR) was recorded with a factory calibrated LiCor LI190sb sensor. Temperature was measured using Omega 44005 thermistors suspended next to the pH electrode in each aquarium, calibrated to 0.1 °C precision. All thermistors were calibrated every 6 months at 6 temperatures (5 to 30 °C) using a temperature-controlled water bath (Fisher Scientific Isotemp). Salinity in each tank was measured multiple times in May and June 2013 with a hand-held refractometer (data not shown), prior to installation of the CTD. There were no differences in measured salinity among

the tanks. Consequently, salinity was monitored from June 2013 to October 2014 using a factory calibrated SeaBird SBE-37 MicroCAT CTD permanently mounted in one of the ambient (no CO<sub>2</sub> addition) aquaria (Fig. 1). As with pH, light, temperature, and salinity were continuously monitored (except during calibration) and recorded every 10 minutes using a National Instruments data acquisition and control system and custom software written in LabVIEW®. Monthly seawater chemistry measurements (NH<sub>4</sub><sup>+</sup>, NO<sub>3</sub><sup>-</sup> and PO<sub>4</sub><sup>3-</sup>) from May 2013 to October 2014 were performed by the Virginia Aquarium and Marine Science Center staff and provided by Mark Swingle.

### **2.2.2 Source population**

In May 2013, *Zostera marina* L. (eelgrass) shoots were carefully collected by SCUBA divers from a donor population near Wreck Island in South Bay, Virginia, USA (37.225° N, 75.840° W). Within 24 hours, vegetative shoots containing roots and at least 5 rhizome internodes each were transplanted into rectangular fiberglass reinforced plastic containers (0.04 m<sup>3</sup> volume, 0.075 m<sup>2</sup> surface area) with sandy sediments from the Elizabeth River (Norfolk, Virginia) to an initial density of 50 shoots per tray. The 100 containers were randomly distributed among the 20 aquaria and placed at a water depth of 0.85 m, positioning the canopy top 0.5 m below the water surface at the start of the experiment. Eelgrass remained under ambient conditions (no CO<sub>2</sub> added) for a month to allow recovery from transplantation shock and to establish a baseline performance for future CO<sub>2</sub> treatment comparisons within and among groups.

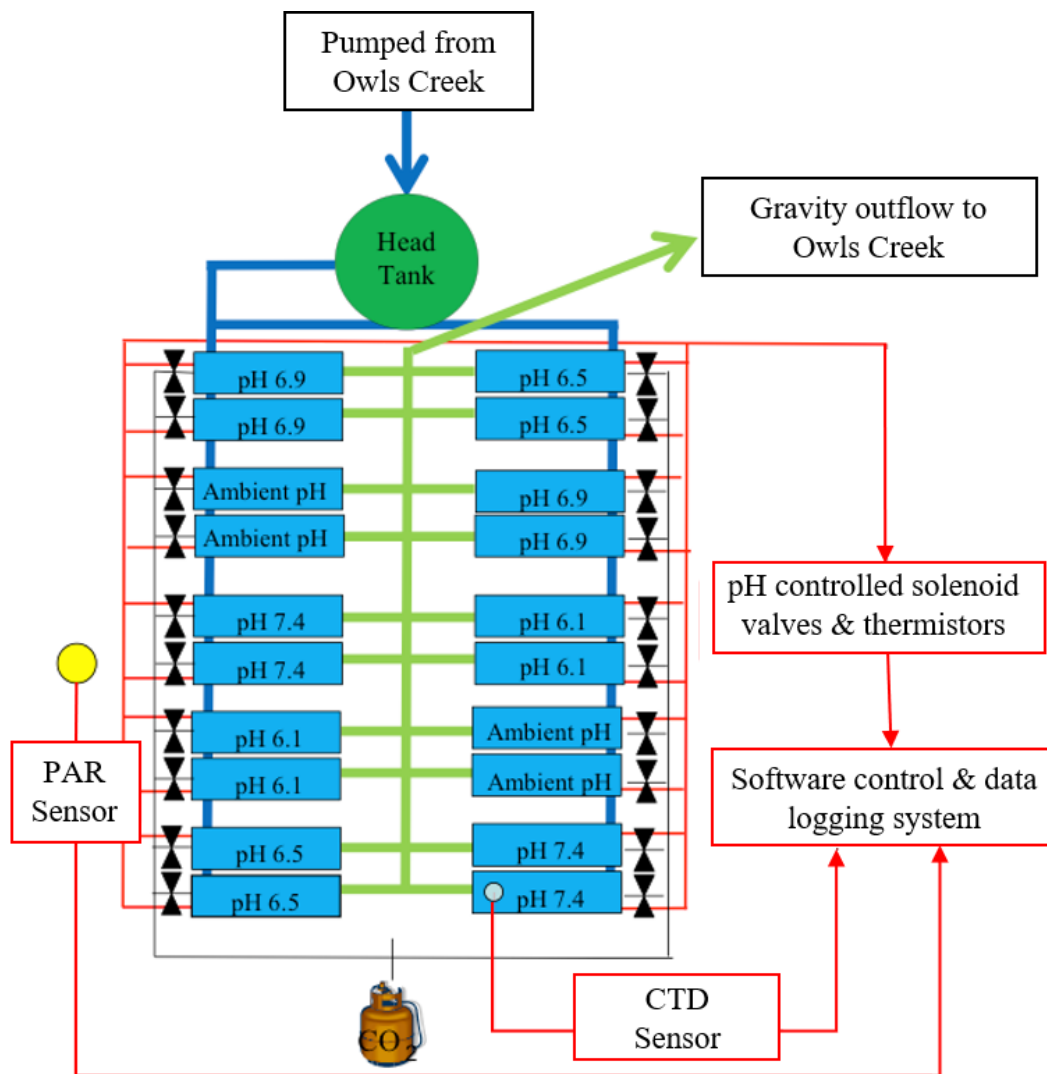


**Fig. 1.** Outdoor CO<sub>2</sub> enrichment facility located at the Virginia Aquarium for Marine Science (Virginia Beach, VA) (originally published by Zimmerman et al. (2017)). Schematic diagram illustrates experimental tanks (blue rectangles, 3 m<sup>3</sup> each), water inflow (blue lines/arrow) pumped into a 70 m<sup>3</sup> holding tank and gravity fed into each fiberglass (3 m<sup>3</sup>), water outflow (green lines/arrow), CO<sub>2</sub> supply (tank) and delivery (black lines), pH-controlled valves (black hourglass symbols), and environmental control and monitoring system (red box and lines).

### 2.2.3 Growth rates and survival

Growth rates were measured in each aquarium as shoot elongation each month using the hole-punch technique (Zieman 1974; Zimmerman et al. 1996). One randomly selected shoot from each container was designated, tagged with a colored cable tie to prevent repeated sampling in subsequent months, and marked with a 20-gauge needle. One week later, the cumulative distance (in cm) from the original puncture on sheath bundle to the scar mark on each leaf, along with the entire length of the emerging unmarked leaf was measured to the nearest mm using a flexible tape measure. Leaf width was measured to the nearest 0.1 mm using a digital caliper. Total leaf area ( $\text{cm}^2 \text{ shoot}^{-1}$ ) was calculated by summing the one-sided area (leaf length x leaf width) of all leaves on a shoot. Absolute growth rates ( $\text{cm}^2 \text{ shoot}^{-1} \text{ d}^{-1}$ ) were calculated by dividing the sum of all new leaf area by the time interval (days) between marking and measurement. Specific growth rates ( $\% \text{ d}^{-1}$ ) were calculated by normalizing absolute growth rates ( $\text{cm}^2 \text{ d}^{-1}$ ) against the total leaf area ( $\text{cm}^2$ ) and multiplying by 100. Monthly shoot counts were recorded, and survival rate ( $\% \text{ of original}$ ) was calculated by subtracting the monthly count from the initial count, then multiplying by 100.

### 2.2.4 Tissue chemistry

The second-youngest leaves (Leaf #2) were collected each month from five different plants randomly selected in each aquarium for analysis of sucrose, bulk C, N and S, free amino acids (FAA) and amino acid (AA) composition. Leaves were carefully cleaned of epiphytes, weighed, and then subjected to 48-hour oven drying at 60 °C. The dried tissues were subsequently ground into fine powder using liquid nitrogen and a mortar and pestle before being further dried at 60 °C for 24 hours. Sucrose and FAA were extracted from the dry powder (~15-20 mg dry weight for leaves and rhizomes, 30 mg dry weight for roots) through three successive extractions using hot

80% ethanol at 80 °C for 15 minutes, following the method described by Zimmerman et al. (1989). The extracts were combined, and separate portions were taken for bulk sucrose and total FAA measurements, as well as for FAA composition analysis. Each sample was evaporated to dryness overnight under a continuous stream of air. The resulting dried residue was re-dissolved in distilled water. Sucrose content was assayed using a resorcinol assay and sucrose standard (Huber and Israel 1982). Total FAA were derivatized with *o*-phthalaldehyde (OPA) reagent and 2-mercaptoethanol, and fluorescence was measured after 2 minutes with excitation and emission wavelengths of 342 and 452 nm, respectively. The total fluorescent products were standardized to glycine (Roth 1971).

Amino acid composition of samples from July and December 2013, under ambient and highest CO<sub>2(aq)</sub> (pH 6.1, 2100 μM CO<sub>2(aq)</sub>) conditions were specifically analyzed to compare summer versus winter differences in enriched and unenriched plants using by electron spray ionization liquid chromatography tandem mass spectrometry (ESI-LC-MS/MS) with ion pairing chromatography, standardized to 40 amino acids (McMahon 2018). The samples were spiked with stable isotope internal standards (DL-Cystine, DL-Lysine, L-Aspartic Acid, L-leucine, L-phenylalanine) prior to analysis.

Tissue C, N, and S content (mmol g<sup>-1</sup> DW) were determined using a combustion method (Cutter and Radford-Knoery 1991), utilizing an elemental analyzer (vario MICRO cube, Elementar). Sulfanilamide (C<sub>6</sub>H<sub>8</sub>N<sub>2</sub>O<sub>2</sub>S) was used for standardization. Approximately 3 mg of dried powder leaf samples (root, and rhizome samples were also analyzed at the final sampling time point) were placed into pre-cleaned tins that had been treated with methanol and dichloromethane. These samples were then combusted at high temperature (1150 °C), with Copper (II) Oxide serving as the oxidizing agent. The C:N:S elemental ratio was calculated based on a mole-mole ratio.

Biochemical composition of rhizomes and roots were expressed only as weight specific values (mole content per gram dry weight), whereas leaf tissues were characterized as both weight-specific and area-specific terms (mole content per  $\text{cm}^{-2}$ ). Specific leaf area sucrose, FAA, C and N content were calculated using the leaf area to dry mass ratio as established by Celebi (2016). This enabled present study to assess the distributions of these components relative to the total biomass in response to  $\text{CO}_{2(\text{aq})}$ .

### 2.2.5 Whole shoot assessment

The long-term effects of  $\text{CO}_{2(\text{aq})}$  enrichment on the entire shoot (leaves, roots, and rhizome) were assessed only at the end of the experiment October 2014 because it necessitated destructive sampling of entire plants. From each aquarium, three shoots were carefully harvested to avoid breaking roots and/or rhizomes, cleaned of epiphytes and sediment debris using filtered seawater, and photographed to document differences in shoot size along the  $\text{CO}_{2(\text{aq})}$  gradient. The eelgrass shoot was then divided into three segments: leaves (from tip of the leaf blades to the sheath bundle, rhizome (the first 3 internodes), and roots (roots of the first 5 internodes). After cleaning, samples were patted dry, weighed (gram fresh weight), then oven-dried at  $60\text{ }^{\circ}\text{C}$  and weighed again (gram dry weight). The dried samples were subsequently ground to a fine powder in liquid nitrogen using a mortar and pestle and analyzed for sucrose, FAA, and CN contents as described above.

### 2.2.6 Determining seasonal growth demands

The growth demand of eelgrass for C and N under varying  $\text{CO}_{2(\text{aq})}$  levels was calculated based on measurements collected from May 2013 to October 2014 as follows:

$$\mu_{dC_m} = (C_{(\text{CO}_{2(\text{aq})})} \times \mu_{\text{SGR}})_m \quad (1)$$

$$\mu_{dN_m} = (N_{(CO_2(aq))} \times \mu_{SGR})_m \quad (2)$$

where  $C_{(CO_2(aq))}$  and  $N_{(CO_2(aq))}$  are the observed monthly ( $m$ ) measured aqueous  $CO_2$ -driven C and N content per shoot, and  $\mu_{SGR(m)}$  represents the specific growth rates for month  $m$ . These specific growth rates varied seasonally and typically fell within the range of 1% and 3% per day, regardless of the  $CO_2(aq)$  treatments. The demands exhibited a sinusoidal pattern, therefore, the predicted seasonal C and N demand ( $\mu_{d_i}$ ) was fitted using a non-linear equation in MATLAB R2022a. The equation is as follows:

$$\mu_{d_i} = C + A \sin \left[ \left( \frac{m - b}{12} \right) \times 2\pi \right] \quad (3)$$

where  $A$ ,  $b$ , and  $C$  are the coefficients corresponding to amplitude, monthly phase shift, and vertical growth demand offset, respectively. To enhance the robustness of the model and minimize the influence of potential outliers, a bi-square weighting method (Dumouchel and O'brien 1989) was applied.

The functional relationship between growth demand and  $CO_2(aq)$  concentrations was further evaluated by plotting the maximum  $\mu_{d_i}$  values (i.e. amplitude) determined from Eq. (3) against aqueous  $CO_2$  concentrations. The non-linear relationship was assumed to follow the Michaelis-Menton function:

$$\mu_{d_i(CO_2(aq))} = V_{\max} \frac{[S]}{K_S + [S]} \quad (4)$$

where  $[S]$  is the  $CO_2(aq)$  substrate concentration,  $V_{\max}$  represents the estimated  $CO_2(aq)$  saturated growth demand for C and N, and  $K_S$  represents the estimated half saturation concentration of  $CO_2(aq)$  where  $V_{\max}$  is halved. The minimum demand, which occurred in winter, did not demonstrate significant  $CO_2(aq)$  treatment effects within the 95% error bound, and therefore were not fitted to the above equation.

### 2.2.7 Determining sucrose availability for growth

The amount of non-structural carbon (in the forms of sucrose) available for growth each month is related to canopy productivity and growth demand, both of which are influenced by  $\text{CO}_{2(\text{aq})}$  concentrations. Beginning in May 2013 and ending in October 2014, the canopy productivity (expressed as  $\text{mmol C shoot}^{-1} \text{ d}^{-1}$ ) for the five  $\text{CO}_{2(\text{aq})}$  (or pH) treatments was calculated using the equation:

$$P_{\text{net}} = (P_{\text{m}} \times H_{\text{sat}}) - R \quad (5)$$

where  $P_{\text{m}}$  is the  $\text{CO}_{2(\text{aq})}$  (or pH) driven light saturated rate of photosynthesis (in relative units),  $H_{\text{sat}}$  (daily period (hour) of light saturated photosynthesis) is the median  $H_{\text{sat}}$  value based on  $E_{\text{k}}$  of  $300 \mu\text{mol quanta m}^{-2} \text{ s}^{-1}$  (refer to Fig. 1A), and  $R$  is the respiration rate. The terms  $P_{\text{m}}$  and  $R$  were estimated using the bio-optical model *GrassLight* (Ver. 2.14, Zimmerman et al. (2015)), based on parameters presented in Table 1. This model simulates the vertical propagation of spectral irradiance through a submerged canopy within an optically homogenous water column. It calculates the canopy photosynthetic and respiration rates based on the in-canopy light environment, considering factors like water quality factors (e.g. CDOM, total suspended particles, Chl *a*) and canopy architecture (e.g. shoot density, leaf area index, leaf orientation, leaf morphology) (Zimmerman 2003; Zimmerman 2006). To convert  $P_{\text{m}}$  from relative units to  $\text{mmol C shoot}^{-1} \text{ d}^{-1}$ , data from the net oxygen release rate at pH 8.0 for *Z. marina* (Invers et al. 2001), a photosynthetic quotient of 1.2 ( $\text{O}_2:\text{C}$ ), and the mean shoot mass ( $\text{g DW shoot}^{-1}$ ) were used. Mean shoot mass values were calculated from shoot size ( $\text{cm}^2 \text{ shoot}^{-1}$ ) and leaf density  $\text{g DW cm}^{-2}$  data presented in Fig. 5.

The monthly calculation  $S_{\text{new},m}$  of carbon available as sucrose for new growth, is determined by the formula:

$$S_{\text{new},m} = \int_{m-1}^m P_{\text{net}} dt - \int_{m-1}^m \mu_{\text{dC}_m} dt + S_{m-1} \quad (6)$$

where  $S_{\text{new},m}$  was expressed as mmol C (as sucrose) shoot<sup>-1</sup>. This formula combines net photosynthesis, growth-related parameters, and sucrose content ( $S_{m-1}$ ) from the previous month ( $m-1$ ). The terms  $\int_{m-1}^m P_{\text{net}} dt$  and  $\int_{m-1}^m \mu_{\text{dC}_m} dt$  represent the integrals of shoot-specific net photosynthesis and growth demand, respectively, over the time interval between months  $m-1$  and  $m$ .

Subsequently, the amount of carbon as sucrose set aside for potential future growth each month, considering the demand for carbon during growth, as indicated by  $\mu_{\text{dC}_m}$  is determined by the formula:

$$S_{\text{reserves},m} = \frac{S_{\text{new},m}}{\mu_{\text{dC}_m}} \quad (7)$$

If  $S_{\text{reserves},m}$  is positive, it suggests a surplus of sucrose available for future growth, whereas a low or even a negative value may indicate an immediate utilization of sucrose for ongoing growth demands.

### 2.2.8 Data analyses

Within-aquarium replicates for each measured response were combined each month to produce a mean value for each aquarium, resulting in four independent replicates for each pH (or CO<sub>2(aq)</sub>) treatment. Monthly measurements for various physiological and morphological attributes were repeatedly made from the same twenty aquaria, therefore the impact of long-term effects of CO<sub>2(aq)</sub> enrichment over time was tested using the repeated measure Analysis of Covariance (ANCOVA) approach, implemented within the linear mixed-effect model (LMM) in IBM SPSS

Statistics 26. In this analysis, the aquaria were treated as the repeated subject, time was considered as a fixed effect, and  $\log \text{CO}_{2(\text{aq})}$  were assigned as covariates. Data lacking statistical differences among  $\text{CO}_{2(\text{aq})}$  treatments were combined to increase the degrees of freedom.

A monthly linear regression analysis was executed in IBM SPSS Statistics 26 to determine the impact of  $\text{CO}_{2(\text{aq})}$  on measured responses. Statistical significance of  $\text{CO}_{2(\text{aq})}$  effects on measured responses, as indicated by the slope, was established when  $p$ -value was less than 0.05. Given the non-linear nature of the measured responses to  $\text{CO}_{2(\text{aq})}$ , log transformation was applied to  $\text{CO}_{2(\text{aq})}$  concentrations to facilitate linear regression analysis. Variations in the slope from month-to-month were assessed through multiple comparison analysis.

**Table 1.** Fixed parameter values assigned to *GrassLight* runs from May 2013 to October 2014. Monthly photosynthesis:respiration ratios ( $P:R$ ) were estimated at pH (or  $\text{CO}_{2(\text{aq})}$ ) 6.1, 6.5, 6.9, 7.4, and 7.7. Parameters not listed below have their default values commanded in *GrassLight*. See *GrassLight* model and Zimmerman references for details. Mean shoot density ( $\text{shoot m}^{-2}$ ) = Mean shoot number/Area of plant container (m). Mean shoot mass ( $\text{g DW shoot}^{-1}$ ) = Mean shoot size ( $\text{cm}^2 \text{shoot}^{-1}$ )  $\times$  leaf density ( $\text{g DW cm}^{-2}$ ) (computed based on data provided in Fig. 5A and 5B). These calculations were performed monthly from May 2013 to October 2014.

| Parameter                    | Values                  | Units                    |
|------------------------------|-------------------------|--------------------------|
| Latitude                     | 36.8207                 | degree                   |
| Longitude                    | -75.9841                | degree                   |
| Daily mean water temperature | Fig. 2B                 | $^{\circ}\text{C}$       |
| Seawater pH                  | 6.1-7.7                 |                          |
| Median $H_{\text{sat}}$      | Fig. 2A                 | $\text{h d}^{-1}$        |
| Water depth                  | 0.5                     | m                        |
| Canopy height                | 0.1                     | m                        |
| Mean shoot density           | calculated              | $\text{shoot m}^{-2}$    |
| Mean shoot mass              | calculated              | $\text{g DW shoot}^{-1}$ |
| Mean shoot number            | Zimmerman et al. (2017) |                          |
| Area of plant container      | 0.098                   | $\text{m}^2$             |

## 2.3 Results

### 2.3.1 Experimental conditions

Downwelling surface irradiance (PAR) followed a sinusoidal pattern due to astronomic changes in local zenith angle and exhibited significant daily fluctuations in light intensity depending on cloud cover. From May 2013 to October 2014, the mean annual variation in natural irradiance was about 4-fold, with larger amplitude in daily irradiance in summer than in winter (Fig. 2A). The  $H_{\text{sat}}$  ( $\text{h d}^{-1}$ ) (daily periods when photosynthesis is light saturated) calculated based on  $E_k$  of  $300 \mu\text{mol quanta m}^{-2} \text{s}^{-1}$  (Zimmerman et al. 1994) varied seasonally, ranging from approximately  $4 \text{ h d}^{-1}$  in winter to  $9 \text{ h d}^{-1}$  in summer. The water temperature followed a seasonal cycle, lagging surface irradiance by 6 to 8 weeks (Fig. 2B). Summers saw water temperature reaching  $30 \text{ }^\circ\text{C}$ , surpassing the  $25 \text{ }^\circ\text{C}$  threshold for eelgrass stress (Evans et al. 1986; Zimmerman et al. 1989; Moore and Jarvis 2008; Moore et al. 2012). In contrast, winter daily temperature averaged around  $5 \text{ }^\circ\text{C}$ , occasionally dropping to  $0 \text{ }^\circ\text{C}$  in February 2014. The daily temperature range was  $\leq 5 \text{ }^\circ\text{C}$ . Salinity showed no seasonal trend and averaged  $24 \pm 3$  (PSS) during the experiment with a recorded minimum and maximum of 8 and 28 depending on the amount of rainfall and freshwater runoff (Fig. 2C).

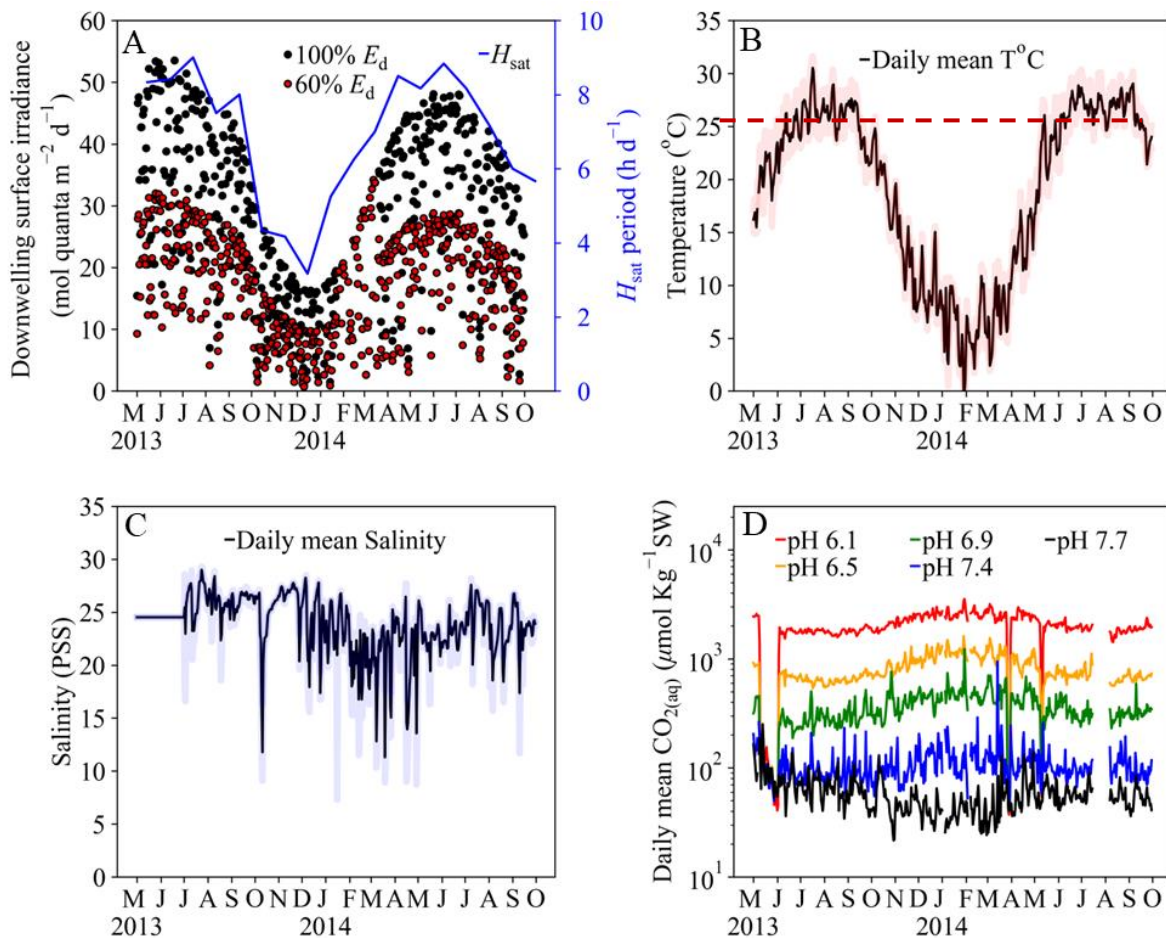


**Fig. 2.** Environmental conditions during the experiment from May, 2013 to October, 2014 for (A) above water natural down-welling irradiance ( $E_d$ ) at 100% (full sun) and 60% (40% shading) light levels, (B) daily mean salinity (PSS), (C) daily mean water temperature ( $^{\circ}\text{C}$ ), and (D) daily mean aqueous  $\text{CO}_2$  concentrations. The blue line in panel (A) represents the median  $H_{\text{sat}}$  value (daily period (hour) of light saturated photosynthesis) calculated based on  $E_k$  of  $300 \mu\text{mol quanta m}^{-2} \text{s}^{-1}$  (Zimmerman et al. 1994). The shading in panels (B) and (C) represents the maximum and minimum values. The red dash line in panel (B) is the temperature threshold for stress in eelgrass (Evans et al. 1986). In panel (D), the colors correspond to  $\text{CO}_{2(\text{aq})}$  concentration gradient ranging from ambient (black line, pH 7.7) to high  $\text{CO}_{2(\text{aq})}$  (red line, pH 6.1). Data were redrawn from values previously published in Zimmerman et al. (2017).

Gaseous CO<sub>2</sub> delivered through the diffuser tubes at the bottom of each aquarium maintained five distinct pH treatments throughout the experiment, except for pH 7.4, which occasionally overlapped with the lower values measured in the ambient treatment (Fig. 2D). In Owls Creek, the pH fluctuated due to the cycle of biological activities (photosynthesis and respiration), with daytime pH exceeding 8.0 and nighttime pH dropping as low as 7.0. Within the CO<sub>2</sub>-enriched tanks, the mean pH (mean ± SE) of each treatment was 6.06 ± 0.02, 6.49 ± 0.01, 6.91 ± 0.01 and 7.42 ± 0.01 and 7.66 ± 0.01, which corresponds to CO<sub>2(aq)</sub> concentrations of 2121 (pH 6.06), 823, 371, 107, and 55 μM Kg<sup>-1</sup> SW (ambient) respectively. Aqueous CO<sub>2</sub> (CO<sub>2(aq)</sub>) concentrations of the enriched tanks were slightly higher in winter than summer due to increased solubility of the gas at low temperature.

Data obtained from the Virginia Beach Aquarium highlighted a significant presence of macronutrients (NH<sub>4</sub><sup>+</sup>, NO<sub>2</sub><sup>-</sup>+NO<sub>3</sub><sup>-</sup>, and PO<sub>4</sub><sup>-</sup>) in the surface water of Owls Creek (Fig. 3A-C). The 18-year dataset displayed a notable variability. There were a few occasional spikes, particularly for NO<sub>2</sub><sup>-</sup>+NO<sub>3</sub><sup>-</sup> and PO<sub>4</sub><sup>3-</sup> likely related to rainfall/runoff events. The highest recorded concentrations were 26 μM for NH<sub>4</sub><sup>+</sup>, 125 μM for NO<sub>2</sub><sup>-</sup>+NO<sub>3</sub><sup>-</sup>, and 31 μM for PO<sub>4</sub><sup>3-</sup>. Nutrient concentrations (NH<sub>4</sub><sup>+</sup>, NO<sub>3</sub><sup>-</sup>, and PO<sub>4</sub><sup>3-</sup>) tended to be higher in the winter compared to summer and spring, primarily because lower temperature and reduced light levels likely led to reduced biological activities. Nutrient concentrations observed between 2013 and 2014 during the experiment were low, with distribution that deviated from normality, as evident from the boxplot in Fig. 3D. Median values were reported at 0.5 μM for PO<sub>4</sub><sup>3-</sup>, 0.8 μM of NO<sub>2</sub><sup>-</sup>+NO<sub>3</sub><sup>-</sup>, and 0.8 μM of NH<sub>4</sub><sup>+</sup>. Interquartile intervals (IQR = 50% of data points located) range from ~1 and 1.7 μM, with the broadest range in NH<sub>4</sub><sup>+</sup> and the narrowest in NO<sub>2</sub><sup>-</sup>+NO<sub>3</sub><sup>-</sup>.

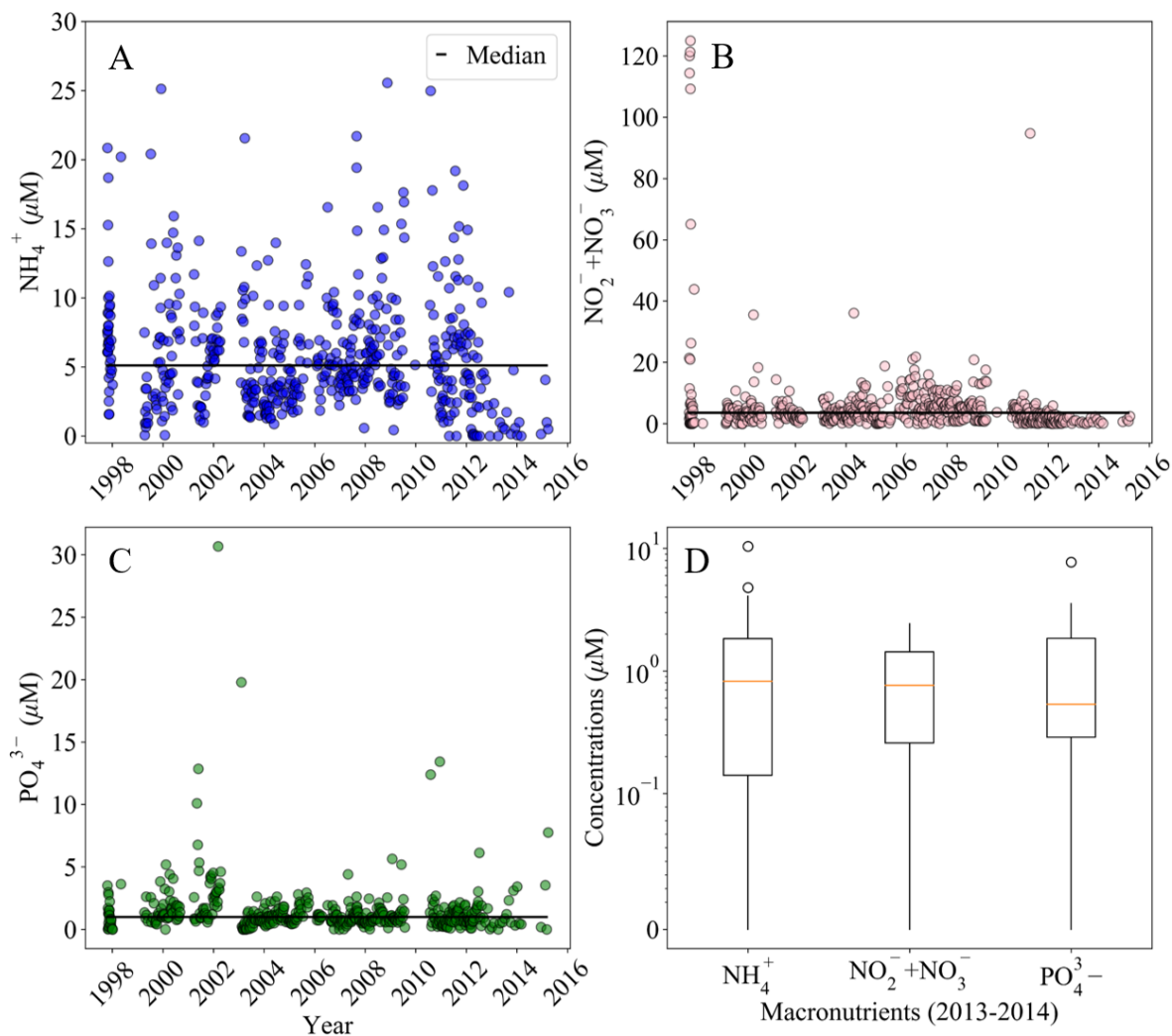


**Fig. 3.** Concentrations of macronutrients ( $\text{NH}_4^+$ ,  $\text{NO}_2^- + \text{NO}_3^-$ , and  $\text{PO}_4^{3-}$ ) in Owls Creek surface water from 1998 to 2016 are presented in panels A, B, and C. Panel D features a box and whisker plot, showing data from 2013-2014 during the experimental period. The box's lower and upper edges represent the 25<sup>th</sup> ( $Q_1$ ) and 75<sup>th</sup> ( $Q_3$ ) percentiles, with medians indicated by the horizontal orange lines. The interquartile intervals (IQR), containing 50% of data, were 1.2, 1.6, and 1.7  $\mu\text{M}$  for  $\text{NO}_2^- + \text{NO}_3^-$ ,  $\text{PO}_4^{3-}$ ,  $\text{NH}_4^+$ , respectively. Vertical whiskers (black lines extending from the box) indicate the data range, not exceeding  $Q_3 + (1.5 \times \text{IQR})$ , with outliers marked as open circles.  $Q_3$  corresponds to the value below which 75% of the data points are located below this upper quartile (additional boxplot statistics are available in the Table 2). Data were provided by the Virginia Aquarium and Marine Science Center (M. Swingle, unpublished).

**Table 2.** Summary statistics for boxplot shown in Fig. 3D.

| Variables                               | NH <sub>4</sub> <sup>+</sup><br>( $\mu$ M) | NO <sub>2</sub> <sup>-</sup> +NO <sub>3</sub> <sup>-</sup><br>( $\mu$ M) | PO <sub>4</sub> <sup>3-</sup><br>( $\mu$ M) |
|---|--|--|---|
| Minimum                                 | 0  | 0  | 0   |
| Maximum                                 | 10.4                                       | 2.4  | 7.8   |
| Mean                                    | 1.6  | 0.9  | 1.4   |
| Median                                  | 0.8  | 0.8  | 0.5   |
| Standard deviation                      | 2.5  | 0.8  | 1.9   |
| 25th lower percentile (Q <sub>1</sub> ) | 0.1  | 0.3  | 0.3   |
| 75th upper percentile (Q <sub>3</sub> ) | 1.8  | 1.4  | 1.8   |
| Interquartile range (IQR)               | 1.7  | 1.2  | 1.6   |

### 2.3.2 Growth rates, shoot size, and total biomass response to CO<sub>2(aq)</sub> enrichment

Within 6 weeks of initiating CO<sub>2(aq)</sub> enrichment, absolute growth rates (AGR) exhibited a positive, logarithmic response to CO<sub>2(aq)</sub> concentrations. The strongest CO<sub>2(aq)</sub> effects were observed during the warm summer months of both 2013 and 2014 (Fig. 4A), where plants grown under elevated CO<sub>2(aq)</sub> (2121  $\mu$ M, pH 6.1) grew 2-3 times faster than plants grown under ambient (55  $\mu$ M CO<sub>2(aq)</sub>, pH 7.7) CO<sub>2(aq)</sub> conditions. In contrast, during winter, the impact of CO<sub>2(aq)</sub> was minimal, resulting in nearly zero slopes, and growth rates remained consistently below 1 cm<sup>2</sup> d<sup>-1</sup> across all CO<sub>2(aq)</sub> treatments due to lower temperature and reduced light levels. When normalized to shoot size, the effects of CO<sub>2(aq)</sub> on specific growth rates (SGR) became non-significant (Table 3). However, it is worth noting that SGR exhibited distinct seasonal patterns, with higher values in the summer and lower values in the winter (Fig. 4B, Table 3). The average specific growth rates ranged from 3% d<sup>-1</sup> ( $\pm$  0.04 SE) in summer, fall, and spring to about 1% d<sup>-1</sup> ( $\pm$  0.05 SE) during the winter (from December 2013 through February 2014).

**Table 3.** Summary ANCOVA tables for the Type III tests of fixed effects using a 1-factor (Month) Linear Mixed-Effects Model in SPSS with  $\log \text{CO}_{2(\text{aq})}$  (pH levels = 6.1, 6.4, 6.9, 7.4, 7.7) as a covariate; DW: dry weight.  $\alpha = 0.05$ .

| Dependent variable                                      | Source   | Effects df | Error df | <i>F</i> | <i>p</i>         |
|---|--|------------|----------|----------|------------------|
| Shoot Size<br>( $\text{cm}^2$ )                         | Month  | 18         | 312.58   | 2.56     | <b>0.001</b>     |
|   | $\log \text{CO}_{2(\text{aq})}$                | 1          | 19.70    | 81.26    | <b>&lt;0.001</b> |
|   | Month $\times$ $\log \text{CO}_{2(\text{aq})}$ | 18         | 312.76   | 3.34     | <b>&lt;0.001</b> |
| Absolute growth rate<br>( $\text{cm}^2 \text{d}^{-1}$ ) | Month  | 18         | 312.33   | 3.21     | <b>&lt;0.001</b> |
|   | $\log \text{CO}_{2(\text{aq})}$                | 1          | 19.49    | 80.35    | <b>&lt;0.001</b> |
|   | Month $\times$ $\log \text{CO}_{2(\text{aq})}$ | 18         | 312.53   | 5.66     | <b>&lt;0.001</b> |
| Specific growth rate<br>( $\text{cm}^2 \text{d}^{-1}$ ) | Month  | 18         | 313.46   | 2.58     | <b>&lt;0.001</b> |
|   | $\log \text{CO}_{2(\text{aq})}$                | 1          | 20.66    | 0.05     | 0.82             |
|   | Month $\times$ $\log \text{CO}_{2(\text{aq})}$ | 18         | 313.63   | 1.29     | 0.19             |
| Sucrose<br>( $\mu\text{mol g}^{-1} \text{DW}$ )         | Month  | 17         | 291.43   | 3.97     | <b>&lt;0.001</b> |
|   | $\log \text{CO}_{2(\text{aq})}$                | 1          | 18.99    | 223.02   | <b>&lt;0.001</b> |
|   | Month $\times$ $\log \text{CO}_{2(\text{aq})}$ | 17         | 291.46   | 3.64     | <b>&lt;0.001</b> |
| Sucrose<br>( $\mu\text{mol cm}^{-2}$ )                  | Month  | 17         | 291.84   | 4.40     | <b>&lt;0.001</b> |
|   | $\log \text{CO}_{2(\text{aq})}$                | 1          | 19.04    | 213.72   | <b>&lt;0.001</b> |
|   | Month $\times$ $\log \text{CO}_{2(\text{aq})}$ | 17         | 291.98   | 6.90     | <b>&lt;0.001</b> |
| FAA<br>( $\mu\text{mol g}^{-1} \text{DW}$ )             | Month  | 17         | 267.06   | 3.56     | <b>&lt;0.001</b> |
|   | $\log \text{CO}_{2(\text{aq})}$                | 1          | 20.52    | 5.99     | <b>0.02</b>      |
|   | Month $\times$ $\log \text{CO}_{2(\text{aq})}$ | 17         | 267.28   | 5.63     | <b>&lt;0.001</b> |
| FAA<br>( $\mu\text{mol cm}^{-2}$ )                      | Month  | 17         | 266.66   | 2.97     | <b>&lt;0.001</b> |
|   | $\log \text{CO}_{2(\text{aq})}$                | 1          | 19.97    | 38.72    | <b>&lt;0.001</b> |
|   | Month $\times$ $\log \text{CO}_{2(\text{aq})}$ | 17         | 266.89   | 5.53     | <b>&lt;0.001</b> |
| Total C<br>( $\text{mmol g}^{-1} \text{DW}$ )           | Month  | 17         | 294.64   | 3.23     | <b>&lt;0.001</b> |
|   | $\log \text{CO}_{2(\text{aq})}$                | 1          | 21.29    | 20.94    | <b>&lt;0.001</b> |
|   | Month $\times$ $\log \text{CO}_{2(\text{aq})}$ | 17         | 294.83   | 2.14     | <b>0.01</b>      |
| Total C<br>( $\mu\text{mol cm}^{-2}$ )                  | Month  | 17         | 295.25   | 1.45     | 0.11             |
|   | $\log \text{CO}_{2(\text{aq})}$                | 1          | 22.38    | 233.26   | <b>&lt;0.001</b> |
|   | Month $\times$ $\log \text{CO}_{2(\text{aq})}$ | 17         | 295.38   | 3.89     | <b>&lt;0.001</b> |
| Total N<br>( $\text{mmol g}^{-1} \text{DW}$ )           | Month  | 17         | 293.37   | 5.15     | <b>&lt;0.001</b> |
|   | $\log \text{CO}_{2(\text{aq})}$                | 1          | 18.95    | 43.17    | <b>&lt;0.001</b> |
|   | Month $\times$ $\log \text{CO}_{2(\text{aq})}$ | 17         | 293.50   | 3.89     | <b>&lt;0.001</b> |

**Table 3.** Summary ANCOVA tables continued.

| Dependent variable                      | Source                                 | Effects df | Error df | <i>F</i> | <i>p</i>         |
|---|--|------------|----------|----------|------------------|
| Total N<br>( $\mu\text{mol cm}^{-2}$ )  | Month                                  | 17         | 293.51   | 1.25     | 0.228            |
|   | log CO <sub>2(aq)</sub>                | 1          | 19.65    | 18.72    | <b>&lt;0.001</b> |
|   | Month $\times$ log CO <sub>2(aq)</sub> | 17         | 293.71   | 2.59     | <b>0.001</b>     |
| Total S<br>( $\mu\text{mol g}^{-1}$ DW) | Month                                  | 17         | 293.98   | 2.66     | <b>&lt;0.001</b> |
|   | log CO <sub>2(aq)</sub>                | 1          | 20.21    | 20.92    | <b>&lt;0.001</b> |
|   | Month $\times$ log CO <sub>2(aq)</sub> | 17         | 294.18   | 1.84     | <b>0.02</b>      |
| Total S<br>( $\mu\text{mol cm}^{-2}$ )  | Month                                  | 17         | 294.08   | 1.23     | 0.24             |
|   | log CO <sub>2(aq)</sub>                | 1          | 20.43    | 40.54    | <b>&lt;0.001</b> |
|   | Month $\times$ log CO <sub>2(aq)</sub> | 17         | 294.28   | 1.90     | <b>0.02</b>      |
| C:N<br>(mole:mole)                      | Month                                  | 17         | 292.79   | 2.88     | <b>&lt;0.001</b> |
|   | log CO <sub>2(aq)</sub>                | 1          | 18.20    | 52.46    | <b>&lt;0.001</b> |
|   | Month $\times$ log CO <sub>2(aq)</sub> | 17         | 292.89   | 5.98     | <b>&lt;0.001</b> |
| N:S<br>(mole:mole)                      | Month                                  | 17         | 293.59   | 3.43     | <b>&lt;0.001</b> |
|   | log CO <sub>2(aq)</sub>                | 1          | 20.04    | 8.78     | <b>0.01</b>      |
|   | Month $\times$ log CO <sub>2(aq)</sub> | 17         | 293.79   | 2.26     | <b>0.003</b>     |

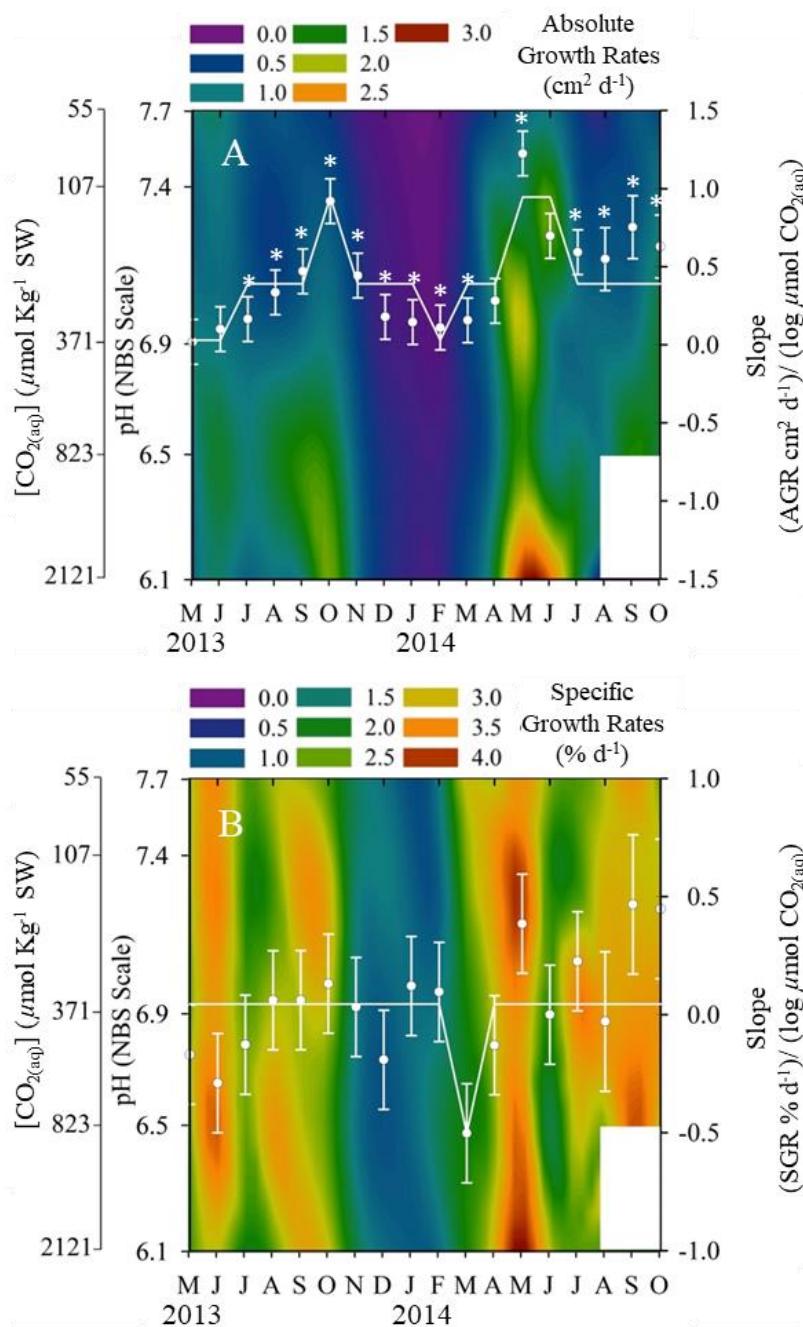


**Fig. 4.** Heat maps of (A) absolute growth rates, and (B) specific growth rates of *Zostera marina* L. contoured as a function of pH or CO<sub>2(aq)</sub> treatments (vertical left axis) and months (horizontal axis) from May 2013 until October 2014. White symbols on each plot represent the slope of the response variable vs. log CO<sub>2(aq)</sub> concentrations (vertical right axis) estimated from linear regression analysis as described in section 2.2.2, with statistically significant slope annotated with asterisk symbols. Error bars represent  $\pm 1$  SE of the regression slope. The white horizontal line connects the slopes that are not statistically different based on multiple comparison analysis. Plants from pH 6.1 treatment were harvested in August 2014; therefore, no data was present from this period onward. Data were previously published in Zimmerman et al. (2017).

In response to  $\text{CO}_{2(\text{aq})}$  enrichment, mean shoot size ( $\text{cm}^2$  leaf per shoot) exhibited a logarithmic increase after 8 weeks, with consistently positive slopes (mean shoot size vs  $\log \text{CO}_{2(\text{aq})}$ ) throughout the experiment (Fig. 5A). The greatest  $\text{CO}_{2(\text{aq})}$  effects were observed during the summers of 2013 and 2014, while winter showed weakened  $\text{CO}_2$  effects, indicated by shallower slopes, which coincided with lower temperature and reduced light levels. By the end of the experiment, shoot size in high  $\text{CO}_{2(\text{aq})}$  treatment had doubled in comparison to eelgrass grown under ambient  $\text{CO}_{2(\text{aq})}$  conditions.

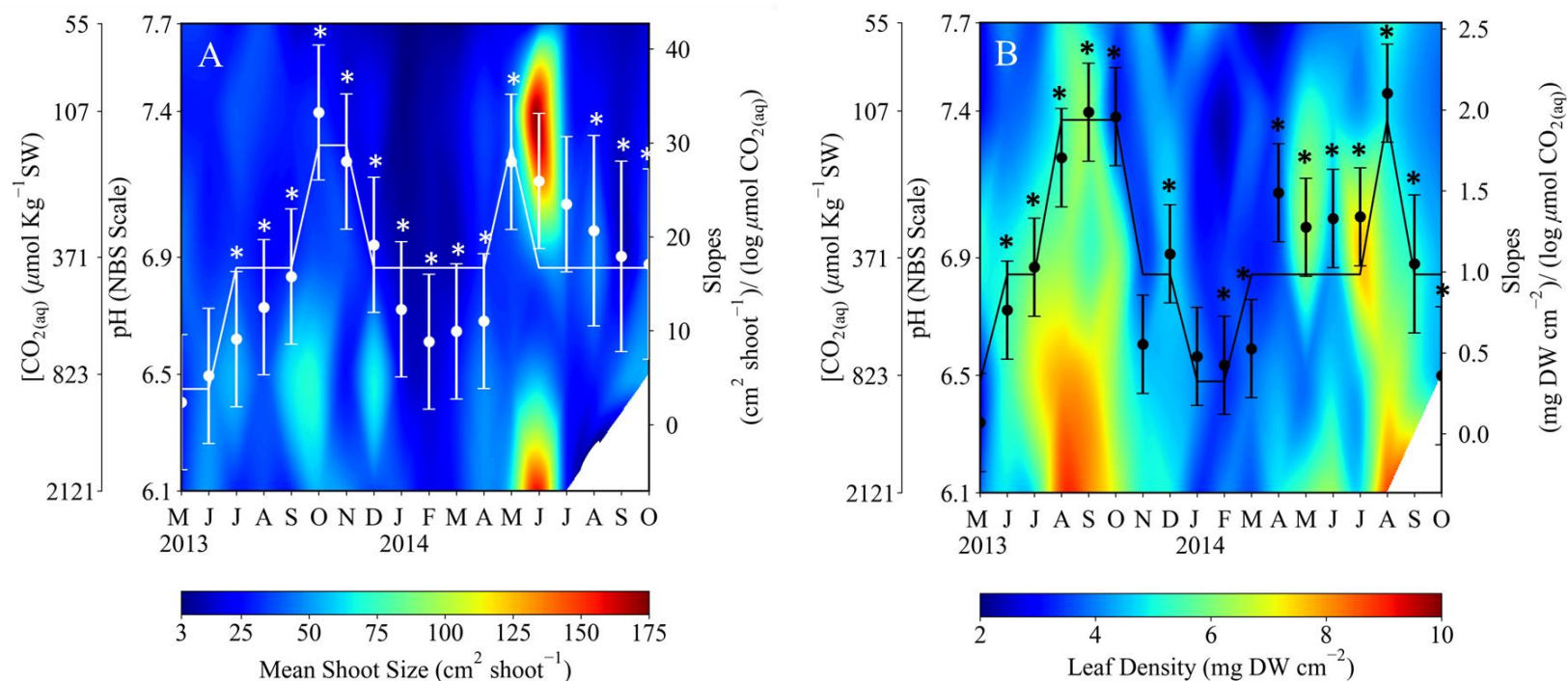


**Fig. 5.** Heat maps of (A) mean shoot size, and (B) leaf density contoured as a function of pH or  $\text{CO}_{2(\text{aq})}$  treatments (vertical left axis) and months (horizontal axis) from May 2013 to October 2014. Black and white symbols on each plot represent the slope of the measured response variable vs.  $\log \text{CO}_{2(\text{aq})}$  concentrations (vertical right axis) estimated from linear regression analysis as described in section 2.2.2, with statistically significant slope annotated with asterisk symbols. Error bars represent  $\pm 1\text{SE}$  of the regression slope. The black and white horizontal lines connect the slopes that are not statistically different based on multiple comparison analysis. Plants from pH 6.1 treatment were harvested in August 2014; therefore, no data was present from this period onward. (A) was redrawn from data previously published in (Zimmerman et al. 2017).

### 2.3.3 Leaf sucrose and leaf free amino acids in response to CO<sub>2(aq)</sub> enrichment

In May 2013, prior to the start of CO<sub>2(aq)</sub> enrichment, leaf sugar (as sucrose) and free amino acids (FAA) contents exhibited no significant differences among the CO<sub>2(aq)</sub> treatment aquaria (Fig. 6 and 7). The mean sucrose and FAA concentrations were  $106.23 \pm 3.70 \mu\text{mol g}^{-1} \text{DW}$  and  $0.18 \pm 0.06 \mu\text{mol g}^{-1} \text{DW}$ .

After 4 weeks of continuous CO<sub>2(aq)</sub> enrichment, both biomass-specific ( $\text{g}^{-1} \text{DW}$ ) and area specific ( $\text{cm}^{-2}$ ) leaf sucrose content increased logarithmically with [CO<sub>2(aq)</sub>], as indicated by consistently positive slope values (repeated measure ANCOVA,  $p < 0.001$ , Table 3) throughout the experiment (Fig. 6A and 6B ). The most pronounced response to CO<sub>2(aq)</sub> concentrations was initially observed during the summer and fall of 2013, with slopes nearly doubling those seen during the same period in 2014, particularly for biomass-specific sucrose content. Seasonal effects were also statistically significant (repeated measure ANCOVA,  $p < 0.001$ , Table 3), with slight differences in the trends between biomass-specific and area-specific sucrose concentration, particularly noticeable during the winter months. Biomass-specific sucrose concentrations were highest across all CO<sub>2(aq)</sub> treatments in January and February 2014, coinciding with the slowest growth rates ( $1\% \text{d}^{-1}$ ). This slower growth allowed sucrose concentrations to accumulate in leaves, reaching nearly  $700 \mu\text{mol g}^{-1} \text{DW}$  during this period, representing approximately 28% of the total carbon in leaf tissues. These substantial soluble carbon reserves are poised for utilization as growth rates increase during spring and summer. In contrast, higher area-specific sucrose contents were evident during spring and summer, rather than in the winter, and coincided with the concurrent increase in mean shoot size due to CO<sub>2(aq)</sub> enrichment (ref. Fig. 5A).

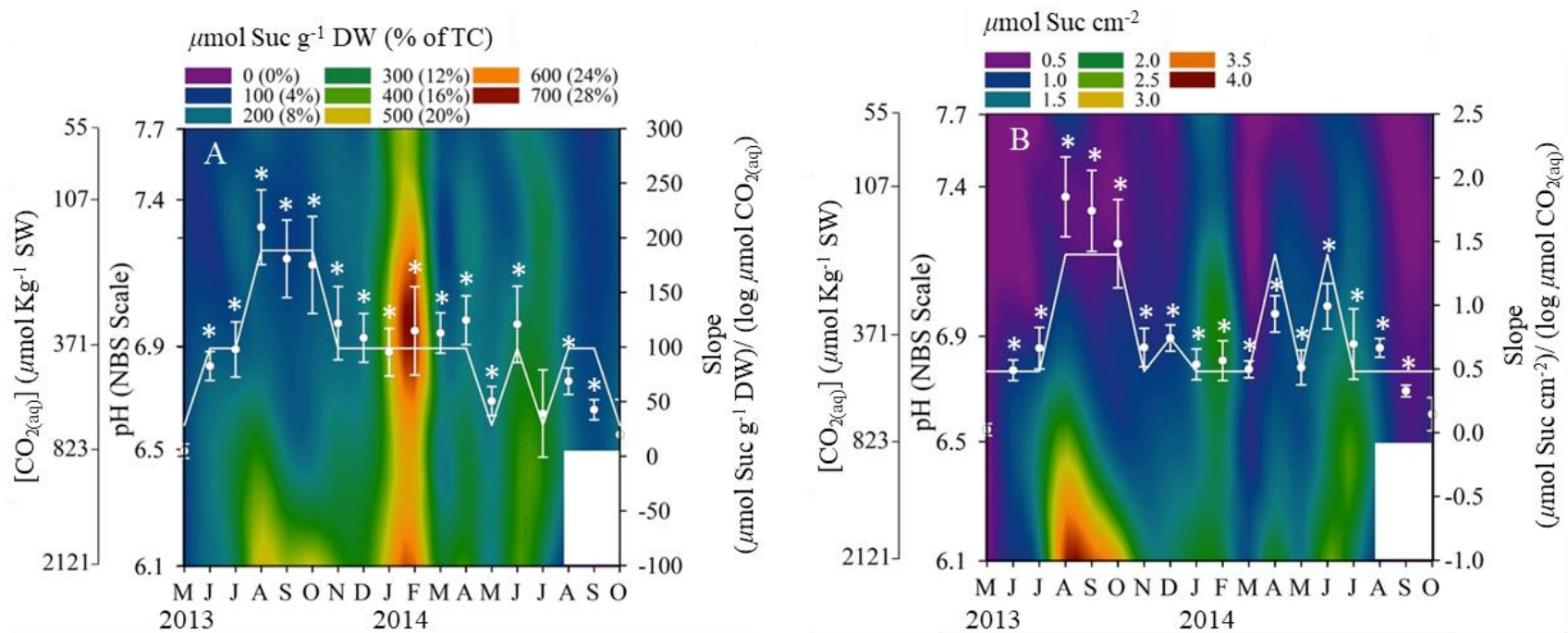


**Fig. 6.** Heat maps of (A) biomass-specific sucrose concentrations, and (B) area-specific sucrose concentrations in leaf tissues contoured as a function of pH or  $\text{CO}_{2(\text{aq})}$  treatments (vertical left axis) and months (horizontal axis). In panel (A), the values in parentheses indicate the percentage of total C as sucrose. White symbols on each plot represent the slope of the response variable vs.  $\log \text{CO}_{2(\text{aq})}$  concentrations (vertical right axis) estimated from linear regression analysis as described in section 2.2.2, with statistically significant slope annotated with asterisk symbols. Error bars represent  $\pm 1\text{SE}$  of the regression slope. The white horizontal line connects the slopes that are not statistically different based on multiple comparison analysis. Plants from pH 6.1 treatment were harvested in August 2014; therefore, no data was present from this period onward. (A) was redrawn from data previously published in (Zimmerman et al. 2017).

Leaf FAA concentrations were initially close to zero for the first three months of the experiment. However, they increased uniformly across all  $\text{CO}_{2(\text{aq})}$  treatments through fall and winter as growth rates declined (Fig. 7A, 7B). In spring, with the recovery of growth rates, FAA concentrations declined. A significant positive effect of  $\text{CO}_{2(\text{aq})}$  on leaf FAA content was observed, with the most substantial impact occurring in December and January. For eelgrass exposed to high  $\text{CO}_{2(\text{aq})}$  treatment, both biomass-specific and area specific FAA content more than doubled compared to ambient  $\text{CO}_{2(\text{aq})}$  treatment. Leaf FAA constitute a small fraction of total nitrogen in leaves estimated to be between 1 and 6%, depending on the seasons.

The predominant amino acids in leaf tissues were glutamine (Gln),  $\gamma$ -Aminobutyric acid (GABA), proline (Pro), and alanine (Ala), collectively comprising over 90% of the total FAA pool (Fig. 8). The relative abundance of these amino acids exhibited variations dependent on time and  $\text{CO}_{2(\text{aq})}$  treatments. In December, high  $\text{CO}_{2(\text{aq})}$  levels facilitated the accumulation of Gln, a precursor of protein synthesis, constituting approximately 50% of the total FAA pool (Fig. 8). However, in July, Gln decreased to approximately 10%, likely a response to increased growth demand as growth rates recovered during the summer. The Gln levels in eelgrass leaves subjected to ambient  $\text{CO}_{2(\text{aq})}$  condition were relatively unchanged between December and July. Both  $\text{CO}_2$  enriched and unenriched (or ambient  $\text{CO}_{2(\text{aq})}$ ) eelgrass accumulated more Pro in leaves in December compared to July, likely in response to low temperatures (winter daily temperature averaged around 5 °C, as shown in Fig. 2B). GABA, a non-proteinogenic amino acid related to stress response (Guo et al. 2023), was approximately two times higher in December than in July for  $\text{CO}_{2(\text{aq})}$  enriched plants. Similar to Gln, GABA exhibited no difference between December and July for ambient  $\text{CO}_{2(\text{aq})}$  conditioned eelgrass.

### 2.3.4 Total C, N, and S in leaf tissues

The total C, N, and S contents in leaf tissues were uniform across all aquaria in May 2013 prior to CO<sub>2(aq)</sub> enrichment, with mean concentrations of 28.5 mmol C g<sup>-1</sup> DW ( $\pm 0.2$ ; n=20), 1.8 mmol N g<sup>-1</sup> DW ( $\pm 0.2$ ; n=20), and 153.1  $\mu$ mol S g<sup>-1</sup> DW ( $\pm 5.0$ ; n=20), respectively (Fig. 9A, 9C, and 9E). However, after this stable period, significant CO<sub>2</sub> treatment effects were observed, but the responses varied depending on the specific response variables.

Total leaf C increased linearly with log CO<sub>2(aq)</sub> concentrations, with statistically significant positive slopes (determined through repeated measure ANCOVA,  $p < 0.001$ , Table 3). The positive CO<sub>2(aq)</sub> treatment effects were particularly evident when leaf C content was normalized to leaf area (Fig. 9B). The slopes for area-specific leaf carbon content ( $\mu$ mol cm<sup>-2</sup>) vs log CO<sub>2(aq)</sub> concentrations consistently remained significantly positive throughout the experiment. These slopes were highest from August to October 2013, declining during the winter months when CO<sub>2(aq)</sub> effects were less pronounced and growth rates decreased. In this period of low growth, leaves accumulated more C per gram of biomass in the form of sucrose, constituting approximately 28% of total carbon, as illustrated in Fig. 6A. In contrast, sucrose made up no more than 20% of total carbon in high CO<sub>2(aq)</sub> (2121  $\mu$ M, pH 6.1) enriched eelgrass in summer and spring.

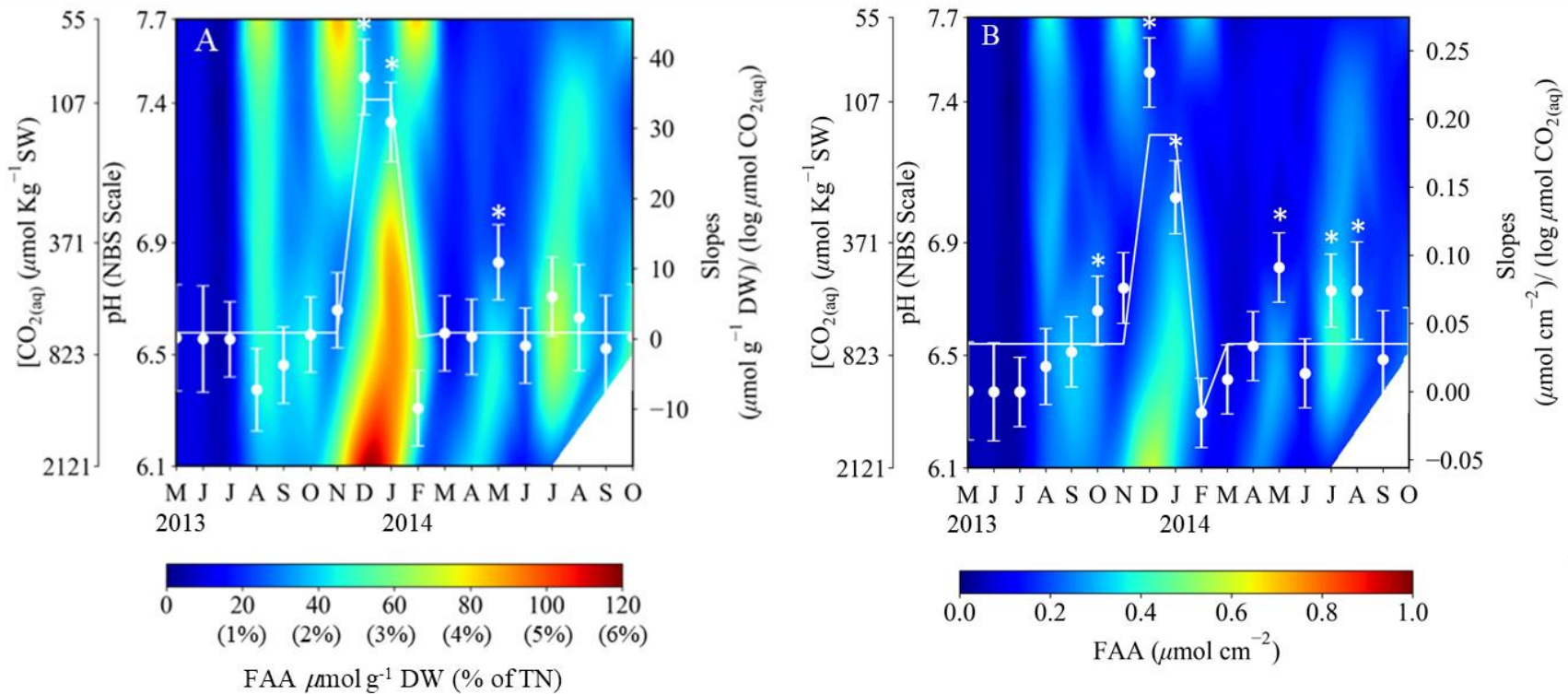


**Fig. 7.** Heat maps of (A) biomass-specific free amino acids (FAA), and (B) area-specific FAA concentrations contoured as a function of pH or  $\text{CO}_{2(\text{aq})}$  treatments (vertical left axis) and months (horizontal axis). In panel (A), the values in parentheses indicate the percentage of total N as FAA. White symbols on each plot represent the slope of the response variable vs.  $\log \text{CO}_{2(\text{aq})}$  concentrations (vertical right axis) estimated from linear regression analysis as described in section 2.2.2, with statistically significant slope annotated with asterisk symbols. Error bars represent  $\pm 1\text{SE}$  of the regression slope. The white horizontal line connects the slopes that are not statistically different based on multiple comparison analysis. Plants from pH treatment 6.1 were harvested in August 2014; therefore, no data was present from this period onward.

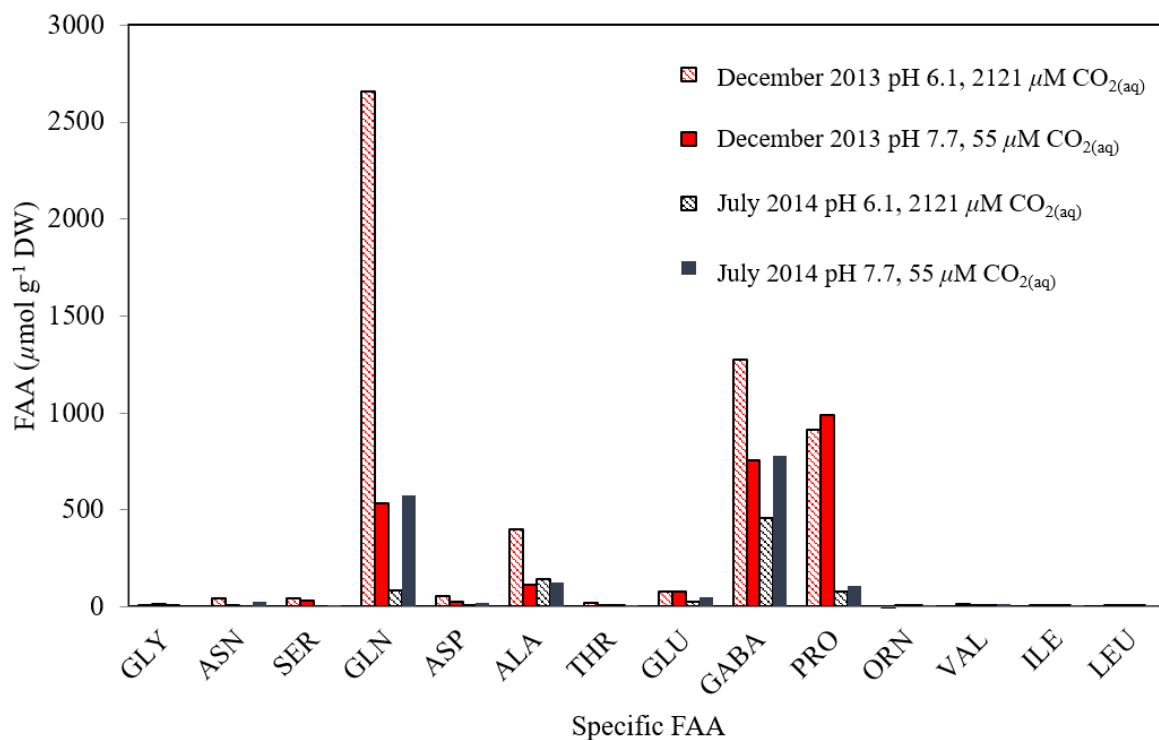


**Fig. 8.** Concentrations of specific free amino acids (FAA) concentrations in *Zostera marina* L. leaf tissues from the highest  $\text{CO}_{2(\text{aq})}$  (hash lines) and ambient  $\text{CO}_{2(\text{aq})}$  (solid color) treatments, contrasting between December 2013 (red) and July 2014 (black). Specific FAA and abundance were analyzed using electron spray ionization liquid chromatography tandem mass spectrometry (ESI-LC-MS/MS) with ion pairing chromatography. Amino acids include: glycine (GLY), asparagine (ASN), serine (SER), glutamine (GLN), aspartic acid (ASP), alanine (ALA), threonine (THR), glutamic acid (GLU),  $\gamma$ -Aminobutyric acid (GABA), proline (PRO), ornithine (ORN), valine (VAL), isoleucine (ILE), and leucine (LEU).

Leaf N content per gram dry weight decreased linearly with increasing  $\log \text{CO}_{2(\text{aq})}$  concentrations, with significant negative  $\text{CO}_{2(\text{aq})}$  treatment effects evident in 10 out of the 18 months, primarily during summer and spring (Fig. 9C, Table 3). In these periods, eelgrass exposed to elevated  $\text{CO}_{2(\text{aq})}$  (2121  $\mu\text{M}$ , pH 6.1) conditions had leaf N content approximately 20-30% lower than those under ambient  $\text{CO}_{2(\text{aq})}$  condition (55  $\mu\text{M}$ , pH 7.7). Biomass-specific leaf N content exhibited a seasonal pattern, being lower during high-growth summer months and higher during low-growth winter months, with no significant impact from  $\text{CO}_{2(\text{aq})}$  treatments during winter (slopes = 0, Fig. 9C).

In contrast, area-specific leaf N content exhibited a linear increase with increasing  $\log \text{CO}_{2(\text{aq})}$  concentrations, but this effect was limited to specific months (Fig. 9D, Table 3). Notably,  $\text{CO}_2$ -induced changes were observed in October and December 2013, as well as May and August 2014, with significant positive slopes. The highest slopes occurred in October and December, with N content approximately 1.5 times higher under high  $\text{CO}_{2(\text{aq})}$  compared to ambient  $\text{CO}_{2(\text{aq})}$  conditions. Leaves contained the lowest N content (per leaf area) during late winter and early spring (February to beginning of April), measuring at less than 6  $\mu\text{mol cm}^{-2}$  across all  $\text{CO}_{2(\text{aq})}$  treatments. The positive response of area-specific leaf N content to  $\text{CO}_{2(\text{aq})}$  treatments closely mirrored the pattern observed for leaf FAA, where significant  $\text{CO}_2$ -stimulated increase in area-specific leaf FAA concentrations were observed during the same months, as shown in Fig. 7B.

Similarly, area-specific leaf S content in Fig. 9F followed a similar pattern observed in leaf FAA in Fig. 7B, suggesting that the presence of S in leaves is likely associated with sulfur containing amino acids. When normalized to biomass, total S content in leaves responded negatively to increasing  $\log \text{CO}_{2(\text{aq})}$ , but the slopes were not consistently negative throughout the course of the experiment.

The CO<sub>2</sub>-stimulated increase in leaf C and the simultaneous decrease in leaf N led to a significant increase in the molar C:N ratio in all months, with the exceptions of May and November 2013 and July 2014 (Fig. 10A). The slopes were consistently positive throughout the experiment, except for these specific months. During the peak of summer and fall of 2013, when CO<sub>2(aq)</sub> treatment effects were most pronounced, the slopes were at their highest, but they weakened considerably in the winter, dropping nearly four times compared to the warmer seasons. During these warmer months, the area-specific leaf C content for CO<sub>2</sub>-enriched eelgrass was nearly two times higher than those grown under ambient CO<sub>(aq)</sub> condition, with approximately 20% of this carbon present as soluble sucrose (ref. Fig. 6A).

The molar N:S ratios in Fig. 10B, which fell within the range of 6 and 20, exhibited seasonal variations that tracked the changes in N content and, to a lesser extent, S content in leaves. The highest values were observed between November and February during the colder months. The N:S ratio in spring, summer, and fall typically ranged between 6 and 15, with lowest N:S ratio observed in late spring in May 2014. Despite this seasonal pattern, there were inconsistent CO<sub>2(aq)</sub> treatment effects (Table 3). Typically, the molar N:S ratios decreased with increasing log CO<sub>2(aq)</sub> concentrations, except for December when the slope was positive.

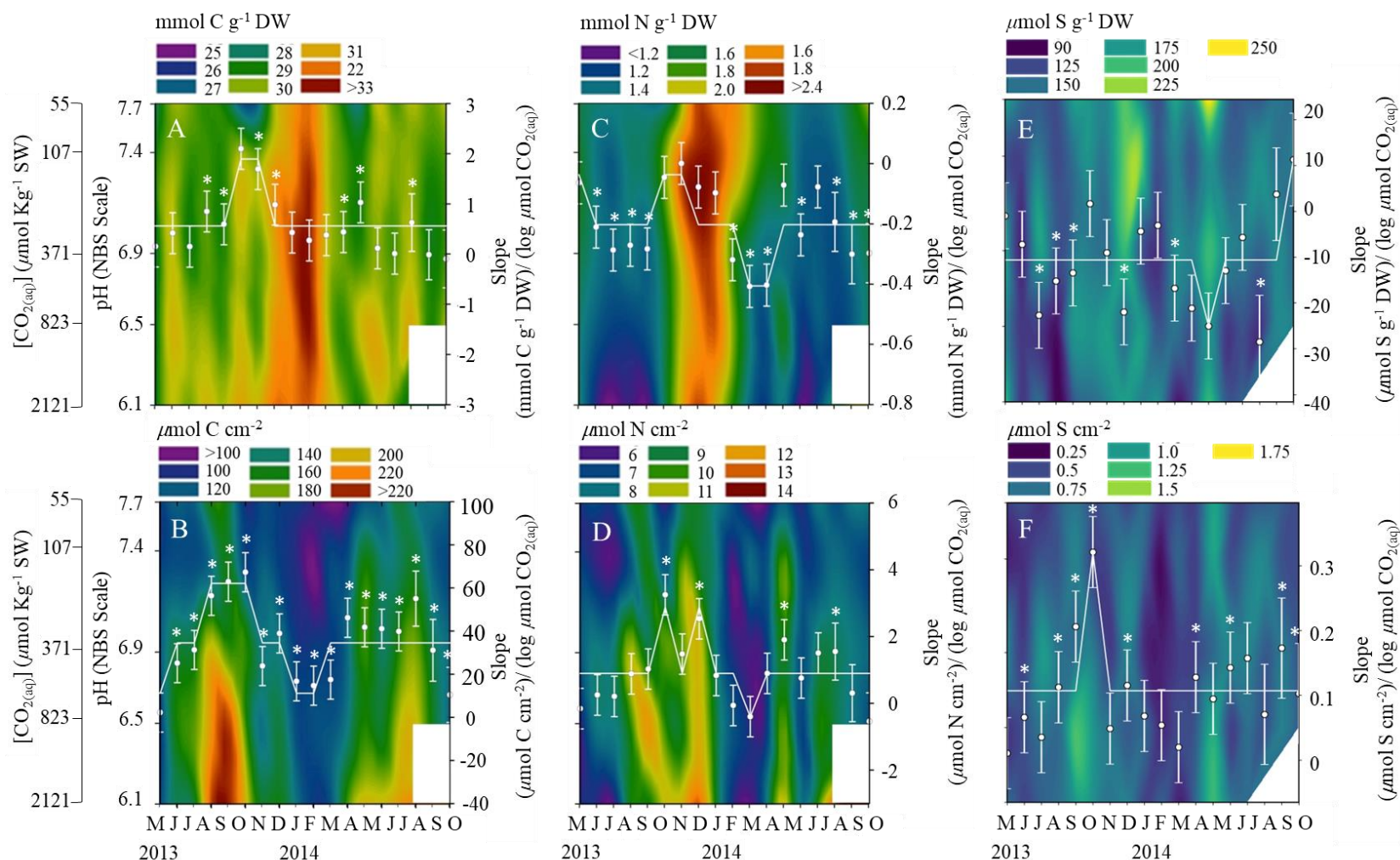


**Fig. 9.** Heat maps of carbon (A, B), nitrogen (C, D), and sulfur (E, F) content in leaves normalized to biomass (top row) or leaf area (bottom row) contoured as a function of pH (or CO<sub>2(aq)</sub>) treatments and months. White symbols on each plot represent the slope of the response variable to log CO<sub>2(aq)</sub>, with statistically significant slope annotated with asterisk symbols. Error bars represent ± 1 SE of the regression slope. The white horizontal line connects the slopes that are not statistically different based on multiple comparison analysis. Plants from pH 6.1 treatment were harvested in August 2014; therefore, no data was present from this period onward.

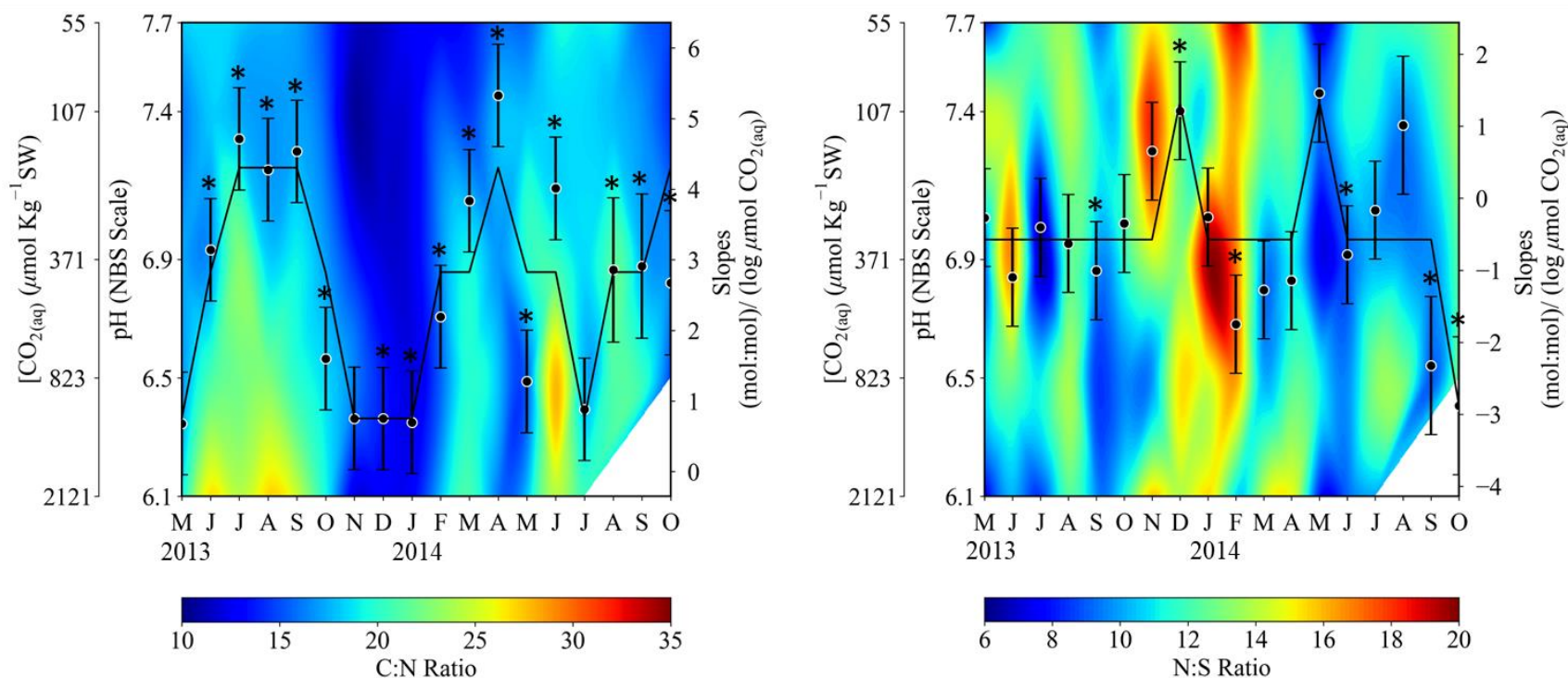


**Fig. 10.** Heat maps of (A) molar C:N ratio, and (B) molar N:S ratio contoured as a function of pH or CO<sub>2(aq)</sub> treatments (vertical left axis) and months (horizontal axis). Black symbols on each plot represent the slope of the response variable vs. log CO<sub>2(aq)</sub> concentrations (right vertical axis) estimated from linear regression analysis, with statistically significant slope annotated with asterisk symbols. Error bars represent  $\pm 1$ SE of the regression slope. The black horizontal line connects the slopes that are not statistically different based on multiple comparison analysis. Plants from pH 6.1 treatment were harvested in August 2014; therefore, no data was present from this period onward.

### 2.3.5 Whole plant comparisons in October 2014

After the 18-month experiment concluded, eelgrass subjected to the highest  $\text{CO}_{2(\text{aq})}$  treatment more than doubled their above- and belowground biomass, evident in Fig. 11 and supported by the shoot size data in Fig. 5A. Simultaneously, sucrose concentrations ( $\mu\text{mol g}^{-1} \text{DW}$ ) in leaves and rhizome measured in October 2014 increased linearly with increasing  $\text{CO}_{2(\text{aq})}$  levels, while roots remained unaffected. The rhizomes, exhibited the strongest response to  $\text{CO}_{2(\text{aq})}$  treatment (as indicated by higher slopes shown in Fig. 12 and Table 4), experienced a nearly two-fold increase in sucrose concentrations compared to the ambient  $\text{CO}_{2(\text{aq})}$  condition. Even under ambient  $\text{CO}_{2(\text{aq})}$  conditions, the rhizome contained more sucrose compared to other plant tissues.



**Fig. 11.** Differences in eelgrass shoot sizes across pH (or  $\text{CO}_{2(\text{aq})}$ ) gradient at the end of the experiment in October 2014. Image was previously published in (Zimmerman et al. 2017).

**Table 4.** Linear regression for the effect of CO<sub>2(aq)</sub> on sucrose, FAA, total C and N contents on leaf, rhizome, and roots at the termination of the experiment (October 2014) after 18 months of CO<sub>2</sub> enrichment at treatments: 55, 107, 371, 823 and 2121  $\mu\text{mol CO}_2 \text{ Kg}^{-1} \text{ SW}$ . ( $\alpha = 0.05$ ).

| Dependent variable                            | Slope | SE (slope) | Intercept | $r^2$ | ANOVA |        |       |              |
|---|-------|------------|-----------|-------|-------|--------|-------|--------------|
|   |       |            |           |       | df    | MS     | $F$   | $p$          |
| Sucrose ( $\mu\text{mol g}^{-1} \text{ DW}$ ) |       |            |           |       |       |        |       |              |
| Leaf  | 0.17  | 0.05       | 185.78    | 0.49  | 1     | 41354  | 12.66 | <b>0.004</b> |
| Rhizome                                       | 0.28  | 0.10       | 215.69    | 0.35  | 1     | 115781 | 7.50  | <b>0.016</b> |
| Root  | 0.08  | 0.04       | 92.56     | 0.20  | 1     | 9494   | 3.51  | 0.082        |
| FAA ( $\mu\text{mol g}^{-1} \text{ DW}$ )     |       |            |           |       |       |        |       |              |
| Leaf  | 0.004 | 0.01       | 21.12     | 0.01  | 1     | 24     | 0.18  | 0.681        |
| Rhizome                                       | -0.06 | 0.02       | 72.70     | 0.44  | 1     | 5360   | 11.19 | <b>0.005</b> |
| Root  | -0.01 | 0.00       | 24.90     | 0.26  | 1     | 119    | 4.65  | 0.05         |
| Total C ( $\text{mmol g}^{-1} \text{ DW}$ )   |       |            |           |       |       |        |       |              |
| Leaf  | -0.10 | 0.48       | 30.14     | 0.00  | 1     | 0.03   | 0.04  | 0.837        |
| Rhizome                                       | 1.38  | 0.58       | 25.32     | 0.29  | 1     | 6.3    | 5.70  | <b>0.032</b> |
| Root  | 0.55  | 0.44       | 24.91     | 0.10  | 1     | 1.01   | 1.55  | 0.233        |
| Total N ( $\text{mmol g}^{-1} \text{ DW}$ )   |       |            |           |       |       |        |       |              |
| Leaf  | -0.30 | 0.13       | 2.56      | 0.28  | 1     | 0.3    | 5.48  | <b>0.035</b> |
| Rhizome                                       | -0.72 | 0.20       | 2.68      | 0.50  | 1     | 1.74   | 13.73 | <b>0.002</b> |
| Root  | -0.11 | 0.05       | 0.96      | 0.26  | 1     | 0.04   | 4.86  | <b>0.045</b> |

A significant  $\text{CO}_{2(\text{aq})}$  treatment effect on FAA concentrations was only observed in the rhizome, where concentrations decreased linearly with increasing  $\text{CO}_{2(\text{aq})}$  levels (Fig. 12). Eelgrass subjected to elevated  $\text{CO}_{2(\text{aq})}$  treatment demonstrated a significant two-fold reduction in FAA content in the rhizome compared to those grown under ambient conditions in October 2014 (Table 4).

Rhizome C content increased logarithmically with  $\text{CO}_{2(\text{aq})}$  treatments ( $r^2 = 0.29$ ,  $p = 0.032$ ) (Fig. 13 and Table 4).  $\text{CO}_{2(\text{aq})}$  enrichment led to a maximum increase of 6% in rhizome C content, with no observed impact on leaf and root C contents at this last measurement. In contrast, the N content of all plant tissues decreased linearly with log  $\text{CO}_{2(\text{aq})}$  concentrations, and the slopes for leaves, rhizome, and roots were significantly different from each other (Fig. 13, Table 4, and Table 5).  $\text{CO}_{2(\text{aq})}$  enrichment resulted in a reduction of N content ranging from 20 to 60 % across all plant tissues in October 2014. The most significant reduction occurred in the rhizome, indicating robust  $\text{CO}_{2(\text{aq})}$  treatment effects, with slopes twice as high as in leaves and six times higher than in roots (Fig. 13 and Table 4). A marked difference in the molar C:N ratio emerged with increasing  $\text{CO}_{2(\text{aq})}$  concentrations between above- and belowground tissues, with the ratio increasing by approximately 150% in rhizome over 24% in leaves and roots.

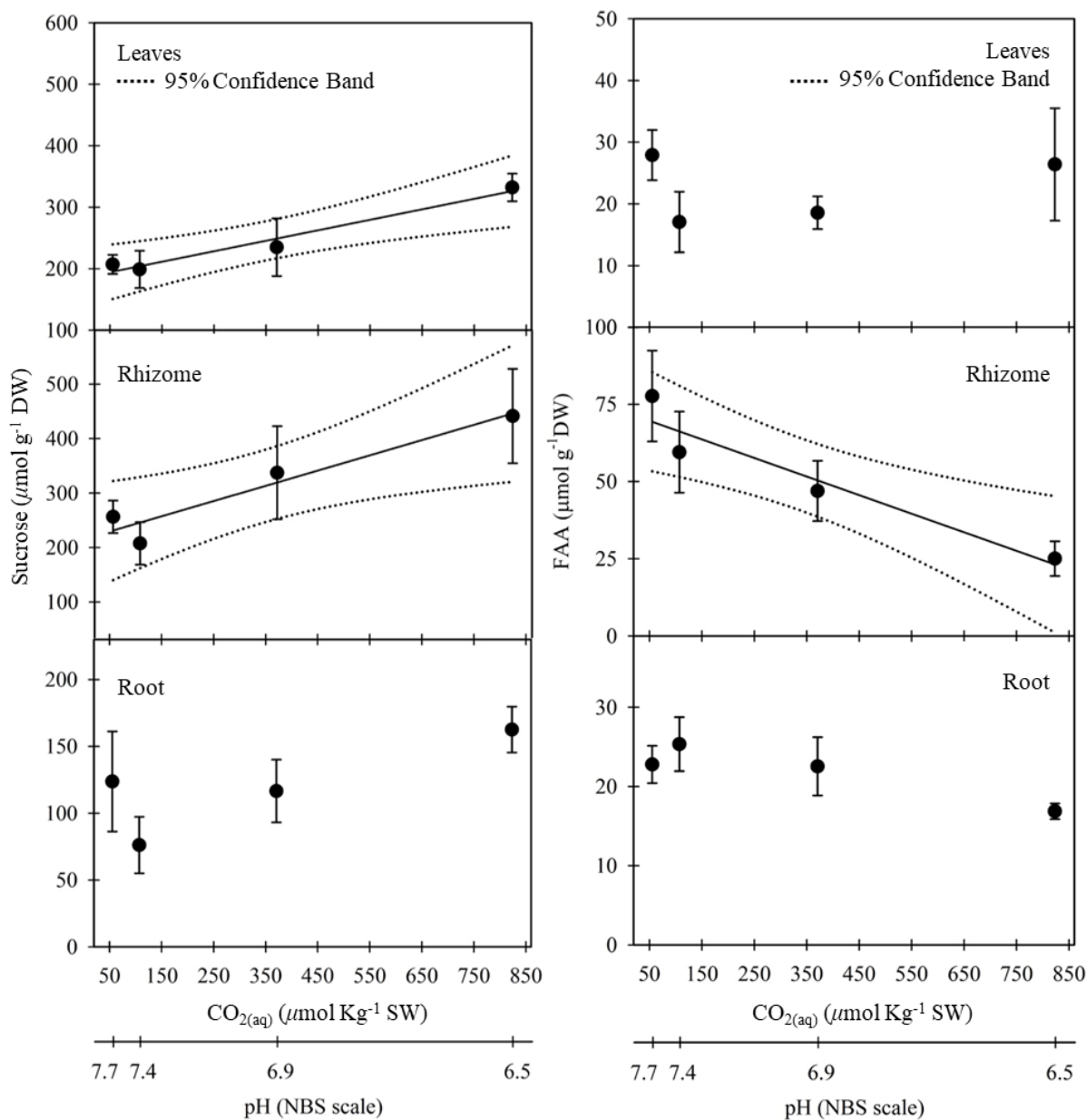


**Fig. 12.** Sucrose (left) and free amino acids (FAA) (right) concentrations for leaves (top), rhizome (middle), and roots (bottom) plotted against  $\text{CO}_{2(\text{aq})}$  concentrations with corresponding pH scale presented on the secondary x-axis. The above data represent sucrose and FAA contents measured at the end of the 18-month experiment in October 2014. The solid line represents linear regression through all data points ( $n = 4$ , replicates = 16). The dotted line represents the 95% confidence limit on the regression line. Error bars are  $\pm 1$  SE.

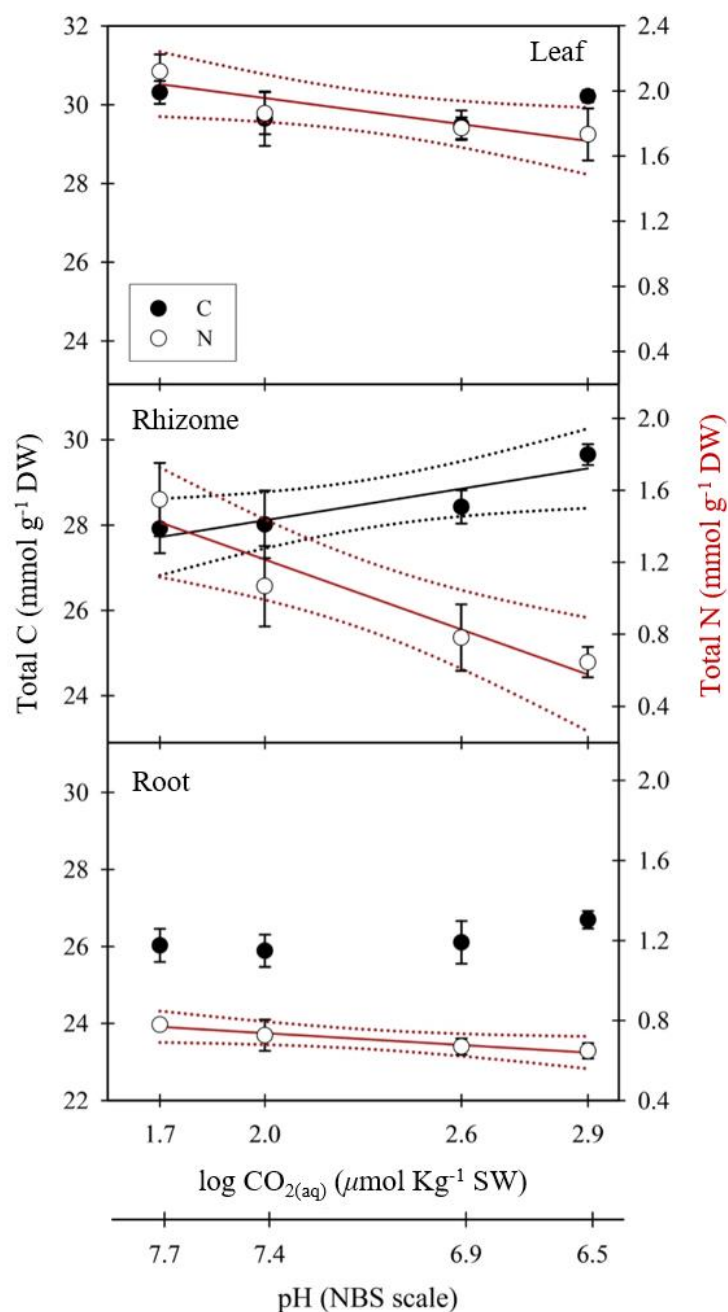


**Fig. 13.** Leaf, rhizome, and root total C (left axis) and N (right axis) content in *Zostera marina* L., shown as a function of  $\log \text{CO}_{2(\text{aq})}$  concentrations and pH (secondary x-axis). Data were collected experiment's conclusion in October 2014. The solid line represents the linear regression fit to all data points ( $n = 4$  for all treatments, except for  $\log \text{CO}_{2(\text{aq})} = 2.9$ , where  $n = 3$ ). The dotted line is the 95% confidence limit on the regression line. The error bars indicate  $\pm 1$  SE.

**Table 5.** Summary ANCOVA tables for Type III tests of fixed effects (Tissue types) using the mixed linear model routine performed in SPSS with  $\log \text{CO}_{2(\text{aq})}$  as a covariate. DW: dry weight.  $\alpha = 0.05$ . Test was performed for total N content measured in tissues collect in October 2014.

| Dependent variable                   | Source  | df | SS    | MS   | <i>F</i> | <i>p</i>       |
|--------------------------------------|---|----|-------|------|----------|----------------|
| Total N<br>(mmol g <sup>-1</sup> DW) | Tissue types  | 2  | 11.70 | 5.85 | 92.91    | < <b>0.001</b> |
|                                      | $\log \text{CO}_{2(\text{aq})}$                     | 1  | 1.42  | 1.42 | 22.54    | < <b>0.001</b> |
|                                      | Tissue types $\times \log \text{CO}_{2(\text{aq})}$ | 2  | 0.66  | 0.33 | 5.21     | <b>0.010</b>   |

### 2.3.6 Growth demand

The initial growth demands for carbon and nitrogen, calculated using Eq. (1) and Eq. (2), were uniform across all  $\text{CO}_{2(\text{aq})}$  treatments, with mean concentrations of  $90.6 (\pm 8.1 \text{ SE}) \mu\text{mol C shoot}^{-1} \text{ d}^{-1}$  and  $5.7 (\pm 0.5 \text{ SE}) \mu\text{mol N shoot}^{-1} \text{ d}^{-1}$ , respectively. After 4 weeks of  $\text{CO}_{2(\text{aq})}$  enrichment, growth demand for both carbon and nitrogen increased in response to  $\text{CO}_2$ -stimulated growth rates (as depicted in Fig. 4A), resulting in seasonal patterns in C and N demands (Fig. 14 and 15). Higher growth rates in the summer resulted in higher growth demands. The maximum growth demand was predicted to occur July and September, with the minimum growth demand projected for January and February.

Both C and N demand exhibited a hyperbolic increase with  $\text{CO}_{2(\text{aq})}$  concentrations, especially during the summer, reaching asymptotic values of  $369 \mu\text{mol C shoot}^{-1} \text{ d}^{-1}$  and  $18 \mu\text{mol N shoot}^{-1} \text{ d}^{-1}$ , respectively (Fig. 16). These values represent the maximum  $\text{CO}_2$ -saturated C and N uptake rates, constrained by growth rates. Predictions suggest that eelgrass under elevated  $\text{CO}_{2(\text{aq})}$  ( $2121 \mu\text{M}$ , pH 6.1) should undergo a two-fold increase in C and N demand when growth rates peak at  $3\% \text{ d}^{-1}$ . Conversely, as growth rates decrease to  $1\% \text{ d}^{-1}$  in the winter, growth demands declined dramatically, remaining uniformly low across all  $\text{CO}_{2(\text{aq})}$  treatments.

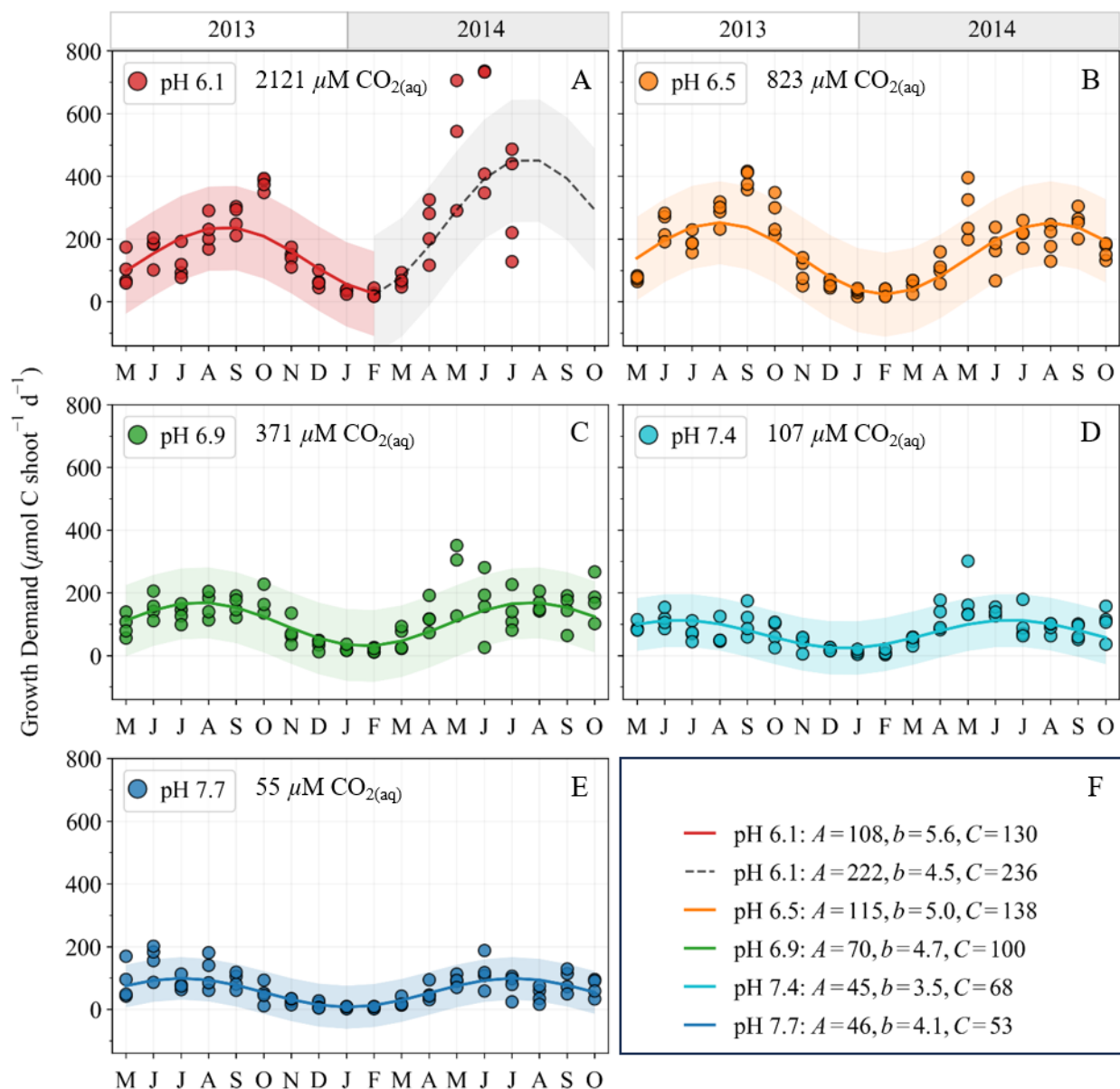


**Fig. 14.** Seasonal patterns of *Zostera marina* L. C demand in response to pH (or  $\text{CO}_{2(\text{aq})}$ ) treatments, depicted in scatter plot with observations spanning from May 2013 until October 2014. The solid and dash lines represent non-linear Least Square fits to observations using Eq. (3).  $A$ ,  $b$ , and  $C$  are the coefficients corresponding to amplitude, monthly phase shift, and vertical growth demand offset, respectively.

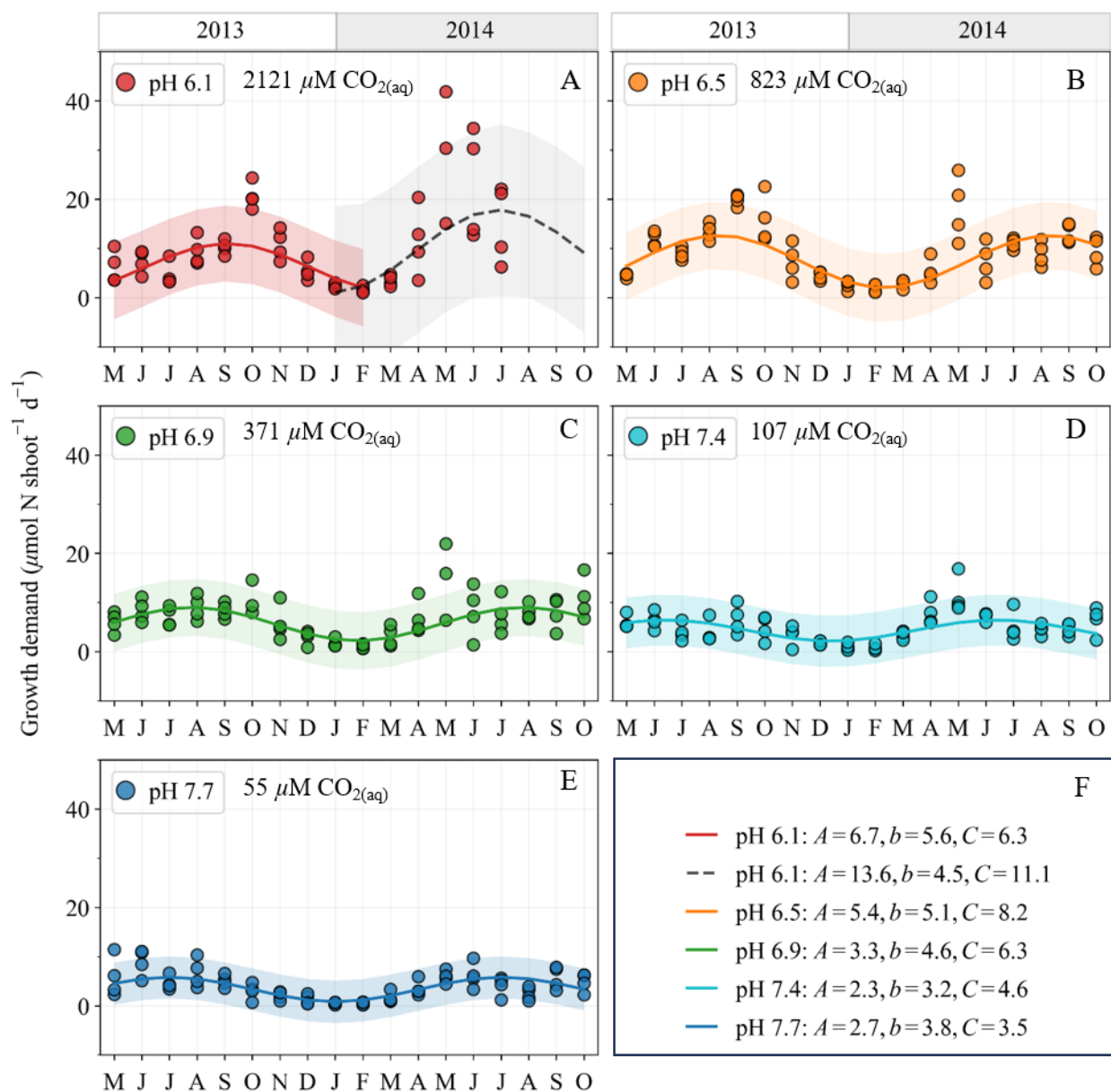


**Fig. 15.** Seasonal patterns of *Zostera marina* L. N demand in response to pH (or  $\text{CO}_{2(\text{aq})}$ ) treatments, depicted in scatter plot with observations spanning from May 2013 until October 2014. The solid and dash lines represent non-linear Least Square fits to observations using Eq. (3). A, b, and C are the coefficients corresponding to amplitude, monthly phase shift, and vertical growth demand offset, respectively.

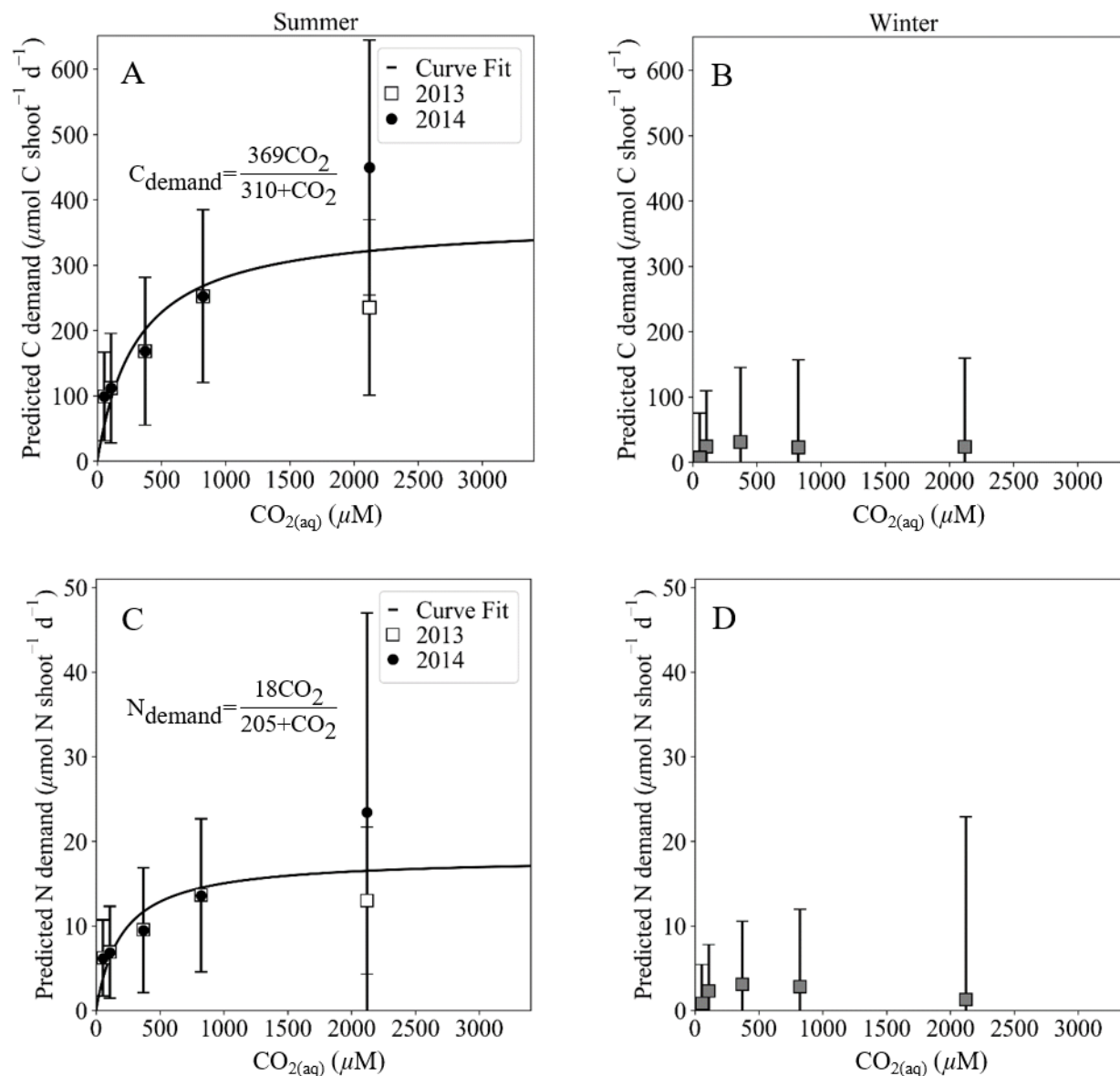


**Fig. 16.** Predicted growth demand for carbon (A, B) and for nitrogen (C, D) in summer vs winter as a function of aqueous CO<sub>2</sub> (CO<sub>2(aq)</sub>) concentrations. The solid line represents non-linear curve fit (MATLAB 2022a) through coefficient *A*, maximum growth demand, estimated by using Eq. (3) (also refer to Fig. 15). No CO<sub>2(aq)</sub> effects on growth demand were observed in the winter.

### 2.3.7 Sucrose reserves

With the exception of the ambient  $\text{CO}_{2(\text{aq})}$  treatment (pH 7.7) in September and October 2014, all monthly estimates of sucrose available for new growth ( $S_{\text{new},m}$ ), calculated using Eq. 6, were positive (Fig. 17). This indicates a deficit, signifying that growth demand during September and October 2024 exceeded the metabolic carbon production during those months ( $P_{\text{net}}$  in Eq. 5), resulting in a negative sucrose reserve, as shown in Fig. 18. The seasonal variation in  $S_{\text{new}}$  was evident, with more sucrose available for growth demand during the summer than in winter. Additionally, the amount of sucrose available for growth was influenced by  $\text{CO}_{2(\text{aq})}$  treatment, increasing with  $\text{CO}_{2(\text{aq})}$  concentrations. Even during peak summer growth demand, eelgrass had approximately 15 to 35 times more sucrose per shoot in the highest  $\text{CO}_{2(\text{aq})}$  treatment (pH 6.1) compared to ambient  $\text{CO}_{2(\text{aq})}$  (pH 7.7) condition, with the latter observed in 2014. This represents between 80 and 140 days of sucrose reserves to support growth (ref. Fig. 18).

There was a notable difference in sucrose reserves between summer and winter. Generally, more sucrose reserves were present during winter months across all  $\text{CO}_{2(\text{aq})}$  treatments due to lower growth rates and reduced growth demand. In particular, between January and February, eelgrass contained approximately 20 to 160 days of sucrose reserves depending on the  $\text{CO}_{2(\text{aq})}$  treatment.

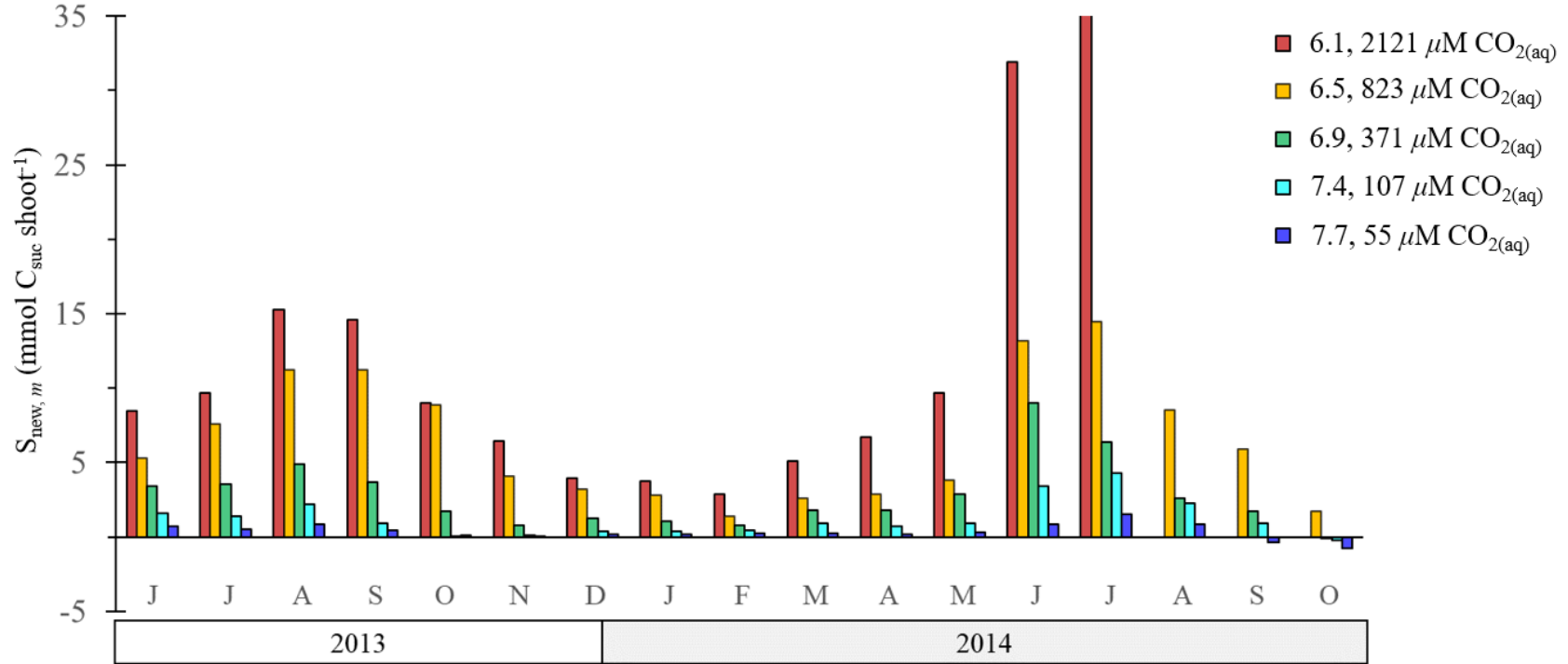


**Fig. 17.** Time series depiction of the effects of  $CO_{2(aq)}$  (or pH) on the abundance of carbon as sucrose ( $C_{sucrose}$ ) per shoot available for new growth, from June 2013 until October 2014. Monthly estimates of  $S_{new, m}$  was calculated using Eq. (6). Negative values indicate that the growth demand surpasses the available supply.

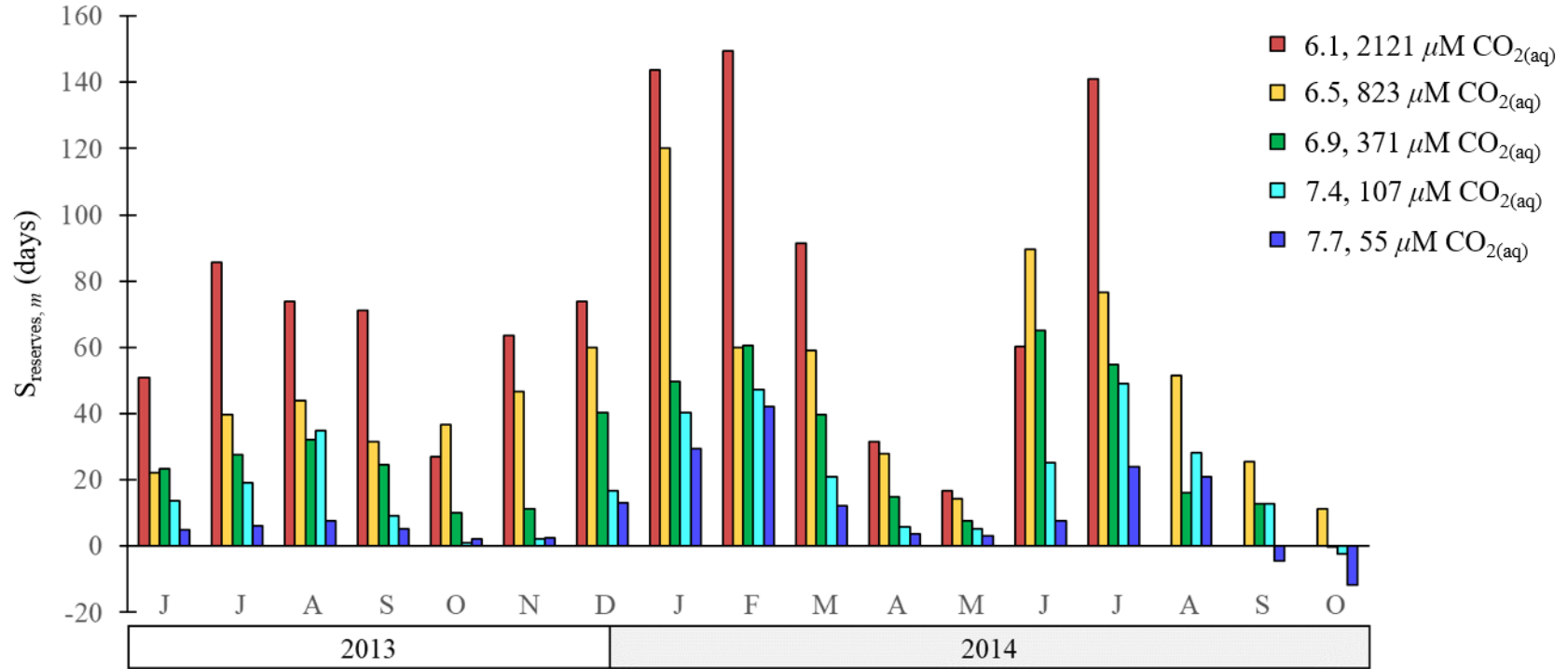


**Fig. 18.** Time series depiction of the effects of  $\text{CO}_{2(\text{aq})}$  (or pH) on sucrose reserves from June 2013 until October 2014. Monthly estimates of  $S_{\text{reserves}, m}$  was calculated using Eq. (7). Negative values denote a sucrose deficit resulting from high growth demand surpassing the supply.

## **2.4 Discussion**

This study explored the intricate dynamics of long-term (18 months) and continuous  $\text{CO}_{2(\text{aq})}$  enrichment on eelgrass physiology, revealing both seasonal and tissue-specific responses. A noticeable lag response to  $\text{CO}_{2(\text{aq})}$  enrichment was observed, with measurable effects taking up to 6 weeks to manifest. However, once established, the overall responses exhibited statistically linear trends across various  $\text{CO}_{2(\text{aq})}$  treatments, producing measurable functional responses to  $\text{CO}_{2(\text{aq})}$ . Positive impacts on growth rates contrasted with findings from shorter-term (<6 weeks) studies (Ow et al. 2015; Ow et al. 2016), but aligned with results from other long-term (~1 year) studies (Palacios and Zimmerman 2007; Zimmerman et al. 2017). This study underscores the importance of longer experimentation, spanning multiple plastochron intervals, which denote the time between successive events of leaf initiation, to effectively assess the influence of  $\text{CO}_2$  on plant performance. Additionally, shoot sizes, leaf density, and growth demands for carbon and nitrogen increased with increasing  $\text{CO}_{2(\text{aq})}$  concentrations, displaying pronounced seasonal patterns. Summer months saw a two- to three-fold increase in these parameters, while minimal effects were observed in winter, likely due to cold temperature and reduced light levels, which tend to slow down metabolic activities.

### **2.4.1 Enhanced plant performance compositions under increasing $\text{CO}_{2(\text{aq})}$ concentrations**

Over the 18-month experiment,  $\text{CO}_{2(\text{aq})}$  enrichment significantly increased sucrose accumulation in eelgrass leaves, even during two summer periods of prolonged thermal stress (25 °C for eelgrass established by Evans et al. (1986)). Elevated  $\text{CO}_{2(\text{aq})}$  stimulated sucrose production in leaves, surpassing growth demands and resulting in sucrose reserves three to six times higher than those observed in eelgrass under ambient  $\text{CO}_{2(\text{aq})}$  conditions (see Fig. 18). This increased

sucrose content provided shoots with abundant carbon reserves, leading to at least a doubling in growth rates and shoot size, especially during the second year. The accumulation of reserves was highest during the cold winter months due to slow growth and low C demand. Labile sucrose constitutes nearly a third of the total C pool in leaf tissues of eelgrass subjected to highest  $\text{CO}_{2(\text{aq})}$  treatments, serving as readily available metabolizable carbon reserves for vegetative and flowering shoots in the following spring and summer. In a concurrent  $\text{CO}_{2(\text{aq})}$  enrichment study that employed the same plants, Zimmerman et al. (2017) observed high flowering rates in the spring of 2014 and a subsequent doubling of shoot numbers in the highest  $\text{CO}_{2(\text{aq})}$  aquaria, attributable to significant sucrose reserves resulted from  $\text{CO}_{2(\text{aq})}$  enrichment. Moreover, within the same study, the documented shoot losses during late summer 2014, in the absence of  $\text{CO}_{2(\text{aq})}$  treatments, seemed to align with a deficiency in sucrose reserves determined in this study. During that specific summer, the eelgrass experienced a prolonged period of high water temperature exceeding 25 °C for 124 consecutive days (Celebi-Ergin et al. 2021). This prolonged exposure to high temperature likely led to increased carbon demand to sustain high respiratory metabolism, consequently depleting the sucrose reserves, and leading to shoot loss.

The impact of  $\text{CO}_{2(\text{aq})}$  treatments on FAA content was generally positive, though it was not consistently observed throughout the experiment.  $\text{CO}_2$ -stimulated growth tended to maintain relatively low FAA concentrations, except during winter months when FAA accumulation in leaves became apparent, particularly under elevated  $\text{CO}_{2(\text{aq})}$  conditions. In winter, with low N demand for growth, the effects of  $\text{CO}_{2(\text{aq})}$  were most pronounced, leading to a three-fold accumulation in leaf FAA concentrations. As growth rates and growth N demand rebounded in the spring and summer, FAA levels decreased and consistently remained low, not exceeding 3% of the total N pool. While modest, the 1-6% range of FAA measured in this study corresponds to the

lower end observed in previous research. Earlier studies have shown that FAA levels in seagrass can vary widely, ranging from less than 1% to greater than 60% of the total N pool in seagrass (Pirc 1985; Pirc and Wollenweber 1988).

It is likely that the CO<sub>2</sub>-stimulated growth led to rapid depletion of FAA concentrations, as protein synthesis and biomass production increased under elevated CO<sub>2(aq)</sub> conditions (Platt and Bassham 1978; Andrews et al. 2018). Various metabolic pathways also stimulated by CO<sub>2</sub>, particularly those involving photosynthetic metabolism (Apostolaki et al. 2014; Zhao et al. 2019; Zayas-Santiago et al. 2020) can exert greater demand for FAA, as synthesis of photosynthesis-related proteins is up-regulated (Zhao et al. 2019). In recent molecular studies, long-term exposure to elevated CO<sub>2</sub> levels led to an increase in proteins related to light harvesting in *Cymodocea nodosa* (Piro et al. 2020). Similar responses are expected to occur in *Z. marina*, potentially drawing down FAA concentrations to low levels, especially during peak growth.

The differences in the accumulation patterns of specific FAA between the highest CO<sub>2(aq)</sub> and ambient CO<sub>2(aq)</sub> treatments could offer additional insights into the feedback regulation of CO<sub>2</sub> on N metabolic pathways. Because glutamine (Gln) represents the first amino acid formed from the assimilation of NH<sub>4</sub><sup>+</sup>, higher levels of Gln in the highest CO<sub>2(aq)</sub> treatment compared to ambient CO<sub>2(aq)</sub> treatment suggests enhanced N assimilation driven by CO<sub>2(aq)</sub> concentrations. These findings are consistent with increased N uptake and the abundance of N assimilation metabolites observed in both terrestrial C<sub>3</sub> plants (Andrews et al. 2018) and marine plants (Zayas-Santiago et al. 2020). Additionally, reduced  $\gamma$ -Aminobutyric acid (GABA) levels under elevated CO<sub>2(aq)</sub> in July, during prolonged high-temperature periods, may indicated a stress mitigation effect by CO<sub>2(aq)</sub>. GABA, a non-protein amino acid, typically accumulates in stressed plants, often

exceeding levels observed in amino acids involved in protein synthesis (Kinnersley and Turano 2000).

The decrease in the biomass-specific N content in leaves under increasing  $\text{CO}_{2(\text{aq})}$  concentrations was associated with increased leaf density and thickness resulting from  $\text{CO}_{2(\text{aq})}$  enrichment. The increased mass per unit area in  $\text{CO}_2$ -enriched eelgrass leaves resulted from an increased number of mesophyll cells rich in carbon (as cellulose, carbohydrates), contributing to thicker leaves. Micrograph analysis of leaf cross-sections from  $\text{CO}_2$ -enriched eelgrass leaves, obtained from a concurrent study with the same plants (Celebi-Ergin et al. 2021), revealed increased thickness in the mesophyll and air lacunae layers, with minor changes noted in the epidermis layer, where most of the N (as proteins, enzymes, chloroplasts, etc.) is concentrated (Kuo and Hartog 2006). Consequently, the reduction in N content per gram of leaf was likely a result of dilution effects caused by the significant  $\text{CO}_2$ -stimulated accumulation of carbon in thicker leaves, rather than being a result of N-limitation. Further evidence against N-limitation in this study includes the positive growth responses observed under elevated  $\text{CO}_{2(\text{aq})}$  conditions, coupled with higher leaf N content on a per-area basis.

Examining the N:S ratio offers an additional means to assess N-limitation in plants, given its role as an indicator of nutritional quality and a proxy for N-limitations in terrestrial plants (Gülüt and Hoşgökdelen 2021). This is due to the interconnectedness of N and S in protein synthesis, which influences the availability of these elements within plants. The established N:S for optimal plant growth (7:1 to 15:1) can vary widely depending on plant species and environmental conditions but generally averages around 12:1, as reported in various literature values (Martin and Matocha 1973; Gülüt and Hoşgökdelen 2021; Zenda et al. 2021). If the optimal molar N:S ratios in eelgrass are comparable to those in terrestrial plants, the findings in this study suggest that

eelgrass is not limited by N based on the observed N:S ratios, which ranged between 6:1 and 20:1 as illustrated in Fig. 10B, even during periods of high growth induced by  $\text{CO}_{2(\text{aq})}$  enrichment.

The dilution of N by C resulted in the elevated molar C:N ratio in  $\text{CO}_2$ -enriched eelgrass leaf tissues in this study. At highest  $\text{CO}_{2(\text{aq})}$  level ( $2121 \mu\text{M CO}_{2(\text{aq})}$ ), the leaf C:N ratio increased by more than 35% compared to the established elemental ratio of 16C:1N (Duarte 1990), except during the winter when the ratio remained comparable to the established value. The  $\text{CO}_2$ -induced shift in nutrient status followed the trend observed in many marine phytoplankton (Burkhardt et al. 1999) and is consistent with values reported for *Thalassia* spp. under both field and laboratory conditions (Jiang et al. 2010; Campbell and Fourqurean 2013). The transition to a higher C:N ratio in the nutrient stoichiometry carries significant ecological consequences for marine ecosystem, particular in sediment biogeochemistry. Leaf nutrient quality serves as a robust indicator of the litter decomposition rates (Enríguez et al. 1993; Ouyang and Lee 2022) and high C:N ratio, indicative of reduced N content or an elevated carbon-nitrogen balance, may lead to slower decomposition rates due to lower microbial activities associated with low litter quality (Goldman et al. 1987). Slow decomposition rates can enhance carbon sequestration as more organic carbon can be retained in the sediment over time rather than being released to the atmosphere as  $\text{CO}_2$  (Gu et al. 2023). Predicted future  $\text{CO}_2$  concentrations may, therefore, promote blue carbon storage in sediments. However, high  $\text{CO}_2$  conditions may have less favorable impacts on trophic interactions, potentially altering nutritional quality of eelgrass based on the observed patterns in molar leaf C:N and N:S ratios in this study.

Although the ocean pH is not expected to decline to 6.1 (the lowest pH treatment in this study) in the near future, a 0.3 unit drop is expected by 2100 (Bindoff et al. 2019). Using the linear relationship established for C:N vs. pH (or  $\text{CO}_{2(\text{aq})}$ ), the C:N ratio of eelgrass in the Chesapeake

Bay is predicted to experience a 12% increase by 2100. If nitrogen is the benchmark for nutritional quality, the shift towards heavier C:N ratio means lowering of nutritional quality, which in turn may influence plant-herbivore interactions (Zvereva and Kozlov 2006; Stiling and Cornelissen 2007; Hernán et al. 2016). How grazers respond to lower nutritional quality will depend on the nutrient requirement of the grazers but consumption is expected to increase since grazers must consume more leaf tissue to compensate for the decreased N content. In two separate feeding experiments, the sea urchin consumptions of *Cymodocea nodosa* (Jiménez-Ramos et al. 2017) and *Posidonia oceanica* leaves and seedlings (Hernán et al. 2016) showed positive correlation to CO<sub>2</sub> concentrations. CO<sub>2</sub> enrichment decreased the N content of *P. oceanica* seedlings and >50% of these seedlings were consumed by sea urchins relative to the unenriched seedlings. Using pH levels as indicators of CO<sub>2</sub> concentrations, Jiménez-Ramos et al. (2017) found that sea urchins preferred CO<sub>2</sub> enriched over unenriched *C. nodosa* leaves, which contained lower phenolic acids, a grazing deterrent compound. All things considered, seagrasses in future ocean will likely face greater risk from increased grazing pressure that may counter the positive effects of CO<sub>2</sub> availability.

#### **2.4.2 Whole plant response under increasing CO<sub>2(aq)</sub> concentrations**

CO<sub>2(aq)</sub> enrichment had a distinctly positive impact on the carbon balance of eelgrass shoot consistent with terrestrial C<sub>3</sub> plants (Leakey et al. 2009), fleshy marine macroalgae (Gao et al. 1991; Suárez-Álvarez et al. 2011) and many other seagrass species (Jiang et al. 2010). Sucrose availability affects the sugar sensing system in higher plants and modulates the gene expressions that controls resource allocations between plant compartments, storage and utilization (Koch 1996). Although sucrose production occurred in the leaves, most of it accumulated in the rhizomes, then leaves and little in the roots, a trend consistent with other *Z. marina* and seagrass studies

(Touchette and Burkholder 2000b). There was also evidence of downward translocation of sucrose from leafy shoot to rhizome based on increasing rhizome sucrose contents (8% to 15% dry weight) with increasing  $\text{CO}_{2(\text{aq})}$  concentrations. Mobilization of substrates between plant structures have been documented based on direct measurements from short term  $^{14}\text{C}$  incubation studies (Harrison 1978; Zimmerman and Alberte 1996; Marbà et al. 2002), therefore it was not surprising to see higher net sucrose accumulation in the rhizome than leaves with the  $\text{CO}_2$  subsidy. Increased accumulation of sucrose and storage in rhizomes provide carbon reserves to support a doubling of absolute growth rates during the second year. This finding suggests that sucrose reserves may play an important role in regulating and signaling growth rates. Furthermore, large sucrose reserves can lead to earlier flowering shoot initiation and increased flowering rates as discussed earlier. We expected the roots to respond similarly, however, roots sucrose content was consistently at 4% dry weight regardless of  $\text{CO}_2$  treatment and lacked any appreciable trend.

This 18-month study highlights eelgrass responses to prolonged  $\text{CO}_{2(\text{aq})}$  enrichment, emphasizing the need for seasonal experimental durations for accurate assessments of plant performance. Increased  $\text{CO}_{2(\text{aq})}$  availability could improve seagrass resilience to climate change by enhancing their C and N metabolism, resulting in positive carbon balance to support increased growth. Increased  $\text{CO}_{2(\text{aq})}$  concentrations may not always lead to N-limitation as nutrient status depends on the balance between the growth demand and N supply. In addition, seagrasses are also sensitive to environmental changes, including light, temperature, and nutrient levels. The interactive effects of  $\text{CO}_{2(\text{aq})}$  and these factors can lead to complex responses in seagrass ecosystems. For instance, while  $\text{CO}_2$ -stimulated growth and productivity, other environmental stressors, such as eutrophication could offset these benefits. Understanding the intricate

relationship between  $\text{CO}_{2(\text{aq})}$  and environmental variables is essential for predicting the future health and resilience of seagrass habitats in the face of ongoing climate change.

## CHAPTER 3

### IMPACTS OF ELEVATED CO<sub>2</sub> AND SEDIMENT EUTROPHICATION ON *ZOSTERA MARINA* L.: AN ENRICHMENT STUDY

#### 3.1 Introduction

Seagrass ecosystems are increasingly exposed to multiple anthropogenic stressors that can act to enhance or limit vegetative survival and reproductive success. Anthropogenic CO<sub>2</sub> is not the only global antagonists in future ocean invoking physiological changes in seagrass. Seagrasses are also dealing with a more localized stressors such as eutrophication, sediment loading and physical disturbance. Though these global and local stressors can individually influence seagrass growth and survival, they rarely act in isolation. In particular, the response of seagrasses to a changing climate will also depend on how they respond to these local stresses.

Eutrophication is a chronic problem in coastal system and implicated as the major cause of large-scale seagrass habitat loss worldwide (Orth et al. 2006; Burkholder et al. 2007; Koch et al. 2007; Waycott et al. 2009). Nitrogen pollution from point and non-point sources can stimulate nuisance algal growth in coastal waters, reducing light available for seagrass photosynthesis (Burkholder et al. 2007). In addition to light reduction, eutrophication can exert a more direct physiological impact from nitrogen (N) toxicity (Burkholder et al. 1992; van der Heide et al. 2008a). The thresholds for N toxicity vary widely depending on the seagrass species, the form of nitrogen (e.g., NO<sub>3</sub><sup>-</sup> vs. NH<sub>4</sub><sup>+</sup>) the source (water column vs. sediment) and the duration of exposure (days vs. weeks), but dissolved inorganic N (DIN) as low as 30 μmol L<sup>-1</sup> can cause irreversible damage to the leaves, resulting in shoot mortality of *Zostera marina* L. (eelgrass) (van Katwijk et

al. 1997; Brun et al. 2002; Govers et al. 2014). The exact underlying mechanism responsible for toxicity related death remains inconclusive but it is known that  $\text{NH}_4^+$  additions can cause a reduction in carbohydrate (sugar) content and instigate internal carbon and nitrogen imbalance in both terrestrial (Matsumoto et al. 1971; Lindt and Feller 1987) and aquatic plants (Brun et al. 2002; Cao et al. 2004). High  $\text{NH}_4^+$  concentrations can quickly exhaust fixed carbon reserves, particularly  $\alpha$ -ketoglutarate, during rapid detoxification of  $\text{NH}_4^+$  into amino acids (Givan 1979; Lancien et al. 2000; Cruz et al. 2006). The depletion of carbon skeleton may exert negative feedback on N assimilation allowing  $\text{NH}_4^+$  to accumulate inside the cell to levels that are detrimental to metabolic functions and survival (Kosegarten et al. 1997; Britto et al. 2001; Qin et al. 2011). These observations have led some to suggest carbon limitation as the leading cause of N toxicity related seagrass death in eutrophic environment (Kaldy et al. 2022).

In eutrophic environments, the deposition of large quantities of organic materials (OM) resulting from algal blooms and seagrass detritus can enhance the anaerobic OM decomposition and consequently sulfide ( $\text{H}_2\text{S}$ ) production in these anoxic sediments (Jørgensen et al. 2019). In the absence of oxygen, sulfate reduction is the predominant mineralization process responsible for up to 90% of the organic carbon oxidation in highly productive, estuarine and marine sediments (Jørgensen 1982; Burdige 2006). The accelerated rate of this process can lead to elevated concentrations of  $\text{H}_2\text{S}$ , particularly in carbonate sediments that possess a low iron content. Reactive iron in siliciclastic sediments may reduce  $\text{H}_2\text{S}$  concentrations by facilitating the formation of iron monosulfide precipitates. These precipitates render  $\text{H}_2\text{S}$  biologically unavailable (Canfield 1989; Kraal et al. 2013). However, when  $\text{H}_2\text{S}$  levels are high, the iron buffering capacity can become overwhelmed, leading to the accumulation of toxic concentrations that can harm seagrasses. Toxicity occurs as a result of  $\text{H}_2\text{S}$  intrusions through the roots into the lacunae and the meristem

tissues, causing various adverse physiological damages. Sulfide is a potent phytotoxin and extremely harmful to seagrass even at low concentrations. Studies have shown that a 1-10  $\mu\text{M}$   $\text{H}_2\text{S}$  can cause disruption to meristematic cell division (Garcias-Bonet et al. 2008), and concentrations  $>100 \mu\text{M}$  can stop photosynthetic activity, reduce carbohydrate reserves in roots, inhibit growth and cause death (Holmer and Bondgaard 2001; Koch and Erskine 2001; Mascaró et al. 2009; Dooley et al. 2013).

To prevent  $\text{H}_2\text{S}$  intrusion and its deleterious effects, seagrasses rely on the oxygen produced during daily photosynthesis to support root aerobiosis and detoxify  $\text{H}_2\text{S}$  (Smith et al. 1984; Hasler-Sheetal et al. 2015). Since only a small fraction, between 4 and 10% of the photosynthetic oxygen produced is transported through the aerenchyma to the belowground structures, and about 1% of that is leaked from the roots to the surrounding rhizosphere, the ability to curtail  $\text{H}_2\text{S}$  intrusion can become increasingly challenging in organic-rich sediments and in low light environments (Borum et al. 2005; Borum et al. 2006; Burdige et al. 2008). However,  $\text{CO}_2$  stimulated photosynthesis should enhance the oxygen transport to the roots and rhizomes thus influencing the seagrass-sulfide dynamics and alleviate toxicity.

The response of seagrasses to future climate change will depend on many factors that act simultaneously and interactively. The goal of this study was to examine how  $\text{CO}_2$ , nutrient availability and organic matter loading together act to influence biochemical composition, growth, and survival of eelgrass. This study hypothesized that  $\text{CO}_2$  enrichment will increase the survival of eelgrass in nutrient and organic carbon enriched sediments.

## **3.2 Materials and methods**

### **3.2.1 Sediment and plant collections**

Both sediments and plants were collected in April 2014. Sediments were collected from the Elizabeth River (Virginia, USA), an intertidal system of the lower Chesapeake Bay, about 3 meters from the shoreline. The grain size distribution was determined using a laser diffraction technique on the Malvern Mastersizer 2000 (Particle Size Analyzer). The sediment contained a mixture of fine to coarse-grained sand and debris including plant materials, algae, and shell fragments. The presence of these debris could potentially interfere with the experiment; therefore, they were preemptively removed by hand as a precautionary measure. Eelgrass shoots were collected by hand from the South Bay coastal lagoon on the eastern shore of the DelMarVa Peninsula and transplanted within 24 hours of collection to the outdoor CO<sub>2</sub> experimental facility at Virginia Beach Aquarium (Virginia) as described in Chapter 2.

### **3.2.2 Sediment fertilization and CO<sub>2(aq)</sub> enrichment**

The interactive effects of sediment fertilization and CO<sub>2(aq)</sub> enrichment on plant performance was determined using four fertilization treatments distributed across five pH (or CO<sub>2(aq)</sub>) levels, with two replicates for each fertilizer × pH (or CO<sub>2(aq)</sub>) treatment. The four fertilization treatments included: (i) bare sediment (Control), (ii) sediment enriched with the slow-release commercial plant fertilizer Osmocote® containing N:P:K ratio of 19 (10% ammoniacal, 9% nitrate):6:12 (% wt./wt.), (iii) sediment enriched with organic carbon (OC) consisting of reagent grade starch (C<sub>12</sub>H<sub>22</sub>O<sub>11</sub>) and cellulose (C<sub>6</sub>H<sub>10</sub>O<sub>5</sub>) powder (Sigma-Aldrich®), and (iv) sediment enriched with both Osmocote® and organic carbon (NPKOC treatment) (Fig. 19). The nitrogen and organic carbon dosing were adapted from Govers et al. (2014) to induce toxicity (N

and  $\text{H}_2\text{S}$ ) to plants and enrich porewater to levels comparable to highly eutrophic system (Santamaría et al. 1994; Peralta et al. 2003; Holmer et al. 2005; Koch et al. 2007; Lamers et al. 2013). To simulate the effects of nutrient loading on plant performance, 27 g of Osmocote® pellets were added to 2 Kg of dried sediment (bulk density of  $1.5 \text{ g cm}^{-3}$ ), resulting in a total loading of approximately  $4 \text{ mg N cm}^{-3}$ . Sediments and pellets were thoroughly mixed in a small plastic barrel, manually tumbled until they were well blended.

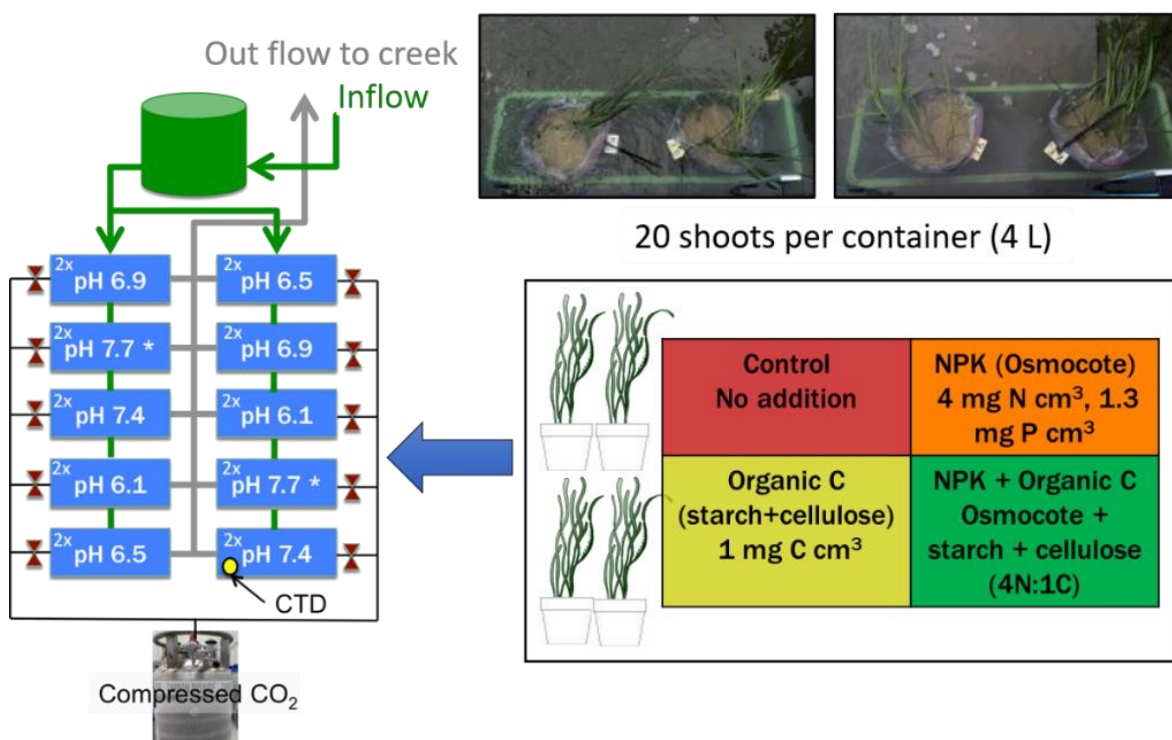


**Fig. 19.** Sediment fertilization and  $\text{CO}_{2(\text{aq})}$  enrichment experimental design. Details of the schematic diagram of the outdoor  $\text{CO}_2$  enrichment facility was provided in Chapter 2 (see Fig. 1). *Zostera marina* L. collected from South Bay (Eastern Shore, Virginia) was transplanted into 4-liter plastic plant pot, each containing 2Kg pre-treatment sediments. The sediment types include: Control (no fertilization) (red), NPK (fertilized with Osmocote®) (orange), organic carbon (yellow), and NPKOC (green). A set of each sediment type (four plant pots in total) was placed in ten of the twenty  $\text{CO}_2$  aquaria poised at 5 pH (or  $\text{CO}_{2(\text{aq})}$ ) levels.

To isolate the effects of H<sub>2</sub>S toxicity in plants, 1.5 g of starch and 1.5 g of cellulose powder were mixed into to 2 Kg of dried sediments to stimulate *in situ* H<sub>2</sub>S production. The additions provided a total loading of approximately 1 mg C cm<sup>-3</sup> sediment. To mimic a eutrophic sediment type, a combination of Osmocote® and organic carbon was added to the NPKOC treatment at a 4N:1C ratio. A control treatment consisting of unenriched sediment was added to the experimental design to provide a baseline comparison of plant performances amongst treatments. All sediment types received identical manual mixing treatments as described above to ensure sediment homogeneity and avoid bias due to mixing.

Twenty healthy eelgrass shoots with intact rhizomes and roots were transplanted into a 1-gallon (4 L) round pots (16.5 cm diameter × 17.8 cm height) lined with plastic. Each pot contained one of the four sediment types: Control, NPK, OC, and NPKOC. Due to limited space caused by concurrent experiment at the CO<sub>2</sub> enrichment facility, a set of each sediment type (four plant pots in total) was placed in ten of the twenty CO<sub>2</sub> aquaria poised at 5 pH (i.e. CO<sub>2(aq)</sub>) levels. The plant pots were positioned near the outflow to flush away any diffused NH<sub>4</sub><sup>+</sup> and H<sub>2</sub>S from the sediments into the overlying water column throughout the two-months study. Detailed descriptions of the outdoor CO<sub>2</sub> experimental design were provided in the Methods section in Chapter 2. To briefly summarize, each aquarium (3 m<sup>3</sup>) was plumbed with running seawater (10 turnovers per day) from the adjacent Owls Creek (mean salinity of 24 ± 3). Each aquarium was continuously enriched with beverage grade, compressed CO<sub>2(g)</sub> from June 2013 to October 2014. The aqueous CO<sub>2</sub> (CO<sub>2(aq)</sub>) level in each aquarium was adjusted individually by using CO<sub>2</sub> bubblers with solenoid valves, which were controlled by Eutech Alpha 190 controller and transmitter equipped with submersible glass electrodes. Five levels of pH (or CO<sub>2(aq)</sub>) concentrations were maintained using this experimental set-up, ranging from ambient (~55 μmol CO<sub>2</sub> Kg<sup>-1</sup> SW, pH 7.7) to 2121 μmol CO<sub>2</sub>

$\text{Kg}^{-1}$  SW (pH 6.1). The treatments were spaced at approximately 0.5 pH unit intervals to achieve the desired range of  $\text{CO}_{2(\text{aq})}$  concentrations. The experiment commenced at the beginning of May of 2014 and terminated when plant mortality in at least 1 treatment exceeded 90% (July 2014).

### 3.2.3 Experimental conditions

Light level (PAR), pH, salinity and water temperature were continuously monitored by the  $\text{CO}_2$  experimental facility (see Chapter 2). Water chemistry in Owls Creek was monitored as part of the water quality monitoring program by the Virginia Beach Aquarium staff at their Water Quality Lab. Time series data of the macronutrient concentrations ( $\text{NH}_4^+$ ,  $\text{NO}_3^-$ , and  $\text{PO}_4^{3-}$ ) from 1998 to 2015 were provided by the Aquarium (M. Swingle unpubl. data). The aquarium conducted weekly monitoring of nutrients in the surface water from 1998 to 2012, transitioning to monthly monitoring from 2012 to 2015.

### 3.2.4 Porewater sampling and analyses

Interstitial porewater were collected weekly for of  $\text{NH}_4^+$ ,  $\text{NO}_x$  ( $\text{NO}_3^- + \text{NO}_2^-$ ),  $\text{PO}_4^{3-}$  and  $\text{H}_2\text{S}$  starting one week after transplantation. Samples were carefully withdrawn from each treatment at 5 cm below the sediment surface using a 15 mL plastic syringe fitted with a 3-way stop cock and a stainless-steel needle. The porewater samples were immediately filtered through a GF/F filter followed by a  $0.2 \mu\text{M}$  nucleopore disposable filter. Approximately 5 mL of filtered samples were collected and stored in a plastic nutrient vial and frozen until analyses.  $\text{NO}_x$  and  $\text{PO}_4^{3-}$  concentrations were analyzed on an Astoria-Pacific auto nutrient analyzer using standard methods (Parsons 2013). Ammonium was analyzed manually using the indophenol-hypochlorite method (Solorzano 1969).

Porewater H<sub>2</sub>S samples were collected from each treatment using a 5 mL gas-tight glass syringe fitted with a 3-way stopcock and a 5 cm long stainless-steel needle. A 1 mL sample was immediately transferred into a crimp-sealed glass serum bottle containing 9 mL fixing solution made up of equal volumes of deoxygenated 10 mM ZnCl<sub>2</sub> and 20 mM NaOH. Oxygen was removed from the headspace by flushing with N<sub>2</sub> gas immediately prior to crimping. The fixed samples were stored in a refrigerator at 4 °C until analysis the next day. Porewater H<sub>2</sub>S concentration was analyzed colorimetrically at 670 nm using the mixed diamine reagent method (Cline 1969) standardized to sodium H<sub>2</sub>S (Na<sub>2</sub>S<sub>9</sub>H<sub>2</sub>O).

### **3.2.5 Growth rates, plant size, and survival**

Shoots in each pot were counted at the beginning of the experiment and every two weeks thereafter until the end of the experiment. Immediately following the shoot count, one shoot per pot was randomly selected and tagged for growth measurements using the hole-punch method as described in Chapter 2 (Zieman 1974; Zimmerman et al. 1996). Subsequently, the tagged plants were evaluated for new growth, total leaf area (cm<sup>2</sup>), absolute growth rates (AGR, cm<sup>2</sup> d<sup>-1</sup>), and specific growth rates (SGR, % d<sup>-1</sup>) following the procedures outlined in the Methods section of Chapter 2. Survival was determined by normalizing the number of shoots to the initial shoot count. This calculation provided a quantification of the survival rate as a percentage at each respective measurement time point.

### **3.2.6 Plant biochemical and elemental compositions**

Plants tagged for growth were sampled for leaf sucrose, bulk free primary amino acid (FAA) contents and total carbon, nitrogen, and sulfur (CNS) compositions. The second youngest

leaf (L2) was collected, cleaned of all epiphytes by gentle scraping with a razor blade, rinsed in deionized water and then oven dried at 60 °C for at least 48 hours. The dried leaves ground to a powder in a mortar and pestle with liquid nitrogen. The powder was subsequently re-dried prior to chemical analysis. Leaf sucrose and FAA contents were extracted from measured aliquots of the dry powder using hot (80 °C) ethanol (Zimmerman et al. 1989). Leaf sucrose was determined colorimetrically using a resorcinol-hydrochloric acid assay and standardized to sucrose (Huber and Israel 1982). Leaf FAA were quantified fluorometrically after derivatization with *o*-phthalaldehyde (OPA) 2-mercaptoethanol (OPA-2MCE) and standardized to glycine.

Elemental C, N and S of leaf sample were quantified following the combustion-reduction method (Cutter and Radford-Knoery 1991) using an elemental analyzer (vario MICRO cube, Elementar) standardized to sulfanilamide ( $C_6H_8N_2O_2S$ ) as described in Chapter 2.

### **3.2.7 Statistical analysis**

All statistical analyses were carried out using the IBM SPSS Statistics 26. The effects of  $CO_{2(aq)}$  on porewater nutrients and  $H_2S$  were nonlinear; therefore, a two-way ANOVA was used to assess the contrasting effects of  $CO_{2(aq)}$  and sediment enrichments at each sampling time point. Where ANOVA results were significant, a post hoc test using Tukey HSD was used for multiple comparisons. Significant changes in plant physical and physiological responses (within subjects) were tested using a repeated measure ANCOVA implemented within the linear mixed model in SPSS. The aquaria were designated as the repeated subject; time and sediment treatments (between subjects) were considered fixed effects while  $\log CO_{2(aq)}$  (i.e. pH) was assigned as the covariate. Data lacking statistical differences amongst  $CO_{2(aq)}$  and/or sediment effects were combined to

increase the degrees of freedom. Any heteroscedastic data was log-transformed to avoid violating the equality of variances assumption in ANOVA.

### **3.3 Results**

#### **3.3.1 Environmental parameter**

Chapter 2 provided a detailed description of PAR levels, salinity, and water temperature. Furthermore, data obtained from the Virginia Beach Aquarium highlighted a significant presence of macronutrients ( $\text{NH}_4^+$ ,  $\text{NO}_2^- + \text{NO}_3^-$ , and  $\text{PO}_4^{3-}$ ) in the surface water of Owls Creek, as presented in Chapter 2, Fig. 3. The distribution of nutrient concentrations was non-normal, as evident from the box plot in Fig. 3D, with median values of  $4.9 \mu\text{M}$  for  $\text{NH}_4^+$ ,  $3.1 \mu\text{M}$  of  $\text{NO}_2^- + \text{NO}_3^-$ , and  $0.9 \mu\text{M}$  of  $\text{PO}_4^{3-}$ . The nutrient dataset exhibited notable variability, although nutrient levels were predominantly low. However, few occasional spikes were observed, particularly for  $\text{NO}_2^- + \text{NO}_3^-$  and  $\text{PO}_4^{3-}$  likely related to meteorological events. The highest record concentrations were  $26 \mu\text{M}$  for  $\text{NH}_4^+$ ,  $125 \mu\text{M}$  for  $\text{NO}_2^- + \text{NO}_3^-$ , and  $31 \mu\text{M}$  for  $\text{PO}_4^{3-}$ . Sediment composition was mostly made up of medium sand grains (70%) with a mixture of very fine sand (13%) and coarse sand grains (17%) (Fig. 20).

#### **3.3.2 Effects of $\text{CO}_{2(\text{aq})}$ and sediment enrichment on porewater chemistry**

The addition of nutrients and organic carbon to the sediments had the anticipated effect of elevating porewater  $\text{NH}_4^+$ ,  $\text{NO}_3^-$ ,  $\text{PO}_4^{3-}$ , and  $\text{H}_2\text{S}$  concentrations (Fig. 21 and 22). In the nutrient enriched sediments, porewater concentrations of  $\text{NH}_4^+$ ,  $\text{NO}_3^-$  and  $\text{PO}_4^{3-}$  exhibited a rapid increase during the initial 30 days of the experiment, followed by a subsequent decline, but the levels remained notably higher than those observed on day 11, which marked the first porewater

measurements. The highest concentrations measured for  $\text{NH}_4^+$ ,  $\text{NO}_3^-$  and  $\text{PO}_4^{3-}$  were between 10 to 10,000 times higher than those observed in the Control or OC treatment. Interestingly, the  $\text{CO}_{2(\text{aq})}$  (or pH) treatments did not exert a significant impact on porewater  $\text{NO}_3^-$  and  $\text{PO}_4^{3-}$  concentrations across any of the four sediment treatments (Table 6). Additionally,  $\text{CO}_{2(\text{aq})}$  enrichment showed no significant impact on porewater  $\text{H}_2\text{S}$  concentrations. Consequently, samples from all  $\text{CO}_{2(\text{aq})}$  treatments were combined, and the effects of OC additions on  $\text{H}_2\text{S}$  levels were assessed. The addition of OC to the sediment significantly increased porewater  $\text{H}_2\text{S}$  levels to over  $600 \mu\text{M}$  by day 10 of the experiment. Subsequently, the  $\text{H}_2\text{S}$  concentrations gradually declined, reaching  $101 \pm 36$  (SE)  $\mu\text{M}$  by the end of the experiment, as illustrated in Fig. 22C. It is important to note that the addition of inorganic nutrients (Osmocote®) appeared to prevent the OC-stimulated production of  $\text{H}_2\text{S}$  in the NPKOC treatment throughout the entire experiment (Fig. 22D). The mean  $\text{H}_2\text{S}$  concentration of the NPKOC treatment was not different from the means of the Control and NPK treatments, as depicted in Table 7. Porewater sulfide concentrations remained low ( $5 - 25 \mu\text{M}$ ) and relatively constant throughout the experiment in the Control, NPK and NPKOC treatments.

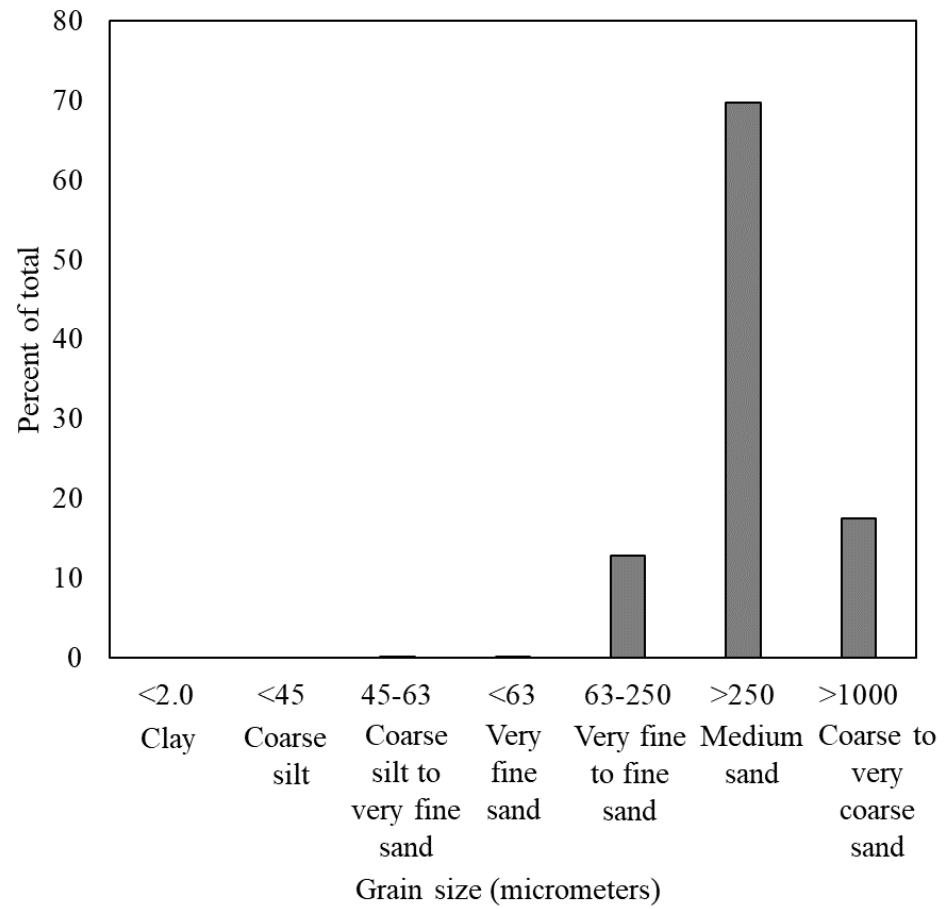


**Fig. 20.** Percentage distribution of sediment grain sizes from Elizabeth River, obtained at the Sailing Center (Old Dominion University, Norfolk, Virginia). The values are representative of the Wentworth size class.

**Table 6.** Two-way ANOVA results for the effects of log CO<sub>2(aq)</sub> (pH levels = 6.1, 6.4, 6.9, 7.4, 7.7) and treatments on pore water NH<sub>4</sub><sup>+</sup>, NO<sub>3</sub><sup>-</sup>, and PO<sub>4</sub><sup>3+</sup> concentrations from May to July 2014. Treatments correspond to the four sediment types: Control, NPK, OC, and NPKOC.

|                                      | NH <sub>4</sub> <sup>+</sup> (mM) |    |       |          |          | NO <sub>3</sub> <sup>-</sup> (mM) |    |       |          |          | PO <sub>4</sub> <sup>3-</sup> (μM) |    |         |          |          |
|--------------------------------------|-----------------------------------|----|-------|----------|----------|-----------------------------------|----|-------|----------|----------|------------------------------------|----|---------|----------|----------|
|                                      | SS                                | df | MS    | <i>F</i> | <i>p</i> | SS                                | df | MS    | <i>F</i> | <i>p</i> | SS                                 | df | MS      | <i>F</i> | <i>p</i> |
| <u>Day 11</u>                        |                                   |    |       |          |          |                                   |    |       |          |          |                                    |    |         |          |          |
| Treatments                           | 26685                             | 3  | 8895  | 165.42   | <0.001   | 1511                              | 3  | 5040  | 26.97    | <0.001   | 297343                             | 3  | 99114   | 29.60    | <0.001   |
| log CO <sub>2(aq)</sub>              | 255                               | 4  | 64    | 1.19     | 0.35     | 230                               | 4  | 57    | 0.31     | 0.87     | 2689                               | 4  | 672     | 0.20     | 0.94     |
| Treatments x log CO <sub>2(aq)</sub> | 562                               | 12 | 47    | 0.87     | 0.59     | 823                               | 11 | 75    | 0.40     | 0.93     | 15902                              | 12 | 1325    | 0.40     | 0.95     |
| Error                                | 1022                              | 19 | 54    |          |          | 2055                              | 11 | 187   |          |          | 66965                              | 20 | 3348    |          |          |
| <u>Day 26</u>                        |                                   |    |       |          |          |                                   |    |       |          |          |                                    |    |         |          |          |
| Treatments                           | 54805                             | 3  | 18268 | 378.20   | <0.001   | 91548                             | 3  | 30516 | 69.57    | <0.001   | 2732551                            | 3  | 910850  | 18.34    | <0.001   |
| log CO <sub>2(aq)</sub>              | 487                               | 4  | 122   | 2.52     | 0.07     | 3712                              | 4  | 928   | 2.12     | 0.12     | 287024                             | 4  | 71756   | 1.45     | 0.26     |
| Treatments x log CO <sub>2(aq)</sub> | 680                               | 12 | 57    | 1.17     | 0.36     | 10244                             | 12 | 854   | 1.95     | 0.09     | 1002318                            | 12 | 83527   | 1.68     | 0.15     |
| Error                                | 966                               | 20 | 48    |          |          | 8334                              | 19 | 439   |          |          | 993495                             | 20 | 49675   |          |          |
| <u>Day 68</u>                        |                                   |    |       |          |          |                                   |    |       |          |          |                                    |    |         |          |          |
| Treatments                           | 34342                             | 3  | 11447 | 159.18   | <0.001   | 38335                             | 3  | 12778 | 59.15    | <0.001   | 3292336                            | 3  | 1097445 | 32.51    | <0.001   |
| log CO <sub>2(aq)</sub>              | 2103                              | 4  | 526   | 7.31     | 0.001    | 3043                              | 4  | 761   | 2.79     | 0.04     | 107664                             | 4  | 26916   | 0.80     | 0.54     |
| Treatments x log CO <sub>2(aq)</sub> | 3712                              | 12 | 309   | 4.30     | 0.002    | 4398                              | 12 | 367   | 1.70     | 0.14     | 364857                             | 12 | 30405   | 0.90     | 0.56     |
| Error                                | 1438                              | 20 | 72    |          |          | 4321                              | 20 | 216   |          |          | 675090                             | 20 | 33755   |          |          |

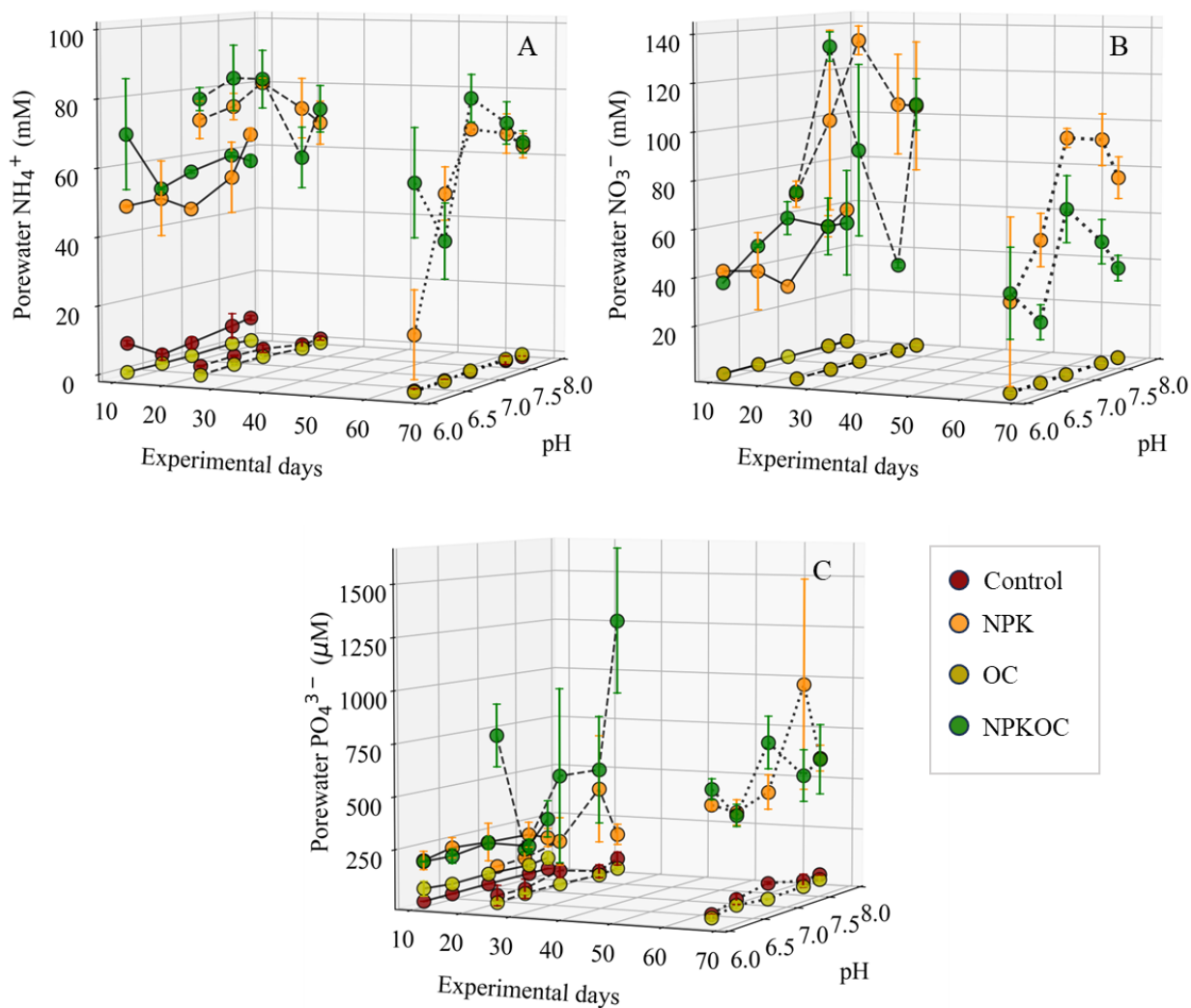


**Fig. 21.** The porewater concentrations of  $\text{NH}_4^+$  (A),  $\text{NO}_3^-$  (B), and  $\text{PO}_4^{3-}$  (C) for each sediment treatment: Control (red), NPK (orange), OC (yellow), NPKOC (green). Concentrations (z-axis) were plotted as a function of pH (NBS scale) (x-axis) and time (y-axis). The plot includes three time points: a solid line represents day 11, dash line represents day 26, and dotted line represents day 68. Each data point represents the mean nutrient concentrations ( $n = 2$ ) of each pH (or  $\text{CO}_{2(\text{aq})}$ ) treatment, with the error bars denoting the standard error (SE) for the measurements.

**Table 7.** Two-way ANOVA results for the effects of log CO<sub>2(aq)</sub> (pH levels = 6.1, 6.4, 6.9, 7.4, 7.7) and treatments (Control, NPK, OC, and NPKOC) on porewater H<sub>2</sub>S concentrations from May to July 2014. Multiple comparisons of H<sub>2</sub>S concentrations amongst sediment treatments were performed and grouped based on result of a Tukey HSD pos hoc analysis. An equal sign between treatments indicated that the means did not differ as *p*-value was >0.05.

|                                      | SS      | df | MS     | <i>F</i> | <i>p</i>         | Pos Hoc Tukey HSD<br>Homogeneous group                                |
|--------------------------------------|---------|----|--------|----------|------------------|---|
| <u>Day 11</u>                        |         |    |        |          |                  |   |
| Treatments                           | 2144270 | 3  | 714757 | 29.05    | <b>&lt;0.001</b> | Control = NPK = NPKOC, <i>p</i> = 1; OC, <i>p</i> = 1                 |
| log CO <sub>2(aq)</sub>              | 89160   | 4  | 22290  | 0.91     | 0.48             |   |
| Treatments x log CO <sub>2(aq)</sub> | 259608  | 12 | 21634  | 0.88     | 0.58             |   |
| Error                                | 418338  | 17 | 24608  |          |                  |   |
| <u>Day 26</u>                        |         |    |        |          |                  |   |
| Treatments                           | 2291387 | 3  | 763796 | 16.78    | <b>&lt;0.001</b> | Control = NPK = NPKOC, <i>p</i> = 1; OC; <i>p</i> = 1                 |
| log CO <sub>2(aq)</sub>              | 156608  | 4  | 39152  | 0.86     | 0.51             |   |
| Treatments x log CO <sub>2(aq)</sub> | 487212  | 12 | 40601  | 0.89     | 0.57             |   |
| Error                                | 864859  | 19 | 45519  |          |                  |   |
| <u>Day 68</u>                        |         |    |        |          |                  |   |
| Treatments                           | 61909   | 3  | 20636  | 4.64     | <b>0.01</b>      | NPK= NPKOC = Control, <i>p</i> = 0.97; Control = OC, <i>p</i> = 0.057 |
| log CO <sub>2(aq)</sub>              | 7507    | 4  | 1877   | 0.42     | 0.79             |   |
| Treatments x log CO <sub>2(aq)</sub> | 21817   | 12 | 1818   | 0.41     | 0.94             |   |
| Error                                | 89051   | 20 | 4453   |          |                  |   |

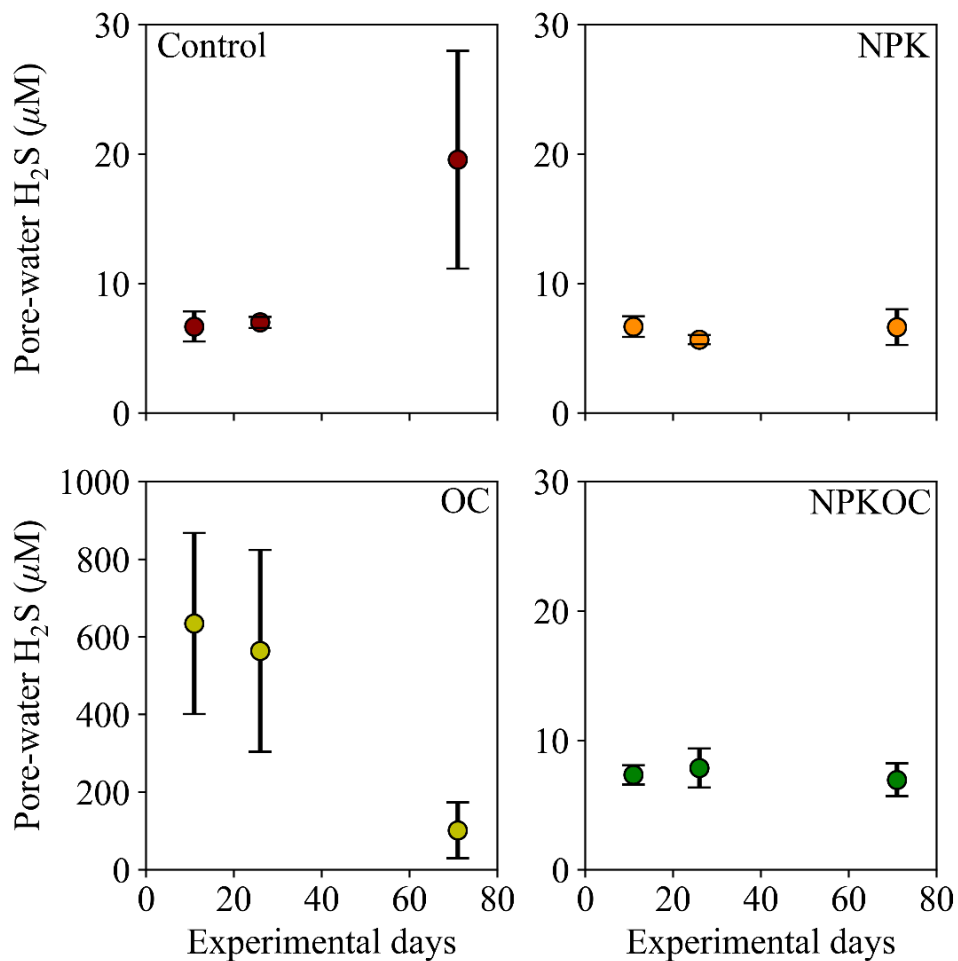


**Fig. 22.** Porewater  $H_2S$  concentrations measured in Control, NPK, OC, and NPKOC sediment treatments from May to July 2014. Each data point represents the average  $H_2S$  concentrations ( $n = 10$ ) calculated from all  $CO_{2(aq)}$  treatments combined (the effects of  $CO_{2(aq)}$  enrichment on porewater  $H_2S$  concentrations were not significant, see Table 7 for 2-way ANOVA summary). The error bars represent the 95% confidence limit.

### 3.3.3 Effects of CO<sub>2(aq)</sub> and sediment enrichment on plant performances

Shoot numbers declined in all sediment treatments over time. Shoot numbers did not respond to CO<sub>2(aq)</sub> enrichment (Table 8), therefore measurement across all CO<sub>2(aq)</sub> treatments were combined to evaluate the effects of sediment treatment types (Fig. 23A) and porewater chemistry (Fig. 24) on survival. A two-way ANOVA was performed to determine if sediment treatments (Control, OC, NPK, NPKOC) and CO<sub>2(aq)</sub> enrichment (pH 6.1 to 7.7) had a significant effect on shoot numbers at days 15 (initial), 32, 46, and 67 (end of experiment). Apart from day 15, sediment treatments significantly reduced shoot numbers (Table 8). Furthermore, Tukey's test for multiple comparisons indicated that shoot numbers in OC treatments were significantly different from NPK and NPKOC treatments, but not significantly different from the Control.

Eelgrass survival (shoot numbers normalized to starting shoot number transplanted) was the highest in the Control treatment (Fig. 23A), though there was a 40% decline in shoot numbers, likely due to the initial stress from transplantation. The impact of sediment manipulation on survival was particularly pronounced in the NPK and NPKOC treatments, where between 80 and 90% of the shoots were dead after 30 days of exposure to elevated nutrients. By day 67, less than 10% of the initially planted shoots survived in these treatments. Compared to the nutrient enriched sediments, more shoots survived (~40%) in the OC treatment suggesting that plants were more tolerant to organic carbon-induced H<sub>2</sub>S production than nutrient loading (i.e. NH<sub>4</sub><sup>+</sup> and NO<sub>3</sub><sup>-</sup>) even though porewater H<sub>2</sub>S approached 1000 μM in the OC treatment (Fig. 23 and 24).

**Table 8.** Two-Way ANOVA results for the effects log CO<sub>2(aq)</sub> (pH levels = 6.1, 6.4, 6.9, 7.4, 7.7) and treatments (Control, NPK, OC, and NPKOC) on log-transformed shoot numbers from May to July 2014. Shoot numbers were log-transformed to remove heteroscedasticity. Multiple comparisons were performed and grouped based on result of a Tukey HSD pos hoc analysis. An equal sign between treatments indicated that the means did not differ as  $p$ -value was  $>0.05$ .

|                                      | Type III SS | df | MS   | $F$    | $p$              | Post Hoc Tukey HSD<br>Homogeneous group                |
|--------------------------------------|-------------|----|------|--------|------------------|--|
| <u>Day 15</u>                        |             |    |      |        |                  |  |
| Treatments                           | 0.04        | 3  | 0.01 | 1.63   | 0.21             | Control = NPK = OC = NPKOC, $p = 0.19$                 |
| log CO <sub>2(aq)</sub>              | 0.03        | 4  | 0.01 | 0.87   | 0.50             |  |
| Treatments x log CO <sub>2(aq)</sub> | 0.12        | 12 | 0.01 | 1.22   | 0.34             |  |
| Error                                | 0.16        | 20 | 0.01 |        |                  |  |
| <u>Day 32</u>                        |             |    |      |        |                  |  |
| Treatments                           | 4.02        | 3  | 1.34 | 26.87  | <b>&lt;0.001</b> | Control = OC, $p = 0.25$ ;<br>NPK = NPKOC, $p = 0.95$  |
| log CO <sub>2(aq)</sub>              | 0.22        | 4  | 0.05 | 1.09   | 0.40             |  |
| Treatments x log CO <sub>2(aq)</sub> | 1.06        | 11 | 0.10 | 1.94   | 0.12             |  |
| Error                                | 0.70        | 14 | 0.05 |        |                  |  |
| <u>Day 46</u>                        |             |    |      |        |                  |  |
| Treatments                           | 3.93        | 3  | 1.31 | 137.68 | <b>&lt;0.001</b> | Control $\neq$ NPK $\neq$ OC $\neq$ NPKOC, $p = 1$     |
| log CO <sub>2(aq)</sub>              | 0.16        | 4  | 0.04 | 4.26   | <b>0.02</b>      |  |
| Treatments x log CO <sub>2(aq)</sub> | 0.48        | 10 | 0.05 | 5.05   | 0.01             |  |
| Error                                | 0.11        | 12 | 0.01 |        |                  |  |
| <u>Day 67</u>                        |             |    |      |        |                  |  |
| Treatments                           | 2.81        | 3  | 0.94 | 34.42  | <b>&lt;0.001</b> | Control = OC, $p = 0.124$ ;<br>NPK = NPKOC, $p = 0.10$ |
| log CO <sub>2(aq)</sub>              | 0.12        | 4  | 0.03 | 1.10   | 0.41             |  |
| Treatments x log CO <sub>2(aq)</sub> | 0.66        | 8  | 0.08 | 3.03   | 0.05             |  |
| Error                                | 0.27        | 10 | 0.03 |        |                  |  |

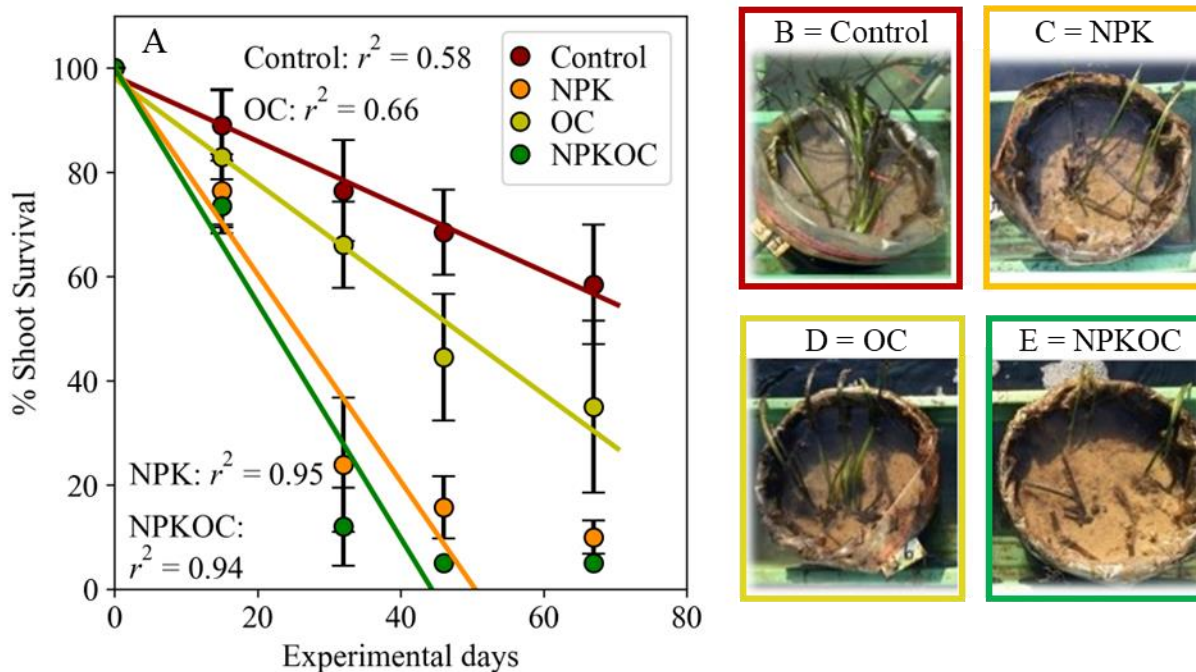


**Fig. 23.** Percent survival (A) plotted as a function of time for the four sediment types: Control (red), NPK (orange), OC (yellow), and NPKOC (green) from May to July 2014. In the Control and OC treatments, percent survival exhibited a linear decrease from days 0-67, while in the NPK and NPKOC treatments, they decreased linearly from days 0-47. Error bars denote 95% confidence interval (CI) error ( $\pm 2$  SE). The slope values (% shoot survival per day) for Control, NPK, OC, and NPKOC are -0.6, -2.0, -1.0, and -2.3, respectively. Panels B-E were photos of shoot survival taken at the end of the experiment in July.

Percent shoot survival decreased linearly in all treatments during the first 32 days, albeit with significantly different slopes (Fig. 23). Survival was highest in the control treatment, followed by the OC, NPK and NPKOC treatments. Since  $\text{CO}_{2(\text{aq})}$  enrichment was not an important predictor of shoot numbers, data from all  $\text{CO}_{2(\text{aq})}$  treatments were combined to compare the effects of sediment treatments on the percent survival during the initial 32 days, where responses were linear. The results indicated that both sediment treatments and time significantly impacted eelgrass survival (Table 9). Specifically, percent survival in the NPK treatment did not significantly differ from the NPKOC treatment, but both were significantly different from the Control and OC treatments (Table 10). On the other hand, percent survival in the OC treatment was comparable to the Control group such that by the end of the experiment, survival in these two sediment types were statistically identical.

**Table 9.** Summary ANCOVA tables for Type III tests of fixed effects (Time and Treatments) using the mixed linear model routine performed in SPSS. Time represents days 0 to 32 where responses were linear for all Treatments (Control, NPK, OC, NPKOC).

| Dependent variable | Source            | Effects df | Error df | <i>F</i> | <i>p</i> |
|--------------------|-------------------|------------|----------|----------|----------|
| Survival (%)       | Time              | 3          | 37.98    | 31.70    | <0.001   |
|                    | Treatments        | 2          | 71.09    | 214.23   | <0.001   |
|                    | Time x Treatments | 1          | 70.35    | 18.24    | <0.001   |

**Table 10.** Tukey's test results comparing the mean percent survival (I) between treatments (J). Mean difference (I-J) with asterisks represents significant difference between sediment treatment types at the 0.05 level.

|              | Treatments (I) | Treatments (J) | Mean Difference (I-J) | Std. Error | p      | 95% Confidence Interval |             |
|--------------|----------------|----------------|-----------------------|------------|--------|-------------------------|-------------|
|              |                |                |                       |            |        | Lower Bound             | Upper Bound |
| Tukey<br>HSD | Control        | NPK            | 20.06*                | 2.96       | <0.001 | 12.33                   | 27.78       |
|              |                | OC             | 4.71                  | 2.96       | 0.39   | -3.01                   | 12.44       |
|              |                | NPKOC          | 16.53*                | 3.08       | <0.001 | 8.50                    | 24.57       |
|              | NPK            | Control        | -20.06*               | 2.96       | <0.001 | -27.78                  | -12.33      |
|              |                | OC             | -15.34*               | 2.98       | <0.001 | -23.14                  | -7.55       |
|              |                | NPKOC          | -3.52                 | 3.10       | 0.67   | -11.62                  | 4.57        |
|              | OC             | Control        | -4.71                 | 2.96       | 0.39   | -12.44                  | 3.01        |
|              |                | NPK            | 15.34*                | 2.98       | <0.001 | 7.55                    | 23.14       |
|              |                | NPKOC          | 11.82*                | 3.10       | <0.001 | 3.72                    | 19.92       |
|              | NPKOC          | Control        | -16.53*               | 3.08       | <0.001 | -24.57                  | -8.50       |
|              |                | NPK            | 3.52                  | 3.10       | 0.67   | -4.57                   | 11.62       |
|              |                | OC             | -11.82*               | 3.10       | <0.001 | -19.92                  | -3.72       |

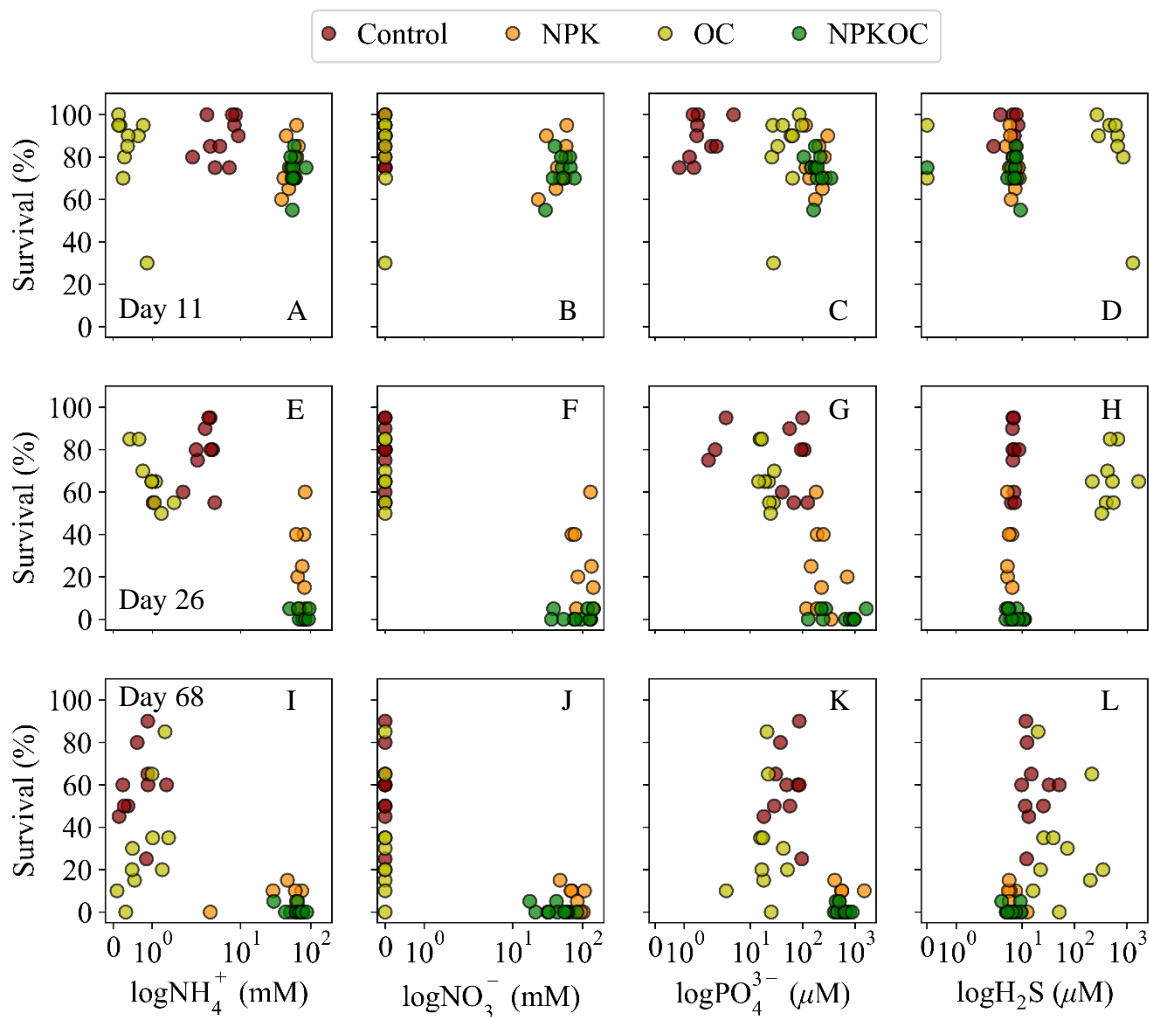


**Fig. 24.** Percent survival plotted as a function of log-nutrient concentrations and log H<sub>2</sub>S concentration for days 11 (start of porewater sampling), 32, and 68 (end of porewater sampling). Color symbols correspond to each sediment treatment: Control, NPK, OC, and NPKOC. CO<sub>2(aq)</sub> enrichment did not impact eelgrass survival therefore all measurements across CO<sub>2(aq)</sub> treatments were combined to evaluate the effects of porewater chemistry on percent survival at days 11, 26, and 68.

Shoot size, measured as total one-sided leaf area ( $\text{cm}^2$ ), decreased over time, and remained unaffected by sediment treatments (Fig. 25, Table 11). The impact of  $\text{CO}_{2(\text{aq})}$  enrichment was only evident in the Control and specifically at the final sampling time point on day 67 (Fig. 25A). Shoot size response to increasing aqueous  $\text{CO}_2$  concentrations ( $\text{CO}_{2(\text{aq})}$ ) was linear, characterized by a positive slope of  $13.19 \pm 3.38$  ( $n = 5$ ,  $r^2 = 0.79$ ,  $p = 0.02$ ). At the conclusion of the experiment, plants cultivated at  $2121 \mu\text{M CO}_{2(\text{aq})}$  (pH 6.1) were 3 times bigger than plants in ambient  $\text{CO}_{2(\text{aq})}$  ( $55 \mu\text{M CO}_{2(\text{aq})}$  or pH 7.7) tanks.

The results presented in Table 11 indicated that sediment treatments and  $\text{CO}_{2(\text{aq})}$  were not significant predictors of growth rates. Initially, the absolute growth rates (AGR) of eelgrass in the NPK, OC and NPKOC treatments exhibited acute responses to sediment treatments (Fig. 26B-D). By day 15, AGR in these treatments decreased by nearly half compared to the Control (Fig. 26A). Subsequently, AGR in all sediment treatments except NPKOC continued to decline. In contrast, eelgrass in NPKOC treatment displayed consistent low growth responses throughout the experiment, with no measurable changes (slope = 0,  $p = 0.905$ ).

Changes in the AGR of plants enriched with NPK (Fig. 26B) mirrored those enriched with OC (Fig. 26C), both yielding slopes of -0.01. However, the specific growth rates (SGR, normalized to shoot size) were not affected by sediment treatment (Fig. 27B-D). Statistically, there were no significant differences in the SGR among the NPK, OC, or NPKOC treatments over time. The combined average SGR for these treatments was  $2.14\% \text{ d}^{-1}$  ( $\pm 0.13 \text{ SE}$ ). The effect of time on SGR was only observed in the Control group, where SGR declined from  $3.02\% \text{ per day}$  ( $\pm 0.35 \text{ SE}$ ) initially to  $2.19\% \text{ per day}$  ( $\pm 0.57 \text{ SE}$ ), as illustrated in Fig. 27A.

**Table 11.** Summary ANCOVA tables for the Type III tests of fixed effects using a 2-factor (Time and Treatment) Linear Mixed-Effects Model in SPSS with log CO<sub>2(aq)</sub> (pH levels = 6.1, 6.4, 6.9, 7.4, 7.7) as a covariate. Shoot size was log-transformed then tested for the significance of sediment and CO<sub>2(aq)</sub> treatment effects. DW: dry weight.

| Dependent variable   | Source                                  | Effects df | Error df | <i>F</i> | <i>p</i>         |
|--|---|------------|----------|----------|------------------|
| Shoot Size<br>(cm <sup>2</sup> )                           | Time                                    | 3          | 83.42    | 53.45    | <b>&lt;0.001</b> |
|  | Treatment                               | 3          | 26.41    | 0.98     | 0.42             |
|  | log CO <sub>2(aq)</sub>                 | 1          | 28.57    | 1.73     | 0.20             |
|  | log CO <sub>2(aq)</sub> x<br>Treatments | 3          | 26.98    | 2.81     | 0.06             |
| Absolute growth rate<br>(cm <sup>2</sup> d <sup>-1</sup> ) | Time                                    | 3          | 65.23    | 6.59     | <b>&lt;0.001</b> |
|  | Treatment                               | 3          | 25.06    | 0.38     | 0.77             |
|  | log CO <sub>2(aq)</sub>                 | 1          | 31.34    | 0.13     | 0.73             |
|  | log CO <sub>2(aq)</sub> x<br>Treatments | 9          | 25.54    | 1.38     | 0.27             |
| Specific growth rate<br>(cm <sup>2</sup> d <sup>-1</sup> ) | Time                                    | 3          | 67.17    | 3.96     | 0.01             |
|  | Treatment                               | 3          | 26.30    | 0.98     | 0.42             |
|  | log CO <sub>2(aq)</sub>                 | 1          | 32.71    | 0.88     | 0.36             |
|  | log CO <sub>2(aq)</sub> x<br>Treatments | 3          | 26.77    | 1.34     | 0.28             |
| Sucrose<br>(μmol g <sup>-1</sup> DW)                       | Time                                    | 3          | 55.39    | 0.75     | 0.53             |
|  | Treatment                               | 2          | 23.42    | 0.17     | 0.84             |
|  | log CO <sub>2(aq)</sub>                 | 1          | 23.35    | 22.39    | <b>&lt;0.001</b> |
|  | log CO <sub>2(aq)</sub> x<br>Treatments | 2          | 22.94    | 0.21     | 0.81             |
| FAA<br>(μmol g <sup>-1</sup> DW)                           | Time                                    | 3          | 53.90    | 1.48     | 0.23             |
|  | Treatment                               | 2          | 20.52    | 5.58     | <b>0.01</b>      |
|  | log CO <sub>2(aq)</sub>                 | 1          | 20.48    | 22.88    | <b>&lt;0.001</b> |
|  | log CO <sub>2(aq)</sub> x<br>Treatments | 2          | 19.90    | 3.28     | 0.06             |
| Total C<br>(μmol g <sup>-1</sup> DW)                       | Time                                    | 4          | 54.27    | 1.03     | 0.40             |
|  | Treatment                               | 3          | 16.99    | 0.45     | 0.72             |
|  | log CO <sub>2(aq)</sub>                 | 2          | 36.52    | 0.85     | 0.36             |
|  | log CO <sub>2(aq)</sub> x<br>Treatments | 3          | 16.96    | 0.46     | 0.71             |

**Table 11.** Summary ANCOVA tables continued.

| Dependent variable                      | Source                                  | Effects df | Error df | <i>F</i> | p                |
|---|---|------------|----------|----------|------------------|
| Total N<br>( $\mu\text{mol g}^{-1}$ DW) | Time                                    | 4          | 82.08    | 33.34    | <b>&lt;0.001</b> |
|   | Treatment                               | 3          | 42.59    | 3.52     | <b>0.02</b>      |
|   | log CO <sub>2(aq)</sub>                 | 1          | 65.28    | 80.09    | <b>&lt;0.001</b> |
|   | log CO <sub>2(aq)</sub> x<br>Treatments | 3          | 42.47    | 2.86     | 0.05             |
| Total S<br>( $\mu\text{mol g}^{-1}$ DW) | Time                                    | 4          | 90.92    | 7.39     | <b>&lt;0.001</b> |
|   | Treatment                               | 3          | 41.83    | 0.63     | 0.60             |
|   | log CO <sub>2(aq)</sub>                 | 1          | 87.16    | 3.07     | 0.08             |
|   | log CO <sub>2(aq)</sub> x<br>Treatments | 3          | 42.31    | 0.48     | 0.70             |
| C:N<br>(mole:mole)                      | Time                                    | 4          | 83.80    | 24.66    | <b>&lt;0.001</b> |
|   | Treatment                               | 3          | 45.09    | 1.70     | 0.18             |
|   | log CO <sub>2(aq)</sub>                 | 1          | 67.43    | 60.46    | <b>&lt;0.001</b> |
|   | log CO <sub>2(aq)</sub> x<br>Treatments | 3          | 44.95    | 1.65     | 0.19             |
| N:S<br>(mole:mole)                      | Time                                    | 4          | 93.92    | 14.50    | <b>&lt;0.001</b> |
|   | Treatment                               | 3          | 50.80    | 2.13     | 0.11             |
|   | log CO <sub>2(aq)</sub>                 | 1          | 91.55    | 16.87    | <b>&lt;0.001</b> |
|   | log CO <sub>2(aq)</sub> x<br>Treatments | 3          | 51.29    | 1.48     | 0.23             |

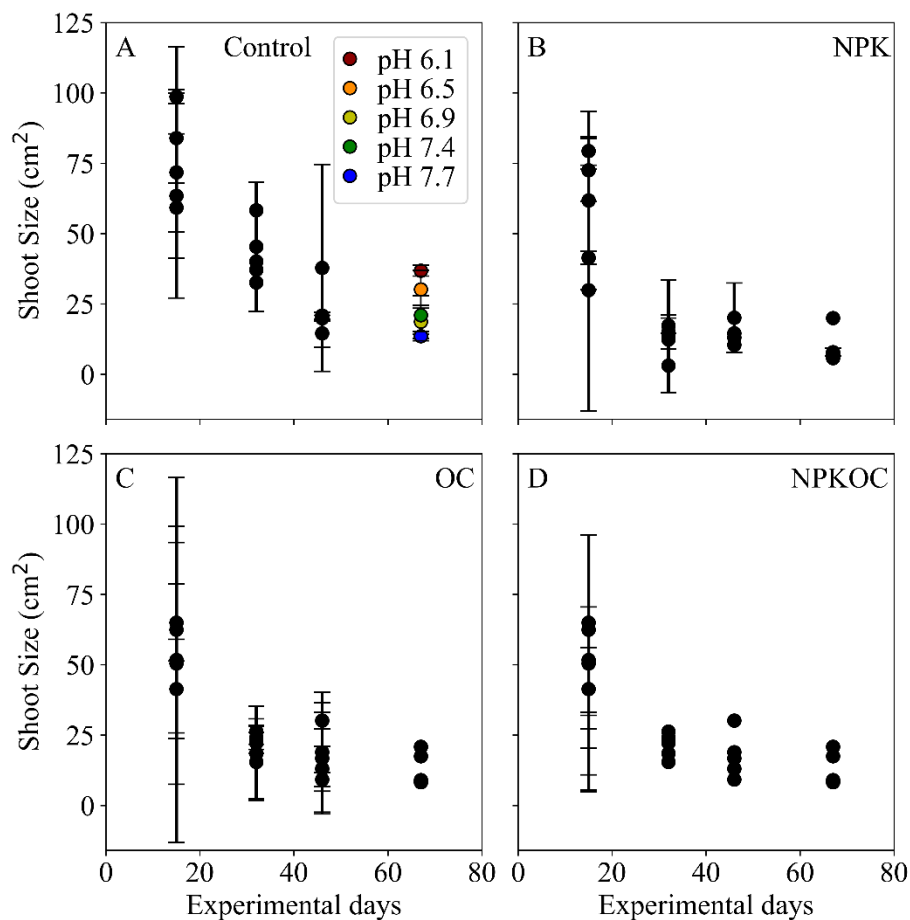


**Fig. 25.** Shoot size (cm<sup>2</sup>) of *Zostera marina* L. plotted as a function of time (in experimental days) for (A) Control, (B) NPK, (C) OC, (D) NPKOC sediment treatments. Each data point represents the mean shoot size obtained from the 5-pH (or CO<sub>2(aq)</sub>) treatments. The solid black symbols were determined to be statistically identical irrespective of CO<sub>2(aq)</sub> enrichment. Colored symbols indicate statistical differences amongst pH (or CO<sub>2(aq)</sub>) treatments based on ANCOVA test. The error bars represent 95% confidence limit.

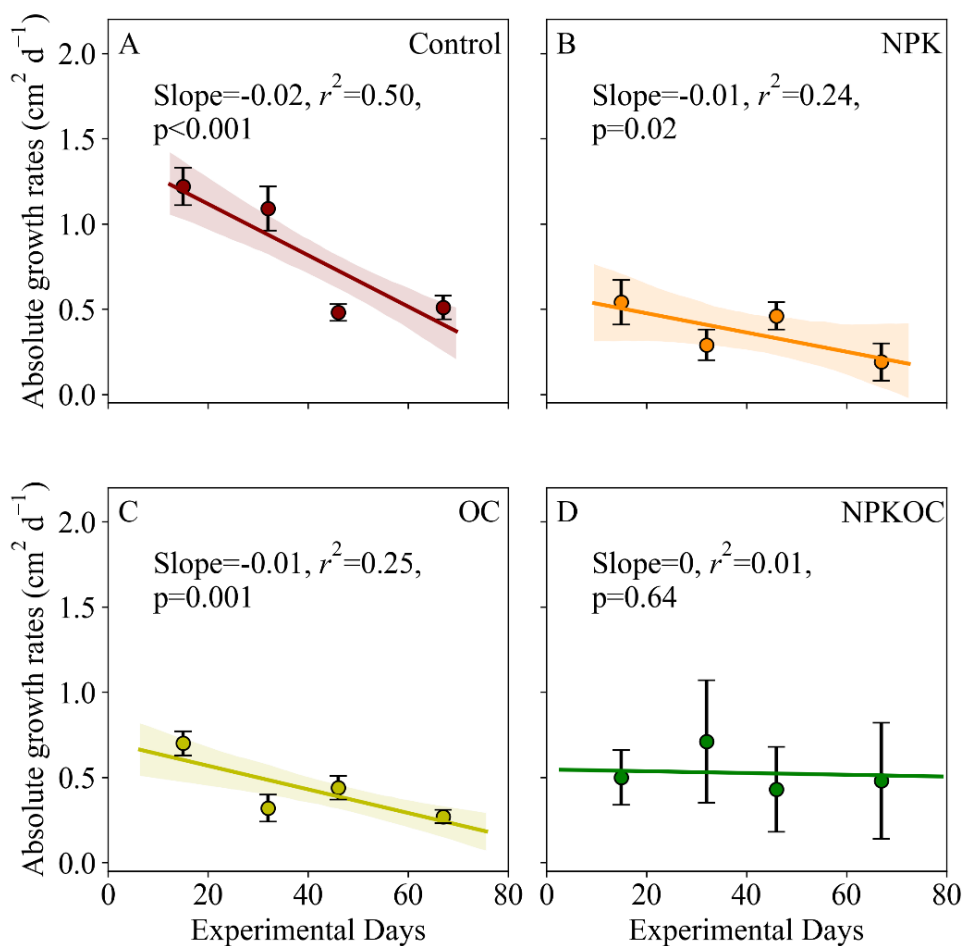


**Fig. 26.** Absolute growth rates (cm<sup>2</sup> d<sup>-1</sup>) of *Zostera marina* L. in Control (A), NPK (B), OC (C), and NPKOC (D) treatments plotted against time. CO<sub>2(aq)</sub> effects were not significant ( $p = 0.7$ , see Table 11), therefore all measurements were combined for each CO<sub>2(aq)</sub> treatments and evaluated for sediment treatment effects. The error bars represent the 95% confidence limit ( $\pm 2$  SE). The lines present linear regression fitted to all observed data. The shaded colors represent the 95% confidence interval on the regression line for those with  $p$ -values  $< 0.05$ .

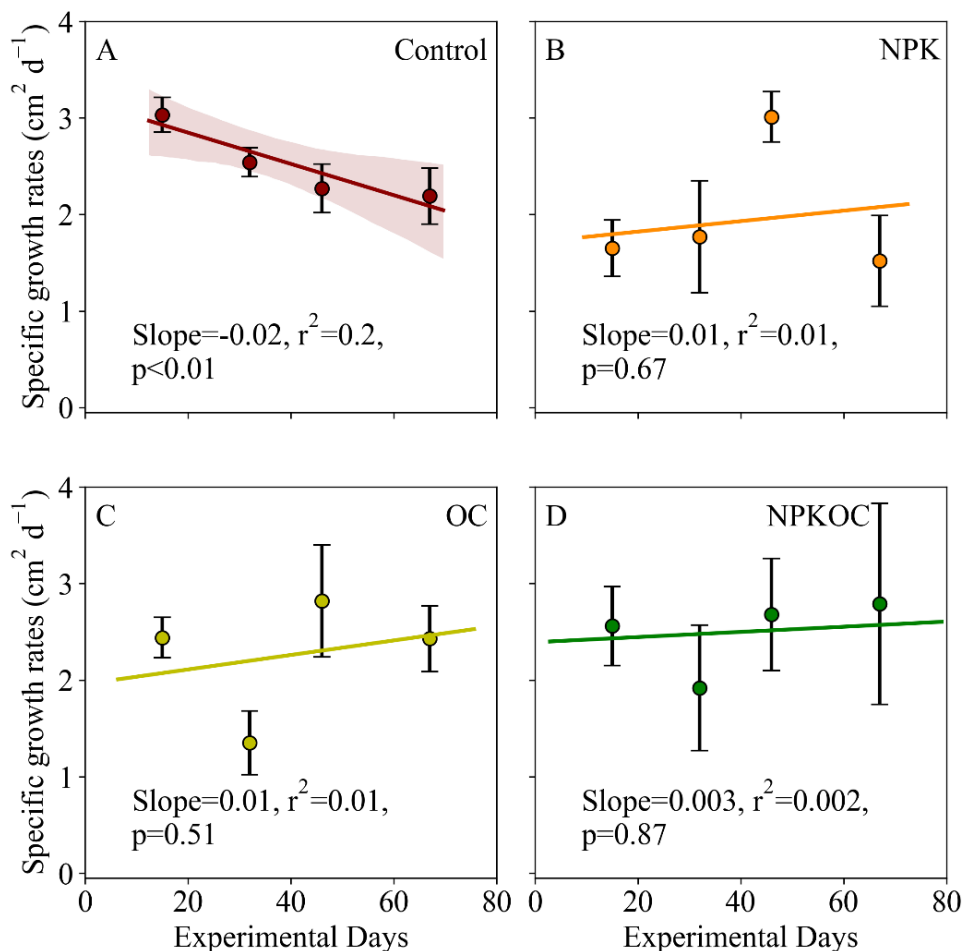


**Fig. 27.** Specific growth rates (SGR) ( $\% \text{d}^{-1}$ ) of *Zostera marina* L. in Control (A), NPK (B), OC (C), and NPKOC (D) treatments plotted against time.  $\text{CO}_{2(\text{aq})}$  effects were not significant ( $p = 0.4$ , see Table 11), therefore all measurements were combined for each  $\text{CO}_{2(\text{aq})}$  treatments and evaluated for sediment treatment effects. The error bars represent the 95% confidence limit ( $\pm 2$  SE). The lines present linear regression fitted to all observed data. The shaded colors represent the 95% confidence interval on the regression line for those with  $p$ -values  $< 0.05$ .

### 3.3.4 Effects of CO<sub>2(aq)</sub> and sediment enrichment on plant sucrose and free amino acids

Leaf sucrose content responded to CO<sub>2(aq)</sub> enrichment but not to sediment treatments (Fig. 28, Table 11). Elevated aqueous CO<sub>2</sub> concentrations led to increased leaf sucrose content after just two weeks of continuous CO<sub>2(aq)</sub> enrichment. After a month of exposure, plants in high CO<sub>2(aq)</sub> conditions (2121  $\mu$ M CO<sub>2(aq)</sub>, pH 6.1) contained twice the sucrose content in leaves than those in ambient CO<sub>2(aq)</sub> conditions. This increase in sucrose accounted for up to 26% of the total leaf C.

The results in Table 11 revealed significant effects of nutrient and organic carbon additions on leaf free amino acids (FAA) concentrations ( $\mu$ mol FAA g<sup>-1</sup> DW). Aqueous CO<sub>2</sub> enrichment effects were only observed in the Control and NPK treatment, albeit not consistently across all time points. Enrichment resulted in decreasing FAA concentrations in leaf tissues, as indicated by the negative slopes (Fig. 29). The effect was greatest with NPK additions, where a 40-fold increase in CO<sub>2(aq)</sub> concentrations led to a substantial 3-to 5-fold reduction in leaf FAA content, in contrast to a less than 1-fold decrease measured in the Control.

Relative to the total nitrogen (N) pool, leaves from plants in high CO<sub>2(aq)</sub> (pH 6.1) condition contained at most 10  $\mu$ mol FAA g<sup>-1</sup> dry weight. In contrast, leaves from ambient CO<sub>2(aq)</sub> (pH 7.7) conditions contained approximately 2-6% higher FAA levels, depending on the sediment treatments. Additionally, the combined effects of high CO<sub>2(aq)</sub> and sediment manipulations were most pronounced with NPK addition, resulting in leaf FAA concentrations to fall below detection limit, especially under the highest CO<sub>2(aq)</sub> condition of pH 6.1 (Fig. 29B).

The combined effects of CO<sub>2(aq)</sub> and NPKOC treatment on leaf FAA and sucrose contents could not be determined, as insufficient tissue samples were available beyond day 30. Consequently, this treatment was excluded from the statistical analysis.

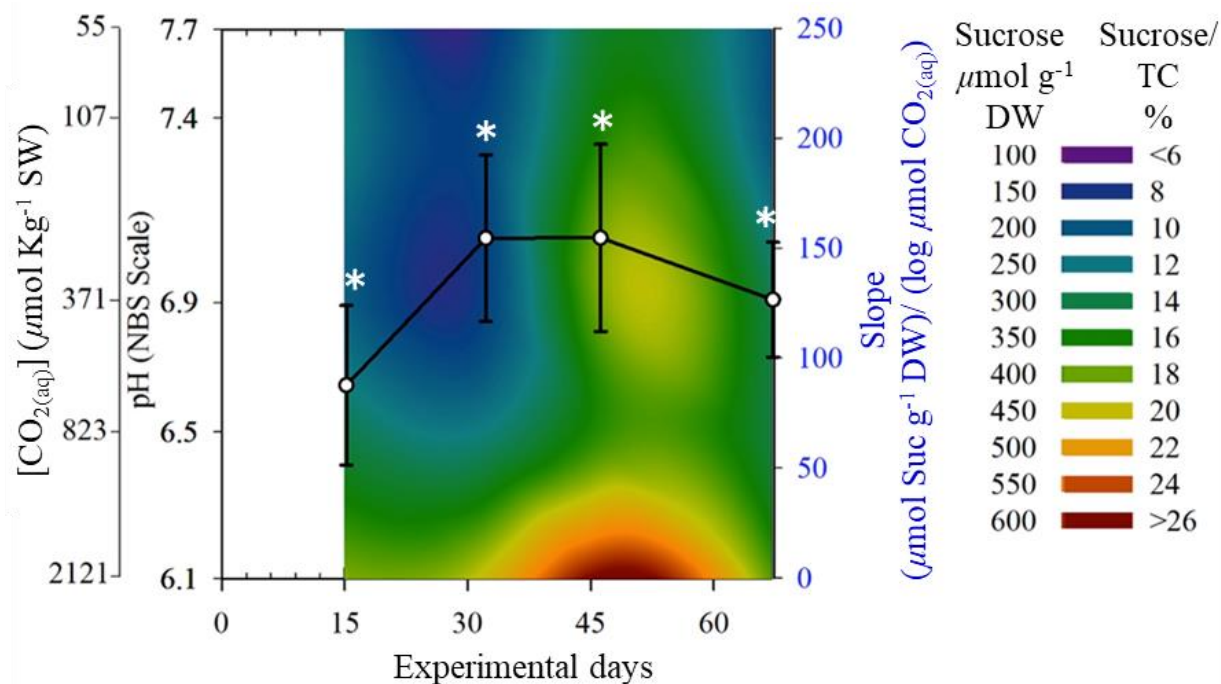


**Fig. 28.** Heat map of leaf sucrose concentrations plotted as a function of pH and corresponding CO<sub>2(aq)</sub> concentrations (left axis) across time for all (except NPKOC) sediment treatments combined (Control, NPK, OC were not significantly different, Table 11). Insufficient tissue samples were available beyond day 30 in the NPKOC treatment, resulting in its exclusion from the statistical analysis. The right axis represents the slope (white circles) derived from the linear regression analysis for sucrose vs. log CO<sub>2(aq)</sub> concentrations. The time points with statistically significant slopes are marked with an asterisk. The error bar represents  $\pm 1$  SE.

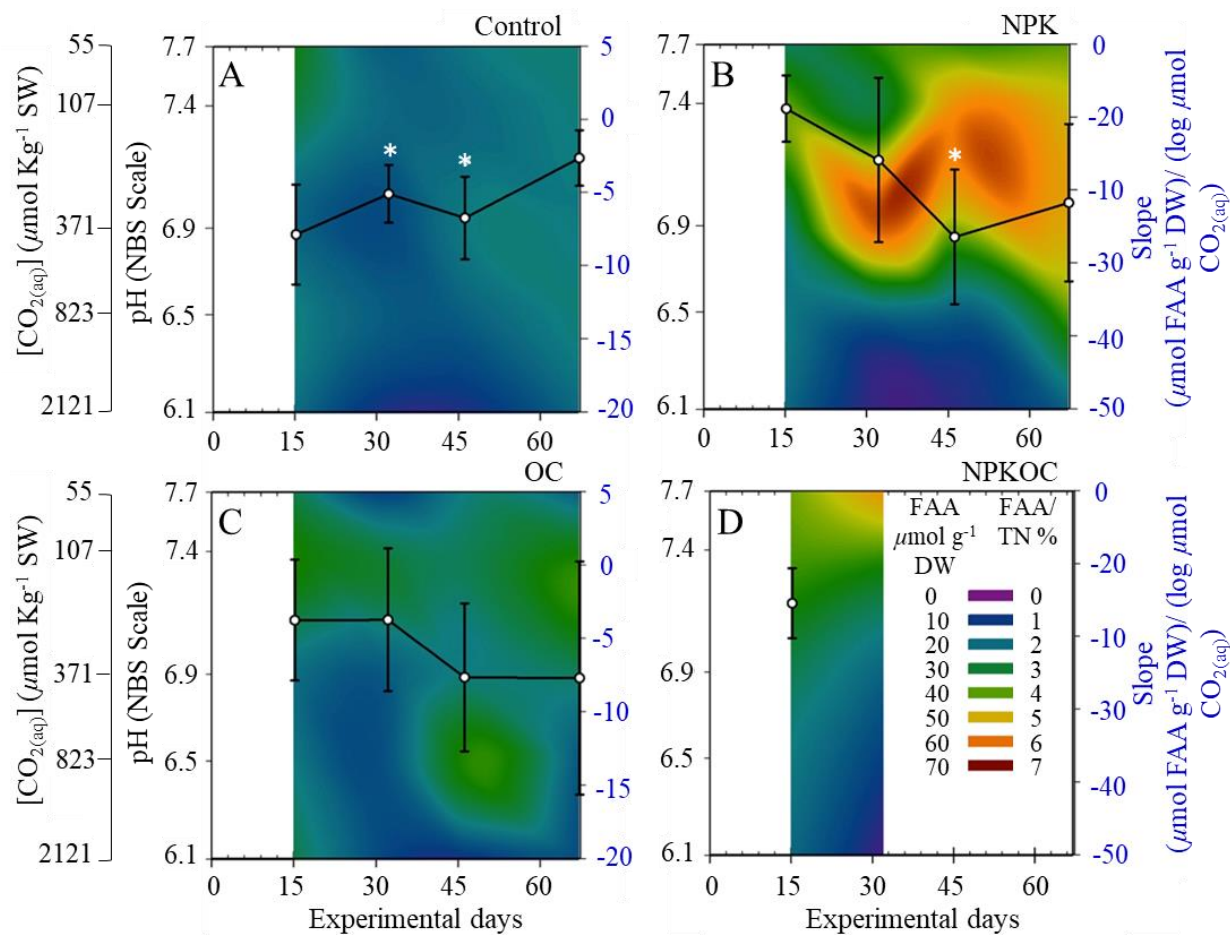


**Fig. 29.** Heat maps of leaf FAA concentrations plotted as a function of pH with the corresponding aqueous  $\text{CO}_2$  concentrations (left axis) across time for Control (A), NPK (B), OC (C), and NPKOC (D) sediment treatments. The right vertical axis represents the slope (white circles) derived from the linear regression analysis for FAA vs.  $\log \text{CO}_{2(\text{aq})}$ . The time points with statistically significant slopes are marked with an asterisk symbol. To the left of the color bar legend is the bulk concentrations of leaf FAA ( $\mu\text{mol g}^{-1}$  dry weight); to the right of the color bar is the FAA content normalized to the total leaf N pool (expressed as %). The error bar represents  $\pm 1$  SE.

### 3.3.5 Effects of CO<sub>2(aq)</sub> and sediment enrichment on plant elemental compositions

The biomass-specific leaf N content in the NPK, OC, and Control treatments decreased with CO<sub>2(aq)</sub> enrichment (Fig. 30). Factors such as time, sediment types, and CO<sub>2(aq)</sub> concentrations were significant predictors of leaf N content and collectively contributed to the observed decline (Table 11). Sediment fertilized with nutrients (NPK) increased leaf N content, but only for eelgrass under ambient CO<sub>2(aq)</sub> conditions (pH 7.7). Eelgrass exposed to the highest CO<sub>2(aq)</sub> concentration (pH 6.1) showed no response to nutrient addition. Interestingly, eelgrass in the NPK treatment exhibited a stronger response to pH (or CO<sub>2(aq)</sub>) treatment than Control plants, containing approximately 4% less N in leaf tissues under the same pH 6.1 condition. While there was some indication of an interactive effect between CO<sub>2(aq)</sub> and nutrient enrichments on leaf N content, this effect remained marginal at best (ANCOVA,  $p = 0.048$ ).

The biomass-specific leaf C (Fig. 31) and S contents (Fig. 32) were neither influenced by CO<sub>2(aq)</sub> enrichment nor sediment treatments (Table 11) at any point during the experiment. The leaf tissue contained on average 29.5 ( $\pm 0.1$ ) mmol C g<sup>-1</sup> DW. Exposure time was a significant factor influencing leaf S content. Total S content declined by 50% between day 15 and day 67, ending below 100  $\mu$ mol g<sup>-1</sup> DW (Fig. 32). Despite the stimulation of H<sub>2</sub>S production from organic carbon addition, TS in OC treatment was not significantly different from other sediment treatment, and was statistically identical to the Control.

Initial analysis of tissue elemental content revealed that eelgrass leaves contained molar C:N and N:S ratios of 24.8 and 8.1, respectively, prior to the start of the enrichment experiment. Both the C:N and N:S ratios showed correlations with CO<sub>2(aq)</sub> levels but not to sediment treatments (Table 11, Fig. 33). The effects of CO<sub>2(aq)</sub> on N:S ratio was statistically significant, despite CO<sub>2(aq)</sub> not affecting TS in leaves. This indicates that changes in the N:S ratio was due to shifts in TN,

influenced by  $\text{CO}_{2(\text{aq})}$  levels. The duration of  $\text{CO}_{2(\text{aq})}$  enrichment exposure notably altered the C:N and N:S ratios over time. The most pronounced  $\text{CO}_{2(\text{aq})}$  effect on these elemental ratios occurred after 30 days of continuous enrichment, causing a 50% increase in C:N ratio and a >25% decrease in N:S ratio.

Due to early high mortality rates in the NPKOC treatment, insufficient samples were available to statistically assess the effects of sediment treatment and  $\text{CO}_{2(\text{aq})}$  enrichment on plant biochemical composition.

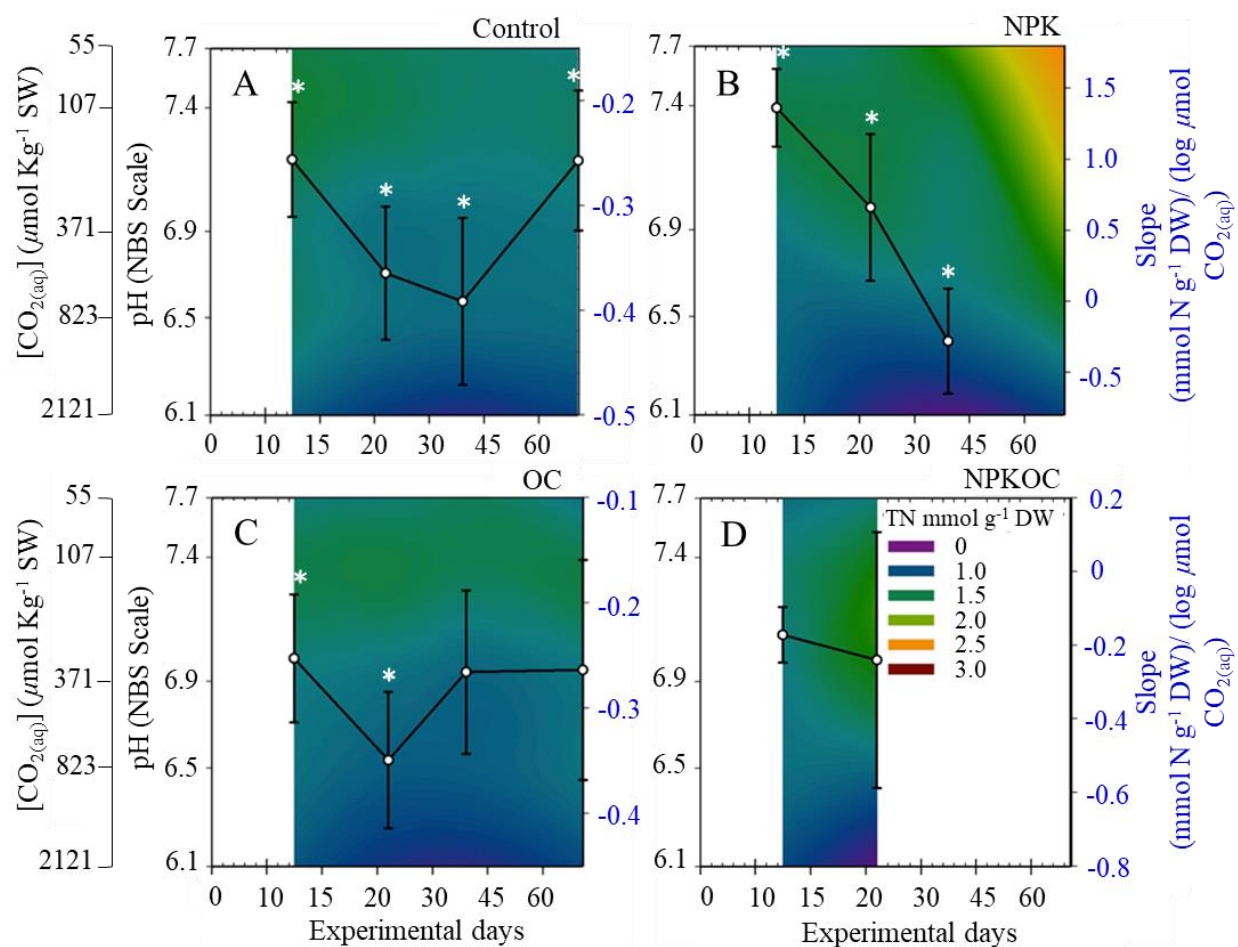


**Fig. 30.** Heat maps of total nitrogen (TN) content per unit dry weight of leaf plotted as a function of pH and corresponding  $\text{CO}_{2(\text{aq})}$  concentrations (left axis) across time for Control (A), NPK (B), OC (C) and NPKOC (D) sediment treatments. The left vertical axis represents the slope (white circles) derived from the linear regression analysis for TN vs.  $\log \text{CO}_{2(\text{aq})}$ . The time points with statistically significant slopes are marked with an asterisk. The error bar represents  $\pm 1$  SE.

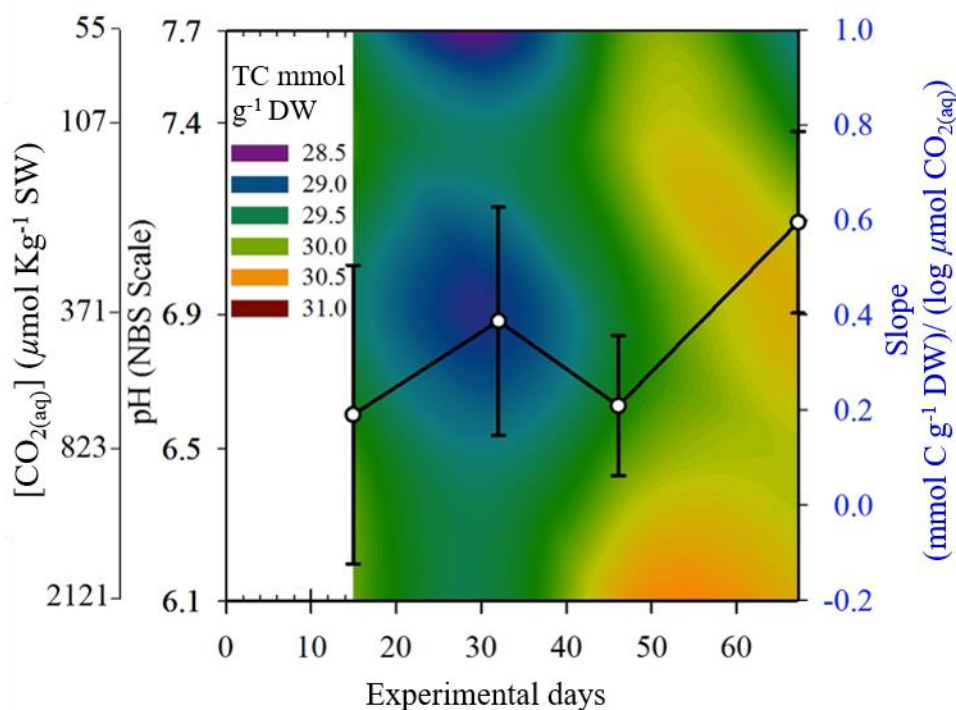


**Fig. 31.** Heat map of total carbon (TC) (mmol g<sup>-1</sup> DW of leaf) plotted as a function of pH and corresponding CO<sub>2(aq)</sub> concentrations (left axis) across time for all sediment treatments combined (Control, NPK, OC and NPKOC were not significantly different, Table 11). The right axis represents the slope (white circles) derived from the linear regression analysis for TC vs. log CO<sub>2(aq)</sub>. No significant effects of CO<sub>2(aq)</sub>, sediment treatments or time on TC were observed. The error bar represents  $\pm 1$  SE.

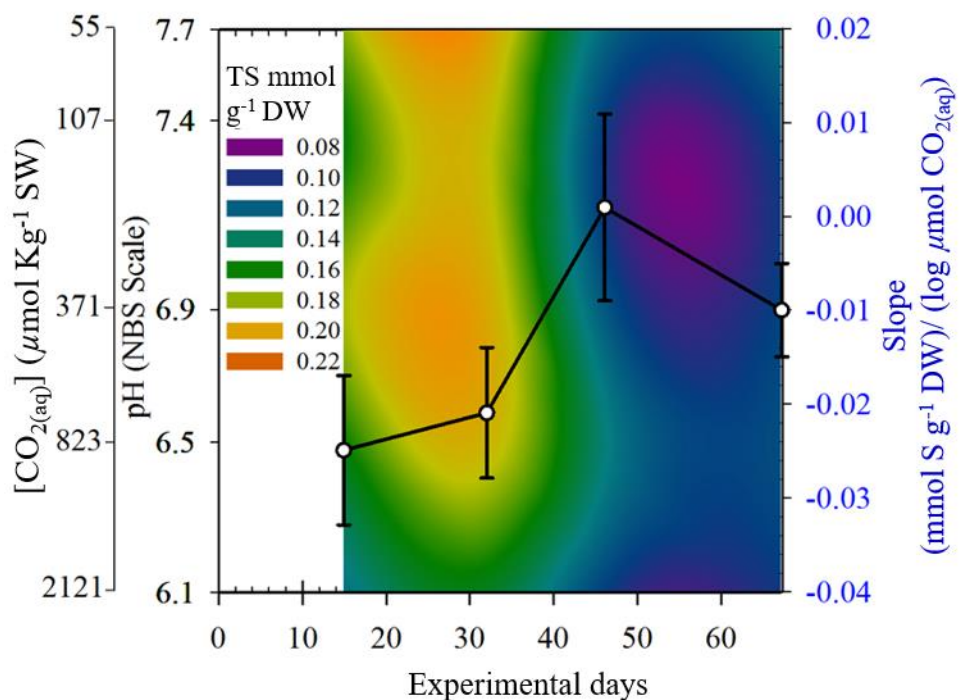


**Fig. 32.** Heat map of total sulfur (TS) (mmol g<sup>-1</sup> DW of leaf) plotted as a function of pH and corresponding CO<sub>2(aq)</sub> concentrations (left axis) across time for all sediment treatments combined (Control, NPK, OC and NPKOC were not significantly different, Table 11). The right axis represents the slope (white circles) derived from the linear regression analysis for TC vs. log CO<sub>2(aq)</sub>. No significant effect of CO<sub>2(aq)</sub> on TS was observed. TS varied with time (p<0.001). The error bar represents ± 1 SE.

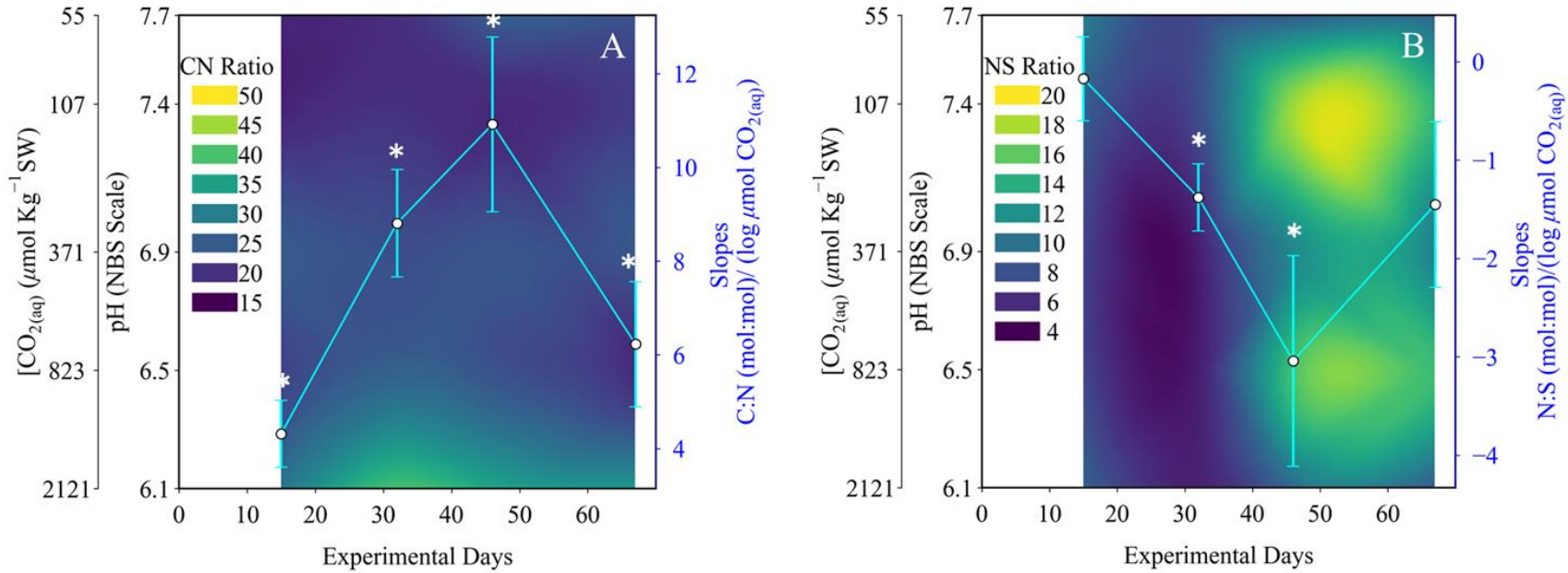


**Fig. 33.** Heat maps of C:N (A) and N:S (B) ratios (mole:mole) plotted as a function of pH and corresponding  $\text{CO}_2(\text{aq})$  concentrations (left axis) across time for all sediment treatments combined (Control, NPK, OC and NPKOC were not significantly different, Table 11). The left vertical axis represents the slope (white circles) derived from the linear regression analysis for C:N vs.  $\log \text{CO}_2(\text{aq})$  and N:S vs.  $\log \text{CO}_2(\text{aq})$ . The time points with statistically significant slopes are marked with an asterisk. The error bar represents  $\pm 1$  SE.

### 3.4 Discussion

Nutrient and organic carbon enrichment had a detrimental impact on the survival of *Z. marina* by increasing inorganic N and H<sub>2</sub>S to toxic levels. The rapid decrease in survival, growth rates, and shoot sizes were mainly acute in nature and seemed to be unrelated to the overall carbon balance. Despite stimulation of H<sub>2</sub>S production from organic carbon addition, survival in the OC treatment was not significantly different from the Control, which appears to counter to published reports about sulfide toxicity in eelgrass (Holmer and Bondgaard 2001; Holmer et al. 2005). Eelgrass survival was most affected by the addition of Osmocote®, which increased NH<sub>4</sub><sup>+</sup> and NO<sub>3</sub><sup>-</sup> concentrations in both NPK and NPKOC treatments, reaching levels that were clearly detrimental to eelgrass. This resulted in nearly complete mortality within 60 days of the study. Contrary to the initial hypothesis of this study, the expected enhancement in eelgrass tolerance to sediment eutrophication through CO<sub>2(aq)</sub> enrichment was not observed within the timeframe of the experiment. It is plausible that utilizing pre-conditioned eelgrass at the targeted CO<sub>2(aq)</sub> levels could yield different results. Given that the synthesis of inorganic N into amino acids requires carbon skeleton, it is possible that eelgrass, especially those in high CO<sub>2(aq)</sub> environments, may possess sufficient internal carbon reserves to meet the metabolic demand associated with N assimilation. Further investigation is need to assess the role of carbon-limitation in mitigating the N toxicity effect.

#### 3.4.1 Responses to CO<sub>2(aq)</sub> enrichment

Significant effects of CO<sub>2(aq)</sub> enrichment on amino acids and total N in leaves exhibited variability with sediment treatments but were consistently observed in the Control. Sediment treatments were found to be unrelated to the pattern of sucrose accumulation in leaves, suggesting

the absence of impact on leaf photosynthesis.  $\text{CO}_{2(\text{aq})}$  enrichment resulted in sucrose production levels comparable to those reported in Chapter 2. The lack of clear and consistent  $\text{CO}_{2(\text{aq})}$  effects in the NPK, OC and NPKOC treatments likely stemmed from the overwhelming toxicity to eelgrass survival caused by high concentrations of DIN in the form of  $\text{NH}_4^+$  and  $\text{NO}_3^-$ , as well as elevated  $\text{H}_2\text{S}$  concentrations. These factors imposed limitations on the interpretations of the findings. In contrast to Chapter 2, the lack of  $\text{CO}_2$ -stimulated growth rates in this study could also be attributed to the relatively short duration of the experiment, possibly insufficient to capture the initial stages of the  $\text{CO}_2$ -stimulated growth, a process that may take six weeks or more to manifest (Zimmerman et al. 2017; Zimmerman 2021). As mentioned earlier, utilizing pre-conditioned eelgrass at the intended  $\text{CO}_{2(\text{aq})}$  levels might have resulted in different outcomes and enabled a more accurate assessment of the potential advantages of  $\text{CO}_2$  for eelgrass survival under eutrophic sediment conditions.

Given those caveats mentioned above, this experiment provided no compelling evidence of an interactive effect between  $\text{CO}_{2(\text{aq})}$  and sediment treatments on plant survival, morphology, or tissue biochemistry. The only significant interactions between  $\text{CO}_{2(\text{aq})}$  enrichment and sediment treatment were observed in porewater  $\text{NH}_4^+$  concentrations, specifically in the NPK treatment, and only at the final sampling time point. The combined effects of  $\text{CO}_{2(\text{aq})}$  enrichment and NPK addition had a substantial impact on porewater  $\text{NH}_4^+$  levels, leading to a reduction exceeding 50 mM between ambient (pH 7.7) and high  $\text{CO}_{2(\text{aq})}$  (pH 6.1) treatments. Such a significant reduction of this magnitude could not have resulted from plant uptake, as less than 10% of the initially transplanted shoot survived. The depletion of  $\text{NH}_4^+$  from the sediment may have resulted from diffusive loss from sediment to the overlying water but it is more likely linked to microbial processes. Although this study did not assess the microbial communities in the sediment, microbial

mediated N transformation can become accelerated under ocean acidification (Berlinghof et al. 2023). Their undeniable role in altering the sediment biogeochemistry within the seagrass habitats necessitates attention and further investigation in future studies.

### 3.4.2 Sensitivity to porewater DIN

Eelgrass exhibited a strong response to sediment N-enrichment, with growth and survival being negatively affected by high  $\text{NH}_4^+$  and  $\text{NO}_3^-$  concentrations. Acute toxicity and shoot death were not immediate, rather these effects occurred after 30 days, and at significantly higher concentrations than previously reported (Burkholder et al. 1994; Santamaría et al. 1994; van Katwijk et al. 1997; Burkholder et al. 2007; Govers et al. 2014). The delayed toxicity effect may be attributed, at least in part, to the sediment properties, specifically mineral types, and grain sizes. Certain sediments, such as clay and sand, possess negatively charged mineral surface under typical marine conditions (Burdige 2006) influencing the mobility of  $\text{NH}_4^+$  by selectively adsorbing this cation from solution (Abdulgawad et al. 2009; Alshameri et al. 2018). This selective adsorption can regulate  $\text{NH}_4^+$  availability for plant uptake (Erfemeijer and Middelburg 1993; Lavery et al. 2001). In a particular study, sediment types were identified as important predictor of seagrass resilience, with the  $\text{NH}_4^+$  toxicity threshold notably higher at muddy than sandy sites (Li et al. 2019). This was attributed to a negative correlation between porewater  $\text{NH}_4^+$  concentrations mud content (Douglas et al. 2016). Though sediments utilized in this study was composed mainly of sand, the negative net charge of these mineral surfaces could still influence  $\text{NH}_4^+$  adsorption and availability for plant uptake.

*Z. marina* was exposed to porewater  $\text{NH}_4^+$  concentrations at least 10 times the reported threshold known to exert metabolic stress. While shoot decline has been linked to  $\text{NO}_3^-$

(Burkholder et al. 1992), the adverse effects were more likely associated with  $\text{NH}_4^+$  toxicity. Plants can generally store  $\text{NO}_3^-$  in cells to some extent, but intracellular accumulation of  $\text{NH}_4^+$  can damage in root cells and cell wall structures (Li et al. 2013). Many of the shoots in the nutrient enriched treatments in this study exhibited growth suppression and necrosis at the meristematic base of the shoot, symptoms commonly associated with  $\text{NH}_4^+$  poisoning reported in the literature (Dennison et al. 1987; Santamaría et al. 1994; Britto and Kronzucker 2002). In contrast to leaf necrosis reported by van Katwijk et al. (1997) and van der Heide et al. (2008b), *Z. marina* in this study sustained severe damage at the rhizome-meristem junction and no visible signs of degradation in the leaves. In some dying plants, the meristem was severely disintegrated that the above ground shoot became detached from the belowground structure. Such magnitude of impact has not been previously documented in *Z. marina*, but it should be noted that the DIN concentrations in this study was several orders of magnitude higher than past research. Shoot death, in this case occurred from the bottom up. This is an important observation to make because in many past researches on seagrass and eutrophication, the health estimate has predominantly been gauged from the physiological changes in the above ground shoot components and little attention to the roots and rhizome. Whole shoot assessment may be a cumbersome and quite destructive to plants but necessary step to make when evaluating plant responses to eutrophication.

In the detached shoots, most of the leaves were visibly green, and showed little evidence of blackened or necrotic spots. Even when exposed to  $\text{NH}_4^+$  levels 10 to 100 times the concentrations known to cause die-off (Santamaría et al. 1994; van Katwijk et al. 1997; Govers et al. 2014),  $\text{CO}_{2(\text{aq})}$ -enriched eelgrasses consistently maintained a positive carbon balance based on high sucrose accumulation in leaves (as shown in Fig. 28). The leaves exhibited a 2-fold increase in leaf sucrose content compared to  $\text{CO}_{2(\text{aq})}$ -unenriched leaves throughout the entire experiment,

indicating that sediment treatment did not adversely affect leaf photosynthesis. Although  $\text{CO}_{2(\text{aq})}$  treatments had a positive impact on photosynthesis and sugar accumulation, eelgrass mortality still occurred. This suggests that mechanisms other than carbon deprivation may be the primary cause of toxicity-related shoot death. Previous studies on various aquatic and terrestrial plants have proposed that extreme carbon limitation could contribute to toxicity syndromes. The ‘carbon drain’ hypothesis, suggested by Burkholder et al. (1992) and Touchette (1999), was based on the reduction in tissue carbohydrates (i.e. sucrose) contents of *Z. marina* under high  $\text{N-NO}_3^-$  enrichment, leading to observed necrosis and shoot death. Severe photosynthetic  $\text{CO}_{2(\text{aq})}$  limitation has been identified as a direct contributor to shoot mortality (Kaldy et al. 2022). Detoxification of inorganic N into amino acids requires carbon skeletons (e.g.  $\alpha$ -ketoglutarate from Krebs Cycle) and intermediate compounds (e.g. pyruvate from Glycolysis) derived from the breakdown of carbohydrates in central metabolic pathways. However, contrary to those findings, the results of this experiment showed that sucrose accumulated in leaves, demonstrating positive C balance and no internal C limitation. Changes in sucrose, total C contents, or the C:N ratio were independent of nutrient enrichment, responding mainly to  $\text{CO}_{2(\text{aq})}$  levels. Consequently, the results obtained here cannot be explained by toxicity-induced C limitation.

A plausible scenario supporting the study’s outcome, while aligning with existing literature, is as follows: High external  $\text{NH}_4^+$  concentrations can lead to rapid  $\text{NH}_4^+$  accumulation in the cytosol, reaching injurious levels to the roots and rhizomes. This damage inhibits the translocation of carbon resources from sucrose-abundant leaves to the roots, requiring N assimilation to rely on C stored in roots & rhizomes to detoxify  $\text{NH}_4^+$  into amino acids. This finite C pool quickly becomes depleted limiting the assimilation process. The resulting negative feedback on N metabolism may lead to increasing accumulations of unassimilated  $\text{NH}_4^+$ , causing

toxicity and cell damage. Whether C deprivation is the key factor in  $\text{NH}_4^+$  toxicity-induced death remains to be challenged as uncertainties persist regarding the actual mechanism linking N toxicity to eelgrass survival, and the scenario described here requires further investigation. Addressing this question necessitates that we deepen our understanding of the mechanisms regulating both C and N assimilations in these aquatic vascular plants.

### **3.4.3 The effects of $\text{H}_2\text{S}$ toxicity**

Although the OC sediment treatment dramatically stimulated  $\text{H}_2\text{S}$  production, toxicity from  $\text{H}_2\text{S}$  was not evident, even though porewater  $\text{H}_2\text{S}$  concentrations were within the range reported capable of eliciting die-off events (Lamers et al. 2013). Further, the addition of organic C to the sediment did not significantly influence eelgrass survival relative to the Control, even though  $\text{H}_2\text{S}$  concentrations in the OC treatment were 5 to 100 times higher than in the Control. In this study,  $\text{H}_2\text{S}$  concentrations had no impact on the biochemical compositions and the elemental CNS of *Z. marina*, demonstrating that  $\text{H}_2\text{S}$  was not as detrimental to growth and survival as N.

Evidence of  $\text{H}_2\text{S}$  intrusion was not observed, though it could not be completely ruled out as the total S content in the roots and rhizomes was not measured. Numerous studies have demonstrated variable responses of  $\text{H}_2\text{S}$ -driven changes to the total S contents of the above- and belowground components (Holmer et al. 2005; Frederiksen et al. 2008; García et al. 2013; Hasler-Sheetal and Holmer 2015). Depending on the plant's re-oxidation capacity, intruded  $\text{H}_2\text{S}$  can be re-oxidized in the aerenchyma, preventing its upward movement into the leaves. In past study,  $\text{H}_2\text{S}$  accumulations were observed to be greatest in the belowground roots and rhizomes, with little to no impact on the leaves (Frederiksen et al. 2006).

The low porewater H<sub>2</sub>S concentrations at Day 66 may have also contributed to eelgrass survival and could explain why *Z. marina* appeared more tolerant to organic carbon loading than nutrient enrichment, which did not decline during the experiment. The rapid decline in H<sub>2</sub>S concentrations may result from a combination of diffusive loss from sediment into the overlying water and the removal of H<sub>2</sub>S by reactive iron (Fe) oxides in sediments (Canfield 1989; Zhu et al. 2012). However, the diffusive flux would have also removed dissolved nutrients from the sediment, and that was not observed here. The formation of metastable iron monosulfide (FeS) precipitates under anaerobic conditions can occur on a timescale of seconds and is crucial in controlling porewater H<sub>2</sub>S bioavailability and maintaining the stability of porewater alkalinity in marine sediments (Canfield and Berner 1987; Jørgensen et al. 2019). Although Fe content was not measured in this study, some Fe was likely present, as both Fe and FeS are ubiquitous in sediments along the entire axis of the Chesapeake Bay (Young 1968; Zimmerman and Canuel 2000). In addition, the presence of NO<sub>3</sub><sup>-</sup> may also interfere with H<sub>2</sub>S production by replacing sulfate with nitrate as the electron acceptor for sulfate reducing bacteria (SRB) during the oxidation of organic matter (Marietou 2016). Therefore, nitrate respiring SRB provides an alternative explanation for low H<sub>2</sub>S concentrations in treatments with NO<sub>3</sub><sup>-</sup> present (NPKOC).

This study highlights that while elevated atmospheric CO<sub>2</sub> benefits seagrass carbon balance, the positive effects can be constrained by eutrophication stress applied to below-ground structures such as roots and rhizomes. In the presence of nutrients and organic carbon, the benefits of CO<sub>2(aq)</sub> appeared limited, and eelgrass succumbed to toxic NH<sub>4</sub><sup>+</sup> levels, emphasizing sediment chemistry as crucial factor in predicting seagrass survival from multiple stressors. The uncoupling of responses between above- and belowground structures suggest disruptions in translocation processes, potentially impacting crucial resource acquisition and allocation. This study

demonstrated the need for further examination of seagrass responses to multi-stressors, particularly in the context of climate change.

## CHAPTER 4

### MODELING THE EFFECTS OF CO<sub>2</sub> AND LAI ON NITROGEN UPTAKE PATTERN IN *ZOSTERA MARINA* L. (EELGRASS)

#### 4.1 Introduction

Seagrasses are some of the most productive primary producers in coastal marine system producing as much as 2000 g dry wt. m<sup>-2</sup> y<sup>-1</sup> (Jacobs 1979; Roman and Able 1988) or on average 400 g C m<sup>-2</sup> y<sup>-1</sup> (Aioi et al. 1981; Duarte and Chiscano 1999). The net productivity of these marine angiosperms is predicted to rise (Zimmerman et al. 1997; Zimmerman et al. 2017) with ocean acidification (IPCC 2013). However, seagrass productivity will benefit from greater CO<sub>2</sub> abundance only if there are sufficient concentrations of dissolved inorganic nutrients to support the increased growth. Higher productivity means higher nutrient demand (Stitt and Krapp 1999), which means that seagrasses will need to take up more nutrients through the leaves and the roots to support CO<sub>2</sub>-stimulated growth. In environments where nutrients are highly transient or scarce the increased growth demand may induce greater N stress on these marine plants and potentially exhaust the inorganic nitrogen supply and limit growth.

In photosynthetic organisms, carbon (C) and nitrogen (N) metabolisms are interdependent (Turpin et al. 1991; Huppe and Turpin 1994; Kraemer and Alberte 1995; Matt et al. 2001) and the responses to elevated CO<sub>2</sub> depend on whether the N supply could meet the growth demand. Chapter 2 showed that aqueous CO<sub>2</sub> concentrations were positively correlated with the daily N demand of *Zostera marina* L. (eelgrass) but negatively correlated with the leaf N content during peak growth, as total carbon as sugar increased by almost 20% under elevated CO<sub>2</sub> conditions.

This raises the question of whether the observed decline in N content resulted from CO<sub>2</sub> stimulated N demand driving eelgrass to N limitation or simply a dilution effect from increased leaf C content. Other CO<sub>2</sub> studies have reported similar shift in tissue N content in *Thalassia testudinum*. (Jiang et al. 2010; Campbell and Fourqurean 2013), *Cymodocea nodosa* (Apostolaki et al. 2014; Mishra et al. 2021), and *Zostera noltii* (Alexandre et al. 2012). Apart from Campbell and Fourqurean (2013), it was suggested that the decline in N content was related to N limitation.

Significant progress has been achieved in the past few decades in understanding the complex interactions between CO<sub>2</sub> and seagrass through various field studies (Hall-Spencer et al. 2008; Campbell and Fourqurean 2013), mesocosms (Palacios and Zimmerman 2007; Celebi 2016; Zimmerman et al. 2017) and laboratory experiments (Zimmerman et al. 1997; Jiang et al. 2010; McPherson et al. 2015) and numerical models. However, our understanding of the CO<sub>2</sub>-seagrass interactions remains incomplete and sometimes contradictory. The negative relationship observed between CO<sub>2</sub> and N content in various seagrass species is still a subject of debate, and conflicting explanations exist. Terrestrial CO<sub>2</sub>-plant interactions have been used as a reference (Williams et al. 1988; Stitt and Krapp 1999; Schlesinger 2006), but caution must be made when drawing conclusions based on land plants even if the physiological effects of CO<sub>2</sub> are similar. The reported N deficiency in CO<sub>2</sub> enriched land plants is primarily linked to reduced N uptake resulting from improved water use efficiency and changes in stomatal conductance (Ainsworth and Rogers 2007). However, water use efficiency and stomatal conductance are not relevant to seagrasses. Unlike terrestrial plants, seagrasses have the ability to acquire nutrients through both their leaves as well as roots (Thursby and Harlin 1982; Short and McRoy 1984; Pedersen and Borum 1992), and in approximately equal proportions (Iizumi and Hattori 1982; Zimmerman et al. 1987). This increases the potential nutrient resource on which the seagrasses can rely relative to terrestrial plants. Yet,

N-limitation has been invoked to explain low N content in CO<sub>2</sub>-enriched seagrass (Alexandre et al. 2012; Apostolaki et al. 2014; Mishra et al. 2021).

To close some of these knowledge gaps, Zimmerman et al. (1987) conducted a modeling study that aimed to investigate the partitioning of DIN uptake between leaves and roots of *Z. marina* (eelgrass) under varying light and nutrient conditions. That model demonstrated the significance of light levels as predictors of NO<sub>3</sub><sup>-</sup> uptake in leaves and NH<sub>4</sub><sup>+</sup> uptake in roots, as N assimilation relies on photosynthetic and respiratory carbon metabolism to provide reducing energy, photoassimilates and carbon skeletons necessary for synthesizing inorganic N into amino acids (Foyer and Noctor 2002). Notably, in high light environment, the model predicted a slight shift in the nutrient uptake dynamics, with roots playing an increasingly important role in absorbing NH<sub>4</sub><sup>+</sup> from the sediment. This led to the roots increasing their contributions to the overall N uptake, transitioning from roughly equal contributions between leaves and roots to approximately 60%. As with light, high CO<sub>2</sub> conditions should also positively affect leaf and root N uptake activities since elevated CO<sub>2</sub> is known to stimulate photosynthesis and promote the production of fixed carbon (Invers et al. 2002; Palacios and Zimmerman 2007; Zimmerman et al. 2017).

The effects of CO<sub>2</sub> on N uptake can be further complicated by changes in the canopy architecture caused by increased aboveground biomass due to CO<sub>2</sub> stimulated growth. Laboratory measurements (Enríquez et al. 2002) and bio-optical models (Zimmerman 2003; Hedley and Enríquez 2010) have demonstrated that the light environment within seagrass canopy is heterogenous, influenced by canopy structures, and strongly dependent on leaf area index (LAI) (Hedley et al. 2014). Leaf area index serves as an important indicator of photosynthetic capacity of seagrass and is strongly correlated to shoot density and aboveground biomass (Szajnowski 1973;

Lebrasse et al. 2022). In a dense seagrass canopy with high LAI, intense self-shading can significantly reduce light level (Dalla Via et al. 1998; Enríquez and Pantoja-Reyes 2005), and lead to a decrease in canopy-scale photosynthesis (Enríquez et al. 2002). Consequently, in order to provide a mechanistic understanding of how photosynthesis influences N uptake in seagrass, it is crucial to incorporate both CO<sub>2</sub> levels and the structural characteristics of the canopy.

This study utilized a modeling approach to explore the dynamics of CO<sub>2</sub> and N in seagrass. By integrating the nutrient uptake model previously developed by Zimmerman et al. (1987) with *GrassLight* (version 2.14, Zimmerman et al. 2015), a two-flow radiative transfer bio-optical model for submerged aquatic plants, the effects of CO<sub>2</sub> and CO<sub>2</sub>-driven photosynthesis on N requirements for growth were explored. Specifically, this study examined how CO<sub>2</sub>-stimulated photosynthesis influences N uptake patterns by leaves and roots over varying aqueous CO<sub>2</sub> (CO<sub>2(aq)</sub>) concentrations. The objective was to identify conditions where CO<sub>2</sub>-stimulated photosynthesis increases N demand to the point of becoming growth-limiting and to evaluate the likelihood of eelgrass experiencing N-limitation in the future oceanic conditions.

## ***4.2 Materials and methods***

### **4.2.1 The model overview**

The N-growth model is conceptualized using the energy symbol of Odum (1983) (Fig. 34) that illustrates the different components, or state variables, under investigation and their interactions. The specific details describing the mathematical formulations along with the model parameters are detailed below. The *Z. marina* shoot, depicted as a large bullet-shaped symbol (yellow/green), is subdivided into the aboveground leaf and belowground root and rhizome (labeled A and B). Key model components are represented by a storage tank symbol, which

fluctuate during the simulation based on the dissolved inorganic nitrogen (DIN) concentrations,  $\text{CO}_{2(\text{aq})}$ , and light field within the canopy determined by the leaf area index (LAI).  $\text{CO}_2$ -stimulated photosynthesis, in addition to light and the dissolved inorganic nitrogen (DIN) concentrations are assumed to be the major drivers of N uptake by leaves and roots here.

Circular symbols represent the non-depletable resources that are in constant supply. Dissolved inorganic N and  $\text{CO}_{2(\text{aq})}$  concentrations are considered non-depletable resources in this study, while in-water light is considered as a pool (storage tank) and varies with LAI. Porewater  $\text{NH}_4^+$  is also categorized as non-depleting, operating under the assumption that all biomass losses are remineralized in the sediment, thus regenerating  $\text{NH}_4^+$ .

The internal carbon and oxygen pools are positively influenced by  $\text{CO}_{2(\text{aq})}$ , and the magnitude of this influence is determined by LAI. This is because photosynthesis, which drives the accumulation of carbon and oxygen, is directly affected by  $\text{CO}_{2(\text{aq})}$  concentration, and indirectly affected by LAI through self-shading effects of the plant canopy. While the explicit modeling of the effects  $\text{CO}_{2(\text{aq})}$  and LAI on metabolic C balance was not conducted in this study, both of these parameters are embedded into *GrassLight*, and the results do reflect the influence of C on N metabolism.

The oxygen content in the leaves, roots, and rhizomes undergo diurnal fluctuations as a result of photosynthesis, which is driven by  $\text{CO}_{2(\text{aq})}$  and LAI. About 10% of the photosynthetically produced  $\text{O}_2$  pool is transported downward from the leaves to roots and rhizomes where it facilitates aerobic root metabolism, a process crucial to nutrient uptake (Morris and John 1984; Bassirirad 2000; Borum et al. 2006; Bodensteiner 2006). Consequently, aerobic respiration of below-ground roots and rhizomes depends on leaf photosynthesis and its specific formulation is further elaborated in Sections 4.2.2 and 4.2.3.

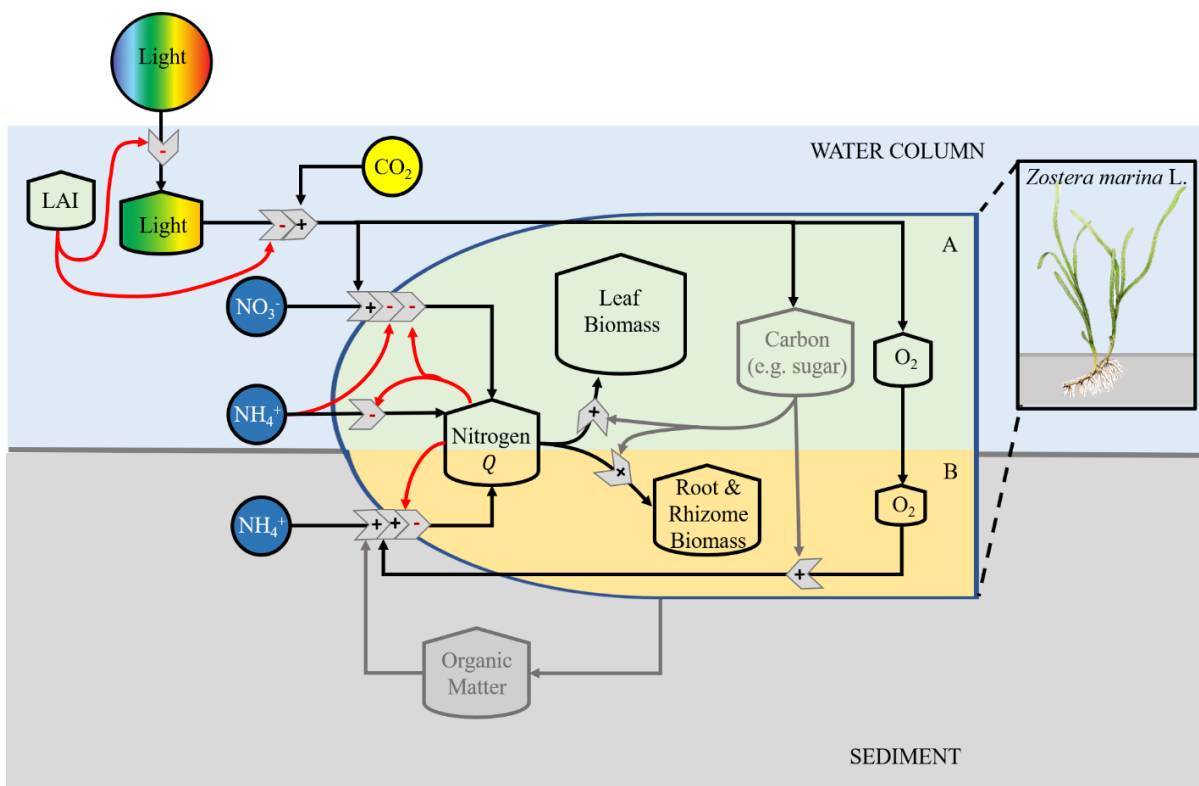


**Fig. 34.** Conceptual diagram illustrating the interactive effects of  $\text{CO}_{2(\text{aq})}$ , light, and nutrient ( $\text{NO}_3^-$ ,  $\text{NH}_4^+$ ) availability on nitrogen (N) uptake in *Zostera marina* L. The symbols used in the diagram are based on the energy symbols of (Odum 1983). The diagram also illustrates how leaf area index (LAI) affects the light available within the canopy for photosynthesis. The arrows represent the flow of energy and substrates, with black arrows indicating positive influences, and red arrows indicating negative influences. Interactions between compartments are represented by grey “work-gate” symbols (block chevrons). The +/- symbols within the work-gates indicate positive or negative interactions. Although the carbon and organic matter pools (represented as grey storage tank symbols) are not explicitly defined in the model, they are included in the diagram due to their important roles in influencing the nitrogen flow. Exploring the dynamics of these components presents a valuable direction for future research.

Leaves are responsible for the uptake of  $\text{NO}_3^-$  and/or  $\text{NH}_4^+$  from the water column, whereas roots only take up  $\text{NH}_4^+$  from the sediment in the model. Porewater  $\text{NO}_3^-$  was not considered in the model based on the assumption that anaerobic N remineralization generates  $\text{NH}_4^+$ , not  $\text{NO}_3^-$  in the porewater (Kelso et al. 1997; Behrendt et al. 2013). The uptake of  $\text{NH}_4^+$  from the sediment by roots depends on aerobic respiratory carbon metabolism, which requires oxygen to facilitate the process. Consequently, the root uptake of  $\text{NH}_4^+$  is modeled as a photosynthesis dependent process.

Leaf uptake of  $\text{NO}_3^-$  from the water column is also modeled as a photosynthesis dependent process because the assimilation of  $\text{NO}_3^-$  requires reducing power, such as NADP and ferredoxin that are generated during photosynthetic electron transport process (Sanz-Luque et al. 2015). However, it is not expected that photosynthesis influences the leaf uptake of  $\text{NH}_4^+$  in this model based on previous results that demonstrate a lack of diurnal variation in the uptake rates for  $\text{NH}_4^+$  in *Zostera* spp. (Iizumi and Hattori 1982; Alexandre et al. 2016).

The rate of N uptake by leaves and roots is dependent on the size of the internal nitrogen quota ( $Q$ ), which is constrained by the upper and lower limit of tissue N content. The size of  $Q$  has a direct impact on N uptake rates, and the balance between uptake (input),  $Q$  (pool), and demand (output) determines the growth of *Z. marina* (Droop 1973). Growth is assumed to occur provided that  $Q$  exceeds the minimum nitrogen quota. The specific mathematical formulation that describes the relationship of  $Q$  on N uptake rate is discussed in detail in sections 4.2.4 through 4.2.6 below. Additionally, the rate of  $\text{NO}_3^-$  uptake by leaves and  $\text{NH}_4^+$  by roots is subjected to feedback inhibition based on the concentration of  $\text{NH}_4^+$  in the water column because  $\text{NO}_3^-$  assimilation is competitively inhibited by  $\text{NH}_4^+$  (Müller and Janiesch 1993). Similarly, there is evidence that  $\text{NH}_4^+$  uptake by roots is inhibited by  $\text{NH}_4^+$  uptake by leaves (Thursby and Harlin 1982). The inhibitory

effect of  $\text{NH}_4^+$  saturation on  $\text{NO}_3^-$  and  $\text{NH}_4^+$  uptake is mathematically expressed in Eq. (18) in section 4.2.5 of the study.

The daily remineralization rate of sedimentary organic matter needed to satisfy the growth demand of eelgrass is not explicitly simulated in this study. Instead, it is calculated post hoc using the model generated results. The N demand at growth saturation, determined by the model, serves as a threshold for comparing model demand to the calculated remineralization rate obtained from the literature. If the remineralization rate is below this threshold, then balance growth cannot be sustained by root uptake activity alone. The calculation of remineralization rate is expressed in Eq. (21) in section 4.2.7.

The parameter space for the model is defined in Fig. 35. The N uptake rates by leaves and roots were simulated for six distinct  $\text{CO}_{2(\text{aq})}$  levels over a range of DIN ( $0\text{-}25 \mu\text{M NO}_3^-$ ,  $0\text{-}25 \mu\text{M NH}_4^+$ , and  $0\text{-}100 \mu\text{M porewater NH}_4^+$ ) concentrations. To mimic the reduction of light level in an increasingly dense canopy, and to explore its impact on photosynthesis and N uptake pattern, simulations were carried out for a range of fixed leaf area index (LAI) values of 0.15, 1.0, 1.5, 2.0, 2.5, and 3.0 ( $\text{m}^2 \text{ leaf m}^{-2} \text{ seafloor}$ ), which are observed in the field (Bostrom and Erik 2000; Barañano et al. 2022). Both N uptake and *GrassLight* models are introduced in further detail in the section directly below. The same parameter space was also used to parameterize the *GrassLight* model used to calculate photosynthesis and respiration rates. Estimates of eelgrass photosynthesis were modeled as a function of pH and LAI.

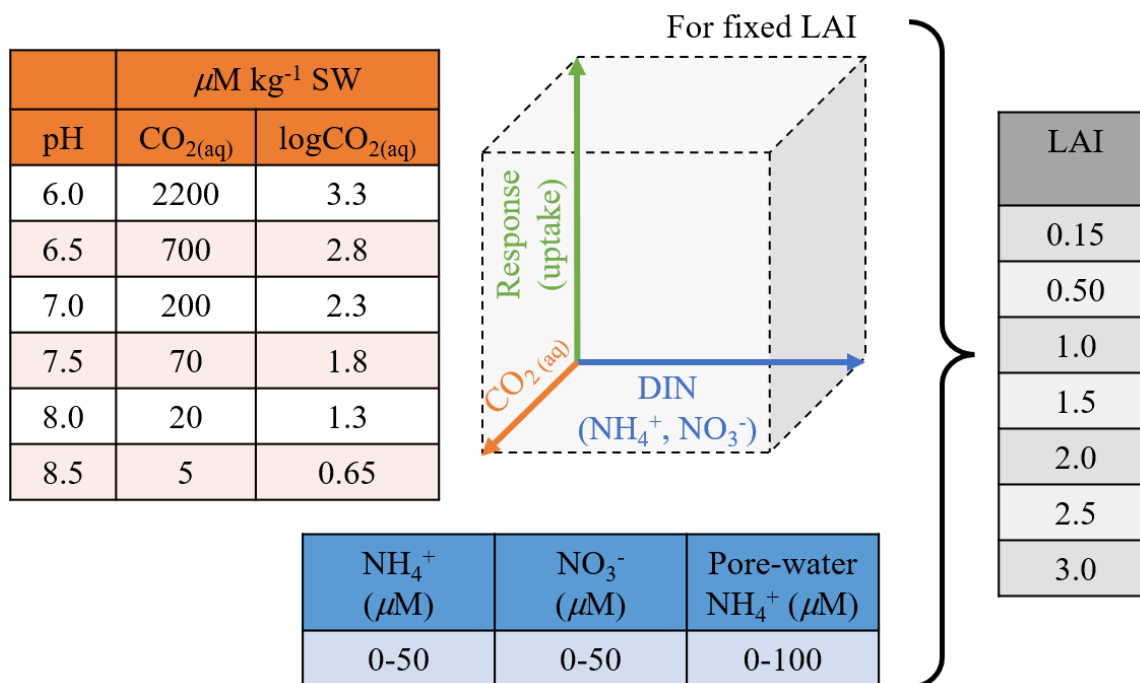


**Fig. 35.** Parameter space defining the N-growth model. For each simulation, responses such as leaf and root uptake rates (green; z-axis) were modeled as a function of  $\text{CO}_{2(\text{aq})}$  (orange; y-axis), dissolved inorganic N (blue; x-axis), for seven distinct levels of LAI (grey) ranging from 0.15 (sparse canopy) to 3.0 (dense canopy). The  $\text{CO}_{2(\text{aq})}$  concentrations were calculated using CO2SYS (Excel version 2.1) (Lewis and Wallace 2006) using temperature, alkalinity and salinity (Table 13) for six distinct pH levels. In this study,  $\text{CO}_{2(\text{aq})} = 2200$  or pH 6.0 represents the highest  $\text{CO}_{2(\text{aq})}$  condition, and  $\text{CO}_{2(\text{aq})} = 5$  or pH 8.5 represents lowest or ambient  $\text{CO}_{2(\text{aq})}$  condition.

**Table 12.** Summary of symbols (in alphabetical order), their definitions, and dimensions.

| Symbol                             | Definition   | Units  |
|------------------------------------|--|--|
| $B_{\text{leaves}}$                | Leaf biomass   | $\text{g DW}^{-1} \text{m}^{-2}$                       |
| $B_{\text{roots}}$                 | Root biomass   | $\text{g DW}^{-1} \text{m}^{-2}$                       |
| $\text{CO}_{2(\text{aq})}$         | Aqueous $\text{CO}_2$  | $\mu\text{M kg}^{-1} \text{SW}$                        |
| $D_b$                              | Dry bulk sediment density  | $\text{g DW m}^{-3}$                                   |
| $dt$                               | Timestep ( $dt = 1/64$ )   | h  |
| DIN                                | Dissolved inorganic nitrogen   | $\mu\text{M}$  |
| DW                                 | Dry weight   | g  |
| $F_{\text{NH}_4^+}$                | Rate limiting term that inhibits the leaf $\text{NO}_3^-$ and root $\text{NH}_4^+$ uptake rates                        | Dimensionless  |
| $kG_N$                             | Remineralization rate of organic nitrogen undergoing first order decay ( $k$ in $\text{d}^{-1}$ )                      | $\text{mmol N m}^{-2} \text{d}^{-1}$                   |
| $K_s$                              | Half saturation constant   | $\mu\text{M}$  |
| LAI                                | Leaf area index  | $\text{m}^2 (\text{leaf}) \text{m}^{-2} (\text{area})$ |
| $N_D$                              | Predicted $\text{CO}_2$ N demand at growth saturation  | $\text{g N m}^{-2} \text{d}^{-1}$                      |
| $P_c$                              | Instantaneous photosynthetic rates of a canopy   | $\mu\text{mol C shoot}^{-1} \text{dt}^{-1}$            |
| $P_E$                              | Light and $\text{CO}_2$ -saturated rate of photosynthesis  |  |
| $P_{\text{lim}}$                   | Photosynthetic constraints that limit the leaf N uptake rate based on the ratio $P_c/P_m$                              | Dimensionless  |
| $P_{\text{max}}$                   | Light saturated rate of photosynthetic   | $\mu\text{mol C shoot}^{-1} \text{dt}^{-1}$            |
| PQ                                 | Photosynthetic quotient  | Dimensionless  |
| $Q$                                | Internal N quota   | % of DW  |
| $Q_D$                              | Rate limiting term that control the uptake rate based on the size of $Q$   | Dimensionless  |
| $Q_{\text{max}}$                   | Maximum N content  | % of DW  |
| $Q_{\text{min}}$                   | Minimum N content  | % of DW  |
| $R_{\text{lim}}$                   | Respiratory constraints that limit the root N uptake based on the ratio $R_{\text{root}}/R_{\text{root}}^{\text{max}}$ | Dimensionless  |
| $R_{\text{root+rhi}}$              | Aerobic respiratory demand for belowground tissues   | $\mu\text{mol O}_2 \text{shoot}^{-1} \text{dt}^{-1}$   |
| $R_{\text{root+rhi}}^{\text{max}}$ | Maximum root+rhizome aerobic respiratory demand  | $\text{mol O}_2 \text{shoot}^{-1} \text{dt}^{-1}$      |
| SW                                 | Seawater   |  |
| $V_{\text{max}}$                   | Maximum uptake rate of DIN   | $\mu\text{mol N shoot}^{-1} \text{d}^{-1}$             |
| $V_p^{\text{LNH}_4}$               | Potential uptake rate of $\text{NH}_4^+$ by leaves   | $\mu\text{mol N shoot}^{-1} \text{d}^{-1}$             |
| $V_p^{\text{LNO}_3}$               | Potential uptake rate of $\text{NO}_3^-$ by leaves   | $\mu\text{mol N shoot}^{-1} \text{d}^{-1}$             |
| $V_p^{\text{RNH}_4}$               | Potential uptake rate of $\text{NH}_4^+$ by roots  | $\mu\text{mol N shoot}^{-1} \text{d}^{-1}$             |
| $V_r^{\text{LNH}_4}$               | Realized uptake rate of $\text{NH}_4^+$ by leaves  | $\mu\text{mol N shoot}^{-1} \text{d}^{-1}$             |
| $V_r^{\text{LNO}_3}$               | Realized uptake rate of $\text{NO}_3^-$ by leaves  | $\mu\text{mol N shoot}^{-1} \text{d}^{-1}$             |
| $V_r^{\text{RNH}_4}$               | Realized uptake rate of $\text{NH}_4^+$ by roots   | $\mu\text{mol N shoot}^{-1} \text{d}^{-1}$             |
| $V_{\text{rmQ}}$                   | Maximum realized N uptake rate constrained by $Q$  | $\mu\text{mol N shoot}^{-1} \text{d}^{-1}$             |
| $z$                                | Sediment depth   | m  |
| $\varphi$                          | Sediment porosity  | Dimensionless  |

#### 4.2.2 Determining photosynthesis using *GrassLight*

Photosynthesis of the eelgrass canopy was calculated using the bio-optical model *GrassLight* (Ver. 2.14), which simulates the vertical propagation of spectral irradiance through a submerged canopy within an optically homogenous water column and calculates the in-canopy light environment where light quality and quantity are a function of water quality (CDOM, total suspended particles, Chl *a*) and canopy architecture (shoot density, leaf area index, leaf orientation, leaf morphology) (Zimmerman 2003; Zimmerman 2006). *GrassLight* calculates photosynthetically utilized radiation (PUR) absorbed by each vertical layer of the seagrass canopy, as described by Zimmerman (2003) and Zimmerman (2006). Using PUR, the biomass-specific instantaneous photosynthetic rate in layer  $z$  of the canopy and the amount is calculated using a non-linear cumulative one-hit Poisson model (Webb et al. 1974; Falkowski and Raven 2007):

$$P(z) = l(z) \cdot P_{\max} \cdot \left\{ 1 - \exp \left[ - \frac{\phi_p \cdot \text{PUR}(z)}{P_{\max}} \right] \right\} \quad (8)$$

where,  $l(z)$  represents the vertical biomass distribution or leaf area index in layer  $z$  [LAI( $z$ )],  $P_{\max}$  represents the light-saturated rate of photosynthesis, and  $\phi_p$  is the quantum yield of photosynthesis ( $1/8 \text{ mol C mol}^{-1} \text{ PUR}$ ). The summation of  $P(z)$  over all layer  $z$  gives the whole canopy production ( $P_c$ ):

$$P_E = 82 \cdot e^{(-0.53\text{pH})} \quad (9)$$

The impact of  $\text{CO}_{2(\text{aq})}$  on the overall canopy photosynthesis,  $P_c$ , was determined by substituting  $P_E$  for  $P_{\max}$  in Eq. (8). To convert  $P_E$  from relative units to  $\mu\text{mol O}_2 \text{ shoot}^{-1} \text{ dt}^{-1}$  ( $\text{dt} = 1/64 \text{ hour}$ ), the net oxygen release rate at pH 8.0 established for *Z. marina* by Invers et al. (2001), along with parameter values for leaf properties (leaf biomass, leaf size) in Table 2, were utilized.

Similar to  $\text{CO}_2$ , changes in shoot density will affect  $P_c$  due to its impact on PUR( $z$ ). Because photosynthesis responds non-linearly to light intensity,  $P_c$  will increase with shoot density

until self-shading effects start to reduce the amount of light delivered to lower portions of the canopy, where most of the leaf biomass resides (Zimmerman 2003; Zimmerman 2006). To investigate the effects of varying shoot density on  $P_c$ , LAI values were simulated across a range of 0.15 (79 shoots  $m^{-2}$ ) to 3.0 (1587 shoots  $m^{-2}$ ) by adjusting the parameter values in the *GrassLight* model.

Canopy photosynthesis was assumed to occur under light saturating condition unless otherwise specified. The parameter  $P_c$  was computed at every timestep (dt), over 24 hours for plants subjected to 14.7 hours of sunlight under cloudless sky on the summer solstice at  $37^\circ$  N (June 21). Other physical parameters required to run *GrassLight* can be found in Table 2. The results were then used to calculate the aerobic respiratory demands of leaves, roots, and rhizomes (section 4.2.3) that were incorporated into the N-growth model to quantify the effects of  $CO_{2(aq)}$  on the photosynthesis dependent N (as  $NH_4^+$  and  $NO_3^-$ ) uptake kinetics (section 4.2.4 and 4.2.5).

#### 4.2.3 Effects of $CO_{2(aq)}$ on aerobic respiration rate of roots+rhizomes

The aerobic respiratory demands of leaves ( $R_{leaf}$ ), roots ( $R_{root}$ ), and rhizomes ( $R_{rhi}$ ) were modeled as a photosynthesis dependent process (assuming 10% of the oxygen produced in leaves was transported belowground (Borum et al. 2006),  $R_{root}$  and  $R_{rhi}$  were quantified by scaling to 10% of  $P_E$ . The effects of  $CO_{2(aq)}$  on the maximum aerobic respiratory demand of leaves, roots, and rhizomes were calculated as follows (Zimmerman et al. 1989):

$$R_{leaf}^{max} = 0.2P_E \quad (10)$$

$$R_{root}^{max} = 0.5R_{leaf}^{max} \quad (11)$$

$$R_{rhi}^{max} = 0.5R_{root}^{max} \quad (12)$$

The sum of  $R_{\text{root}}^{\text{max}}$  and  $R_{\text{rhi}}^{\text{max}}$  represented the maximum respiratory demand of the belowground tissues ( $R_{\text{root+rhi}}^{\text{max}}$ ). The linear relationship between  $R_{\text{root+rhi}}^{\text{max}}$  and  $P_E$  provided the basis for calculating  $R_{\text{root+rhi}}$  based on the modeled daily  $P_c$  predicted for each  $\text{CO}_{2(\text{aq})}$  scenario. The results were then incorporated into the N-growth model to quantify the effects of  $\text{CO}_{2(\text{aq})}$  on the uptake rates of  $\text{NH}_4^+$  by the roots (see section 4.2.6).

#### 4.2.4 Realized Leaf $\text{NH}_4^+$ uptake rate

The potential uptake rate of  $\text{NH}_4^+$  by leaves depended on the dissolved  $\text{NH}_4^+$  concentration in the bulk seawater, according to the Michaelis-Menton equation as:

$$V_p^{\text{LNH}_4} = \frac{V_{\text{max}} \cdot [\text{NH}_4^+]}{K_s + [\text{NH}_4^+]} \cdot B_{\text{leaves}} \quad (13)$$

where  $V_{\text{max}}$  and  $K_s$  were the theoretical maximum uptake rate ( $\mu\text{mol N g DW}^{-1} \text{d}^{-1}$ ) and the half-saturation constant for  $\text{NH}_4^+$  ( $\mu\text{M}$ ) obtained from Thursby and Harlin (1982) (Table 3),  $[\text{NH}_4^+]$  represented the ammonium concentration in seawater, and  $B_{\text{leaves}}$  ( $= \text{LAI} \times \text{leaf mass area}$ ) represented the aboveground (leaf) biomass in units of  $\text{g DW shoot}^{-1}$ . Ammonium uptake by leaves was subjected to feedback inhibition by the internal N quota ( $Q$ ) originally proposed by Droop (1968), which was regulated by the upper and lower N limits as specified in the initial condition presented in Table 3:

$$V_r^{\text{LNH}_4} = V_p^{\text{LNH}_4} \cdot Q_D \quad (14)$$

where  $Q_D$  limited the uptake rate based on the size of  $Q$ :

$$Q_D = 1 - \frac{Q - Q_{\text{min}}}{Q_{\text{max}} - Q_{\text{min}}} \quad (15)$$

When  $Q = Q_{\text{max}}$ , the quota is full and the nutrient uptake goes to 0. When  $Q$  approaches  $Q_{\text{min}}$ ,  $Q_N$  approaches 1 (no feedback inhibition).

#### 4.2.5 Realized leaf NO<sub>3</sub><sup>-</sup> uptake rate

The potential uptake rate of NO<sub>3</sub><sup>-</sup> by the leaves ( $V_p^{LNO_3}$ ) was calculated using the same formulations as for ammonium [Eq. (13) and (14)]. Due to the lack of available data for NO<sub>3</sub><sup>-</sup> uptake by *Z. marina*, the same theoretical constants ( $V_{max}$  and  $K_s$ ) as those used to calculate  $V_r^{LNH_4}$  were employed. However, the uptake rates were modeled as a photosynthesis dependent process as NO<sub>3</sub><sup>-</sup> assimilation relies on energy generated during photosynthesis (Huppe and Turpin 1994). Furthermore, in addition to being constrained by the size of  $Q$ , the uptake of NO<sub>3</sub><sup>-</sup> by leaves was also inhibited by the degree to which NH<sub>4</sub><sup>+</sup> uptake was saturated in leaves (Thursby and Harlin 1982). The combined effects of CO<sub>2</sub>-stimulated photosynthesis, size of  $Q$ , and inhibition from NH<sub>4</sub><sup>+</sup> on the realized rate of NO<sub>3</sub><sup>-</sup> uptake in leaves was quantified as:

$$V_r^{LNO_3} = V_p^{LNH_4} \cdot Q_D \cdot P_{lim} \cdot F_{NH_4^+} \quad (16)$$

where  $Q_D$  was defined in Eq. (15), and  $P_{lim}$  (ratio) represented the photosynthetic constraints that sensitized the uptake rates to CO<sub>2(aq)</sub> availability using pH as proxy:

$$P_{lim} = \frac{P_{c(pH)}}{P_{E(pH8.5)}} \quad (17)$$

The term  $P_{c(pH)}$  represented pH dependent  $P_c$  output from *GrassLight* and  $P_{E(pH8.5)}$  was  $P_E$  at pH 8.5 (low CO<sub>2(aq)</sub> concentration). The feedback effect,  $F_{NH_4^+}$ , was mathematically defined as:

$$F_{NH_4^+} = 1 - \frac{V_r^{LNH_4}}{V_{max}} \quad (18)$$

#### 4.2.6 Realized root $\text{NH}_4^+$ uptake rate

The assimilation of  $\text{NH}_4^+$  by the roots requires aerobic respiration provided by the lacunal transport of photosynthetically produced oxygen from the leaves (Morris 1984; Rosen and Carlson 1984). The root uptake rate of  $\text{NH}_4^+$  from the sediment was therefore, regulated by  $P_c$  and consequently  $R_{\text{root+rhi}}$ . Following a similar mathematical expression as Eq. (16), the realized root  $\text{NH}_4^+$  uptake rate was defined as:

$$V_r^{\text{RNH}_4} = V_p^{\text{RNH}_4} \cdot Q_D \cdot R_{\text{lim}} \cdot F_{\text{NH}_4^+} \quad (19)$$

and  $V_p^{\text{RNH}_4}$  was defined as:

$$V_p^{\text{RNH}_4} = \frac{V_{\text{max}} \cdot \text{porewater}[\text{NH}_4^+]}{K_s + \text{porewater}[\text{NH}_4^+]} \cdot B_{\text{roots}} \quad (20)$$

The term  $V_p^{\text{RNH}_4}$  denoted the potential uptake rate of  $\text{NH}_4^+$  by belowground tissues, which was governed by the theoretical kinetic constants  $V_{\text{max}}$  and  $K_s$  specific to  $\text{NH}_4^+$  uptake by roots (Table 3). The rate of uptake was also determined by porewater  $[\text{NH}_4^+]$  and the amount of belowground biomass ( $B_{\text{roots}}$ ) (g DW shoot<sup>-1</sup>). In Eq. (19), the terms  $Q_D$  and  $F_{\text{NH}_4^+}$  were defined by Eq. (15) and (18), respectively. The parameter  $R_{\text{lim}}$  represented the  $\text{CO}_2$ -dependent  $R_{\text{root+rhi}}$  and was determined by normalizing pH-specific  $R_{\text{root+rhi}}$  to  $R_{\text{root+rhi}}^{\text{max}}$  at pH 8.5. The rationale behind  $R_{\text{lim}}$  was the similar to  $P_{\text{lim}}$ .

#### 4.2.7 Estimates of remineralization rate

A modified version of a basic diagenetic equation of organic matter was used to calculate the rate of organic nitrogen remineralization needed to meet the predicted N uptake requirement at growth saturation as projected by the model. The rate was calculated as follow:

$$kG_N = \frac{N_D}{D_b \cdot \varphi \cdot z} \quad (21)$$

The parameter  $kG_N$  ( $\text{mmol N m}^{-2} \text{ d}^{-1}$ ) was determined for sediment at depth of 20 cm ( $z$ ) with a dry bulk density ( $D_b$ ) of  $1.7 \times 10^6 \text{ g DW m}^{-3}$ , assuming a constant porosity ( $\varphi$ ) of 30%. This calculation was performed under the assumption of no bioturbation and no  $\text{NH}_4^+$  adsorption by the sediments (Mortland 1955).

The term  $N_D$  ( $\text{mmol N m}^{-2} \text{ d}^{-1}$ ) represented the maximum realized rate of N (as  $\text{NH}_4^+$  and  $\text{NO}_3^-$ ) uptake required to achieve growth saturation, as determined from Eq. (14), (16), and (19) at steady state. It was assumed that the remineralization of organic N followed first-order decay rate ( $k$  in  $\text{d}^{-1}$ ).

#### 4.2.8 Model parameterization

The fixed parameters used for running the *GrassLight* model this study are summarized in Table 2. All other parameters (such as chlorophyll  $a$ , CDOM, and turbidity) were maintained at their default values. Shoot density ( $\text{shoots m}^{-2}$ ) was calculated from the LAI values, assuming a shoot leaf area of  $0.002 \text{ m}^2 \text{ shoot}^{-1}$  (Zimmerman unpublished data for *Z. marina* from South Bay population in Eastern Shore, Virginia). The model assumed a clean leaf surface without any epiphyte load. The optical properties of the water were modeled for a water depth of 1 m during the summer solstice in the Northern Hemisphere. The coordinates (latitude and longitude) necessary for generating irradiance profile were parameterize using the location of the  $\text{CO}_2$  experiment presented in Chapter 2. Water temperature was fixed at  $26 \text{ }^\circ\text{C}$  to simulate a typical warm summer, below the  $30 \text{ }^\circ\text{C}$  threshold that elicits thermal stress in eelgrass (Zimmerman et al. 1989; Hammer et al. 2018).

A list of values in Table 3 was used to parameterize the N-growth model. The theoretical constants related to the maximum uptake velocity ( $V_{\max}$ ) and half-saturation constant ( $K_s$ ) for  $\text{NH}_4^+$  and  $\text{NO}_3^-$  uptake kinetics in leaves and roots were obtained from the literature. Growth was capped at  $3\% \text{ d}^{-1}$ , regardless of  $Q$ , a reasonable upper estimate for a productive eelgrass population (Dennison and Alberte 1982; Short 1987; Zimmerman et al. 2017). The values for  $Q$  were constrained not to exceed 4% of DW ( $Q_{\max}$ ) or drop below 0.95% of DW ( $Q_{\min}$ ) for the entire shoot (leaves, roots, and rhizomes combined). The N contents of new leaf and root/rhizome tissues were set at 2% and 1% (of DW), respectively. The values for  $Q_{\max}$  and N content of new leaves were obtained from Chapter 2 and represented the average of the entire leaf N dataset collected over 18 months of experimentation. The values for  $Q_{\min}$  and N content for new roots were based on Zimmerman et al. (1987). Growth was allocated between roots/rhizome and leaves at a constant root:shoot ratio of 1:3 to maintain allometric growth (Duarte 1991). All calculations were performed using a 1/64 (h) timestep and terminated when  $Q$ , growth rates, and N uptake rates stabilized (aka steady state condition). Consequently, all results presented in this study reflect the model's steady state solutions under the specified conditions mentioned earlier.

**Table 13.** Fixed parameter values assigned to each *GrassLight* run. CO<sub>2</sub> simulation was performed for a range of pH (or CO<sub>2(aq)</sub>) condition under different LAI values. The pH (or CO<sub>2(aq)</sub>) values are given in Fig. 35. All runs were conducted for summer solstice with 14.7 hours of sunlight and under cloudless sky. Parameters not listed below have their default values commanded in *GrassLight*. See *GrassLight* model and Zimmerman references for details.  $B_{\text{leaves}} = \text{LAI} \times \text{leaf mass area}$ . Value for leaf mass area is given in Table 14.

| Parameter          | Values   | Units                              |
|--------------------|----------|------------------------------------|
| Latitude           | 36.8207  | degree                             |
| Longitude          | -75.9841 | degree                             |
| Water temperature  | 26       | °C                                 |
| Salinity           | 30       | PSS                                |
| Alkalinity         | 2.2      | mEq L <sup>-1</sup>                |
| Water depth        | 1        | m                                  |
| Canopy height      | 0.3      | m                                  |
| Leaf epiphyte load | 0        | mg cm <sup>-2</sup>                |
| Shoot leaf area    | 0.00189  | m <sup>2</sup> shoot <sup>-1</sup> |
| Shoot density:     |          |                                    |
| LAI 0.15           | 79       | shoot m <sup>-2</sup>              |
| LAI 0.5            | 265      | shoot m <sup>-2</sup>              |
| LAI 1.0            | 529      | shoot m <sup>-2</sup>              |
| LAI 1.5            | 794      | shoot m <sup>-2</sup>              |
| LAI 2.0            | 1058     | shoot m <sup>-2</sup>              |
| LAI 2.5            | 1323     | shoot m <sup>-2</sup>              |
| LAI 3.0            | 1587     | shoot m <sup>-2</sup>              |
| Shoot:Root Ratio   | 3:1      |                                    |

**Table 14.** Fixed parameter values assigned to each N-growth model run. The effects of CO<sub>2(aq)</sub> on N uptake were performed for a range of pH (or CO<sub>2(aq)</sub>) condition for a fixed LAI value (given in Table 13).

| Parameter  | Values                   |       |       |       |       |       | Units  | Source                                   |
|--|--------------------------|-------|-------|-------|-------|-------|--|--|
|  | CO <sub>2(aq)</sub> (pH) |       |       |       |       |       |  |  |
|  | 2200                     | 700   | 200   | 70    | 20    | 5     |  |  |
|  | (6.0)                    | (6.5) | (7.0) | (7.5) | (8.0) | (8.5) |  |  |
| $V_{\max}$ of NH <sub>4</sub> <sup>+</sup> by leaves |                          |       | 20.5  |       |       |       | $\mu\text{M g DW}^{-1} \text{ h}^{-1}$                 | Thursby and Harlin (1982)                |
| $K_s$ of NH <sub>4</sub> <sup>+</sup> by leaves      |                          |       | 9.2   |       |       |       | $\mu\text{M}$  | Thursby and Harlin (1982)                |
| $V_{\max}$ of NO <sub>3</sub> <sup>-</sup> by leaves |                          |       | 20.5  |       |       |       | $\mu\text{M g DW}^{-1} \text{ h}^{-1}$                 | Zimmerman et al. (1987)                  |
| $K_s$ of NO <sub>3</sub> <sup>-</sup> by leaves      |                          |       | 9.2   |       |       |       | $\mu\text{M}$  | Zimmerman et al. (1987)                  |
| $V_{\max}$ of NH <sub>4</sub> <sup>+</sup> by roots  |                          |       | 211   |       |       |       | $\mu\text{M g DW}^{-1} \text{ h}^{-1}$                 | Thursby and Harlin (1982)                |
| $K_s$ of NH <sub>4</sub> <sup>+</sup> by roots       |                          |       | 104   |       |       |       | $\mu\text{M}$  | Thursby and Harlin (1982)                |
| $P_E$  | 0.25                     | 0.19  | 0.15  | 0.11  | 0.09  | 0.07  | $\mu\text{mol O}_2 \text{ shoot}^{-1} \text{ dt}^{-1}$ | Values determined from <i>GrassLight</i> |
| $R_{\text{root+rhi}}^{\max}$                         | 0.025                    | 0.019 | 0.015 | 0.011 | 0.009 | 0.007 | $\mu\text{mol O}_2 \text{ shoot}^{-1} \text{ dt}^{-1}$ | Calculated using Eq. (10-12)             |
| $Q_{\min}$   |                          |       | 0.95  |       |       |       | % of DW  | Zimmerman et al. (1987)                  |
| $Q_{\max}$   |                          |       | 4     |       |       |       | % of DW  | CO <sub>2</sub> experiment (Chapter 2)   |
| N content for new leaf tissue                        |                          |       | 2     |       |       |       | % of DW  | CO <sub>2</sub> experiment (Chapter 2)   |
| N content for new root tissue                        |                          |       | 1     |       |       |       | % of DW  | Zimmerman et al. (1987)                  |
| Maximum SGR  |                          |       | 3     |       |       |       | % d <sup>-1</sup>                                      | CO <sub>2</sub> experiment (Chapter 2)   |
| Root:Shoot ratio                                     |                          |       | 1:3   |       |       |       | $\text{g DW}^{-1} \text{ m}^{-2}$                      | Zimmerman et al. (2015)                  |
| Leaf mass area                                       |                          |       | 100   |       |       |       | $\text{g FW m}^{-2} \text{ leaf}$                      | Zimmerman unpublished data               |
| DW:FW  |                          |       | 0.2   |       |       |       | $\text{g DW}$  | Jinuntuya unpublished data               |

### 4.3 Results

#### 4.3.1 The effects of $\text{CO}_{2(\text{aq})}$ and LAI on photosynthesis and root respiration

The maximum respiration rates for roots/rhizome ( $R_{\text{root+rhi}}^{\text{max}}$ ) based on Eq. (10), (11), and (12), displayed a linear relationship across the  $P_E$  gradient, and ranged between  $2 \times 10^{-4}$  and  $6 \times 10^{-4} \mu\text{mol O}_2 \text{ shoot}^{-1} \text{ dt}^{-1}$  (Fig. 36). This relationship led to the prediction that approximately 2% of the photosynthetically generated oxygen supplied from leaves (assumed to be 10%), was utilized to support root metabolism, while 8% diffused into the sediment.

Because all simulations were performed for the summer solstice, photosynthesis occurred over a daylight period of 14.7 hours. The diurnal pattern in  $P_c$  showed a strong response to pH (or  $\text{CO}_{2(\text{aq})}$ ) during the daylight period (Fig. 37A-F). The daily pattern of canopy photosynthesis closely tracked the sinusoidal pattern of light availability and the effects of canopy self-shading decreased shoot-specific photosynthesis with increasing LAI at pH 6. The effects of LAI on  $P_c$  was greatest at pH 6.0, where the increase in LAI from 0.15 to  $3.0 \text{ m}^2 \text{ m}^{-2}$  resulted in a near 50% drop in  $\text{O}_2$  production.  $P_c$  decreased for all LAI scenarios as pH increased but the self-shading effect from increasing LAI decreased. However, the daily pattern of photosynthesis became more square-wave as  $P_c$  became limited by  $\text{CO}_{2(\text{aq})}$  availability. This plateauing effect was strongest at pH 8.5 but was also observed at pH 7.0 for LAI of  $1.0 \text{ m}^2 \text{ m}^{-2}$  and below.

Utilizing the relationship illustrated in Fig. 36, the estimation of  $R_{\text{root+rhi}}$  based on  $P_c$  exhibited a cascading impact resulting from variations in  $\text{CO}_{2(\text{aq})}$ /pH levels, mirroring the  $P_c$  trends observed in Fig. 37A-F. In contrast to the direct influence of  $\text{CO}_{2(\text{aq})}$  on  $P_c$ , the impact of  $\text{CO}_{2(\text{aq})}$  on  $R_{\text{root+rhi}}$  was mediated by  $\text{O}_2$  production, with the highest level observed under high  $\text{CO}_{2(\text{aq})}$  conditions and lowest under low  $\text{CO}_{2(\text{aq})}$  conditions. As with  $P_c$ ,  $R_{\text{root+rhi}}$  was highest at high  $\text{CO}_{2(\text{aq})}$ /low LAI (Fig. 37G-L) and lowest at low  $\text{CO}_{2(\text{aq})}$ /high LAI. The effects of LAI on  $R_{\text{root+rhi}}$

increased with decreasing  $\text{CO}_{2(\text{aq})}$  concentration, with the impact being smallest under low  $\text{CO}_{2(\text{aq})}$  concentration and became progressively larger as the concentrations increased. Under the highest  $\text{CO}_{2(\text{aq})}$  simulation, increasing LAI from 0.15 to 3.0 resulted in approximately 30% reduction in  $R_{\text{root+rhi}}$ . Further, in this condition,  $R_{\text{root+rhi}}$  never reached  $R_{\text{root+rhi}}^{\text{max}}$  indicating that the respiration rates were not limited by  $\text{CO}_{2(\text{aq})}$  but rather by light.

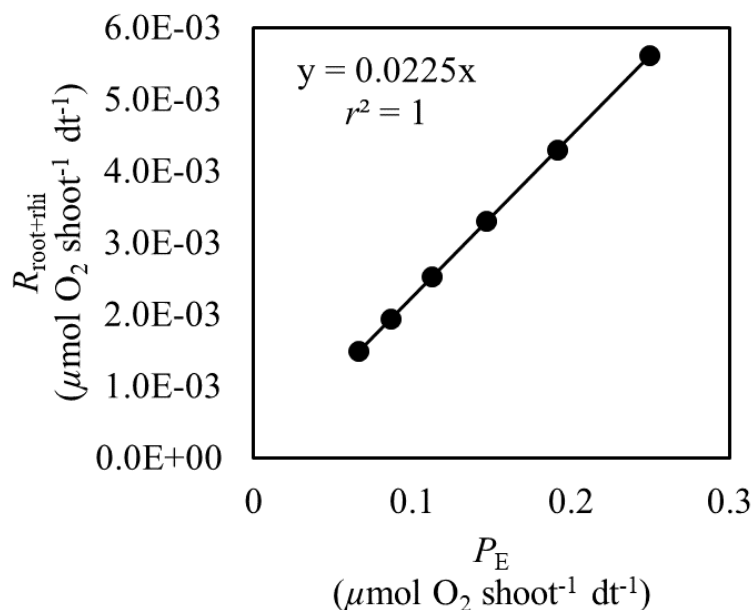


**Fig. 36.** A property-property plot demonstrating the linear relationship between light and  $\text{CO}_2$ -saturated rate of photosynthesis ( $P_E$ ) and maximum aerobic respiratory demand of roots+rhizome ( $R_{\text{root+rhi}}^{\text{max}}$ ) determined for *Zostera marina* L.  $P_E$  values were estimated using *GrassLight* model based on conditions outlined in Table 2 for six pH ( $\text{CO}_{2(\text{aq})}$ ) levels; pH = 6.0 (2200  $\mu\text{M}$ ), pH = 6.5 (700  $\mu\text{M}$ ), pH = 7.0 (200  $\mu\text{M}$ ), pH = 7.5 (70  $\mu\text{M}$ ), pH = 8.0 (20  $\mu\text{M}$ ), and pH = 8.5 (5  $\mu\text{M}$ ). The  $R_{\text{root+rhi}}^{\text{max}}$  was calculated according to Eq. (10), (11), and (12) It was assumed that 10% of  $P_E$  was available to roots for respiration (Borum et al. 2006).

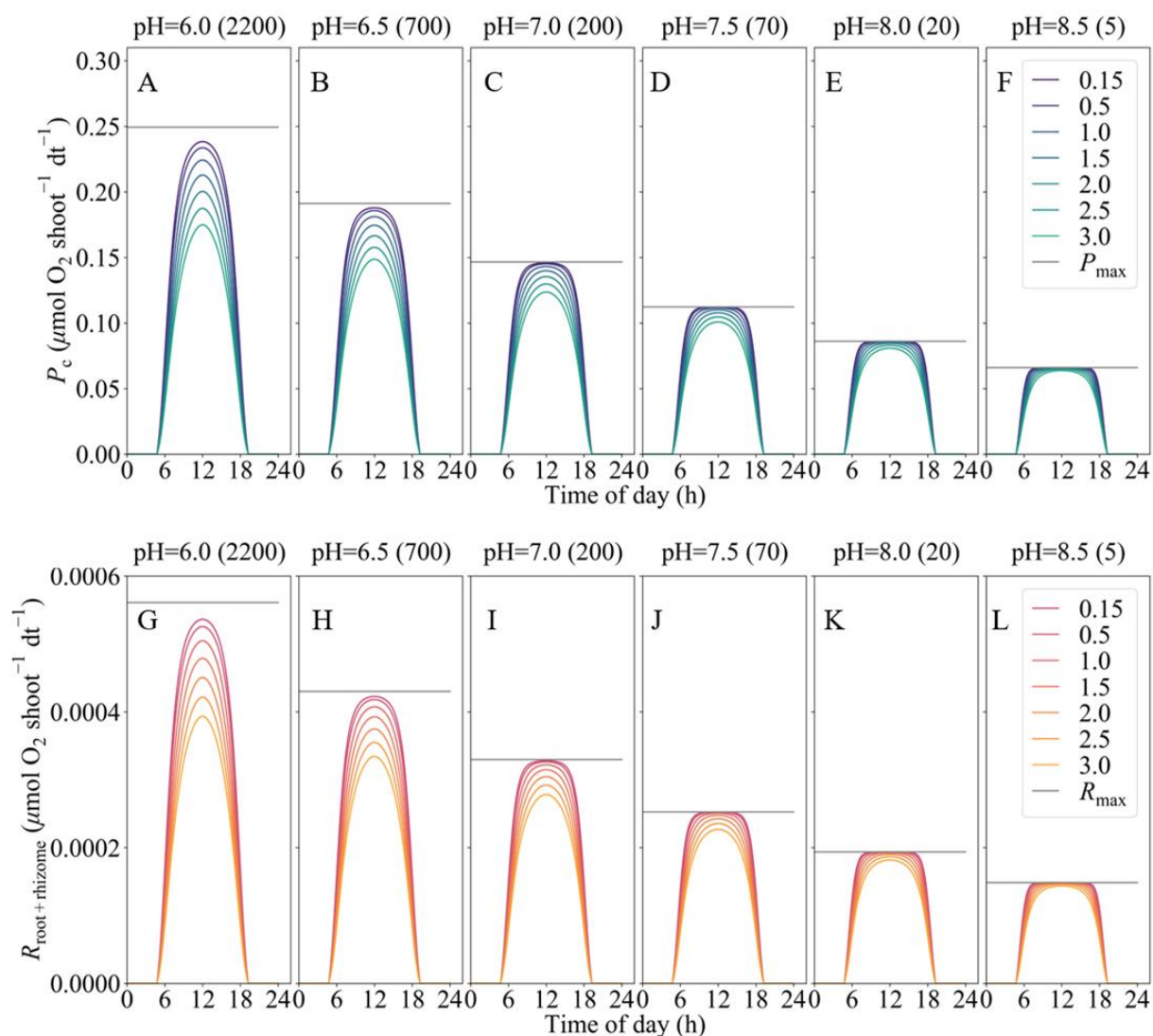


**Fig. 37.** Each panel illustrates the diurnal pattern of (A-F) shoot specific instantaneous canopy photosynthesis ( $P_c$ ), and (G-L) shoot specific instantaneous aerobic respiration for roots+rhizome ( $R_{\text{root+rhi}}$ ) predicted over 14.7 hours of daylength under different  $\text{CO}_{2(\text{aq})}$  treatments. The parameter  $R_{\text{root+rhi}}$  was calculated according to Eqs. (10-12) based on 10% of  $P_c$  (Borum et al. 2006). Each colored line represents response at different LAI specified in the legends. The  $\text{CO}_{2(\text{aq})}$  concentrations were calculated using CO2SYS (Excel version 2.1) (Lewis and Wallace 2006) at temperature, salinity, and alkalinity provided in Table 13 for six distinct pH levels. Solid grey horizontal lines represent the light and  $\text{CO}_{2(\text{aq})}$  saturated rates of photosynthesis ( $P_E$ ; *GrassLight* estimates) and respiratory demand ( $R_{\text{root+rhi}}^{\text{max}}$  calculated according to Eq. (10), (11), and (12)), respectively.

### 4.3.2 Nutrient requirements for growth

The dissolved inorganic N (DIN) concentrations required for growth saturation in eelgrass were predicted to be relatively low. Under steady state conditions, when no alternative sources of DIN were available, a constant water column concentration of  $1.2 \mu\text{M NH}_4^+$  was able to saturate growth, regardless of the LAI or  $\text{CO}_{2(\text{aq})}$  conditions. When  $\text{NO}_3^-$  was the sole source of nitrogen, the model predicted that eelgrass would need concentrations ranging from 1 to  $3 \mu\text{M NO}_3^-$  concentrations to achieve maximum growth (Fig. 38A). Alternatively, when porewater  $\text{NH}_4^+$  was the only N source, eelgrass required between 2 and  $8 \mu\text{M NH}_4^+$  for growth saturation (Fig. 38B). The specific range of  $\text{NO}_3^-$  and porewater  $\text{NH}_4^+$  concentrations depended on the levels of  $\text{CO}_{2(\text{aq})}$  and LAI. Higher  $\text{CO}_{2(\text{aq})}$  concentrations resulted in reduced concentrations of both  $\text{NO}_3^-$  and porewater  $\text{NH}_4^+$  required to saturate growth because of the faster uptake rates with increasing  $\text{CO}_{2(\text{aq})}$  concentrations. However, increasing biomass density (or LAI) required higher concentrations of  $\text{NO}_3^-$  and porewater  $\text{NH}_4^+$  to meet growth demand.

### 4.3.3 Effects of $\text{CO}_{2(\text{aq})}$ and LAI on N uptake

The realized rate of  $\text{NH}_4^+$  uptake by leaves ( $V_r^{\text{LNH}_4}$ ) (Fig. 39),  $\text{NO}_3^-$  by leaves ( $V_r^{\text{LNO}_3}$ ) (Fig. 40), and  $\text{NH}_4^+$  by roots ( $V_r^{\text{RNH}_4}$ ) (Fig. 41) integrated over 24 hours, increased hyperbolically to an asymptotic value of  $1.9 \mu\text{mol shoot}^{-1} \text{d}^{-1}$ . This value represented the maximum realized uptake capacity ( $V_{\text{rmQ}}$ ) at growth saturation that is constrained by  $Q$ . When uptake was not constrained by growth demand, the potential uptake capacity for  $\text{NO}_3^-$  ( $V_p^{\text{LNO}_3}$ ) and  $\text{NH}_4^+$  ( $V_p^{\text{LNH}_4}$ ) by leaves, and  $\text{NH}_4^+$  by roots ( $V_p^{\text{RNH}_4}$ ) were several orders of magnitude higher than  $V_{\text{rmax}}$  for all  $\text{CO}_{2(\text{aq})}$  and LAI scenarios. These results indicated that nitrogen uptake capacity of eelgrass greatly exceeds

the internal N demand required to support growth. This capacity for luxury uptake is a common property of virtually all plants and algae.

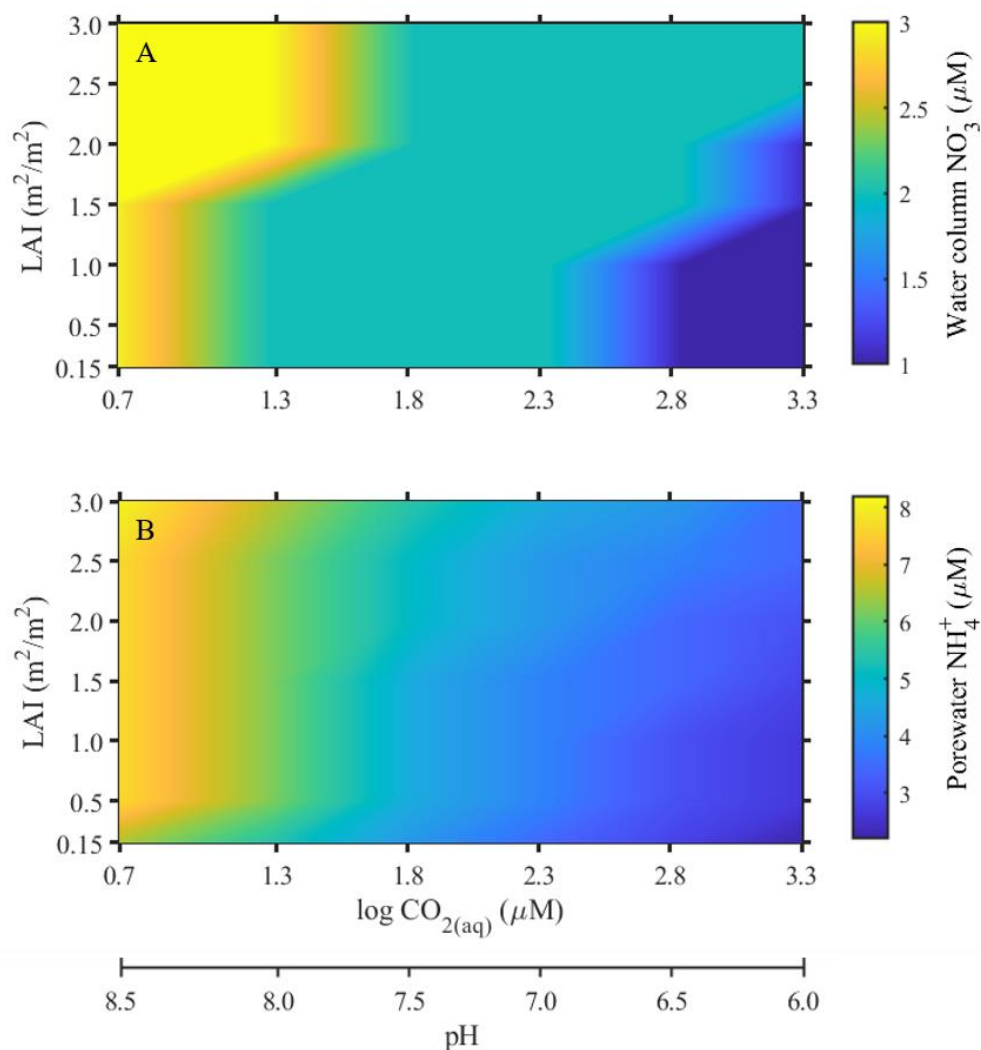


**Fig. 38.** Heatmap illustrating the (A) water column NO<sub>3</sub><sup>-</sup> concentrations, and (B) porewater NH<sub>4</sub><sup>+</sup> concentrations required to saturate eelgrass growth plotted as a function of log CO<sub>2(aq)</sub> (μM) (or pH presented on the secondary x-axis) for fixed LAI values. Nitrogen requirements were estimated based on growth rates of 3% d<sup>-1</sup>.

The effects of  $\text{CO}_{2(\text{aq})}$  and LAI on the N uptake rates varied depending on the source of DIN and the mode of uptake (leaves versus roots). Neither  $\text{CO}_{2(\text{aq})}$  nor LAI had an impact on canopy uptake of  $\text{NH}_4^+$  (Fig. 39). These rates increased with  $\text{NH}_4^+$  concentrations until the internal N reserve reached its capacity defined by the horizontal gray plane, after which the realized canopy uptake was constrained well below  $V_{\text{max}}$ .

In contrast, the daily realized rate of  $\text{NO}_3^-$  uptake by leaves and  $\text{NH}_4^+$  by roots showed variations with  $\text{CO}_{2(\text{aq})}$ , LAI and nutrient concentrations (Fig. 40 and 41). Both leaves and roots exhibited faster uptake of DIN at high  $\text{CO}_{2(\text{aq})}$ , and allowed growth to saturate at  $\leq 1 \mu\text{M}$  of  $\text{NO}_3^-$  or  $\leq 2 \mu\text{M}$  of porewater  $\text{NH}_4^+$ . A drop in  $\text{CO}_{2(\text{aq})}$  concentrations from 2000 to 5  $\mu\text{M}$ , resulted in decreased uptake rates and an increased requirement of DIN (300 to 400%) to achieve  $V_{\text{max}}$ . Increased  $\text{CO}_{2(\text{aq})}$  also increased the potential uptake capacity of eelgrass (colored hyperbolic curves), although these responses were suppressed at high LAI, as demonstrated in Fig. 40 and 41.

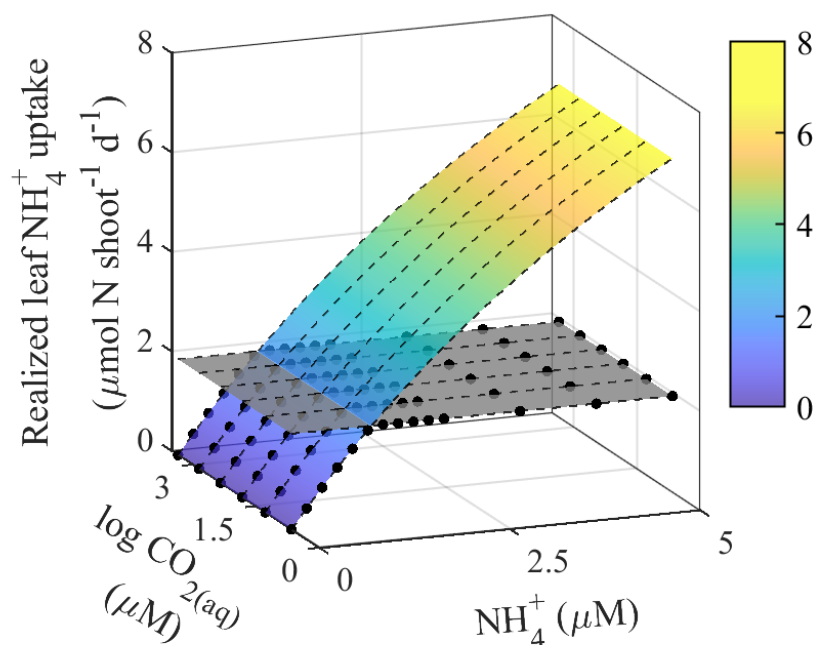


**Fig. 39.** Daily integrated rate of realized ( $V_r^{\text{LNH}_4^+}$ ) (black symbols) and potential ( $V_p^{\text{LNH}_4^+}$ ) (color hyperbolic curve) uptake rate of  $\text{NH}_4^+$  by leaves at steady state plotted as a function of log-transformed  $\text{CO}_{2(\text{aq})}$  concentrations (dash lines) and  $\text{NH}_4^+$  concentrations. The colored surface represents the potential uptake capacity in response to  $\text{NH}_4^+$  and  $\log \text{CO}_{2(\text{aq})}$  concentrations without any constraints from the size of the internal  $Q$ . The grey surface plane depicts the maximum realized uptake rate required to saturate growth ( $V_{\text{rm}Q}$ ) as constrained by  $Q$ .

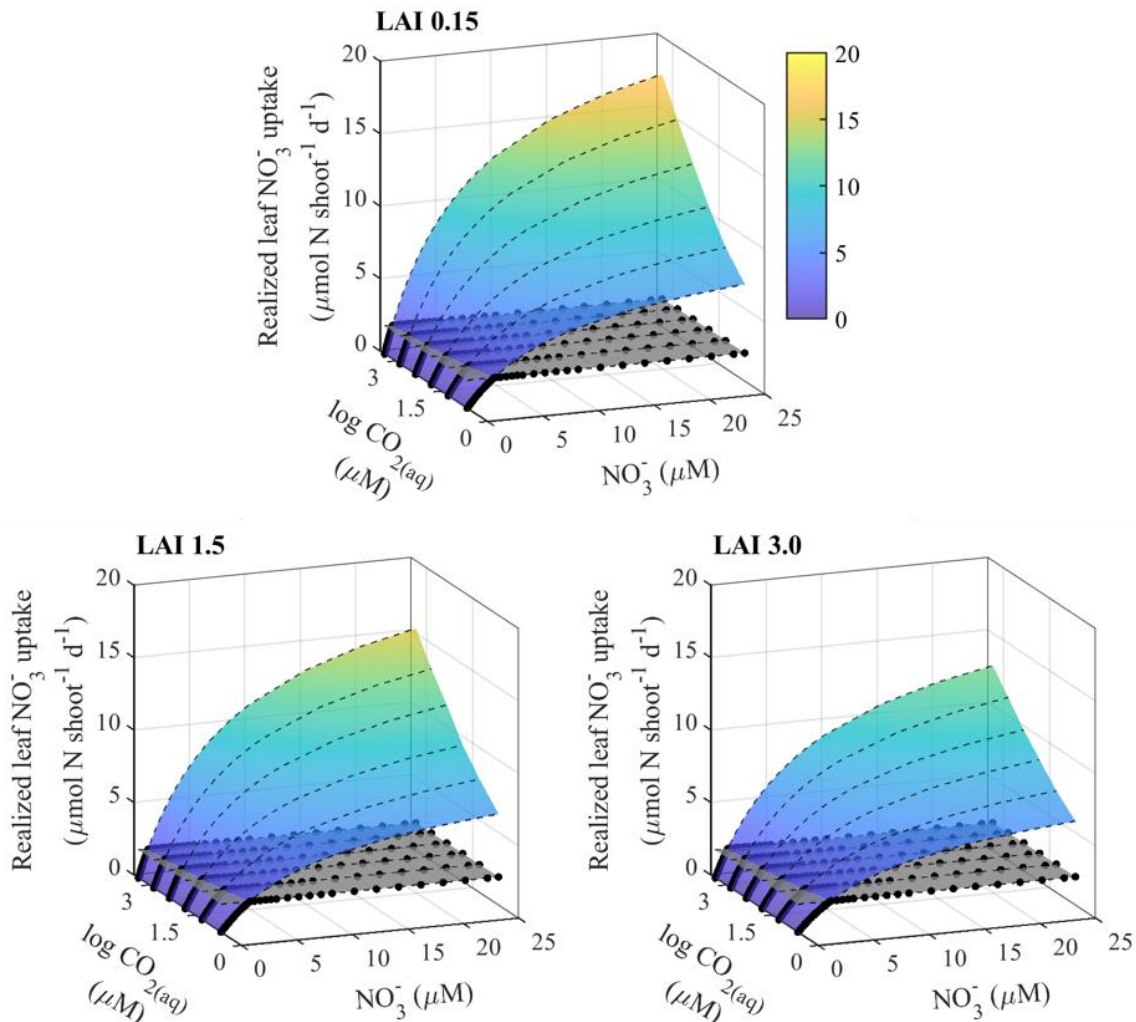


**Fig. 40.** Daily integrated rate of realized ( $V_r^{\text{LNO}_3}$ ) (black symbols) and potential ( $V_p^{\text{LNO}_3}$ ) (color hyperbolic curve) uptake rate of  $\text{NO}_3^-$  by leaves at steady state plotted as a function of log-transformed  $\text{CO}_{2(\text{aq})}$  concentrations (dash lines) and  $\text{NO}_3^-$  concentrations. The colored surface represents the potential uptake capacity in response to  $\text{NO}_3^-$  and  $\log \text{CO}_{2(\text{aq})}$  concentrations without any constraints from the size of the internal  $Q$ . The grey surface plane depicts the maximum realized uptake rate required to saturate growth ( $V_{\text{rm}Q}$ ) as constrained by  $Q$ .

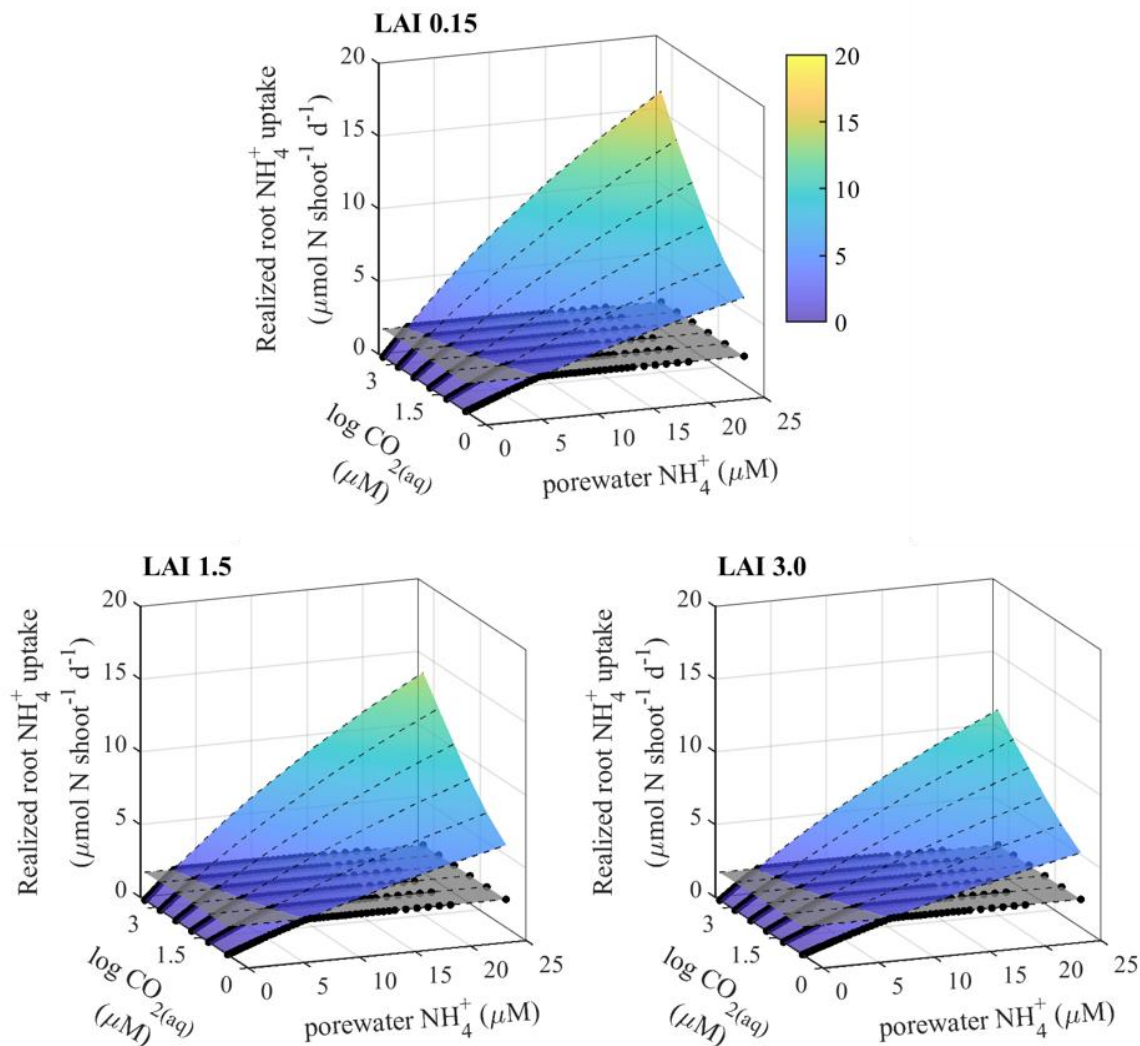


**Fig. 41.** Daily integrated rate of realized ( $V_r^{\text{RNH}_4}$ ) (black symbols) and potential ( $V_p^{\text{RNH}_4}$ ) (color hyperbolic curve) uptake rate of  $\text{NH}_4^+$  by roots at steady state plotted as a function of log-transformed  $\text{CO}_{2(\text{aq})}$  concentrations (dash lines) and  $\text{NO}_3^-$  concentrations. The grey surface plane depicts the maximum realized uptake rate required to saturate growth ( $V_{\text{rm}Q}$ ) as constrained by  $Q$ . The colored surface represents the potential uptake capacity in response to porewater  $\text{NH}_4^+$  and  $\log \text{CO}_{2(\text{aq})}$  concentrations without any constraints from the size of the internal  $Q$ .

#### 4.3.4 Effects of $\text{CO}_{2(\text{aq})}$ and LAI on N uptake kinetics, $V_{\text{max}}$ and $K_s$

Except for leaf uptake of  $\text{NH}_4^+$ , elevated  $\text{CO}_{2(\text{aq})}$  increased the uptake rates of  $\text{NO}_3^-$  by leaves and  $\text{NH}_4^+$  by roots as shown in Fig. 40 and 41. When unrestricted by  $Q$ , the potential N uptake capacity ( $V_{\text{pmax}}$ ) exceeded  $V_{\text{rmQ}}$  as shown in Fig. 42. The maximum potential uptake rates for  $\text{NO}_3^-$  ( $V_{\text{pmax}}^{\text{LNO}_3}$ ) and porewater  $\text{NH}_4^+$  ( $V_{\text{pmax}}^{\text{RNH}_4}$ ) exhibited positive linear slopes with  $\log \text{CO}_{2(\text{aq})}$  (Fig. 42). Although  $\text{CO}_2$ -stimulated  $V_{\text{pmax}}^{\text{LNO}_3}$  and  $V_{\text{pmax}}^{\text{RNH}_4}$ , increasing LAI (i.e. shoot density) attenuated the  $\text{CO}_{2(\text{aq})}$  effects. Increasing LAI from 0.15 to 3 ( $\text{m}^2 \text{m}^{-2}$ ) resulted in a 30% reduction in the slopes of  $V_{\text{pmax}}^{\text{LNO}_3}$ , declining from 5.2 to 3.5 ( $\mu\text{M N shoot}^{-1} \text{d}^{-1} \mu\text{M}^{-1} \log \text{CO}_{2(\text{aq})}$ ). Similar effects were observed for  $V_{\text{pmax}}^{\text{RNH}_4}$ . This reduction in  $\text{CO}_{2(\text{aq})}$  stimulated  $V_{\text{pmax}}$  was due to the self-shading impact of increasing LAI on  $P_c$  (Fig. 37A-F), as the assimilation of  $\text{NO}_3^-$  in leaf and  $\text{NH}_4^+$  in root tissues depended on  $P_c$ . The influence of LAI was more pronounced at high  $\text{CO}_{2(\text{aq})}$  than at low  $\text{CO}_{2(\text{aq})}$  where eelgrass photosynthesis was  $\text{CO}_2$ -limited (evidenced by the plateauing of the  $P_c$  curves). Increasing LAI suppressed the maximum uptake capacity of both  $V_{\text{pmax}}^{\text{LNO}_3}$  and  $V_{\text{pmax}}^{\text{RNH}_4}$  by approximately 20% under elevated  $\text{CO}_{2(\text{aq})}$  conditions and by around 10% under low  $\text{CO}_{2(\text{aq})}$ .

The half-saturation constant ( $K_s$ ) for water column  $\text{NH}_4^+$  ( $K_s^{\text{NH}_4^+}$ ) remained constant at 9.7  $\mu\text{M}$ , indicating that the leaf uptake for  $\text{NH}_4^+$  was not influenced by  $\text{CO}_{2(\text{aq})}$  or LAI manipulations (Fig. 43A). In contrast, the  $K_s$  values for water column  $\text{NO}_3^-$  ( $K_s^{\text{NO}_3^-}$ ) and for porewater  $\text{NH}_4^+$  ( $K_s^{\text{pwNH}_4^+}$ ) decreased logarithmically with increasing  $\text{CO}_{2(\text{aq})}$  and the rate of change also varied with LAI, as evident in the slopes in Fig. 43B and 43C. At low  $\text{CO}_{2(\text{aq})}$  concentrations, variations in LAI values had minimal effect on  $K_s^{\text{NO}_3^-}$  and  $K_s^{\text{pwNH}_4^+}$ . Under such conditions, the difference in  $K_s$  values between LAI values of 0.15 and 3 was predicted to less than 2%. However, as  $\text{CO}_{2(\text{aq})}$  concentrations increased, the difference in the  $K_s$  values increased approximately 10 times.

Similarly, the  $\text{NO}_3^-$  uptake affinity ( $\alpha = V_{\text{pmax}}/K_s$ ) for leaves and  $\text{NH}_4^+$  uptake affinity for roots were two to three times higher at high  $\text{CO}_{2(\text{aq})}$  compared to low  $\text{CO}_{2(\text{aq})}$  concentrations (Table 15). The  $\alpha$  of leaves for  $\text{NO}_3^-$  was much higher than the  $\alpha$  of roots for  $\text{NH}_4^+$ .

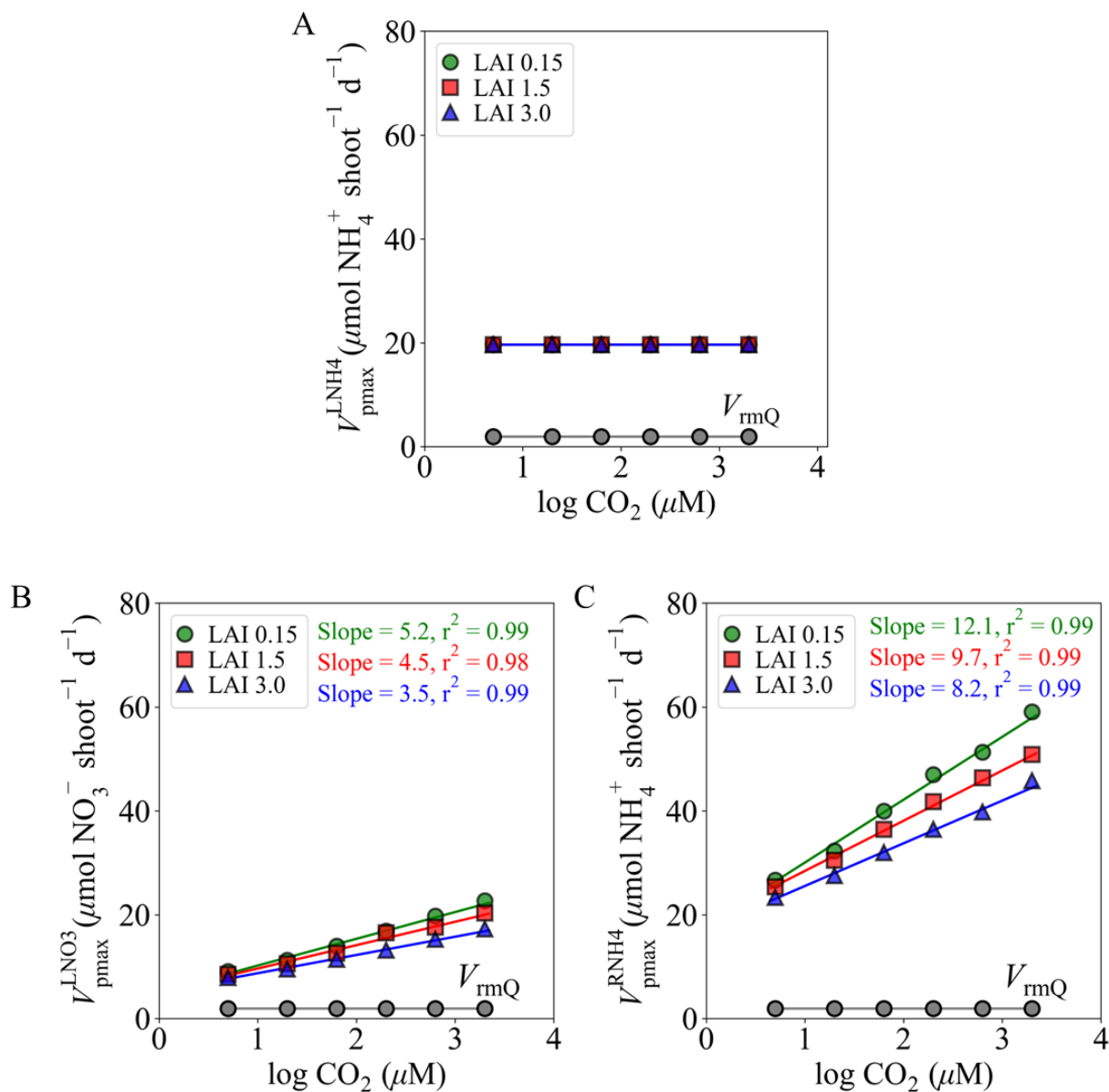


**Fig. 42.** Effects of CO<sub>2(aq)</sub> concentrations and LAI on the daily integrated maximum potential uptake rate for (A) NH<sub>4</sub><sup>+</sup> by leaves ( $V_{\text{pmax}}^{\text{LNH}_4}$ ), (B) NO<sub>3</sub><sup>-</sup> by leaves ( $V_{\text{pmax}}^{\text{LNO}_3}$ ), and (C) porewater NH<sub>4</sub><sup>+</sup> by roots ( $V_{\text{pmax}}^{\text{RNH}_4}$ ). The CO<sub>2(aq)</sub> concentrations are expressed in log scale. The horizontal grey symbols represent the predicted maximum realized N uptake rate constrained by Q as determined from Eq. (13), (14), and (15).

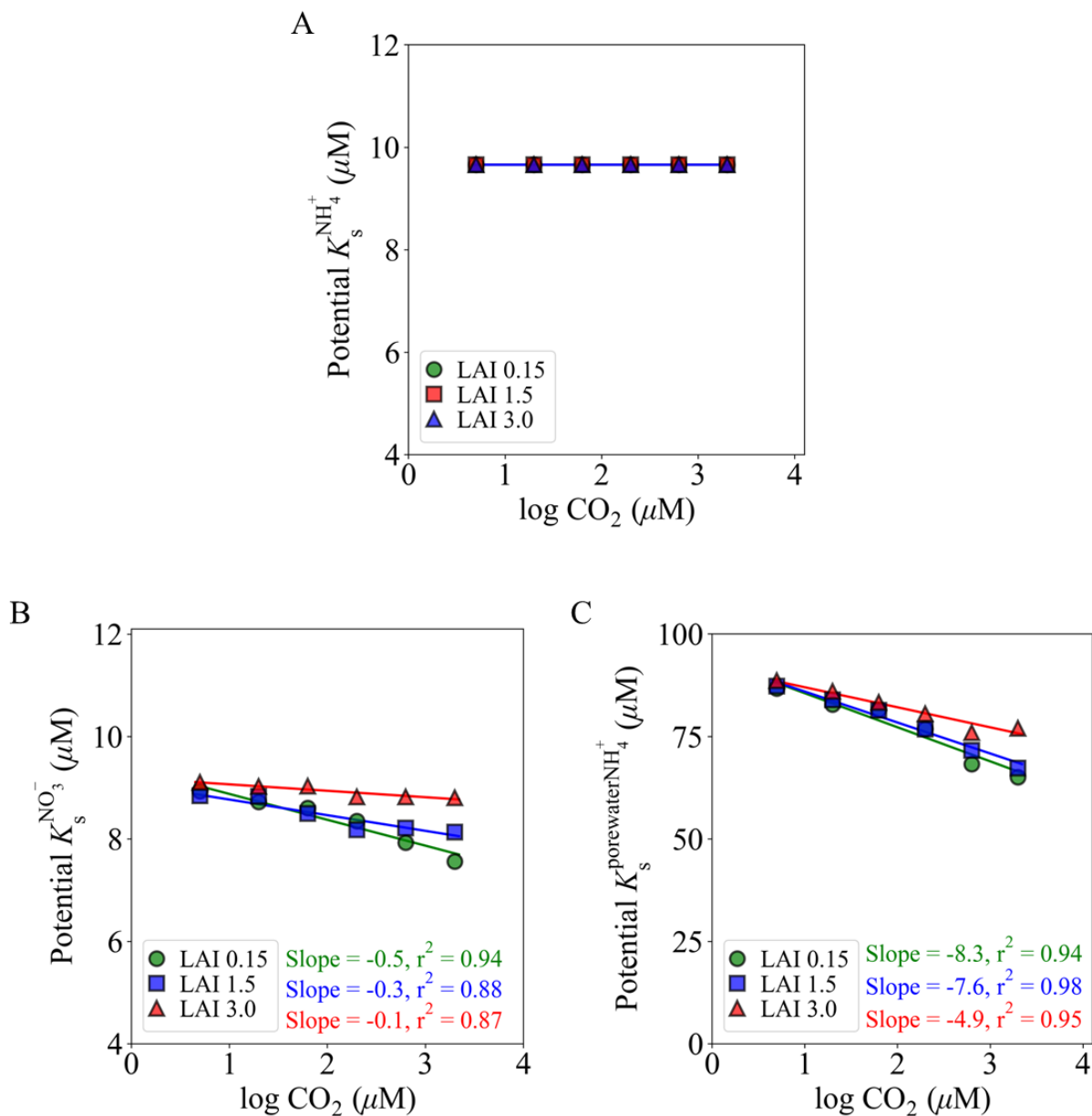


**Fig. 43.** Effects of  $\text{CO}_{2(\text{aq})}$  and LAI on the half-saturation constants ( $K_s$  in  $\mu\text{M}$ ) of leaves for (A)  $\text{NH}_4^+$ , (B)  $\text{NO}_3^-$ , and of roots for (C) porewater  $\text{NH}_4^+$ . The  $\text{CO}_{2(\text{aq})}$  concentrations are expressed as a log scale.

**Table 15.** Effects of  $\text{CO}_{2(\text{aq})}$  on uptake kinetics: maximum potential uptake rate,  $V_{\text{pmax}}$  ( $\mu\text{mol shoot}^{-1} \text{d}^{-1}$ ), half-saturation constant,  $K_s$  ( $\mu\text{M}$ ), and affinity coefficient  $\alpha$  ( $V_{\text{pmax}}/K_s$ ) of ammonium and nitrate in leaves and roots. Values in parentheses represent the corresponding pH values.

| Parameter                               | $V_{\text{pmax}}$ |       |       | $K_s$ |       |       | $\alpha$ |      |      |
|---|-------------------|-------|-------|-------|-------|-------|----------|------|------|
|   | LAI               |       |       | LAI   |       |       | LAI      |      |      |
|   | 0.15              | 1.5   | 3.0   | 0.15  | 1.5   | 3.0   | 0.15     | 1.5  | 3.0  |
| Leaf $\text{NO}_3^-$ :                  |                   |       |       |       |       |       |          |      |      |
| $\text{CO}_{2(\text{aq})} = 2200$ (6.0) | 22.69             | 22.33 | 17.26 | 7.56  | 8.14  | 8.8   | 3.00     | 2.50 | 1.96 |
| 700 (6.5)                               | 19.75             | 17.58 | 15.24 | 7.93  | 8.21  | 8.82  | 2.49     | 2.14 | 1.73 |
| 200 (7.0)                               | 16.87             | 15.37 | 13.16 | 8.35  | 8.54  | 8.82  | 2.02     | 1.80 | 1.49 |
| 70 (7.5)                                | 13.97             | 12.58 | 11.41 | 8.61  | 8.50  | 9.03  | 1.62     | 1.48 | 1.26 |
| 20 (8.0)                                | 11.25             | 10.56 | 9.52  | 8.73  | 8.83  | 9.03  | 1.29     | 1.20 | 1.06 |
| 5 (8.5)                                 | 9.07              | 8.49  | 7.88  | 8.93  | 8.84  | 9.10  | 1.02     | 0.96 | 0.87 |
| Leaf $\text{NH}_4^+$ :                  |                   |       |       |       |       |       |          |      |      |
| 2200 – 5 (6.0 – 8.5)                    | 19.66             | 19.66 | 19.66 | 9.66  | 9.66  | 9.66  | 2.04     | 2.04 | 2.04 |
| Root $\text{NH}_4^+$ :                  |                   |       |       |       |       |       |          |      |      |
| 2200 (6.0)                              | 59.07             | 50.87 | 45.80 | 65.06 | 67.27 | 76.96 | 0.91     | 0.76 | 0.60 |
| 700 (6.5)                               | 51.33             | 46.39 | 39.80 | 68.22 | 72.58 | 75.91 | 0.75     | 0.65 | 0.52 |
| 200 (7.0)                               | 46.98             | 41.75 | 36.44 | 76.84 | 76.76 | 80.52 | 0.61     | 0.54 | 0.45 |
| 70 (7.5)                                | 39.97             | 36.42 | 31.96 | 81.48 | 81.34 | 83.25 | 0.49     | 0.45 | 0.38 |
| 20 (8.0)                                | 32.29             | 30.49 | 27.52 | 82.78 | 83.95 | 85.98 | 0.39     | 0.36 | 0.32 |
| 5 (8.5)                                 | 26.65             | 25.38 | 23.30 | 86.67 | 87.29 | 88.61 | 0.31     | 0.29 | 0.26 |

#### 4.3.5 The effects of $\text{CO}_{2(\text{aq})}$ , LAI and nutrient availability on leaves and roots uptake pattern

For a typical DIN profile encountered *in situ* ( $5 \mu\text{M}$  water column  $\text{NH}_4^+$ ,  $5 \mu\text{M}$  water column  $\text{NO}_3^-$  and  $100 \mu\text{M}$  porewater  $\text{NH}_4^+$ ), the model predicted that roots assimilated 60% and leaves assimilated 40% of the total N when  $\log \text{CO}_{2(\text{aq})} < 1 \mu\text{M}$  (or pH 8.0) (Fig. 44). Under this specific condition, when water column  $\text{NO}_3^-$  and  $\text{NH}_4^+$  were present in equal amounts, leaf uptake favored  $\text{NH}_4^+$  over  $\text{NO}_3^-$  and represented about 30% of the total N assimilated. As  $\log \text{CO}_{2(\text{aq})}$  increased to  $3.3 \mu\text{M}$  (pH 6.0), the uptake of  $\text{NH}_4^+$  from the water column declined followed by a slight increase in the  $\text{NO}_3^-$  uptake. At elevated  $\log \text{CO}_{2(\text{aq})}$ , leaves assimilated N as  $\text{NH}_4^+$  and  $\text{NO}_3^-$  in roughly equal amount and made up about 30% of the total N in plants when combined. The effects of increasing LAI were relatively minor, or completely absent when  $\text{NH}_4^+$  was the only N source for leaves.

Leaves took up more  $\text{NH}_4^+$  at low  $\text{CO}_{2(\text{aq})}$  regime and high LAI, than at high  $\text{CO}_{2(\text{aq})}$  regime and low LAI (Fig. 45). In general, leaves and roots took up more  $\text{NO}_3^-$  (Fig. 46) and porewater  $\text{NH}_4^+$  (Fig. 47), respectively, under high  $\text{CO}_{2(\text{aq})}$  and low LAI, than in low  $\text{CO}_{2(\text{aq})}$  and high LAI, if these nutrient concentrations were above water column  $\text{NH}_4^+$  concentrations. The percentage of total N assimilated as  $\text{NH}_4^+$  by leaves increased asymptotically with increasing  $\text{NH}_4^+$  concentrations in the water column. For seawater with  $\text{CO}_{2(\text{aq})}$  concentrations less than  $5 \mu\text{M}$  ( $\log \text{CO}_{2(\text{aq})} \sim 1 \mu\text{M}$ , pH 8.5), the model predicted that leaves assimilated as much as 50% of the total N as  $\text{NH}_4^+$  when the  $\text{NH}_4^+$  was  $\geq 25 \mu\text{M}$  in the water column. Leaf  $\text{NH}_4^+$  uptake decreased with increasing  $\text{CO}_{2(\text{aq})}$  availability and the contributions of total N as  $\text{NH}_4^+$  dropped to  $< 40\%$  at LAI = 3, and  $< 30\%$  at LAI = 0.15. As water column  $\text{NH}_4^+$  concentrations increased beyond  $25 \mu\text{M}$ , the combination of high  $\text{CO}_{2(\text{aq})}$  and high LAI caused the uptake of  $\text{NO}_3^-$  by leaves to decrease asymptotically to about 10% and the contribution of N as  $\text{NH}_4^+$  by roots to decline to 40%.

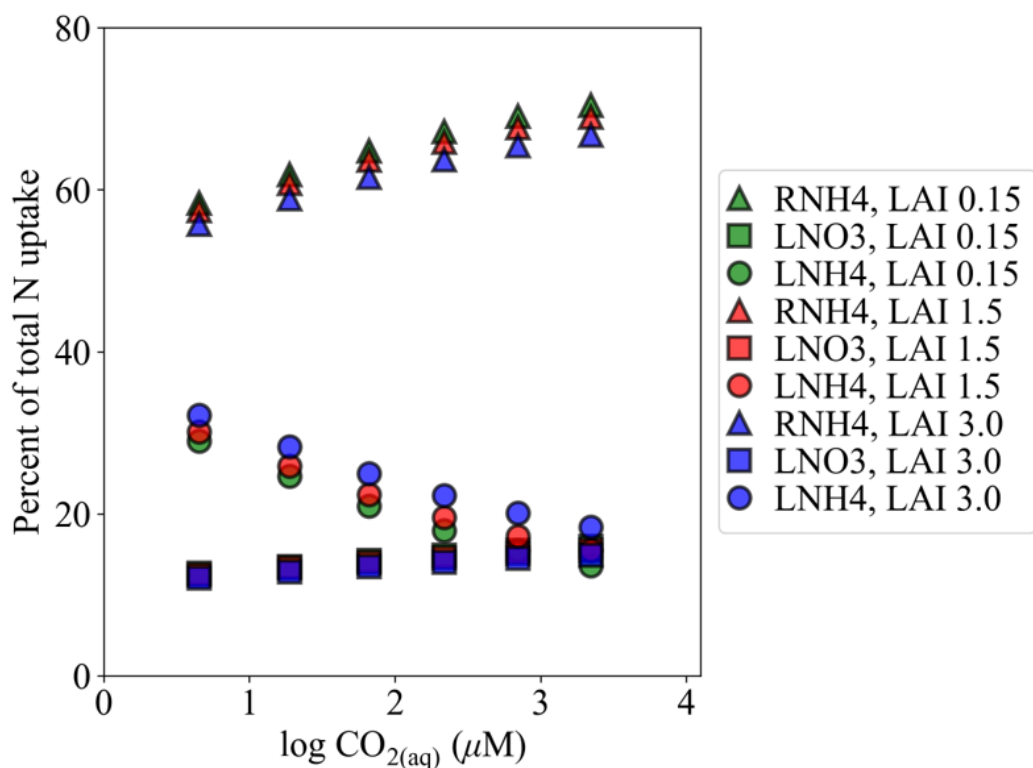


**Fig. 44.** Percentage of total N uptake by leaves and roots under standard nutrient simulation ( $5 \mu\text{M}$  water column  $\text{NH}_4^+$ ;  $5 \mu\text{M}$  water column  $\text{NO}_3^-$ ,  $100 \mu\text{M}$  porewater  $\text{NH}_4^+$ ) plotted as a function of  $\log \text{CO}_{2(\text{aq})}$  concentrations for different leaf area index (LAI) (color). Symbols represent the type of uptake: ( $\Delta$ ) represents root uptake of porewater  $\text{NH}_4^+$  (RNH4); ( $\square$ ) and ( $\circ$ ) represent leaf uptake of water column  $\text{NO}_3^-$  (LNO3) and water column  $\text{NH}_4^+$  (LNH4), respectively.

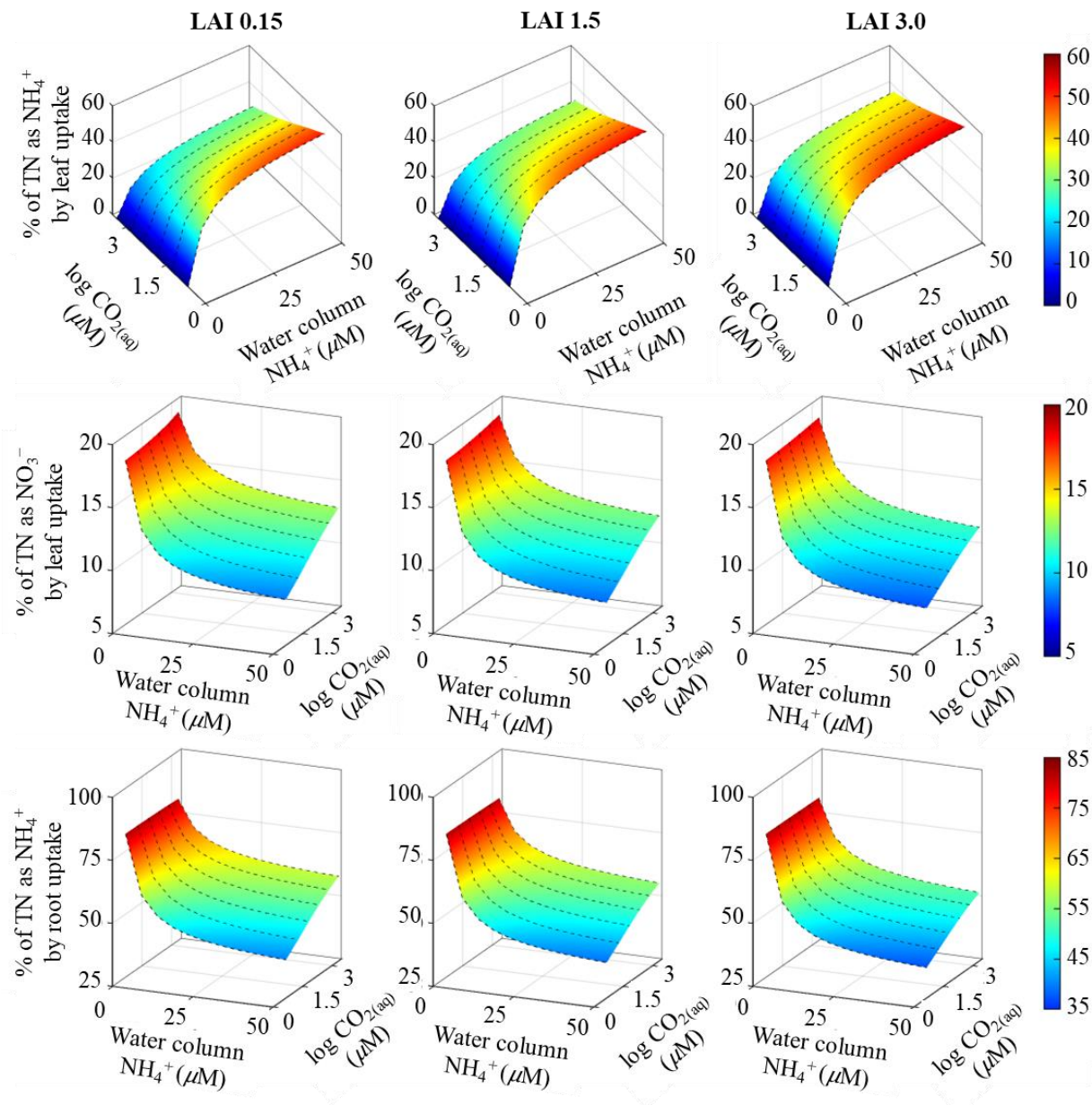


**Fig. 45.** Percentage of total N taken as  $\text{NH}_4^+$  by leaves (top), as  $\text{NO}_3^-$  by leaves (middle), and as porewater  $\text{NH}_4^+$  by roots, plotted as a function of water column  $\text{NH}_4^+$  (0-50  $\mu\text{M}$ ) and log-transformed  $\text{CO}_{2(\text{aq})}$  concentrations for fixed LAI. Water column  $\text{NO}_3^-$  and porewater  $\text{NH}_4^+$  concentrations were fixed at 5 and 100  $\mu\text{M}$ , respectively during each simulation. The colormaps represent the model solutions at steady state condition. Plot orientations are as follow: x-axis = water column  $\text{NH}_4^+$  concentrations, y-axis = log  $\text{CO}_{2(\text{aq})}$  ( $\mu\text{M}$ ), and z-axis = % of total N.

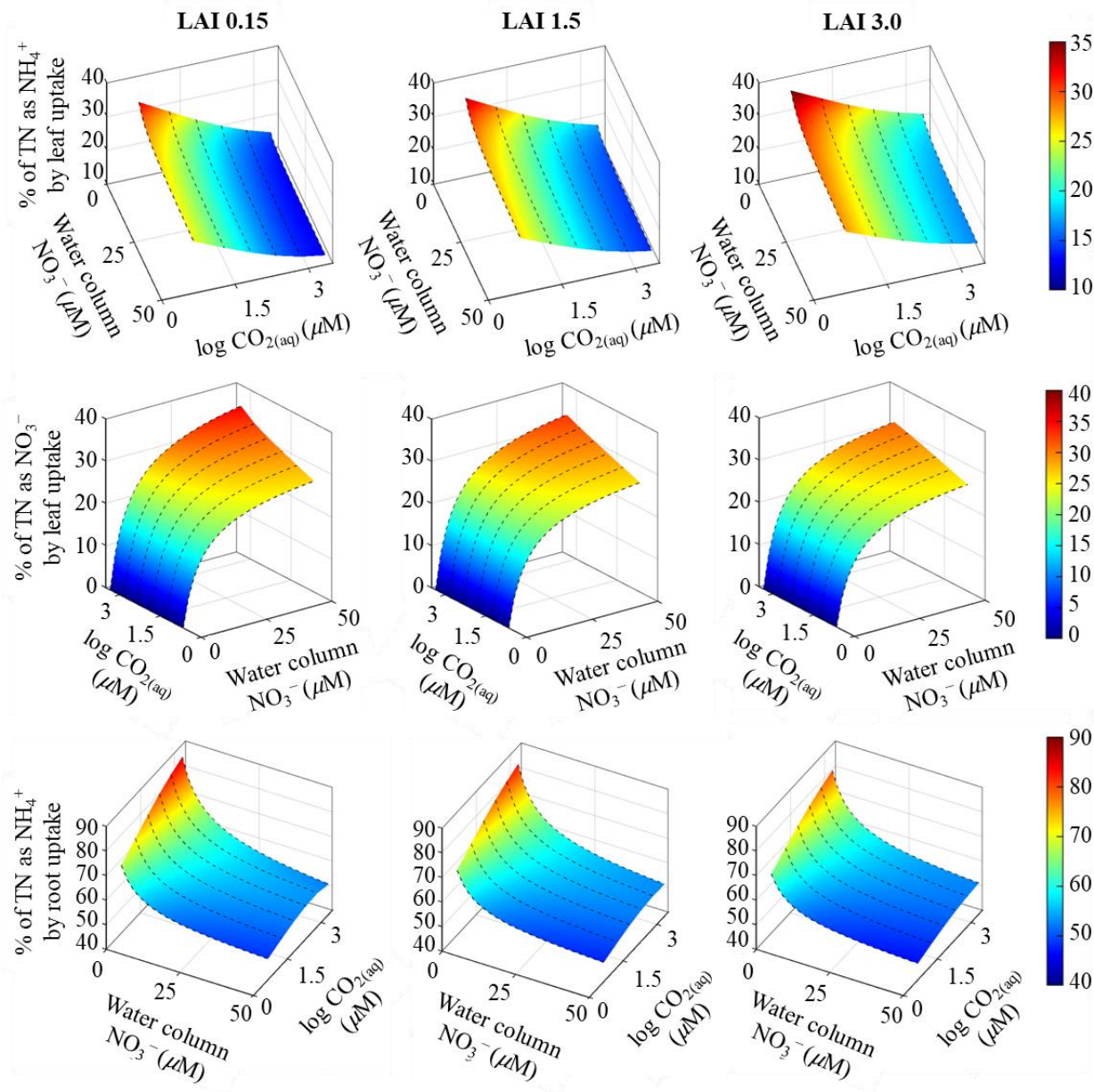


**Fig. 46.** Percentage of total N taken as  $\text{NH}_4^+$  by leaves (top), as  $\text{NO}_3^-$  by leaves (middle), and as porewater  $\text{NH}_4^+$  by roots, plotted as a function of water column  $\text{NO}_3^-$  (0-50  $\mu\text{M}$ ) and log-transformed  $\text{CO}_{2(\text{aq})}$  concentrations for fixed LAI. Water column  $\text{NH}_4^+$  and porewater  $\text{NH}_4^+$  concentrations were fixed at 5 and 100  $\mu\text{M}$ , respectively during each simulation. The colormaps represent the model solutions at steady state condition. Plot orientations are as follow: x-axis = water column  $\text{NO}_3^-$  concentrations, y-axis =  $\log \text{CO}_{2(\text{aq})}$  ( $\mu\text{M}$ ), and z-axis = % of total N.

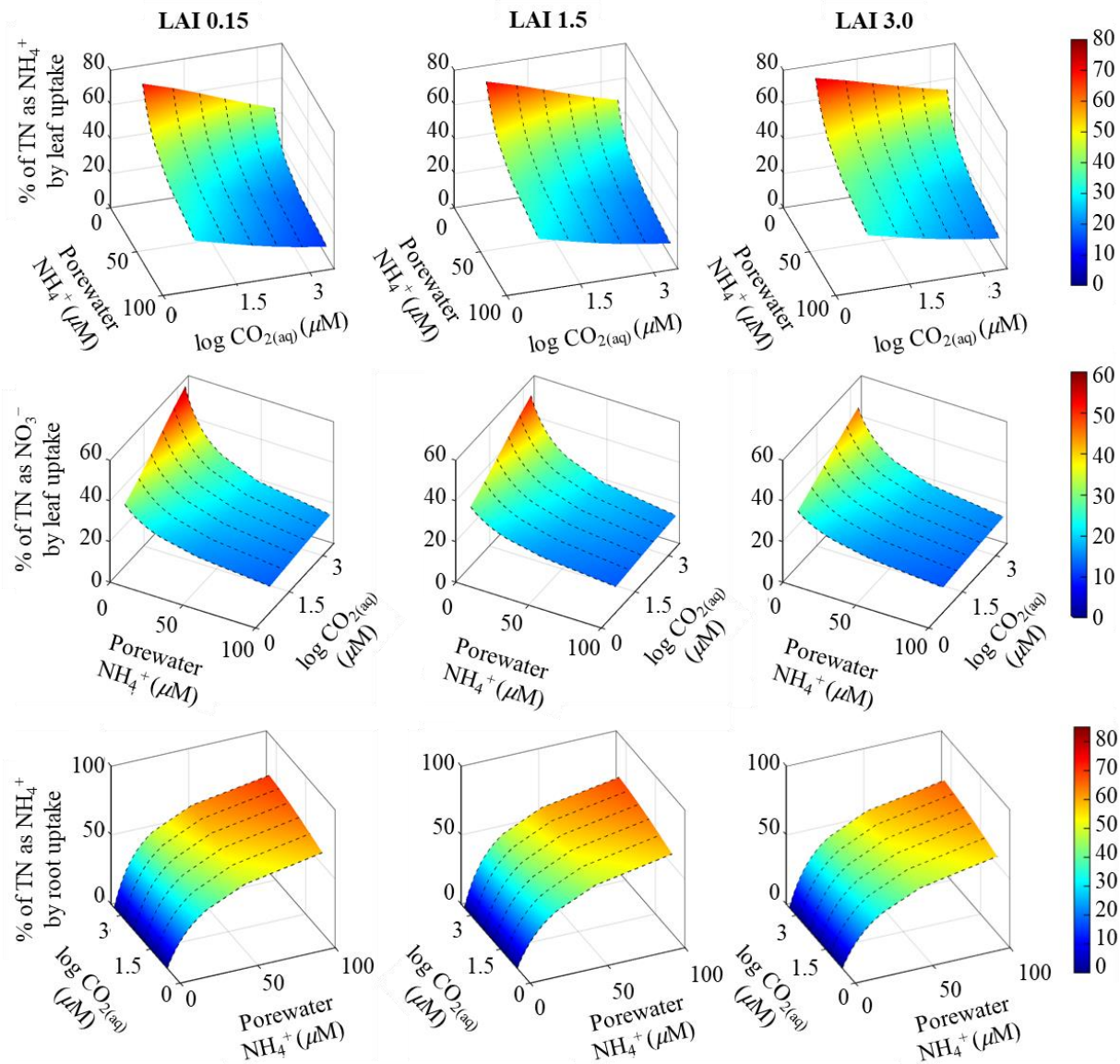


**Fig. 47.** Percentage of total N taken as  $\text{NH}_4^+$  by leaves (top), as  $\text{NO}_3^-$  by leaves (middle), and as porewater  $\text{NH}_4^+$  by roots, plotted as a function of porewater  $\text{NH}_4^+$  (0-100  $\mu\text{M}$ ) and log-transformed  $\text{CO}_{2(\text{aq})}$  concentrations for fixed LAI. Water column  $\text{NO}_3^-$  and  $\text{NH}_4^+$  concentrations were fixed at 5  $\mu\text{M}$  during each simulation. The colormaps represent the model solutions at steady state condition. Plot orientations are as follow: x-axis = porewater  $\text{NH}_4^+$  concentrations, y-axis =  $\log \text{CO}_{2(\text{aq})}$  ( $\mu\text{M}$ ), and z-axis = % of total N.

The leaf uptake of  $\text{NO}_3^-$  increased asymptotically with increasing  $\text{NO}_3^-$  concentrations (Fig. 46). This increase in leaf uptake of  $\text{NO}_3^-$  led to a 10-20% reduction in the leaf  $\text{NH}_4^+$  uptake, and a 30-40% reduction in the root  $\text{NH}_4^+$  uptake depending on  $\text{CO}_{2(\text{aq})}$  and LAI. The interactive effects of decreasing  $\text{CO}_{2(\text{aq})}$  concentrations and increasing LAI resulted in a 20% reduction in the contribution of  $\text{NO}_3^-$  to the total N in eelgrass. Leaves never assimilated more than 35% of N as  $\text{NO}_3^-$ , even when the nutrient concentrations reached  $50 \mu\text{M}$ . These results indicated that  $\text{NO}_3^-$  represented a minor source of N in eelgrass even in a high  $\text{CO}_{2(\text{aq})}$  environment.

Over the concentration range of porewater  $\text{NH}_4^+$  (0-100  $\mu\text{M}$ ) utilized in the model, roots + rhizome assimilated a higher proportion of N as  $\text{NH}_4^+$  under elevated  $\text{CO}_{2(\text{aq})}$  and LAI conditions (Fig. 47). Under low  $\text{CO}_{2(\text{aq})}$  conditions, roots + rhizome assimilated between 50 and 60% of N as  $\text{NH}_4^+$ . As  $\text{CO}_{2(\text{aq})}$  concentrations increased, the contribution of roots + rhizome to the total N in eelgrass increased to over 70% (not exceeding 80%) in response to increased  $\text{CO}_{2(\text{aq})}$  concentrations. In such circumstances, the contributions from leaves to the total N decreased to 30%. Roots and leaves contributed equally to the total N when porewater  $\text{NH}_4^+$  was at least  $27 \mu\text{M}$  (also see Fig. 48).

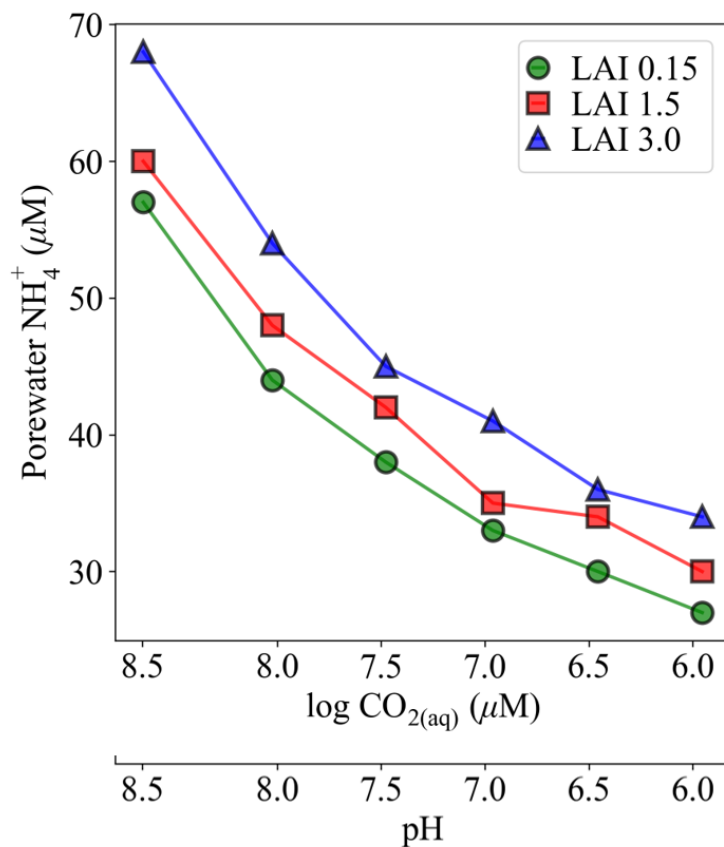


**Fig. 48.** Isoleth of equal (50%) N uptake by leaves and roots/rhizome defined by  $\text{CO}_{2(\text{aq})}$  (in log scale) and porewater  $\text{NH}_4^+$  concentrations for LAI values ranging from 0.15 to 3.0. The pH values are provided along the secondary x-axis. Leaves dominate N uptake below the lines; roots dominate above the lines.

### 4.3.6 Remineralization requirements

The sediment  $\text{NH}_4^+$  regeneration rate was assumed to be equivalent to the maximum realized N demand or  $V_{\text{rmQ}}$  predicted by the model. When scaled to different LAI values,  $V_{\text{rmax}}$  increased linearly, ranging from 0.15 to 3.1  $\text{mmol N m}^{-2} \text{d}^{-1}$  (Fig. 49). This range was significantly lower, by several orders of magnitude, than the global average ammonification rates of  $29.8 (\pm 6 \text{ SE}) \text{ mmol N m}^{-2} \text{d}^{-1}$  calculated from values reported for vegetated sediments across latitudes (Dennison 1987; Caffrey and Kemp 1990; Herbert 1999). Based on this global average, this rate of ammonification would be able to sustain well over 13,000 shoots  $\text{m}^{-2}$ , which is equivalent to LAI of 25.

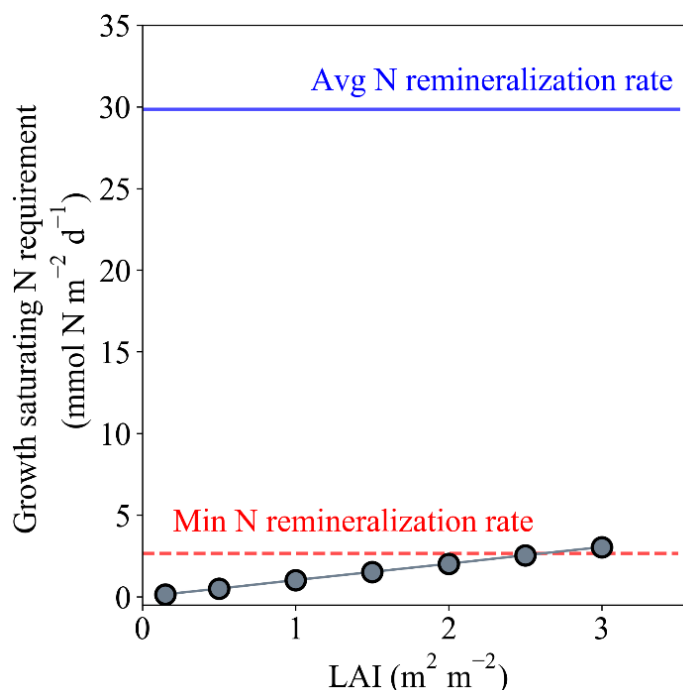


**Fig. 49.** Comparison of N uptake rate (i.e. N demand) and N remineralization rate (blue solid and red dash lines; values obtained from the literature) across different LAI. The data points are model results of the maximum N uptake rate of *Zostera marina* L. required to sustain growth rates of  $3\% \text{d}^{-1}$ .

#### **4.4 Discussion**

The model predicted low N demand for eelgrass ( $<2 \mu\text{mol N shoot}^{-1} \text{d}^{-1}$ ) across all  $\text{CO}_{2(\text{aq})}$  conditions. Eelgrass required  $1.2 \mu\text{M}$  of  $\text{NH}_4^+$  or  $1\text{-}3 \mu\text{M}$   $\text{NO}_3^-$  from the water column, or  $2\text{-}8 \mu\text{M}$   $\text{NH}_4^+$  from the sediment pool to maintain balanced growth. Leaf uptake of  $\text{NO}_3^-$  and root uptake of  $\text{NH}_4^+$  increased due to higher photosynthesis and respiration rates influenced by changes in  $\text{CO}_{2(\text{aq})}$  and LAI. Roots played a key role in N uptake (as  $\text{NH}_4^+$ ) across various  $\text{CO}_{2(\text{aq})}$  and LAI scenarios, indicating their importance in N acquisition strategy as  $\text{CO}_{2(\text{aq})}$  levels increased. Overall, present study highlights the importance of photosynthesis in regulating N assimilation and acquisition between the above- and belowground components, and suggest that most eelgrass meadows are unlikely to experience N limitation, even in high  $\text{CO}_{2(\text{aq})}$  environments.

##### **4.4.1 Variable photosynthetic rates in leaves in response to changing $\text{CO}_{2(\text{aq})}$ and LAI**

The influence of LAI on photosynthetic rates revealed the significance of canopy architecture, especially in a density-dependent manner, as suggested by Zimmerman (2003). Eelgrass canopies with high LAI, indicative of high shoot density, exhibited a negative impact on photosynthetic rates, possible due to canopy self-shading (Enríquez and Pantoja-Reyes 2005; Enríquez et al. 2019). Self-shading effects were most pronounced under elevated  $\text{CO}_{2(\text{aq})}$  conditions, leading to a one third reduction in  $P_E$  values between dense (LAI = 3.0) and sparse (LAI = 0.15) canopies. Conversely, in low  $\text{CO}_{2(\text{aq})}$  environment, the impact of self-shading on  $P_E$  was limited to at most 5%. The limited impact of canopy self-shading on overall  $P_C$  and  $P_E$  under low  $\text{CO}_{2(\text{aq})}$  conditions suggests that eelgrass was already  $\text{CO}_2$ -limited, as evident from plateauing of  $P_C$  curves across much of the photoperiod (14.7 hours). Although not a robust predictor of photosynthesis in present day  $\text{CO}_{2(\text{aq})}$  conditions, this study proposes that LAI could play a crucial

role in driving net primary productivity of eelgrass and influencing metabolic activities that depend on photosynthesis in future CO<sub>2</sub>-enriched oceans.

#### **4.4.2 Variable respiration rates in roots in response to changing CO<sub>2(aq)</sub> and LAI**

In this model, the rates of aerobic respiration in eelgrass roots (and rhizomes) were controlled by the transport of O<sub>2</sub> from shoot photosynthesis, allowing for the impacts of CO<sub>2(aq)</sub> and LAI on belowground metabolism to be quantified. The results predicted that increased CO<sub>2(aq)</sub> availability would lead to higher rates of below-ground respiration due to increased oxygen production at higher CO<sub>2(aq)</sub> levels. Root respiration, like other forms of cellular respiration, relies on oxygen transported from the leaves to convert carbohydrates (such as sucrose) into energy to support metabolic processes such as nutrient uptake and assimilation (Zimmerman et al. 1989; Foyer et al. 2011).

Not all the photosynthetically produced oxygen was available to roots and rhizomes. Assuming that 10% of oxygen produced during photosynthesis was transported down to the roots (Borum et al. 2006; Bodensteiner 2006), this study predicted that approximately 2% of the oxygen produced in the leaves and transported would be utilized by roots for respiration. This was based on the relationship observed between the respiration rates of roots + rhizomes and the light and CO<sub>2</sub>-saturated rate of photosynthesis determined at different CO<sub>2(aq)</sub> concentrations (as shown in Fig. 4). The remaining 8% is assumed to diffuse into the surrounding rhizosphere where it can have significant impacts on diagenetic processes in otherwise anoxic sediments. The release of O<sub>2</sub> may, for example, restrict sulfide production and its intrusion into vulnerable roots (Brodersen et al. 2015; Martin et al. 2019). It may also promote nitrification, reducing porewater concentrations of NH<sub>4</sub><sup>+</sup> that have been shown to be highly toxic to eelgrass (Chapter 3). The positive gradient

caused by enhanced photosynthesis at elevated  $\text{CO}_{2(\text{aq})}$  concentrations would benefit eelgrass by providing protection against detrimental toxic sulfide intrusions affecting survival.

Like the trends observed for photosynthetic rates (ref. Fig. 37A-F), the extent of the positive effects of  $\text{CO}_{2(\text{aq})}$  on respiration rates was found to depend on LAI. Less stimulation of root respiration at high  $\text{CO}_{2(\text{aq})}$  concentrations in heavily shaded areas, characteristics of eelgrass canopy with high LAI, may be limited by oxygen availability due to reduced photosynthetic rates caused by self-shading (Pérez and Romero 1992; Marchiori et al. 2014). Conversely, reduced stimulation of root respiration rates at low  $\text{CO}_{2(\text{aq})}$  concentrations may be attributed to low oxygen as well as low sucrose availabilities, resulting from reduced carbon fixation at low  $\text{CO}_{2(\text{aq})}$  levels. Evidence from Chapter 2 supports lower sucrose concentrations in leaves, roots, and rhizome at low  $\text{CO}_{2(\text{aq})}$  concentrations.

#### **4.4.3 Leaf and root uptake dynamics in response to DIN, $\text{CO}_{2(\text{aq})}$ , and LAI**

When not constrained by growth rates, both eelgrass leaves and roots exhibited greater uptake capacities for  $\text{NO}_3^-$  and porewater  $\text{NH}_4^+$  than necessary for optimal growth, as illustrated by the color hyperbolic curves in Fig. 40 and 41. Previous uptake experiments (Iizumi and Hattori 1982; Thursby and Harlin 1982; Short and McRoy 1984) demonstrated the ability of eelgrass to rapidly absorb large amounts of nutrients from the environment, possibly as a strategy to capitalize on transient pulses of nutrients that pass through the meadow. Despite possessing high uptake capacity, this study predicted low N demand for eelgrass, owing to their low specific growth rates compared to other fast growing micro- and macroalgae (Nielsen et al. 1996; Young and Gobler 2017). Nitrogen demand was estimated to be less than  $2 \mu\text{mol N shoot}^{-1} \text{d}^{-1}$  (i.e.  $V_{\text{rmax}}$ ), which was within the range reported for *Z. marina* from field observations (Dennison et al. 1987).

The N uptake model presented in this study highlights the important role of photosynthesis and aerobic respiration in regulating N metabolism. The observed increases in  $\text{NO}_3^-$  uptake rate by leaves and  $\text{NH}_4^+$  uptake rate by roots (and rhizomes) for *Z. marina* were attributed to increased photosynthesis and respiration rates, which were impacted by changes in  $\text{CO}_{2(\text{aq})}$  and LAI as anticipated by the model. The uptake and assimilation of dissolved inorganic nitrogen (DIN) in photosynthetic organisms are an active metabolic process that requires energy (such as ATP, NADPH etc.), and reductant and fixed carbon (such as sucrose) that are generated during photosynthesis (Flores et al. 2005; Nunes-Nesi et al. 2010). The model outcome proposed that leaves under elevated  $\text{CO}_{2(\text{aq})}$  would respond to  $\text{NO}_3^-$  availability similarly to illuminated leaves, where higher uptake rates correlate with light-stimulated photosynthesis (Zimmerman et al. 1987). This formulation aligns with prior studies that suggested a positive relationship between photosynthetic activity and  $\text{NO}_3^-$  assimilation in plants (Lillo 2008; Walker et al. 2014; Kinoshita and Kinoshita 2022) and algae (Weger and Turpin 1989; Huppe and Turpin 1994). This study also highlighted the dependence of root  $\text{NH}_4^+$  uptake on photosynthesis, as root and rhizome respiration were found to be strongly influenced by photosynthetic rates in the leaves (Smith et al. 1984). This relationship ultimately governs root  $\text{NH}_4^+$  uptake rate in the model. Photosynthesis is thus critical in nutrient uptake and assimilation, especially when  $\text{NO}_3^-$  is an N source, as the assimilation of  $\text{NO}_3^-$  is particularly (photo)energy-intensive, requiring between 20 to 30% of the electrons generated by photosynthesis (Peuke and Kaiser 1996). While changes in  $\text{CO}_{2(\text{aq})}$  and LAI positively impacted  $\text{NO}_3^-$  leaf uptake rates, they had no direct impact on leaf  $\text{NH}_4^+$  uptake rate of *Z. marina*. Given that  $\text{NH}_4^+$  uptake occurs in both light and dark conditions (Rubio et al. 2007), the absorption of  $\text{NH}_4^+$  by leaf is independent of photosynthesis. Consequently, the  $\text{NH}_4^+$  leaf uptake pattern produced by the model is consistent with typical observations of N uptake/assimilation in plants

and algae (Britto and Kronzucker 2002; Alexandre et al. 2016; Reidenbach et al. 2017), confirming the model's accuracy in demonstrating the diurnal responses of  $\text{NH}_4^+$  uptake pattern and its contributions to total N in eelgrass. This study implies that the forms of DIN present in the environment will be important for eelgrass to meet their N requirement in future oceans.

Under elevated  $\text{CO}_{2(\text{aq})}$  conditions, eelgrass leaves and roots exhibited increased N uptake capacity ( $V_{\text{pmax}}$ ) and greater responsiveness to low concentrations of  $\text{NO}_3^-$  and porewater  $\text{NH}_4^+$ . The decreasing  $K_s$  values are a result of the model's formulation, driven by increasing photosynthesis ( $P_{\text{lim}}$ ) root respiration ( $R_{\text{lim}}$ ), which are influenced by changes in  $\text{CO}_{2(\text{aq})}$  and LAI. Lower  $K_s$  indicated that both leaves and roots exhibited higher affinity for these nutrients at low concentrations under increasing  $\text{CO}_{2(\text{aq})}$  concentrations. The enhanced nutrient uptake efficiency was further supported by the higher affinity coefficient ( $\alpha = V_{\text{pmax}}/K_s$ ), which evaluates nutrient uptake efficiency (Harrison et al. 1989). Specifically, the affinity coefficient of leaves for  $\text{NO}_3^-$  and roots for porewater  $\text{NH}_4^+$  was at least twice as high under high  $\text{CO}_{2(\text{aq})}$  compared to low  $\text{CO}_{2(\text{aq})}$ , indicating a faster uptake of these nutrients under high  $\text{CO}_{2(\text{aq})}$  conditions. Data on the interactive effects of  $\text{CO}_2$  and nutrient uptake in seagrass are limited, but one study suggested that  $\text{CO}_2$  may stimulate the nitrogen transporter gene responsible for higher DIN uptake in  $\text{CO}_2$ -enriched *Posidonia oceanica* living near a volcanic vent (Ravaglioli et al. 2017). However, a study by Alexandre et al. (2012) reported no significant effects of  $\text{CO}_2$  enrichment on the  $\text{NO}_3^-$  uptake rates in *Z. noltii*. It should be noted in that study, *Z. noltii* was exposed to seawater with pH levels of 8.13 and 7.91, which roughly corresponds to  $\sim 20 \mu\text{M}$   $\text{CO}_{2(\text{aq})}$  in current study. This narrow range of  $\text{CO}_{2(\text{aq})}$  levels may have limited the ability to detect any potential impacts of  $\text{CO}_{2(\text{aq})}$  on the  $\text{NO}_3^-$  uptake kinetics in that study. The current study predicted that eelgrass leaves with improved photosynthetic activity (high  $\text{CO}_{2(\text{aq})}$ , low LAI) can effectively utilize even low levels of  $\text{NO}_3^-$ ,

enabling the uptake of both  $\text{NH}_4^+$  and  $\text{NO}_3^-$ . Moreover, in the highest  $\text{CO}_{2(\text{aq})}$  conditions, the model predicted nearly equal uptake of  $\text{NH}_4^+$  and  $\text{NO}_3^-$  by leaves when both nutrients were present in similar concentrations, despite  $\text{NO}_3^-$  being more energetically costly to absorb and assimilate than  $\text{NH}_4^+$  (Guo et al. 2006). This dual capacity to efficiently assimilate both DIN species benefits eelgrass in meeting its growth requirements, particularly in low nutrient environments.

The influence of  $\text{CO}_{2(\text{aq})}$  on the nutrient uptake efficiency depended on the canopy density. The study revealed that  $\text{CO}_{2(\text{aq})}$ -enriched eelgrass with a dense canopy, characterized by high LAI, exhibited lower  $\alpha$ -values ( $\alpha = V_{\text{pmax}}/K_s$ ) compared to eelgrass with a sparse canopy, characterized by low LAI. Increasing the LAI by three-fold effectively reduced the positive effects of  $\text{CO}_{2(\text{aq})}$  on the nutrient uptake efficiency by up to 20% likely from self-shading. The self-shading effect led to a decline in photosynthetic activity (Enríquez and Pantoja-Reyes 2005), which in turn limited the photosynthesis-dependent uptake of nutrients by leaves and root in the model. Despite a 20% reduction in efficiency, *Z. marina* still met their growth requirements in heavily shaded canopy due to their low N demand.

The model predicted that eelgrass required low nutrient concentrations to satisfy growth demand under all  $\text{CO}_{2(\text{aq})}$  and LAI conditions. This study estimated that eelgrass requires  $1.2 \mu\text{M}$  of  $\text{NH}_4^+$  or between 1 and  $3 \mu\text{M}$   $\text{NO}_3^-$  from the water column, or between 2 and  $8 \mu\text{M}$   $\text{NH}_4^+$  from the sediment pool to achieve balanced growth. While these concentrations may appear high compared to open ocean levels, they are commonly found within seagrass meadows, particularly in the marine sediments (Touchette and Burkholder 2000a). In a typical eelgrass bed, sediment  $\text{NH}_4^+$  concentrations can range from 50 to  $>500 \mu\text{M}$ , depending on factors such as the sediment types, compositions, organic matter decomposition rates, microbial activities, and environmental conditions (Dennison et al. 1987; Short 1987). These concentrations are significantly higher than

the predicted threshold of 2-8  $\mu\text{M}$  for porewater  $\text{NH}_4^+$ , even at the lower limit of the reported range.

The current study suggests that root uptake of  $\text{NH}_4^+$  is expected to provide sufficient support for growth. Despite the enhanced nutrient uptake efficiency induced by increased photosynthesis in high  $\text{CO}_{2(\text{aq})}$  environment, the regeneration of  $\text{NH}_4^+$  in sediment was found to be more than adequate to meet the increased uptake rates in roots. Based on N remineralization rates observed in various seagrass studies, the rate was found to be at least 6 to 30 times higher than the growth N requirement, as illustrated in Fig. 15. Therefore, according to this model, *Z. marina* in the field is unlikely to experience N-limitation, even in the event of water column nutrient depletion.

Between leaves and roots, roots were by far the most important plant components in taking up N (as  $\text{NH}_4^+$ ) across the broad range of  $\text{CO}_{2(\text{aq})}$  and LAI simulations. For an environment with nutrient concentrations typically encountered in the field, leaves and roots contributed roughly equivalent to the total N assimilated in *Z. marina*. This prediction agrees with as the *in-situ*  $\text{CO}_{2(\text{aq})}$  concentrations increased; the model predicted that the  $\text{NH}_4^+$  acquired by the roots represented the largest proportion of N assimilated for plant growth. There was a shift in the percentage contributions to the whole plant N by the leaves and the roots, going from roughly equal contributions in current  $\text{CO}_{2(\text{aq})}$  condition to a 30:70 split favoring the roots at elevated  $\text{CO}_{2(\text{aq})}$ . This is because root  $\text{NH}_4^+$  uptake is highly sensitive to  $\text{O}_2$  (Morris and John 1984) and its metabolic activity is a photosynthesis dependent process (Smith et al. 1984). As long as sediment  $\text{NH}_4^+$  was above 50  $\mu\text{M}$ , roots assimilated no less than 50% of the total N in eelgrass even with adequate  $\text{NO}_3^-$  and  $\text{NH}_4^+$  in the water column to saturate growth and even when photosynthesis was severely  $\text{CO}_{2(\text{aq})}$  limited. This makes root activity pivotal to shoot growth and will likely play a central role

in dictating their N acquisition strategy with rising  $\text{CO}_{2(\text{aq})}$ . The heavier reliance on the root system also makes the sediment and sediment biogeochemistry important components of N source for eelgrass in future carbonated ocean.

Although this study focuses on *Z. marina*, the model can be applied to other seagrass species with similar nutrient uptake requirements. In summary, N-limitation in *Z. marina* under current or future  $\text{CO}_2$  climate appears unlikely. However, it is important to note that this study assumes a closed system for the purpose of balancing the N budget within the system. The model does not consider the biomass loss through export beyond the meadow, which could account for up to 30% of the seagrass net primary production (Duarte and Krause-Jensen 2017). This non-sequestered detritus can significantly impact on nutrient availability in the sediments, where root uptake serves as the primary source of N for eelgrass. Therefore, it is crucial to incorporate the effects of biomass exports in future studies on nitrogen-seagrass dynamics, particularly in the context of climate change.

## CHAPTER 5

### CONCLUSION

This study provides comprehensive understanding of long-term  $\text{CO}_{2(\text{aq})}$  exposure on *Zostera marina* L. with regard to nitrogen utilization and potential toxicity. While the lag response to  $\text{CO}_{2(\text{aq})}$  enrichment was evident, taking at least 6 weeks to manifest for some parameters, the established overall responses were statistically linear across various  $\log \text{CO}_{2(\text{aq})}$  concentrations and consistent with past research (Zimmerman et al. 2017). The established linear pattern is an important predictive tool, as the impact of  $\text{CO}_{2(\text{aq})}$  on seagrass can be extrapolated into the future well beyond 2100. Emphasizing the importance of longer experimentation design, especially considering seasonal patterns, this long-term  $\text{CO}_2$ -enrichment study, spanning over 18 months, provided unique insights into both seasonal and tissue-specific responses of eelgrass within the context of climate change.

*Z. marina* currently faces carbon limitation in today's ocean, but stands to benefit from increasing aqueous  $\text{CO}_2$  concentrations in the future. The study revealed positive physiological and morphological traits in eelgrass, with marked improvements in growth rates, plant size, and leaf density. These enhancements were evident even during periods of prolonged thermal stress in two consecutive summers, facilitated by increased sucrose accumulation in leaves and rhizomes. The sucrose reserves in the rhizomes likely played an important role in regulating growth rates, and led to significant doubling of the absolute growth rates and plant size in the second year of the experiment. These results support previous model predictions that  $\text{CO}_2$  can offset the negative temperature effect and enable survival in warming ocean (Zimmerman et al. 2015). The anticipated

global average temperature rise of 2 °C in the next 50 years is expected to have a profound impact on eelgrass habitats, especially those living at the southern limit of their distribution, such as those in the Chesapeake Bay. The net carbon gain resulting from rising CO<sub>2</sub> levels holds the potential to mitigate the adverse effects of global climate warming for these eelgrass populations.

Exploring the impact of CO<sub>2</sub> on amino acid content, particularly during winter months, uncovered positive effects, suggesting enhanced N assimilation under elevated CO<sub>2(aq)</sub> conditions. However, the study also observed a decrease in biomass-specific N content, attributed to dilution effects caused by CO<sub>2</sub>-stimulated increase in carbon content in thicker leaves. This decline in biomass-specific N content did not result from CO<sub>2</sub>-induced N-limitation, as N content increased per unit area of leaf with increasing CO<sub>2(aq)</sub> concentrations and growth rates were stimulated by CO<sub>2(aq)</sub> enrichment. Furthermore, the dissolved inorganic nitrogen in the environment was at least twice above the minimum N threshold for growth as established by Zimmerman et al. (1987) and by the modeling analysis performed in Chapter 4 of this dissertation, throughout the entire experiment. Additionally, the present study predicted low N demand even at the highest CO<sub>2(aq)</sub> conditions owing to their low specific growth rates compared to other fast growing micro- and macroalgae (Nielsen et al. 1996; Young and Gobler 2017). Optimal growth was easily achieved as long as water column NH<sub>4</sub><sup>+</sup> or NO<sub>3</sub><sup>-</sup> were maintained at 1.2 μM or 3 μM, respectively, or porewater NH<sub>4</sub><sup>+</sup> concentration was kept above 8 μM.

This study utilized a model to predict the N demand and uptake dynamics of *Zostera marina* L. under varying CO<sub>2(aq)</sub> conditions and leaf area index (LAI). The results suggested efficient assimilation of both NH<sub>4</sub><sup>+</sup> and NO<sub>3</sub><sup>-</sup> under elevated CO<sub>2(aq)</sub> environments. Despite considering factors like canopy density and architecture, which can hinder N uptake and assimilation by modulating photosynthesis and aerobic root respiration, the model predicted that

eelgrass was unlikely to experience N-limitation, highlighting the important role of root  $\text{NH}_4^+$  uptake in supporting shoot growth. Moreover, model simulations spanning a wide range of  $\text{CO}_{2(\text{aq})}$  and LAI values indicated an anticipated increase in root activities going forward as atmospheric  $\text{CO}_2$  concentrations continue to escalate. These  $\text{CO}_2$ -enhanced root activities, while influencing nutrient cycling in the sediments, may extend their impact on sediment biogeochemistry by altering the sediment redox potential through promotion of rhizosphere oxygenation (Borum et al. 2016; Li et al. 2024) and protect against sulfide toxicity.

Despite the beneficial impacts of  $\text{CO}_2$  on *Z. marina* documented in Chapter 2, this study recognizes the susceptibility of seagrass to sediment eutrophication. The study explored the intricate dynamics of  $\text{CO}_{2(\text{aq})}$  treatment on biochemical compositions, focusing on sucrose, amino acids and total C and N in eelgrass under four sediment types. Even though sucrose accumulated in leaves to levels comparable to those measured in Chapter 2, the positive C reserve did not prevent plants from N- $\text{NH}_4^+$  toxicity, as hypothesized. This suggests that shoot mortality was unrelated to the overall carbon balance.

The lack of clear and consistent  $\text{CO}_{2(\text{aq})}$  effects in nutrient enriched sediments was due to the unanticipated overwhelming  $\text{NH}_4^+$  toxicity effects on eelgrass survivals, imposing limitations on result interpretations. Acknowledging the experimental constraints, the study highlighted the sensitivity of eelgrass to porewater DIN rather than  $\text{H}_2\text{S}$  concentrations resulting from organic carbon loading. Despite porewater  $\text{H}_2\text{S}$  concentrations above levels that could elicit die-offs (Lamers et al. 2013),  $\text{H}_2\text{S}$  toxicity was not observed. In addition, this study also proposed plausible scenarios emphasizing the roles of sediment properties in predicting the sediment chemistry and, consequently, eelgrass survival.

Base on the conclusion of this study, there is a clear imperative for further research into the dynamics of sediment biogeochemistry and its influence on seagrass ecosystems, especially within the context of climate change. The intricate interaction between  $\text{CO}_{2(\text{aq})}$  and sediment biogeochemistry, whether synergistic or antagonistic, may give rise to complex responses in seagrass communities. Therefore, there is a need to unravel these relationships comprehensively, as understanding these dynamics is crucial for making accurate predictions regarding the future health and resilience of seagrasses amidst the ongoing challenges posed by climate change.

## REFERENCES

- Abdulgawad, F., E. B. Bockelmann, D. Sapsford, K. P. Williams, and R. Falconer. 2009. Ammonium ion adsorption on clays and sand under freshwater and seawater conditions, p. 656-661. *Advances in Water Resources and Hydraulic Engineering*. Springer Berlin Heidelberg.
- Ainsworth, E. A., and S. P. Long. 2005. What have we learned from 15 years of free-air CO<sub>2</sub> enrichment (FACE)? A meta-analytic review of the responses of photosynthesis, canopy properties and plant production to rising CO<sub>2</sub>. *New Phytol.* **165**: 351-372.
- Ainsworth, E. A., and A. Rogers. 2007. The response of photosynthesis and stomatal conductance to rising [CO<sub>2</sub>]: Mechanisms and environmental interactions. *Plant Cell Environ.* **30**: 258-270.
- Aioi, K., H. Mukai, I. Koike, M. Ohtsu, and A. Hattori. 1981. Growth and organic production of eelgrass (*Zostera marina* L.) in temperate waters of the pacific coast of Japan II. Growth analysis in winter. *Aquat. Bot.* **10**: 175-182.
- Alexandre, A., J. Silva, P. Buapet, M. Björk, and R. Santos. 2012. Effects of CO<sub>2</sub> enrichment on photosynthesis, growth, and nitrogen metabolism of the seagrass *Zostera noltii*. *Ecol. Evol.* **2**: 2625-2635.
- Alexandre, A., J. Silva, and R. Santos. 2016. Nitrogen uptake in light versus darkness of the seagrass *Zostera noltei*: Integration with carbon metabolism. *Mar. Ecol.* **37**: 1050-1056.
- Alshameri, A., H. He, Y. Xi, R. Zhu, L. Ma, and Q. Tao. 2018. Adsorption of ammonium by different natural clay minerals: characterization, kinetics and adsorption isotherms. *Appl. Clay Sci.* **159**: 83-93.

- Andrews, M. and others 2018. Elevated CO<sub>2</sub> effects on nitrogen assimilation and growth of C<sub>3</sub> vascular plants are similar regardless of N-form assimilated. *J. Exp. Bot.* **70**: 683-690.
- Apostolaki, E. T., S. Vizzini, I. E. Hendriks, and Y. S. Olsen. 2014. Seagrass ecosystem response to long-term high CO<sub>2</sub> in a Mediterranean volcanic vent. *Mar. Environ. Res.* **99**: 9-15.
- Azevedo, L. B., A. M. De Schryver, A. J. Hendriks, and M. A. J. Huijbregts. 2015. Calcifying species sensitivity distributions for ocean acidification. *Environ. Sci. Technol.* **49**: 1495-1500.
- Barañano, C., E. Fernández, P. Morán, P. Urbieta, and G. Méndez. 2022. Population dynamics of a fragmented subtidal *Zostera marina* population affected by shell fishing. *Est. Coast. Shelf Sci.* **269**: 107818.
- Bassirirad, H. 2000. Kinetics of nutrient uptake by roots: Responses to global change. *New Phytol.* **147**: 155-169.
- Beer, S., and E. Koch. 1996. Photosynthesis of marine macroalgae and seagrasses in globally changing CO<sub>2</sub> environments. *Mar. Ecol. Prog. Ser.* **141**: 199-204.
- Behrendt, A., D. de Beer, and P. Stief. 2013. Vertical activity distribution of dissimilatory nitrate reduction in coastal marine sediments. *Biogeosciences* **10**: 7509-7523.
- Berlinghof, J. and others 2023. Accelerated nitrogen cycling on seagrass leaves in a high-CO<sub>2</sub> world. *bioRxiv*: 2023.2005.2019.541481.
- Bindoff, N. L. and others 2019. Changing ocean, marine ecosystems, and dependent communities. *In* D. C. R. H.-O. Pörtner, V. Masson-Delmotte, P. Zhai, M. Tignor, E. Poloczanska, K. Mintenbeck, A. Alegría, M. Nicolai, A. Okem, J. Petzold, B. Rama, N.M. Weyer [ed.], IPCC Special Report on the Ocean and Cryosphere in a Changing Climate. In press.

- Bodensteiner, L. E. 2006. The impact of light availability on benthic oxygen release by seagrasses. Master's Theses. San Jose State University.
- Borum, J. and others 2005. The potential role of plant oxygen and sulphide dynamics in die-off events of the tropical seagrass, *Thalassia testudinum*. *J. Ecol.* **93**: 148-158.
- Borum, J. and others 2016. Photosynthetic response to globally increasing CO<sub>2</sub> of co-occurring temperate seagrass species. *Plant Cell Environ.* **39**: 1240-1250.
- Borum, J., K. Sand-Jensen, T. Binzer, O. Pedersen, and T. M. Greve. 2006. Chapter 10. Oxygen movement in seagrasses, p. 255-270. *In* A. W. D. Larkum, R. J. Orth and C. M. Duarte [eds.], *Seagrasses: Biology, ecology and conservation*. Springer Netherlands.
- Bostrom, C., and B. Erik. 2000. Zoobenthic community establishment and habitat complexity - The importance of seagrass shoot-density, morphology and physical disturbance for faunal recruitment. *Mar. Ecol. Prog. Ser.* **205**: 123-138.
- Britto, D. T., and H. J. Kronzucker. 2002. NH<sub>4</sub><sup>+</sup> toxicity in higher plants: a critical review. *J. Plant Physiol.* **159**: 567-584.
- Britto, D. T., M. Y. Siddiqi, A. D. Glass, and H. J. Kronzucker. 2001. Futile transmembrane NH<sub>4</sub><sup>+</sup> cycling: A cellular hypothesis to explain ammonium toxicity in plants. *Proc. Natl. Acad. Sci. U. S. A.* **98**: 4255-4258.
- Brodersen, K. E., D. A. Nielsen, P. J. Ralph, and M. Kühl. 2015. Oxic microshield and local pH enhancement protects *Zostera muelleri* from sediment derived hydrogen sulphide. *New Phytol.* **205**: 1264-1276.
- Brun, F. G., H. I., V. J.J., P. G., and P.-L. J.L. 2002. Assessing the toxicity of ammonium pulses to the survival and growth of *Zostera noltii*. *Mar. Ecol. Prog. Ser.* **225** : 177–187.

- Burdige, D. J. 2006. The components of marine sediments, p. 5-26. *Geochemistry of Marine Sediments*. Princeton University Press.
- Burdige, D. J., R. C. Zimmerman, and X. Hu. 2008. Rates of carbonate dissolution in permeable sediments estimated from pore-water profiles: The role of sea grasses. *Limnol. Oceanogr.* **53**: 549-565.
- Burkhardt, S., I. Zondervan, and U. Riebesell. 1999. Effect of CO<sub>2</sub> concentration on C: N: P ratio in marine phytoplankton: A species comparison. *Limnol. Oceanogr.* **44**: 683-690.
- Burkholder, J. M., H. B. J. Glasgow, and J. E. Cooke. 1994. Comparative effects of water-column nitrate enrichment on eelgrass *Zostera marina*, shoalgrass *Halodule wrightii*, and widgeongrass *Ruppia maritima* *Mar. Ecol. Prog. Ser.* **105**: 121-138.
- Burkholder, J. M., K. M. Mason, and H. B. J. Glasgow. 1992. Water-column nitrate enrichment promotes decline of eelgrass *Zostera marina* : Evidence from seasonal mesocosm experiments. *Mar. Ecol. Prog. Ser.* **81**: 163-178.
- Burkholder, J. M., D. A. Tomasko, and B. W. Touchette. 2007. Seagrasses and eutrophication. *J. Exp. Mar. Biol. Ecol.* **350**: 46-72.
- Caffrey, J. M., and W. M. Kemp. 1990. Nitrogen cycling in sediments with estuarine populations of *Potamogeton perfoliatus* and *Zostera marina*. *Mar. Ecol. Prog. Ser.* **66**: 147-160.
- Campbell, J. E., and J. W. Fourqurean. 2018. Does nutrient availability regulate seagrass response to elevated CO<sub>2</sub>? *Ecosystems* **21**: 1269-1282.
- . 2013. Effects of in situ CO<sub>2</sub> enrichment on the structural and chemical characteristics of the seagrass *Thalassia testudinum*. *Mar. Biol.* **160**: 1465-1475.
- Canfield, D. E. 1989. Reactive iron in marine sediments. *Geochim. Cosmochim. Acta* **53**: 619-632.

- Canfield, D. E., and R. A. Berner. 1987. Dissolution and pyritization of magnetite in anoxic marine sediments. *Geochim. Cosmochim. Acta* **51**: 645-659.
- Cao, T., L. Ni, and P. Xie. 2004. Acute biochemical responses of a submersed macrophyte, *Potamogeton crispus* L., to high ammonium in an aquarium experiment. *J. Freshw. Ecol.* **19**: 279-284.
- Celebi-Ergin, B., R. C. Zimmerman, and V. J. Hill. 2022. Photorespiration in eelgrass (*Zostera marina* L.): A photoprotection mechanism for survival in a CO<sub>2</sub>-limited world. *Front. Plant Sci.* **13**.
- Celebi-Ergin, B., R. C. Zimmerman, and V. J. Hill. 2021. Impact of ocean carbonation on long-term regulation of light harvesting in eelgrass *Zostera marina*. *Mar. Ecol. Prog. Ser.* **671**: 111-128.
- Celebi, B. 2016. Potential impacts of climate change on photochemistry of *Zostera Marina* L. Doctor Dissertation. Old Dominion University.
- Cline, J. D. 1969. Spectrophotometric determination of hydrogen sulfide in natural waters. *Limnol. Oceanogr.* **14**: 454-458.
- Cruz, C., A. F. M. Bio, M. D. Domínguez-Valdivia, P. M. Aparicio-Tejo, C. Lamsfus, and M. A. Martins-Loução. 2006. How does glutamine synthetase activity determine plant tolerance to ammonium? *Planta* **223**: 1068-1080.
- Cummings, M. E., and R. C. Zimmerman. 2003. Light harvesting and the package effect in the seagrasses *Thalassia testudinum* Banks ex König and *Zostera marina* L.: Optical constraints on photoacclimation. *Aquat. Bot.* **75**: 261-274.

- Cutter, G. A., and J. Radford-Knoery. 1991. Determination of carbon, nitrogen, sulfur, and inorganic sulfur species in marine particles, p. 57-63. *Marine Particles: Analysis and Characterization*. American Geophysical Union.
- Dalla Via, J. and others 1998. Light gradients and meadow structure in *Posidonia oceanica*: Ecomorphological and functional correlates. *Mar. Ecol. Prog. Ser.* **163**: 267-278.
- Delgado, O., J. Ruiz, M. Perez, J. Romero, and E. Ballesteros. 1999. Effects of fish farming on seagrass (*Posidonia oceanica*) in a Mediterranean bay: Seagrass decline after organic loading cessation. *Oceanol. Acta* **22**: 109-117.
- Dennison, W. C. 1987. Effects of light on seagrass photosynthesis, growth and depth distribution. *Aquat. Bot.* **27**: 15-26.
- Dennison, W. C., and R. S. Alberte. 1982. Photosynthetic responses of *Zostera marina* L. (eelgrass) to *in situ* manipulations of light intensity. *Oecologia* **55**: 137-144.
- Dennison, W. C., R. C. Aller, and R. S. Alberte. 1987. Sediment ammonium availability and eelgrass (*Zostera marina*) growth. *Mar. Biol.* **94**: 469-477.
- Dickson, A. G., and F. J. Millero. 1987. A comparison of the equilibrium constants for the dissociation of carbonic acid in seawater media. *Deep Sea Res. Part I Oceanogr. Res. Pap.* **34**: 1733-1743.
- Dlugokencky, E. J., B. D. Hall, S. A. Montzka, G. Dutton, J. Mühle, and J. W. Elkins. 2019. Atmospheric composition [in state of the climate in 2018, Chapter 2: Global climate]. *Bulletin of the American Meteorological Society* **100**: S48-S50.
- Dooley, F. D., S. Wyllie-Echeverria, M. B. Roth, and P. D. Ward. 2013. Tolerance and response of *Zostera marina* seedlings to hydrogen sulfide. *Aquat. Bot.* **105**: 7-10.

- Douglas, E. J., C. A. Pilditch, L. V. Hines, C. Kraan, and S. F. Thrush. 2016. *In situ* soft sediment nutrient enrichment: A unified approach to eutrophication field experiments. *Mar. Pollut. Bull.* **111**: 287-294.
- Droop, M. R. 1973. Some thoughts on nutrient limitation in algae. *J. Phycol.* **9**: 264-272.
- . 1968. Vitamin B<sub>12</sub> and marine ecology. IV. The kinetics of uptake, growth and inhibition in *Monochrysis lutheri*. *J. Mar. Biol. Assoc. U. K.* **48**: 689-733.
- Duarte, C. C. 1991. Allometric scaling of seagrass form and productivity. *Mar. Ecol. Prog. Ser.* **77**: 289-300.
- Duarte, C. M. 1990. Seagrass nutrient content. *Mar. Ecol. Prog. Ser.* **6**: 201-207.
- Duarte, C. M., and C. L. Chiscano. 1999. Seagrass biomass and production: A reassessment. *Aquat. Bot.* **65**: 159-174.
- Duarte, C. M., and D. Krause-Jensen. 2017. Export from seagrass meadows contributes to marine carbon sequestration. *Front. Mar. Sci.* **4**.
- Dumouchel, W., and F. O'brien. 1989. Integrating a robust option into a multiple regression computing environment, p. 297-302. *Computer science and statistics: Proc. 21st symp. interface*. American Statistical Association Alexandria, VA.
- Durako, M. J. 1993. Photosynthetic utilization of CO<sub>2(aq)</sub> and HCO<sub>3</sub><sup>-</sup> in *Thalassia testudinum* (*Hydrocharitaceae*). *Mar. Biol.* **115**: 373-380.
- Enríquez, S., C. M. Duarte, and K. Sand-Jensen. 1993. Patterns in decomposition rates among photosynthetic organisms: The importance of detritus C:N:P content. *Oecologia* **94**: 457-471.

- Enrriquez, S., M. Merino, and R. Iglesias-Prieto. 2002. Variations in the photosynthetic performance along the leaves of the tropical seagrass *Thalassia testudinum*. *Mar. Biol.* **140**: 891-900.
- Enrriquez, S., I. Olivé, N. Cayabyab, and J. D. Hedley. 2019. Structural complexity governs seagrass acclimatization to depth with relevant consequences for meadow production, macrophyte diversity and habitat carbon storage capacity. *Sci. Rep.* **9**: 14657.
- Enrriquez, S., and N. I. Pantoja-Reyes. 2005. Form-function analysis of the effect of canopy morphology on leaf self-shading in the seagrass *Thalassia testudinum*. *Oecologia* **145**: 234-242.
- Erfteimeijer, P. L. A., and J. J. Middelburg. 1993. Sediment-nutrient interactions in tropical seagrass beds: A comparison between a terrigenous and a carbonate sedimentary environment in South Sulawesi (Indonesia). *Mar. Ecol. Prog. Ser.* **102**: 187-198.
- Evans, A. S., K. L. Webb, and P. A. Penhale. 1986. Photosynthetic temperature acclimation in two coexisting seagrasses, *Zostera marina* L. and *Ruppia maritima* L. *Aquat. Bot.* **24**: 185-197.
- Falkowski, P., and J. Raven. 2007. *Aquatic photosynthesis*, 2nd ed. Princeton Univ. Press.
- Flores, E., J. E. Frías, L. M. Rubio, and A. Herrero. 2005. Photosynthetic nitrate assimilation in cyanobacteria. *Photosynth. Res.* **83**: 117-133.
- Fonseca, M. S. 1989. Sediment stabilization by *Halophila decipiens* in comparison to other seagrasses. *Est. Coast. Shelf Sci.* **29**: 501-507.
- Fourqurean, J. W. and others 2012. Seagrass ecosystems as a globally significant carbon stock. *Nat. Geosci.* **5**: 505-509.

- Foyer, C. H., and G. Noctor. 2002. Photosynthetic nitrogen assimilation: Inter-pathway control and signaling, p. 1-22. *In* C. H. Foyer and G. Noctor [eds.], Photosynthetic Nitrogen Assimilation and Associated Carbon and Respiratory Metabolism. Springer Netherlands.
- Foyer, C. H., G. Noctor, and M. Hodges. 2011. Respiration and nitrogen assimilation: targeting mitochondria-associated metabolism as a means to enhance nitrogen use efficiency. *J. Exp. Bot.* **62**: 1467-1482.
- Frederiksen, M. S., M. Holmer, J. Borum, and H. Kennedy. 2006. Temporal and spatial variation of sulfide invasion in eelgrass (*Zostera marina*) as reflected by its sulfur isotopic composition. *Limnol. Oceanogr.* **51**: 2308-2318.
- Frederiksen, M. S., M. Holmer, M. Pérez, O. Invers, J. M. Ruiz, and B. B. Knudsen. 2008. Effect of increased sediment sulfide concentrations on the composition of stable sulfur isotopes ( $\delta^{34}\text{S}$ ) and sulfur accumulation in the seagrasses *Zostera marina* and *Posidonia oceanica*. *J. Exp. Mar. Biol. Ecol.* **358**: 98-109.
- Gacia, E., C. M. Duarte, and J. J. Middelburg. 2002. Carbon and nutrient deposition in a Mediterranean seagrass (*Posidonia oceanica*) meadow. *Limnol. Oceanogr.* **47**: 23-32.
- Gao, K., Y. Aruga, K. Asada, T. Ishihara, T. Akano, and M. Kiyohara. 1991. Enhanced growth of the red alga *Porphyra yezoensis* Ueda in high CO<sub>2</sub> concentrations. *J. Appl. Phycol.* **3**: 355-362.
- García, R., M. Holmer, C. M. Duarte, and N. Marbà. 2013. Global warming enhances sulphide stress in a key seagrass species (NW Mediterranean). *Glob Chang Biol.* **19**: 3629-3639.
- Gieskes, J. M., and W. C. Rogers. 1973. Alkalinity determination in interstitial waters of marine sediments. *J. Sediment. Res.* **43**: 272-277.

- Givan, C. V. 1979. Metabolic detoxification of ammonia in tissues of higher plants. *Phytochemistry* **18**: 375-382.
- Goldman, J. C., D. A. Caron, and M. R. Dennett. 1987. Regulation of gross growth efficiency and ammonium regeneration in bacteria by substrate C: N ratio<sup>1</sup>. *Limnol. Oceanogr.* **32**: 1239-1252.
- Govers, L. L. and others 2014. Toxic effects of increased sediment nutrient and organic matter loading on the seagrass *Zostera noltii*. *Aquat. Toxicol.* **155**: 253-260.
- Green, E. P., and F. T. Short. 2003. *World atlas of seagrasses*. University of California Press.
- Gu, X. and others 2023. Changes in mangrove blue carbon under elevated atmospheric CO<sub>2</sub>. *Ecosyst. Health Sustain.* **9**: 0033.
- Gülüt, K. Y., and B. Hoşgökdelen. 2021. Sulfur and nitrogen nutrition status in flag leaf and shoot samples collected from wheat growing areas in Çukurova, Central Anatolia and GAP regions of Turkey. *Saudi J Biol Sci* **28**: 4807-4817.
- Guo, S., Y. Zhou, Q. Shen, and F. Zhang. 2006. Effect of ammonium and nitrate nutrition on some physiological processes in higher plants-growth, photosynthesis, photorespiration, and water relations. *Plant Biol.*: 21-29.
- Guo, Z., J. Gong, S. Luo, Y. Zuo, and Y. Shen. 2023. Role of Gamma-Aminobutyric Acid in Plant Defense Response. *Metabolites* **13**.
- Hall-Spencer, J. M. and others 2008. Volcanic carbon dioxide vents show ecosystem effects of ocean acidification. *Nature* **454**: 96-99.
- Hammer, K. J., J. Borum, H. Hasler-Sheetal, E. C. Shields, K. Sand-Jensen, and K. A. Moore. 2018. High temperatures cause reduced growth, plant death and metabolic changes in eelgrass *Zostera marina*. *Mar. Ecol. Prog. Ser.* **604**: 121-132.

- Harley, C. D. G. and others 2006. The impacts of climate change in coastal marine systems. *Ecol. Lett.* **9**: 228-241.
- Harrison, P. G. 1978. Patterns of uptake and translocations of  $^{14}\text{C}$  by *Zostera americana* Den Hartog in the laboratory. *Aquat. Bot.* **5**: 93-97.
- Harrison, P. J., J. S. Parslow, and H. L. Conway. 1989. Determination of nutrient uptake kinetic parameters: A comparison of methods. *Mar. Ecol. Prog. Ser.* **52**: 301-312.
- Hasler-Sheetal, H., L. Fragner, M. Holmer, and W. Weckwerth. 2015. Diurnal effects of anoxia on the metabolome of the seagrass *Zostera marina*. *Metabolomics* **11**: 1208-1218.
- Hasler-Sheetal, H., and M. Holmer. 2015. Sulfide Intrusion and Detoxification in the Seagrass *Zostera marina*. *PLoS One* **10**: e0129136-e0129136.
- Hatfield, J. L., and C. Dold. 2019. Water-use efficiency: Advances and challenges in a changing climate. *Front Plant Sci* **10**: 103.
- Heck, K. L. J., G. Hays, and R. J. Orth. 2003. Critical evaluation of the nursery role hypothesis for seagrass meadows. *Mar. Ecol. Prog. Ser.* **253**: 123-136.
- Hedley, J., and S. Enríquez. 2010. Optical properties of canopies of the tropical seagrass *Thalassia testudinum* estimated by a three-dimensional radiative transfer model. *Limnol. Oceanogr.* **55**: 1537-1550.
- Hedley, J. D., K. McMahon, and P. Fearn. 2014. Seagrass canopy photosynthetic response is a function of canopy density and light environment: A model for *Amphibolis griffithii*. *PLoS One* **9**: e111454.
- Hemminga, M., and C. M. Duarte. 2000. *Seagrass Ecology*. Cambridge University Press.
- Herbert, R. A. 1999. Nitrogen cycling in coastal marine ecosystems. *FEMS Microbiol. Rev.* **23**: 563-590.

- Hernán, G. and others 2016. Seagrass (*Posidonia oceanica*) seedlings in a high-CO<sub>2</sub> world: from physiology to herbivory. *Sci. Rep.* **6**: 38017.
- Holmer, M., and E. J. Bondgaard. 2001. Photosynthetic and growth response of seagrass to low oxygen and high sulfide concentrations during hypoxic events. *Aquat. Bot.* **70**: 29-38.
- Holmer, M., M. S. Frederiksen, and H. Møllegaard. 2005. Sulfur accumulation in eelgrass (*Zostera marina*) and effect of sulfur on eelgrass growth. *Aquat. Bot.* **81**: 367-379.
- Huber, S. C., and D. W. Israel. 1982. Biochemical basis for partitioning of photosynthetically fixed carbon between starch and sucrose in soybean (*glycine max merr.*) leaves<sup>1</sup>. *Plant Physiol.* **69**: 691-696.
- Huppe, H. C. a., and D. H. Turpin. 1994. Integration of carbon and nitrogen metabolism in plant and algal cells. *Annu. Rev. Plant Physiol. Plant Mol. Biol.* **45**: 577-607.
- Iizumi, H., and A. Hattori. 1982. Growth and organic production of eelgrass (*Zostera marina* L.) in temperate waters of the Pacific coast of Japan. III. The kinetics of nitrogen uptake. *Aquat. Bot.* **12**: 245-256.
- Invers, O., Tom, F. s, M. rez, and J. Romero. 2002. Potential effect of increased global CO<sub>2</sub> availability on the depth distribution of the seagrass *Posidonia oceanica* (L.) Delile: A tentative assessment using a carbon balance model. *Bull. Mar. Sci.* **71**: 1191-1198.
- Invers, O., R. C. Zimmerman, R. S. Alberte, M. Pérez, and J. Romero. 2001. Inorganic carbon sources for seagrass photosynthesis: An experimental evaluation of bicarbonate use in species inhabiting temperate waters. *J. Exp. Mar. Biol. Ecol.* **265**: 203-217.
- IPCC. 2022. Climate change 2022: Impacts, adaptation and vulnerability. Contribution of Working group II to the sixth assessment report of the intergovernmental panel on climate change [H.-O. Pörtner, D.C. Roberts, M. Tignor, E.S. Poloczanska, K. Mintenbeck, A. Alegría, M.

- Craig, S. Langsdorf, S. Löschke, V. Möller, A. Okem, B. Rama (eds.]). Cambridge University Press. Cambridge University Press, Cambridge, UK and New York, NY, USA, 3056 pp., doi:10.1017/9781009325844.
- . 2013. Annex II: Climate system scenario tables [Prather, M., G. Flato, P. Friedlingstein, C. Jones, J.-F. Lamarque, H. Liao and P. Rasch (eds.)]. In: Climate change 2013: The physical science basis. Contribution of working group I to the fifth assessment report of the intergovernmental panel on climate change [Stocker, T.F., D. Qin, G.-K. Plattner, M. Tignor, S.K. Allen, J. Boschung, A. Nauels, Y. Xia, V. Bex and P.M. Midgley (eds.)], p. 1395-1445. Cambridge University Press, Cambridge, United Kingdom and New York, NY, USA.
- . 2014. Climate change 2014: Impacts, adaptation, and vulnerability. Part A: Global and sectoral aspects. Contribution of working group ii to the fifth assessment report of the intergovernmental panel on climate change [Field, C.B., V.R. Barros, D.J. Dokken, K.J. Mach, M.D. Mastrandrea, T.E. Bilir, M. Chatterjee, K.L. Ebi, Y.O. Estrada, R.C. Genova, B. Girma, E.S. Kissel, A.N. Levy, S. MacCracken, P.R. Mastrandrea, and L.L. White (eds.)]. Cambridge University Press.
- Jacobs, R. P. W. M. 1979. Distribution and aspects of the production and biomass of eelgrass, *Zostera marina* L., at Roscoff, France. *Aquat. Bot.* **7**: 151-172.
- Jiang, Z. J., X.-P. Huang, and J.-P. Zhang. 2010. Effects of CO<sub>2</sub> enrichment on photosynthesis, growth, and biochemical composition of seagrass *Thalassia hemprichii* (Ehrenb.) Aschers. *J. Integr. Plant Biol.* **52**: 904-913.

- Jiménez-Ramos, R., L. G. Egea, M. J. Ortega, I. Hernández, J. J. Vergara, and F. G. Brun. 2017. Global and local disturbances interact to modify seagrass palatability. *PLoS One* **12**: e0183256.
- Jørgensen, B. B. 1982. Mineralization of organic matter in the sea bed—the role of sulphate reduction. *Nature* **296**: 643-645.
- Jørgensen, B. B., A. J. Findlay, and A. Pellerin. 2019. The biogeochemical sulfur cycle of marine sediments. *Front. Microbiol.* **10**.
- Kaldy, J. E., C. A. Brown, and S. R. Pacella. 2022. Carbon limitation in response to nutrient loading in an eelgrass mesocosm: influence of water residence time. *Mar. Ecol. Prog. Ser.* **689**: 1-17.
- Kelso, B., R. V. Smith, R. J. Laughlin, and S. D. Lennox. 1997. Dissimilatory nitrate reduction in anaerobic sediments leading to river nitrite accumulation. *Appl. Environ. Microbiol.* **63**: 4679-4685.
- Kinnersley, A. M., and F. J. Turano. 2000. Gamma aminobutyric acid (GABA) and plant responses to stress. *Crit. Rev. Plant Sci.* **19**: 479-509.
- Kinoshita, S. N., and T. Kinoshita. 2022. A win-win scenario for photosynthesis and the plasma membrane H<sup>(+)</sup> pump. *Front. Plant Sci.* **13**: 982485.
- Kleypas, J. A., R. W. Buddemeier, D. Archer, J.-P. Gattuso, C. Langdon, and B. N. Opdyke. 1999. Geochemical consequences of increased atmospheric carbon dioxide on coral reefs. *Science* **284**: 118-120.
- Koch, K. E. 1996. Carbohydrate-modulated gene expression in plants. *Annu. Rev. Plant Physiol. Plant Mol. Biol.* **47**: 509.

- Koch, M. S., and J. M. Erskine. 2001. Sulfide as a phytotoxin to the tropical seagrass *Thalassia testudinum*: Interactions with light, salinity and temperature. *J. Exp. Mar. Biol. Ecol.* **266**: 81-95.
- Koch, M. S., S. A. Schopmeyer, O. I. Neilsen, C. Kyhn-Hansen, and C. J. Madden. 2007. Conceptual model of seagrass die-off in Florida bay: Links to biogeochemical processes. *J. Exp. Mar. Biol. Ecol.* **350**: 73-88.
- Kosegarten, H., F. Grolig, J. Wieneke, G. Wilson, and B. Hoffmann. 1997. Differential ammonia-elicited changes of cytosolic pH in root hair cells of rice and maize as monitored by 2',7'-bis-(2-carboxyethyl)-5 (and -6)-carboxyfluorescein-fluorescence ratio. *Plant Physiol.* **113**: 451.
- Kowalczyk, J. B., and J.-E. Lee. 2022. High CO<sub>2</sub> expands where plants can grow in CESM-CLM4-CNDV. *J. Geophys. Res. Atmos.* **127**: e2021JD035158.
- Kraal, P., E. D. Burton, and R. T. Bush. 2013. Iron monosulfide accumulation and pyrite formation in eutrophic estuarine sediments. *Geochim. Cosmochim. Acta* **122**: 75-88.
- Kraemer, G. P., and R. S. Alberte. 1995. Impact of daily photosynthetic period on protein synthesis and carbohydrate stores in *Zostera marina* L. (eelgrass) roots: implications for survival in light-limited environments. *J. Exp. Mar. Biol. Ecol.* **185**: 191-202.
- Kuo, J., and C. d. Hartog. 2006. Seagrass morphology, anatomy, and ultrastructure, p. 51-87. *Seagrasses: Biology, Ecology and Conservation*. Springer Netherlands.
- Lamers, L. and others 2013. Sulfide as a soil phytotoxin—a review. *Front. Plant Sci.* **4**.
- Lancien, M., P. Gadgil, and M. Hodges. 2000. Enzyme redundancy and the importance of 2-oxoglutarate in higher plant ammonium assimilation. *Plant Physiol.* **123**: 817.

- Lavery, P. S., C. E. Oldham, and M. Ghisalberti. 2001. The use of Fick's First Law for predicting porewater nutrient fluxes under diffusive conditions. *Hydrol. Process* **15**: 2435-2451.
- Leakey, A. D. B., E. A. Ainsworth, C. J. Bernacchi, A. Rogers, S. P. Long, and D. R. Ort. 2009. Elevated CO<sub>2</sub> effects on plant carbon, nitrogen, and water relations: Six important lessons from FACE. *J. Exp. Bot.* **60**: 2859-2876.
- Lebrasse, M. C. and others 2022. Temporal stability of seagrass extent, leaf area, and carbon storage in St. Joseph Bay, Florida: a semi-automated remote sensing analysis. *Estuaries Coast* **45**: 2082-2101.
- Lee, J., B. B. Hughes, K. J. Kroeker, A. Owens, C. Wong, and F. Micheli. 2022. Who wins or loses matters: Strongly interacting consumers drive seagrass resistance under ocean acidification. *Sci. Total Environ.* **808**: 151594.
- Lewis, E., and D. W. R. Wallace. 2006. MS Excel program developed for CO<sub>2</sub> system calculations. ORNL/CDIAC-105a. Carbon dioxide information analysis center, Oak Ridge National Laboratory, U.S. Department of Energy, Oak Ridge, Tennessee. . . .
- Li, J. and others 2024. Elevated CO<sub>2</sub> increases soil redox potential by promoting root radial oxygen loss in paddy field. *J. Environ. Sci.* **136**: 11-20.
- Li, M., C. J. Lundquist, C. A. Pilditch, T. A. V. Rees, and J. Ellis. 2019. Implications of nutrient enrichment for the conservation and management of seagrass *Zostera muelleri* meadows. *Aquat. Conserv.* **29**: 1484-1502.
- Li, S.-X., Z.-H. Wang, and B. A. Stewart. 2013. Chapter 5. Responses of crop plants to ammonium and nitrate N, p. 205-397. *In* D. L. Sparks [ed.], *Advances in Agronomy*. Academic Press.
- Lillo, C. 2008. Signalling cascades integrating light-enhanced nitrate metabolism. *Biochem. J.* **415**: 11-19.

- Lindt, T., and U. Feller. 1987. Effect of nitrate and ammonium on long distance transport in cucumber plants. *Bot. Helv.* **97**: 45-52.
- Marbà, N. and others 2002. Carbon and nitrogen translocation between seagrass ramets. *Mar. Ecol. Prog. Ser.* **226**: 287-300.
- Marchiori, P. E. R., E. C. Machado, and R. V. Ribeiro. 2014. Photosynthetic limitations imposed by self-shading in field-grown sugarcane varieties. *Field Crops Res.* **155**: 30-37.
- Marietou, A. 2016. Nitrate reduction in sulfate-reducing bacteria. *FEMS Microbiol. Lett.* **363**.
- Marsh, J. J. A., W. C. Dennison, and R. S. Alberte. 1986. Effects of temperature on photosynthesis and respiration in eelgrass (*Zostera marina* L.). *J. Exp. Mar. Biol. Ecol.* **101**: 257-267.
- Martin, B. C. and others 2019. Oxygen loss from seagrass roots coincides with colonisation of sulphide-oxidising cable bacteria and reduces sulphide stress. *ISME J.* **13**: 707-719.
- Martin, W., and J. Matocha. 1973. Plant analysis as an aid in the fertilization of forage crops, p. 393-426. *In* L. W. a. J. Beaton [ed.], *Soil Testing and Plant Analysis*. Soil Sci. Soc. Am. Wiley.
- Mascaró, O., T. Valdemarsen, M. Holmer, M. Pérez, and J. Romero. 2009. Experimental manipulation of sediment organic content and water column aeration reduces *Zostera marina* (eelgrass) growth and survival. *J. Exp. Mar. Biol. Ecol.* **373**: 26-34.
- Matsumoto, H., N. Wakiuchi, and E. Takahashi. 1971. Changes of starch synthetase activity of cucumber leaves during ammonium toxicity. *Physiol. Plant.* **24**: 102-105.
- Matt, P., M. Geiger, P. Walch-Liu, C. Engels, A. Krapp, and M. Stitt. 2001. Elevated carbon dioxide increases nitrate uptake and nitrate reductase activity when tobacco is growing on nitrate, but increases ammonium uptake and inhibits nitrate reductase activity when tobacco is growing on ammonium nitrate. *Plant Cell Environ.* **24**: 1119-1137.

- McLeod, E. and others 2011. A blueprint for blue carbon: toward an improved understanding of the role of vegetated coastal habitats in sequestering CO<sub>2</sub>. *Front. Ecol. Environ.* **9**: 552-560.
- McMahon, R. M. 2018. Advances in amino acid analysis for marine related matrices and its application to coastal shelf settings in the canadian arctic. Master's Theses Old Dominion University.
- McPherson, M. L., R. C. Zimmerman, and V. J. Hill. 2015. Predicting carbon isotope discrimination in eelgrass (*Zostera marina* L.) from the environmental parameters—light, flow, and [DIC]. *Limnol. Oceanogr.* **60**: 1875-1889.
- Mehrbach, C., C. H. Culberson, J. E. Hawley, and R. M. Pytkowicz. 1973. Measurement of the apparent dissociation constants of carbonic acid in seawater at atmospheric pressure. *Limnol. Oceanogr.* **18**: 897-907.
- Mishra, A. K., S. Cabaço, C. B. de los Santos, E. T. Apostolaki, S. Vizzini, and R. Santos. 2021. Long-term effects of elevated CO<sub>2</sub> on the population dynamics of the seagrass *Cymodocea nodosa*: Evidence from volcanic seeps. *Mar. Pollut. Bull.* **162**: 111824.
- Moore, K. A., and J. C. Jarvis. 2008. Environmental factors affecting recent summertime eelgrass diebacks in the lower Chesapeake bay: Implications for long-term persistence. *J. Coast. Res.*: 135-147.
- Moore, K. A., R. J. Orth, and J. F. Nowak. 1993. Environmental regulation of seed germination in *Zostera marina* L. (eelgrass) in Chesapeake bay: Effects of light, oxygen and sediment burial. *Aquat. Bot.* **45**: 79-91.

- Moore, K. A., E. C. Shields, D. B. Parrish, and R. J. Orth. 2012. Eelgrass survival in two contrasting systems: Role of turbidity and summer water temperatures. *Mar. Ecol. Prog. Ser.* **448**: 247-258.
- Morris, J. T. 1984. Effects of oxygen and salinity on ammonium uptake by *Spartina alterniflora* Loisel. and *Spartina patens* (Aiton) Muhl. *J. Exp. Mar. Biol. Ecol.* **78**: 87-98.
- Morris, J. T., and W. H. D. John. 1984. Effects of O<sub>2</sub> on ammonium uptake and root respiration by *Spartina alterniflora*. *Am. J. Bot.* **71**: 979-985.
- Mortland, M. M. 1955. Adsorption of ammonia by clays and muck. *Soil Science* **80**: 11-18.
- Müller, E. K. H., and P. Janiesch. 1993. *In vivo* nitrate reductase activity in *Carex pseudocyperus* L.: The influence of nitrate - ammonium concentration ratios and correlation with growth. *J. Plant Nutr.* **16**: 1357-1372.
- Nielsen, S. L., S. Enriquez, C. Duarte, and K. Sand-Jensen. 1996. Scaling maximum growth rates across photosynthetic organisms. *Funct. Ecol.*: 167-175.
- Nunes-Nesi, A., A. R. Fernie, and M. Stitt. 2010. Metabolic and signaling aspects underpinning the regulation of plant carbon nitrogen interactions. *Mol. Plant* **3**: 973-996.
- Odum, H. T. 1983. *Systems Ecology: An Introduction*. Wiley.
- Orr, J. C. and others 2001. Estimates of anthropogenic carbon uptake from four three-dimensional global ocean models. *Global Biogeochem. Cycles* **15**: 43-60.
- Orth, R. J. and others 2006. A global crisis for seagrass ecosystems. *BioScience* **56**: 987-996.
- Ouyang, X., and S. Y. Lee. 2022. Chapter 2. Decomposition of vascular plants and carbon mineralization in coastal wetlands, p. 25-54. *In* X. Ouyang, S. Y. Lee, D. Y. F. Lai and C. Marchand [eds.], *Carbon Mineralization in Coastal Wetlands*. Elsevier.

- Ow, Y. X., C. J. Collier, and S. Uthicke. 2015. Responses of three tropical seagrass species to CO<sub>2</sub> enrichment. *Mar. Biol.* **162**: 1005-1017.
- Ow, Y. X., N. Vogel, C. J. Collier, J. A. M. Holtum, F. Flores, and S. Uthicke. 2016. Nitrate fertilisation does not enhance CO<sub>2</sub> responses in two tropical seagrass species. *Sci. Rep.* **6**: 23093.
- Palacios, S. L., and R. C. Zimmerman. 2007. Response of eelgrass *Zostera marina* to CO<sub>2</sub> enrichment: Possible impacts of climate change and potential for remediation of coastal habitats. *Mar. Ecol. Prog. Ser.* **344**: 1-13.
- Parsons, T. R. 2013. A manual of chemical & biological methods for seawater analysis. elsevier.
- Pedersen, M. F., and J. Borum. 1992. Nitrogen dynamics of eelgrass *Zostera marina* during a late summer period of high growth and low nutrient availability *Mar. Ecol. Prog. Ser.* **80**: 65-73.
- Peralta, G., T. J. Bouma, J. v. Soelen, J. L. Pérez-Lloréns, and I. Hernández. 2003. On the use of sediment fertilization for seagrass restoration: A mesocosm study on *Zostera marina* L. *Aquat. Bot.* **75**: 95-110.
- Pérez, M., and J. Romero. 1992. Photosynthetic response to light and temperature of the seagrass *Cymodocea nodosa* and the prediction of its seasonality. *Aquat. Bot.* **43**: 51-62.
- Peuke, A. D., and W. M. Kaiser. 1996. Nitrate or ammonium uptake and transport, and rapid regulation of nitrate reduction in higher plants, p. 93-113. *In* H. D. Behnke, U. Lüttge, K. Esser, J. W. Kadereit and M. Runge [eds.], *Progress in Botany / Fortschritte der Botanik: Structural Botany Physiology Genetics Taxonomy Geobotany / Struktur Physiologie Genetik Systematik Geobotanik*. Springer Berlin Heidelberg.
- Pirc, H. 1985. Growth dynamics in *Posidonia oceanica* (L.) Delile. *Mar. Ecol.* **6**: 141-165.

- Pirc, H., and B. Wollenweber. 1988. Seasonal changes in nitrogen, free amino acids, and C/N ratio in mediterranean seagrasses. *Mar. Ecol.* **9**: 167-179.
- Piro, A. and others 2020. Leaf proteome modulation and cytological features of seagrass *Cymodocea nodosa* in response to long-term high CO<sub>2</sub> exposure in volcanic vents. *Sci. Rep.* **10**: 22332.
- Platt, S. G., and J. A. Bassham. 1978. Photosynthesis and increased production of protein. *Adv Exp Med Biol* **105**: 195-247.
- Qin, C., K.-k. Yi, and P. Wu. 2011. Ammonium affects cell viability to inhibit root growth in *Arabidopsis*. *J Zhejiang Univ Sci B* **12**: 477-484.
- Quay, P. D., B. Tilbrook, and C. S. Wong. 1992. Oceanic uptake of fossil fuel CO<sub>2</sub>: carbon-13 evidence. *Science* **256**: 74.
- Ravaglioli, C. and others 2017. Nutrient loading fosters seagrass productivity under ocean acidification. *Sci. Rep.* **7**: 13732.
- Reidenbach, L. B. and others 2017. Growth, ammonium metabolism, and photosynthetic properties of *Ulva australis* (Chlorophyta) under decreasing pH and ammonium enrichment. *PLoS One* **12**: e0188389.
- Riebesell, U. 2004. Effects of CO<sub>2</sub> enrichment on marine phytoplankton. *J. Oceanogr.* **60**: 719-729.
- Roman, C. T., and K. W. Able. 1988. Production ecology of eelgrass (*Zostera marina* L.) in a cape cod salt marsh-estuarine system, Massachusetts. *Aquat. Bot.* **32**: 353-363.
- Rosen, C. J., and R. M. Carlson. 1984. Influence of root zone oxygen stress on potassium and ammonium absorption by myrobalan plum rootstock. *Plant Soil* **80**: 345-353.
- Roth, M. 1971. Fluorescence reaction for amino acids. *Anal. Chem.* **43**: 880-882.

- Ruan, Y.-L. 2012. Signaling role of sucrose metabolism in development. *Mol. Plant* **5**: 763-765.
- Rubio, L., A. Linares-Rueda, M. J. García-Sánchez, and J. A. Fernández. 2007. Ammonium uptake kinetics in root and leaf cells of *Zostera marina* L. *J. Exp. Mar. Biol. Ecol.* **352**: 271-279.
- Santamaría, L., C. Dias, and M. J. M. Hootsmans. 1994. The influence of ammonia on the growth and photosynthesis of *Ruppia drepanensis* Tineo from Doñana National Park (SW Spain). *Hydrobiologia* **275-276**: 219-231.
- Sanz-Luque, E., A. Chamizo-Ampudia, A. Llamas, A. Galvan, and E. Fernandez. 2015. Understanding nitrate assimilation and its regulation in microalgae. *Front. Plant Sci.* **6**.
- Schlesinger, W. H., E.S .Bernhardt, E.H. DeLucia, D.S.Ellsworth, A.C.Finzi, G.R.Hendrey, K.S. Hofmockel, J. Lichter, R. Matamala, D. Moore, R. Oren, J.S. Phippen, and R.B. Thomas, . 2006. The Duke forest FACE experiment: CO<sub>2</sub> enrichment of a loblolly pine forest. *Ecol. Stud.* **187**: 197-212.
- Short, F., and C. McRoy. 1984. Nitrogen uptake by leaves and roots of the seagrass *Zostera marina* L. *Bot. Mar.* **27**: 547-556.
- Short, F. T. 1987. Effects of sediment nutrients on seagrasses: Literature review and mesocosm experiment. *Aquat. Bot.* **27**: 41-57.
- Short, F. T., and H. A. Neckles. 1999. The effects of global climate change on seagrasses. *Aquat. Bot.* **63**: 169-196.
- Sisson, M., J. Shen, W.G. Reay, E.J. Miles, A.Y. Kuo, and H. V. Wang. 2010. The development of a management tool to assess bacterial impacts in Rudee Inlet, Virginia Beach. Special reports in applied marine science and ocean engineering (SRAMSOE) No. 423. Virginia Institute of Marine Science, William & Mary. <https://doi.org/10.21220/V5KR07>. : .

- Smith, R. D., W. C. Dennison, and R. S. Alberte. 1984. Role of seagrass photosynthesis in root aerobic processes. *Plant Physiol.* **74**: 1055.
- Solorzano, L. 1969. Determination of ammonia in natural waters by the phenylhypochlorite method. *Limnol. Oceanogr.* **14**: 799-801.
- Stiling, P., and T. Cornelissen. 2007. How does elevated carbon dioxide (CO<sub>2</sub>) affect plant–herbivore interactions? A field experiment and meta-analysis of CO<sub>2</sub>-mediated changes on plant chemistry and herbivore performance. *Glob Chang Biol.* **13**: 1823-1842.
- Stitt, M., and A. Krapp. 1999. The interaction between elevated carbon dioxide and nitrogen nutrition: The physiological and molecular background. *Plant Cell Environ.* **22**: 583-621.
- Suárez-Álvarez, S., J. L. Gómez-Pinchetti, and G. García-Reina. 2011. Effects of increased CO<sub>2</sub> levels on growth, photosynthesis, ammonium uptake and cell composition in the macroalga *Hypnea spinella* (Gigartinales, Rhodophyta). *J. Appl. Phycol.* **24**: 815-823.
- Szajnowski, F. 1973. Relationship between leaf area index and shoot production of *Phragmites communis* Trin. *Pol. Arch. Hydrobiol* **20**: 257-268.
- Thursby, G. B., and M. M. Harlin. 1982. Leaf-root interaction in the uptake of ammonia by *Zostera marina*. *Mar. Biol.* **72**: 109-112.
- Touchette, B. W. 1999. Physiological and developmental responses of eelgrass (*Zostera marina* L.) to increases in water-column nitrate and temperature. Ph.D dissertation. Doctor of Philosophy (PhD), Dissertation, Botany. North Carolina State University.
- Touchette, B. W., and J. M. Burkholder. 2000a. Review of nitrogen and phosphorus metabolism in seagrasses. *J. Exp. Mar. Biol. Ecol.* **250**: 133-167.
- Touchette, B. W., and J. M. Burkholder. 2000b. Overview of the physiological ecology of carbon metabolism in seagrasses. *J. Exp. Mar. Biol. Ecol.* **250**: 169-205.

- Touchette, B. W., Burkholder, J. M., Glasgow, H. 2003. Variations in eelgrass *Zostera marina* L. morphology and internal nutrient composition as influenced by increased temperature and water column nitrate. *Estuaries Coast* **26**: 142-155.
- Turpin, D. H., G. C. Vanlerberghe, A. M. Amory, and R. D. Guy. 1991. The inorganic carbon requirements for nitrogen assimilation. *Can. J. Bot.* **69**: 1139-1145.
- van der Heide, T., A. J. P. Smolders, B. G. A. Rijkens, E. H. v. Nes, E. H. v. Nes, and J. G. M. Roelofs. 2008a. Toxicity of reduced nitrogen in eelgrass (*Zostera marina*) is highly dependent on shoot density and pH. *Oecologia*: 411-419.
- van der Heide, T., A. J. P. Smolders, B. G. A. Rijkens, E. H. van Nes, M. M. van Katwijk, and J. G. M. Roelofs. 2008b. Toxicity of reduced nitrogen in eelgrass (*Zostera marina*) is highly dependent on shoot density and pH. *Oecologia* **158**: 411-419.
- van Heuven, S., D. Pierrot, J. W. R. Rae, E. Lewis, and D. W. R. Wallace. 2011. Matlab program developed for CO<sub>2</sub> system calculations. ORNL/CDIAC-105b. Department of Energy, Oak Ridge, Tennessee.
- van Katwijk, M. M., L. H. T. Vergeer, G. H. W. S. GHW, and J. G. M. Roelofs. 1997. Ammonium toxicity in eelgrass *Zostera marina*. *Mar. Ecol. Prog. Ser.* **157**: 159-173.
- Velthuis, M. and others 2022. Differential effects of elevated *p*CO<sub>2</sub> and warming on marine phytoplankton stoichiometry. *Limnol. Oceanogr.* **67**: 598-607.
- Walker, B. J., D. D. Strand, D. M. Kramer, and A. B. Cousins. 2014. The response of cyclic electron flow around photosystem I to changes in photorespiration and nitrate assimilation. *Plant Physiol.* **165**: 453-462.
- Waycott, M. and others 2009. Accelerating loss of seagrasses across the globe threatens coastal ecosystems. *Proceedings of the National Academy of Sciences* **106**: 12377.

- Webb, W. L., M. Newton, and D. Starr. 1974. Carbon dioxide exchange of *Alnus rubra*. *Oecologia* **17**: 281-291.
- Weger, H. G., and D. H. Turpin. 1989. Mitochondrial respiration can support  $\text{NO}_3^-$  and  $\text{NO}_2^-$  reduction during photosynthesis 1: interactions between photosynthesis, respiration, and n assimilation in the n-limited green alga *Selenastrum minutum*. *Plant Physiol.* **89**: 409-415.
- Wigley, T. M. L. 1983. The pre-industrial carbon dioxide level. *Climatic Change* **5**: 315-320.
- Williams, W. E., K. Garbutt, and F. A. Bazzaz. 1988. The response of plants to elevated  $\text{CO}_2$  • V. performance of an assemblage of serpentine grassland herbs. *Environ. Exp. Bot.* **28**: 123-130.
- Young, C. S., and C. J. Gobler. 2017. The organizing effects of elevated  $\text{CO}_2$  on competition among estuarine primary producers. *Sci. Rep.* **7**: 1-15.
- Young, D. K. 1968. Chemistry of southern Chesapeake bay sediments. *Chesap. Sci* **9**: 254-260.
- Zayas-Santiago, C. C., A. Rivas-Ubach, L.-J. Kuo, N. D. Ward, and R. C. Zimmerman. 2020. Metabolic profiling reveals biochemical pathways responsible for eelgrass response to elevated  $\text{CO}_2$  and temperature. *Sci. Rep.* **10**: 4693.
- Zeebe, R. E. 2012. History of seawater carbonate chemistry, atmospheric  $\text{CO}_2$ , and ocean acidification. *Annu. Rev. Earth Planet. Sci.* **40**: 141-165.
- Zenda, T., S. Liu, A. Dong, and H. Duan. 2021. Revisiting sulphur—the once neglected nutrient: It's roles in plant growth, metabolism, stress tolerance and crop production. *Agriculture* **11**: 626.
- Zhao, X. and others 2019. Elevated  $\text{CO}_2$  concentration promotes photosynthesis of grape (*Vitis vinifera* L. cv. 'Pinot noir') plantlet in vitro by regulating RbcS and Rca revealed by proteomic and transcriptomic profiles. *BMC Plant Biol.* **19**: 42.

- Zhu, M.-X., J. Liu, G.-P. Yang, T. Li, and R.-J. Yang. 2012. Reactive iron and its buffering capacity towards dissolved sulfide in sediments of Jiaozhou bay, China. *Mar. Environ. Res.* **80**: 46-55.
- Zieman, J. C. 1974. Methods for the study of the growth and production of turtle grass, *Thalassia testudinum* König. *Aquaculture* **4**: 139-143.
- Zimmerman, A. R., and E. A. Canuel. 2000. A geochemical record of eutrophication and anoxia in Chesapeake bay sediments: anthropogenic influence on organic matter composition. *Mar. Chem.* **69**: 117-137.
- Zimmerman, R., D. Kohrs, and R. Alberte. 1996. Top-down impact through a bottom-up mechanism: The effect of limpet grazing on growth, productivity and carbon allocation of *Zostera marina* L. (eelgrass). *Oecologia* **107**: 560-567.
- Zimmerman, R. C. 2021. Scaling up: predicting the impacts of climate change on seagrass ecosystems. *Estuaries Coast* **44**: 558-576.
- . 2003. A biooptical model of irradiance distribution and photosynthesis in seagrass canopies. *Limnol. Oceanogr.* **48**: 568-585.
- . 2006. Chapter 13. Light and photosynthesis in seagrass meadows, p. 303-321. *In* A. W. D. Larkum, R. J. Orth and C. M. Duarte [eds.], *Seagrasses: Biology, ecology and conservation*. Springer Netherlands.
- Zimmerman, R. C., and R. S. Alberte. 1996. Effect of light/dark transition on carbon translocation in eelgrass *Zostera marina* seedlings. *Mar. Ecol. Prog. Ser.* **136**: 305-309.
- Zimmerman, R. C., A. Cabello-Pasini, and R. S. Alberte. 1994. Modeling daily production of aquatic macrophytes from irradiance measurements: a comparative analysis. *Mar. Ecol. Prog. Ser.*: 185-196.

- Zimmerman, R. C., V. J. Hill, and C. L. Gallegos. 2015. Predicting effects of ocean warming, acidification, and water quality on Chesapeake region eelgrass. *Limnol. Oceanogr.* **60**: 1781-1804.
- Zimmerman, R. C. and others 2017. Experimental impacts of climate warming and ocean carbonation on eelgrass *Zostera marina*. *Mar. Ecol. Prog. Ser.* **566**: 1-15.
- Zimmerman, R. C., D. G. Kohrs, D. L. Steller, and R. S. Alberte. 1995. Carbon partitioning in eelgrass (regulation by photosynthesis and the response to daily light-dark cycles). *Plant Physiol.* **108**: 1665-1671.
- Zimmerman, R. C., D. G. Kohrs, D. L. Steller, and R. S. Alberte. 1997. Impacts of CO<sub>2</sub> enrichment on productivity and light requirements of eelgrass. *Plant Physiol.* **115**: 599-607.
- Zimmerman, R. C., R. D. R.D. Smith, and R. S. Alberte. 1987. Is growth of eelgrass nitrogen limited? A numerical simulation of the effects of light and nitrogen on the growth dynamics of *Zostera marina*. *Mar. Ecol. Prog. Ser.* **41**: 167-176.
- Zimmerman, R. C., R. D. Smith, and R. S. Alberte. 1989. Thermal acclimation and whole-plant carbon balance in *Zostera marina* L. (eelgrass). *J. Exp. Mar. Biol. Ecol.* **130**: 93-109.
- Zvereva, E. L., and M. V. Kozlov. 2006. Consequences of simultaneous elevation of carbon dioxide and temperature for plant–herbivore interactions: a metaanalysis. *Glob Chang Biol.* **12**: 27-41.

## VITA

Malee Jinuntuya  
 Department of Ocean and Earth Sciences  
 Old Dominion University, Elkhorn Ave, Norfolk, VA 23529  
 Email: mjinuntu@gmail.com

### EDUCATION

2024 (Expected) Ph.D. Oceanography, Old Dominion University, Virginia  
 2007 M.S. Environmental Geochemistry, Michigan State University, Michigan  
 2003 B.S. Marine Biology, Michigan State University, Michigan

### PROFESSIONAL EXPERIENCE

2019 Research Technician, Old Dominion University, Virginia  
 2015-2016 Teaching Assistant, Old Dominion University, Virginia  
 2011-2014 Graduate Research Assistant, Old Dominion University, Virginia  
 2007-2008 Teaching Assistant, Old Dominion University, Virginia  
 2008-2009 Graduate Research Assistant, Old Dominion University, Virginia  
 2003-2007 Teaching Assistant, Michigan State University, Michigan  
 2002-2003 Research Technician, Department of Entomology, Michigan State University

### PUBLICATIONS

2008 **Jinuntuya, M.**, R.L. Sutka, P.H. Ostrom, H. Gandhi, N.E. Ostrom. 2008. Isotopologue fractionation during microbial reduction of N<sub>2</sub>O within soil mesocosms as a function of water filled pore space. *Soil Biology and Biochemistry*, 40: 2273-2280.  
 2017 Zimmerman, R.C., V.J. Hill, **M. Jinuntuya**, B. Celebi, D. Ruble, M. Smith, T. Cedeno, W.M. Swingle. 2017. Experimental impacts of climate warming and ocean carbonation on eelgrass, *Zostera marina*. *Marine Ecology Progress Series*, 566: 1-15.

### AWARDS

2015 Dorothy Brown Smith (DBS) Travel Award to attend Aquatic Sciences Meeting, Granada, Spain  
 2014 DBS Travel Award to attend Ocean Sciences Meeting, Honolulu, Hawaii  
 2013 DBS Travel Award to attend Graduate Climate Conference, Woods Hole, MA  
 2014 Jacques S. Zaneveld Endowed Scholarship (annual competition)  
 2013 Jacques S. Zaneveld Endowed Scholarship (annual competition)  
 2011 Jacques S. Zaneveld Endowed Scholarship (annual competition)  
 2009-2010 Dorothy Brown Smith Scholarship (annual competition)  
 2006 Council of Graduate Students (COGS) Degree Completion Grants from Michigan State University  
 2005 Travel Grant from Biogeosphere-Atmosphere Stable Isotope Network to attend the workshop at Fall AGU meeting  
 2005-2006 Shell Oil Company Fellowship (annual competition)